The Dissertation Committee for Nikola Petrov Petrov
Certifies that this is the approved version of the following dissertation:

Methods of Dynamical Systems, Harmonic Analysis and Wavelets Applied to Several Physical Systems

Committee:

Rafael de la Llave, Supervisor

Richard D. Hazeltine

Hans Koch

Philip J. Morrison

Jack B. Swift

Mikhail M. Vishik

Methods of Dynamical Systems, Harmonic Analysis and Wavelets Applied to Several Physical Systems

by

Nikola Petrov Petrov, B.S.

DISSERTATION

Presented to the Faculty of the Graduate School of

The University of Texas at Austin

in Partial Fulfillment

of the Requirements

for the Degree of

DOCTOR OF PHILOSOPHY

THE UNIVERSITY OF TEXAS AT AUSTIN

December 2005

Dedicated to my wife Adriana.

Acknowledgments

First I would like to thank my advisor, Rafael de la Llave, a great mentor and person. He taught me so much mathematics, physics, nonlinear dynamics, programming... My work with him was a wonderful journey from physics to programming to number theory to harmonic analysis...

He was always supportive when I get stuck, always ready to answer my questions, always ready to spend hours with me when I cannot find a bug in a program.

His work is a source of inspiration for me and I hope that in the future we will keep our professional contacts as well as our friendship.

I would like to mention the names of the professors whose courses (besides being very enjoyable) taught me a lot: Rafael de la Llave, Hans Koch, Misha Vishik, John Gilbert, Todd Arbogast, Jack Xin, and Anatoly Neishtadt from the Department of Mathematics, Jack Swift, Bryce DeWitt, and Qian Niu from the Department of Physics, and Takis Konstantopoulos from the Department of Electrical Engineering.

Thanks also to John Vano, Juan Abad, and Henrik Kalisch — fellow graduate students from the Department of Mathematics with whom I had many interesting discussions. In particular, John noticed the simple argument for the importance of the boundary conditions given in Section 2.6.1, and

Masaru Yamaguchi kindly sent me his articles and preprints related to my research.

I would also like to thank some people who generously made their software products freely available – Paul J. Turner for the plotting tool `ACE/gr`, Keith Briggs for the `doubledouble` routines, and the team developing the library for arbitrary precision arithmetic GNU MP.

Going back in time, I would like to acknowledge the crucial role played by my high-school Physics teachers, Vassilka Aretova and Zdravka Dimova, and my high school Mathematics teacher, the late Gavrail Poslannikov, in "converting" me from chemistry to physics and mathematics.

I would like also to thank my aunt Elena Stefanova, who was a high-school Physics teacher. During the wonderful summer vacations I spent at her house in my early teenage years, the world of physics was brought to me for the first time through her books. I still remember vividly how excited I was when reading Faraday's *The Chemical History of a Candle* and Einstein and Infeld's *The Evolution of Physics*.

The years spent in Austin were a great time thanks to our friends in Austin – I would like to mention Hani Kaldas, Liziane and Sandro da Rocha, Gergana Drandova and Sergey Cheshkov, Evelina Bozhankova and Steftcho Dokov, Margarita Marinova, Enrico Rossi, Evstati Evstatiev, Jon Chang, Ves-

was a very pleasant distraction from my teaching and research, and I think that it was the main thing that helped me keep my sanity. In the beginning of this period, Kenneth Meyer told me that this was going to be one of the best years of my life, and I think he was right. Thanks, Pepi!

I would like to thank my wife, Adriana, for bearing with me during the whole "graduate school" adventure.

Finally, it is a great pleasure for me to thank my parents, Maria Petrova and Petar Petrov, and my sister, Nadezhda Petrova, for their love and encouragement over the years.

Methods of Dynamical Systems, Harmonic Analysis and Wavelets Applied to Several Physical Systems

Publication No. ⎯⎯⎯⎯⎯⎯

Nikola Petrov Petrov, Ph.D.
The University of Texas at Austin, 2005

Supervisor: Rafael de la Llave

We consider the electromagnetic field in a one-dimensional optical resonator with one stationary and one periodically moving perfectly reflecting boundaries. We show that the problem of the asymptotic behavior of the electromagnetic field in the resonator can be reformulated as a problem of the dynamical behavior of a circle map associated with the motion of the boundary. We illustrate that mathematical theory of circle maps leads to several physical predictions. Notably, well-known mathematical results imply that there are intervals of parameters where the waves in the cavity concentrate in wave packets whose width decreases exponentially and whose energy grows exponentially. Even though these intervals are dense for typical motions of the boundary, in the complement there is a positive measure set of parameters where the energy remains bounded.

We also study the problem of the asymptotic behavior of the electromagnetic field in the resonator if the mirror is moving quasiperiodically (with

$d \geq 2$ incommensurate frequencies). In this case we reduce the problem to a study of the long-time behavior of the iterates of a map of d-dimensional torus. We describe the class of torus maps that occur in the description of the physical problem (in particular, they preserve a foliation). We study several dynamical features of such maps and translate them into into properties for the field in the cavity. The mathematical predictions are illustrated with numerical simulations.

In the second part of the dissertation we develop numerical implementations of several criteria to asses the regularity of functions. The criteria are based on the method of finite differences and methods of harmonic analysis, namely, Littlewood-Paley theory and wavelet analysis.

As an application of the methods, we study the regularity of conjugacies between critical circle maps with golden mean rotation number. These maps have a very well developed mathematical theory as well as a wealth of numerical studies. We compare the results produced by our methods among themselves and with theorems in the mathematical literature. We confirm that several of the features that are predicted by the mathematical results are observable by numerical computation. Some universal numbers predicted can be computed reliably.

Table of Contents

List of Figures

xvii

Chapter 1

Introduction

The present dissertation is devoted to applications of theory of dynamical systems and methods of harmonic/wavelet analysis to physical systems and numerical methods.

It consists of two parts. In the first part (Chapters 2 and 3), we apply methods of dynamical systems to the study of the asymptotic behavior of the electromagnetic field in a one-dimensional optical cavity one mirror of which is moving periodically or quasiperiodically. It the case of a periodically moving mirror, we reformulate the problem to the study of an orientation-preserving homeomorphism of the circle (explicitly defined for any given physically admissible motion of the mirror). If the mirror is moving quasiperiodically, we show that the problem can be translated into the problem of the long-time behavior of the iterates of a map of the d-dimensional torus (if the motion of the mirror is a quasiperiodic function of time with d incommensurate frequencies). The torus maps occurring in this situation are of a very particular kind – they preserve an invariant foliation on the torus. This is a very severe restriction on the torus map, so the general theorems about torus maps do not apply. We study numerically and analytically some features of these torus maps, and

give physical interpretation of the mathematical results.

In the second part of the dissertation (Chapter 4), we study numerically the global Hölder regularity of conjugacies between circle maps of different types – circle diffeomorphisms or "critical" circle maps, i.e., circle homeomorphisms that have one point at which their derivative is zero. We use several methods to study numerically the regularity of the conjugacies – finite differences method, two methods based on Littlewood-Paley theorem (studying the rate of decrease of the dyadic Fourier sums or of the convolution of the function with the Poisson kernel), and two wavelet methods (studying the rate of decrease of the wavelet coefficients or the rate of approximation by truncated wavelet series).

The main results of the dissertation have been published in the articles/preprints [131, 190] (Chapter 2), [160] (Chapter 3), [132] (Chapter 4).

Chapter 2

Circle Maps and a Periodically Pulsating Cavity

The goal of this chapter is to show that the problem of predicting the asymptotic behavior of the solutions of the one-dimensional wave equation in a spatially bounded domain with with a periodically moving boundary can be easily reformulated in terms of the study of long term behavior of circle maps and, therefore, that many well known results in theory of circle maps lead to physically important predictions.

In Chapter 3, we apply a similar dynamical systems approach to describe the electromagnetic field in the cavity if instead of periodically, the wall is moving quasiperiodically.

The main results in this chapter were published in [131] and [190].

2.1   Literature Review

In this section, we give pointers to the literature on the problem, trying to emphasize the papers that are more relevant to our approach.

2.1.1 Early Studies

The description of waves in changing domains has been studied for a long time. It is directly related to the Maxwell's theory of the electromagnetic field and has been analyzed in connection with the radiation pressure in the late XIX and early XX century.

Lord Rayleigh [172] (reprinted in [173, vol. V, pp. 41–48]) and Sir Joseph Larmor [125] gave a dynamical illustration of the radiation pressure. Their methods were applied by Havelock [91] and Nicolai [154], who considered the motion of a string one end of which is fixed and the other one is moving and calculated the pressure exerted by the string on the moving end.

2.1.2 Minkowski Space-Time and D'Alembert Method

The advent of the geometrical picture of the space-time given by Minkowski [144] (English translation: [136, pp. 73–91]) shed new light on the connection between the mathematics and the physics of the wave equation. D'Alembert method of solving the wave equation in the case of one spatial dimension is an example of the fact that the spatial and the temporal variables should be treated on equal footing. Moreover, this method has a transparent physical interpretation – namely, the disturbances in a field of zero mass propagate along the future light cone.

The space-time representation (i.e., the method of characteristics) for solving the one-dimensional wave equation in the presence of moving boundaries was used by Balazs [8].

2.1.3 Periodically Oscillating Boundaries in the Mathematics Literature

The problem of the behavior of the solutions of the wave equation in presence of (periodically) moving boundaries in one or more spatial dimensions has been studied intensively by Cooper and his collaborators.

In [30], Cooper studied the case of a plane electromagnetic wave normally incident on a moving perfectly conducting flat surface. He used the physically correct boundary conditions (see Section 2.3.3), calculated the Doppler factor at reflection (Section 2.3.4), and constructed an approximate solution taking into account the Doppler shift.

In [32], Cooper analyzed the long-time behavior and the energy growth of the electromagnetic field in a pulsating optical resonator. He used the method of characteristics to reformulate the time evolution of the field in terms of a map of the interval. Then he analyzed the iterates of this map (for periodically moving boundary) and found that under certain assumptions the energy of the field grows unboundedly. In [31], he used similar methods to find the asymptotic behavior of the vibrations of a string with varying length.

Cooper and Koch [33] studied the Dirichlet problem for the one-dimensional wave equation in a spatially bounded domain one of whose boundaries is stationary and the other one is moving periodically, by analyzing the operator of evolution through one period, T, of the motion of the boundary. If u is the solution of the boundary-value problem, and

$$U : (u(0, \cdot), u_t(0, \cdot)) \mapsto (u(T, \cdot), u_t(T, \cdot))$$

stands for the time-T evolution operator, Cooper and Koch showed that the properties of the spectrum of U are related to the properties of a circle map associated with the motion of the boundary. Their map is essentially the same as our circle map g [131] (see Section 2.3.5). One can try to give physical interpretation of Theorem 2.4 of [33] after reading Sections 2.3–2.6. Cooper and Koch made the interesting observation that in certain cases the solutions of the boundary value problem can go to 0 as $t \to \infty$ in some Sobolev norms, but grow in others. This is related to the surprising difference between the behavior of the solutions of the Dirichlet and the Neumann boundary problems which we give in Section 2.6.1 [190].

Yamaguchi and his collaborators have proven the existence and analyzed the behavior of the solutions of the Dirichlet boundary value problem for one-dimensional hyperbolic partial differential equations with (quasi)periodic coefficients/forcing terms and/or in a changing domain.

In [199], Yamaguchi proved the existence of almost periodic and quasi-periodic solutions in the case of a quasiperiodically (see Definition 3.3.2) varying forcing term and coefficients that are periodic in t and whose frequencies satisfy some Diophantine relation (Definition 2.4.4).

Yamaguchi [198] proved the existence of exactly one almost periodic solution to the wave equation with a quasiperiodic forcing term under some conditions on the Diophantine properties of the frequencies of the forcing term. In a similar situation, he and Imai [205] found classes of periodic forcing terms for which the problem has no bounded (hence, no periodic) solutions for any

choice of the initial data; again, Diophantine properties of the frequencies constituted a necessary condition for that (for fixed length of the spatial domain). In [200], Yamaguchi extended these results.

In [201, 202], Yamaguchi studied the (quasi)periodic solutions of the Dirichlet boundary problem for the homogeneous one-dimensional wave equation in a pulsating domain. In these articles, he explicitly constructed a circle map (the map F defined by (2.19)) and related the number-theoretic properties of its rotation number with the existence of (quasi)periodic solutions. In [206], he and Yoshida gave a generalization of this approach in the presence of a driving term in the right-hand side of the wave equation.

Dittrich *et al* [53] studied the stability (i.e., the boundedness of the energy) of the solutions of the Dirichlet or Neumann boundary problems for the one-dimensional wave equation in a periodically pulsating domain. In their analysis, they explicitly used theory of circle maps. Some of their statements for the case of Neumann boundary conditions, however, are not correct – we found [190] a counterexample to their conclusions (see Section 2.6.1).

2.1.4 One-Dimensional Changing Domains in the Physics Literature

Although we are not going to discuss the quantum aspects of the problem, let us discuss briefly what has been done and give some references. Quantum effects are present even if the two boundaries are at rest (the Casimir effect [21]; see also the book by Mostepanenko and Trunov [151]). The generalization

to the case of a moving boundary is important for the the high precision measurements with a Michelson interferometer with mirrors attached to strings or a Fabry-Perot cavity related to gravitational wave detection (see the references in [27]).

Moore [146] considered the quantum theory of the electromagnetic field in a one-dimensional cavity with variable length. He imposed homogeneous Dirichlet boundary conditions on the electromagnetic vector potential (which in this formalism is an operator-valued distribution) and showed that one cannot construct a Hamiltonian, hence, Schrödinger picture does not exist. Indeed, the existence of a Hamiltonian would imply the existence of a unitary evolution operator, $\hat{U}(t, t_0) = \exp\{-i(t - t_0)\hat{H}\}$ with the property

$$\hat{A}(t, x) = \hat{U}^\dagger(t, t_0)\,\hat{A}(t_0, x)\,\hat{U}(t, t_0)\ ,$$

which, in turn, implies that if the point (t_0, x) belongs to the world line of the mirror (and, therefore, $\hat{A}(t_0, x) = 0$), then one would not be able to obtain a nonzero value for $\hat{A}(t, x)$ at the same spatial point x at any moment $t > t_0$.

Since we will not to treat the quantum case in detail, we leave out all complications Moore had to overcome in the development of a quantization scheme, and discuss only one particular result of his treatment. [1] Namely, he pointed out that one has to look for an expansion of the field operator $\hat{A}(t, x)$

---

[1]Fulling and Davies [76] and Castagnino and Ferraro [22] continued the line of investigation of Moore, while Razavy and Terning [174] developed an alternative approach.

in mode functions

$$A_k(t, x) = e^{\pi i k R(t+x)} + e^{\pi i k R(t-x)} \ , \qquad k \in \mathbb{N} \ ,$$

where the function $R : \mathbb{R} \to \mathbb{R}$ satisfies

$$R(t + a(t)) = R(t - a(t)) + 2 \ . \tag{2.1}$$

Most authors studying the quantum aspects of the problem analyzed, in fact, the properties of the solution of the functional equation (2.1). In Section 2.6.4, we give a method for analyzing the properties of the function $R(z)$, based on theory of circle maps.

Let us emphasize that the authors of all papers mentioned below discussed the Dirichlet boundary problem only.

Fulling and Davies [76] (see also Mostepanenko and Trunov [151, Section 2.7]) calculated the expectation values of the energy-momentum tensor in the presence of a moving boundary (using the "point-splitting" method of DeWitt). They found that (after discarding some infinite constants), each of the four components of the energy-momentum tensor is equal (up to multiplicative constants) to the Schwarzian derivative of certain function – we give more details about this interesting fact in Section 2.6.6.

Calucci [20] adopted a formalism different from Moore's and estimated the number of emitted photons for the case of a very slow motion of the boundary by using the formalism of adiabatic approximation. His results, however, do not apply to the long-time behavior of the field or to the case of

9

resonant motion of the boundary (i.e., when the wall oscillates with a small amplitude and with frequency equal to a multiple of the time a light ray needs to traverse the unperturbed length of the cavity twice).

Dodonov *et al* [61] considered the case of resonant motion of the boundary within Moore's formalism. They studied a slightly sinusoidally perturbed motion of the boundary,

$$a(t) = a_0 \left(1 + \varepsilon \sin \frac{q\pi t}{a_0} \right) \ , \quad q = 1, \, 2, \, \dots \, , \quad \varepsilon \ll 1 \ ,$$

and expanded $R(\xi)$ in powers of ε, obtaining an approximate solution valid for $\varepsilon t \gg 1$. For this boundary motion, they calculated the long-time asymptotics of the number of photons generated in the mth mode as well as the back reaction on the oscillating wall from the field. [2] They mentioned that the force between the mirrors can be enhanced significantly in the resonant case, but without recognizing the presence of wave packets, although in some cases they found some moderate squeezing, i.e., formation of narrow wave packets (squeezing was mentioned also in Dodonov *et al* [59]).

Dittrich *et al* [54] studied the behavior of a string one of whose ends is moving periodically. They used the method of characteristics, constructed a map identical to our map F (2.19), and mentioned that the behavior of the iterates of this map can explain the energy growth. They, however, failed to

---

[2]The same authors [60] studied the quantized electromagnetic field in time-dependent nonuniform media, and calculated the number of photons due to the change in time of the dielectric constant of the medium.

notice that this map is a lift of a circle map, so they did not use the rich theory of circle maps to make physical predictions.

Sassaroli *et al* [177] studied the photon production in the case of a cavity whose length is changing periodically, but discontinuously (arguably, a quite non-physical situation) using a method similar to the one use by Calucci [20]. They gave some arguments supporting the (quite controversial) idea of Schwinger that sonoluminescence can be explained through the dynamical Casimir effect (i.e., Casimir effect between moving boundaries).

Law [127] studied the quantum field in a cavity with a moving boundary and filled with a medium with time-dependent index of refraction. He took as a starting point Moore's approach and derived an approximate effective Hamiltonian, which made an approximate Schrödinger picture possible. He used the "instantaneous" set of mode functions and "instantaneous" creation/annihilation operators. Since several authors have used the method of "instantaneous" eigenfuncions, here we give a brief sketch of it. In order to solve the homogeneous Dirichlet boundary value problem for the wave equation in the domain $\{(x,t)|x \in [0, a(t)], \ t \geq 0\}$, one can look for a solution in the form

$$u(t,x) = \sum_{k \in \mathbb{N}} Q_k(t)\, \psi_k(t,x) \ ,$$

where

$$\psi_k(t,x) = \sin \frac{2\pi k x}{a(t)} \ . \tag{2.2}$$

The functions $\psi_k(t,x)$ obviously satisfy the boundary conditions. If $a(t) =$

$a_0 = $ const, they would be solutions of the corresponding Sturm-Liouville problem, and the functions $Q_k(t)$ would satisfy the equation of the harmonic oscillator with frequency $\frac{2\pi k}{a_0}$. After substituting the above expansion in the wave equation, one obtains an infinite system of coupled second order ordinary differential equations for the functions $Q_k(t)$. This system can be solved approximately after truncations based on assumptions for smallness of some of the parameters of the physical system. This method, however, approximates the true solutions well only for small times. Law [127] found numerically growth of the photon number in the lowest resonant motions of the mirror for small times. His results were extended by Ying Wu *et al* [197].

In [128], Law proposed an exact analytic solution for $R(z)$ (2.1) for a particular 2-parameter family of motions of the boundary,

$$
a(t) = \begin{cases} a_0 \;, & t < 0 \;, \\ a_0 + \dfrac{a_0}{2\pi}\left[\arcsin\left(\sin\theta\cos\dfrac{2\pi t}{a_0}\right) - \theta\right] \;, & t \geq 0 \;, \end{cases} \tag{2.3}
$$

where θ is a parameter describing the amplitude of the mirror's motion. In this case,

$$
R(2na_0 + \zeta) = 2n + \frac{1}{2} - \frac{1}{\pi}\arctan\left(\cot\frac{\pi\zeta}{a_0} - 2n\tan\theta\right) \;, \tag{2.4}
$$

where n is an arbitrary positive integer, and $\zeta \in (-a_0, a_0]$. Using the expression for the energy density due to Fulling and Davies [76], Law found that the field in the cavity develops two wave packets which become narrower in time and whose energy grows.

12

Law's solution (2.3), (2.4) was generalized by Ying Wu et al [196], who gave an explicit solution for R for motion of the boundary given by

$$
a_m(t) = \begin{cases} a_0 \, , & t < 0 \, , \\ a_0 + \dfrac{a_0}{m\pi} \left[\arcsin \left(\sin \theta_m \cos \dfrac{m\pi t}{a_0} \right) - \theta_m \right] , & t \geq 0 \, , \end{cases}
$$

where $m = 2,\ 3,\ \ldots$, and θ_m is a parameter (related to the amplitude ε of the mirror's motion by $\tan \theta_m \approx \frac{\varepsilon m\pi}{2a_0}$). They found

$$
R_m((2n-1)a_0 + \zeta) = 2n - \frac{1}{4} + \frac{1}{m\pi} \operatorname{arccot} \left(\cot \frac{m\pi\zeta}{a_0} - 2n \tan \theta_m \right) \, .
$$

Law's solution is the particular case with $m = 2$. For $a_m(t)$, the field develops m wave packets whose width decrease and whose energy increase with time.

Cole and Schieve [28] (see also Cole's thesis [27]) proposed a method of constructing numerically the function $R(z)$ for an arbitrary wall motion with $a(t) = a_0 = \text{const}$ for $t < 0$, based on the D'Alembert solution. They found numerically that for resonant wall motions the field develops wave packets and its energy grows in time. Their procedure, however, did not allow them to make general predictions about the long-time behavior of the field and its energy.

Johnston and Sarkar [110] pointed out that, although the similarity between a constant-length cavity filled with a medium with time-varying index of refraction and an empty cavity with time-varying length seems intuitively appealing (since in both cases the optical path length changes), it needs to be studied in detail. They presented an explicit calculation for the spectral

13

distribution of generated photons in the two cases (using Moore's method [146] in the case of moving mirrors), and found serious qualitative differences. The question studied by them is interesting even in the purely classical case and certainly deserves attention.

In [111], Johnston and Sarkar developed a procedure for quantizing the field in an empty cavity with a moving mirror, different from the quantization method of Moore [146]. They introduced a new, "time-dependent", spatial variable, such that the boundaries do not move in the new coordinates, and then quantized the transformed quantities in the standard way. They showed that Moore's method is consistent with their procedure.

Dodonov and Klimov [58] studied in detail the problem of an empty cavity with a periodically vibrating wall. They adopted Moore's method and used the "instantaneous" basis (2.2), thus arriving at an infinite system of coupled second order ordinary differential equations. Then they employed the presence of two different time scales in the problem – the usual ("fast") one, related to the oscillations of the mirror, and a "slow" one, which accounts for the cumulative resonance effect. In the resonant case, for small amplitudes of the mirror's motion, they averaged over the fast oscillations to extract the slowly changing coefficients. They found that the energy of the field in the cavity increases exponentially.

Méplan and Gignoux [139] developed a method for solving the wave equation in an empty cavity with a moving mirror very similar in spirit to the method developed by us in [131]. By using the method of characteristics, they

reduced the physical problem to a two-dimensional area-preserving map and studied the iterates of this map. Let us consider one particular characteristics ("light ray") and let t_n be the time at which this characteristics reaches the stationary mirror for the nth time, and let μ_n is the "energy" of this light ray right before it reaches the stationary mirror (for more details, see the original article [139]). Using a complicated argument, they derived the map

$$\begin{aligned} \mu_{n+1} &= D((\mathrm{Id}-a)^{-1}(t_n))\,\mu_n \\ t_{n+1} &= (\mathrm{Id}+a) \circ (\mathrm{Id}-a)^{-1}(t_n) \;, \end{aligned}$$

where $D(t) = \frac{1-\dot{a}(t)}{1+\dot{a}(t)}$ is the Doppler factor at reflection at time t (cf. (2.16)). In fact, their map giving t_{n+1} as a function of t_n (the second equation in the system above) is nothing but our map F defined by (2.19). However, as we showed in [131], the dynamical properties of the physical system can be described by a one-dimensional map, which makes the description of the system much simpler.

Janovicz [104] solved the wave equation in the pulsating cavity by introducing new variables in which both mirrors are stationary, but the equation becomes much more complicated, and looked for solutions that satisfy the new equation approximately, but satisfy the boundary conditions exactly. The system of ordinary differential equations he arrived at is the same as the one analyzed in [126] and [58].

Dodonov [56] used a method similar to the one in [58] to analyze the behavior of the field in the case of a small "detuning" from the exact resonance

between the mechanical modes (the mirror) and the field modes. As we will see later, within our – purely classical – treatment, small enough detuning from resonance does not change the qualitative features of the behavior of the field in the cavity; moreover, we can find explicitly for what detuning the behavior of the field will change dramatically. Dodonov and Andreata [57] and Andreata and Dodonov [1] continued the line of research of [56] and studied in detail the packet formation in a resonantly pulsating resonator.

Ji *et al* [106] calculated the number of photons in a cavity with a wall vibrating resonantly with a small amplitude. They used the "instantaneous" basis method, after which they introduced new variables (related to the coordinate and the momentum like the creation/annihilation operators) to obtain an infinite system of coupled first order ordinary differential equations, which they solved perturbatively to first order in the amplitude of the mirror's motion.

Dalvit and Mazzitelli [40] solved (2.1) for small-amplitude motions of the wall using the renormalization-group technique for finding asymptotic expansions in singularly perturbed problems developed in [23, 24]. In agreement with the previous treatments, they found that in the case of a resonantly moving wall the energy of the field grows exponentially.

2.1.5 Ideas from Dynamical Systems

Since the method we develop in this and the following chapter relies heavily on theory of circle and torus maps, we would like to explicitly quote

the articles that have used ideas from dynamical systems to study the problem at hand.

The possibility to use the properties of iterated maps in order to explain the behavior of the field was pointed out by Cooper [32], Dittrich *et al* [54], Méplan and Gignoux [139].

Circle maps were used as a tool by Cooper and Koch [33], Gonzalez [82, 83], Dittrich *et al* [53], Yamaguchi [201, 202, 206].

2.1.6   Two Moving Mirrors

Our approach can be easily generalized to the case of two periodically moving mirrors. In Section 2.6.5, we explain how to reduce the problem in this case either to a circle map, or to a map of the 2-torus, depending on whether the frequencies of the motion of the two mirrors are commensurate (i.e., rationally related) or not.

The case of two moving mirrors has been studied – without resort to dynamical systems – by Dalvit and Mazzitelli [41], Ji *et al* [107].

2.1.7   More than One Spatial Dimension

In the case of more than one spatial dimension, the problem of electromagnetic waves reflected off moving obstacles is much more complicated. The main difficulty is that the rays do not simply bounce back and forth between the obstacles as in the case of one spatial dimension, but may diverge and leave the domain between the moving obstacles. Therefore, one has to impose

conditions on the geometry of the problem that guarantee the existence of rays "trapped" between the obstacles. These rays undergo multiple reflections, and their energy may grow exponentially. Since this goes beyond the scope of the present dissertation, we will not discuss it further, and will just mention the papers of Cooper and Strauss [34, 35], Popov and Rangelov [164].

In the physics literature, waves in a changing domain in more than one spatial dimension are studied from different points of view by Dodonov and Klimov [58], Ji *et al* [108], Colanero and Chu [26], Mkrtchian and v. Baltz [145], Crocce *et al* [37], Yamaguchi [203].

Mundarain and Maia Neto [152] calculated the photon generation in the nonrelativistic approximation for the more realistic case of two plane parallel perfectly reflecting mirrors the field between which can be polarized in an arbitrary direction.

2.1.8   Interaction with the Boundary

Although we have not studied the effect of the radiation pressure on the motion of the boundary, we would like to point out that this problem has been studied by Law [126]; see also Cole and Schieve [29] and the references therein.

2.1.9   Other Applications of Circle Maps

Thomas Kwok-keung Au and Xiao-Song Lin [6] used circle maps to study caustics in off-center reflections in a mirrored circle, using symplectic

18

topology as a tool. Their results might be useful in the semiclassical treatment of the short-wavelength modes in two-dimensional optical cavities (see, e.g., Nöckel and Chang [155] and the references therein).

Yamaguchi [203] studied the wave equation in spherically symmetric domain with periodically pulsating boundaries.

2.1.10   Fermi Acceleration

The problem of the behavior of the electromagnetic field between two parallel perfectly reflecting mirrors is different from the so-called Fermi acceleration ([73]; see also Chapter 3.4 of the book by Lichtenberg and Lieberman [129]). Fermi proposed the growth of the speed of a particle bouncing elastically between two parallel planes (in the absence of any other forces) as a mechanism for acceleration of particles in the cosmic rays. Another model with similar dynamical features is that of a particle moving in a vertical direction in a homogeneous gravity field and bouncing off a horizontal plate oscillating periodically up and down. In Appendix A, we showed the derivation of the (full) map describing Fermi acceleration.

Although sometimes it is said that the problem of the wave equation in a periodically pulsating domain is a "string" analogue of the Fermi accelerator [54], it turns out – somewhat surprisingly – that the dynamics of the former is described by a one-dimensional map, while for the latter one needs to use a two-dimensional map whose behavior is much more complicated.

Ulam [188] considered Fermi acceleration as a model for studying the

approach to statistical equilibrium.

Zharnitsky [210] used reparametrization of the temporal variable to "stop the walls" of the Fermi accelerator, i.e., to reduce the problem to the study of an equivalent system of a particle moving in a time-dependent quadratic potential between two stationary walls.

Fermi acceleration has been studied with dynamical systems tools by Pustyl'nikov [166] Douady [62], Dovbysh [63] Krüger *et al* [117], Zharnitsky [211, 212].

The generalization of Fermi acceleration to two spatial dimensions (i.e., to the problem of a motion of a ball bouncing elastically off the walls of a time-dependent billiard) have been studied by and Koiller *et al* [115] and Oliffson Kamphorst and Pinto de Carvalho [156].

2.1.11 Experimental Aspects

Smith [181] and Henneberger and Schulte [93] have found experimentally the formation of short laser pulses in a laser with a moving mirror.

We note that the experimental situation does not necessarily require that there be a physically moving mirror. One experimental possibility – among others – would be to have a material that is a good conductor or not, depending on whether a magnetic field of sufficient intensity is applied to it, and then have a magnetic field applied to it in a changing region. This induces reflecting boundaries that are moving with time. Note that the boundaries of this region could move even faster than the speed of light, hence the study of

mirrors moving at a speed comparable to the speed of light is not unphysical (even if in that case one would also have to discuss corrections to the boundary conditions depending on the details of the experimental realizations).

2.2   Plan of the Exposition

The plan of this chapter is the following. In Section 2.3 we give a description of the physical system and show how the physical problem can be formulated in terms of circle maps. Section 2.4 contains a brief exposition of the necessary facts from the theory of circle maps, and in Section 2.5 these facts are applied to the problem at hand and illustrated numerically. Section 2.6 is devoted to several topics related to the physical problem and its mathematical treatment: the role of the correct boundary conditions, the problem of finding the motion of the mirror from the circle map, remarks about the universality class of circle maps associated with pulsating resonators and about the quantum treatment of the problem within our approach, details on the case of two moving mirrors, and a discussion of the appearance of Schwarzian derivative in the quantum treatment of the problem.

2.3   Physical Setting

2.3.1   Description of the System

We consider a one-dimensional optical resonator consisting of two parallel perfectly reflecting mirrors. For simplicity of notation, we consider only the situation in which one of them is at rest at the origin of the x axis while
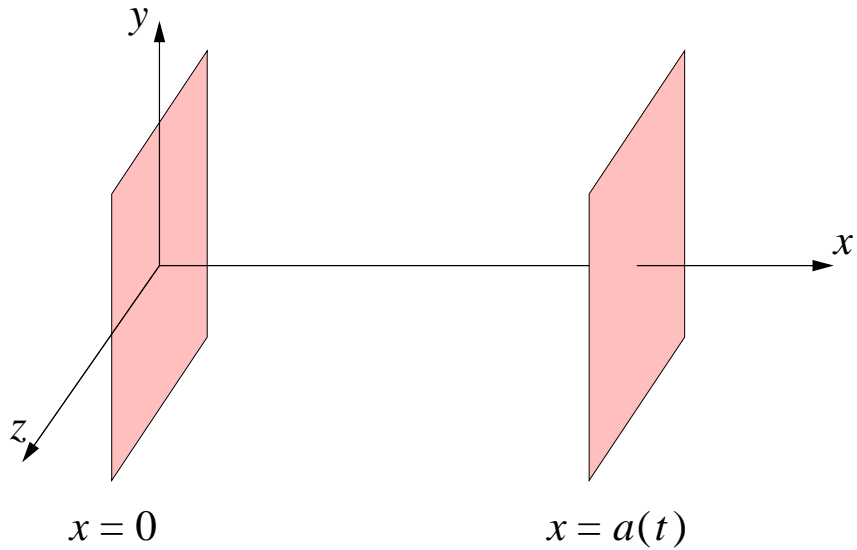
Figure 2.1: The pulsating resonator.

the other one is moving periodically with period T – See Figure 2.1. The case where the two mirrors are moving periodically with a common period can be treated in a similar manner. We assume that the resonator is empty, so that the speed of the electromagnetic waves in it is equal to the speed of light, c. The speed of the moving mirror cannot exceed c (see, however, Section 2.1.11).

We use dimensionless time t and length ℓ connected with the physical (i.e., dimensional) time t_{phys} and length ℓ_{phys} by $t := t_{\text{phys}}/T$, $\ell := \ell_{\text{phys}}/(cT)$.

Let the coordinate of the moving mirror be $x = a(t)$, where a is a C^k function ($k = 1, \ldots, \infty, \omega$) satisfying the conditions

$$a(t) > 0 , \qquad |a'(t)| < 1 , \qquad a(t+1) = a(t) . \tag{2.5}$$

The meaning of the first condition is that the cavity does not collapse, the second one means that the speed of the moving mirror cannot exceed the

22

speed of light, and the third one is that the mirror's motion is periodic of period 1. An example which we will use for numerical illustrations is

$$a(t) = \frac{\alpha}{2} + \beta \sin 2\pi t \qquad \left(|\beta| < \frac{1}{2\pi} \, , \quad 0 < |\beta| < \frac{\alpha}{2} \right) . \tag{2.6}$$

Since there are no charges and no currents, we impose Coulomb gauge conditions

$$A_0 = 0 \, , \qquad \nabla \cdot \mathbf{A} = 0$$

on the 4-potential $A^\mu = (A^0, \mathbf{A})$ (Jackson [101, Section 6.5]) and obtain that $\mathbf{A}$ satisfies the homogeneous wave equation. We consider plane waves traveling in x-direction, so that without loss of generality, we assume that

$$\mathbf{A}(t, x) = A(t, x) \, \mathbf{e}_y \, ,$$

therefore

$$\begin{aligned}
\mathbf{E}(t, x) &= -\nabla A_0 - \frac{\partial \mathbf{A}}{\partial t} &&= -\, A_t(t, x) \, \mathbf{e}_y \\
\mathbf{B}(t, x) &= \nabla \times \mathbf{A} &&= A_x(t, x) \, \mathbf{e}_z
\end{aligned} \tag{2.7}$$

(the subscripts of A always denote the corresponding derivatives). The vector potential $A(t, x)$ must satisfy the homogeneous one-dimensional wave equation,

$$A_{tt}(t, x) - A_{xx}(t, x) = 0 \, , \tag{2.8}$$

in the domain $\Sigma := \{(t, x) \in \mathbb{R}^2 \,|\, t_0 < t, \; 0 < x < a(t)\}$. It will also need to satisfy some boundary conditions that will be specified in Section 2.3.2, and appropriate initial conditions,

$$A(t_0, x) = \psi_1(x) \, , \qquad A_t(t_0, x) = \psi_2(x) \, . \tag{2.9}$$

2.3.2　Method of Characteristics

Before discussing the boundary conditions and the method of solving the boundary-value problem in the domain Σ, let us discuss the way of solving (2.8) in the absence of spatial boundaries, i.e., in the domain $\{t_0 < t, \ x \in \mathbb{R}\}$. It is well-known that in this case, the solution of the problem (2.8), (2.9) at some particular space-time point (t, x) can be written as

$$A(t, x) = \Psi^-(x_0^-) + \Psi^+(x_0^+) \ , \tag{2.10}$$

where $x_0^\pm := x \pm (t - t_0)$, and Ψ^- and Ψ^+ are functions of one variable that are selected to match the initial conditions (2.9). The explicit expressions for $\Psi^\pm$ follow from the D'Alembert's formula

$$\Psi^\pm(s) = \frac{1}{2} \left[\psi_1(s) \pm \int_\kappa^s \psi_2(s') \, ds' \right] \ , \tag{2.11}$$

where κ is an arbitrary constant (the same for Ψ^+ and Ψ^-).

The representation (2.10) has a simple geometrical meaning: the value of $A(t, x)$ is a superposition of two functions, $\Psi^-(x_0^-)$ and $\Psi^+(x_0^+)$, the former being constant along the lines $\{x - t = \mathrm{const}\}$, and the latter being constant along $\{x + t = \mathrm{const}\}$. The disturbances at a space-time point (T, X) propagate in the space-time diagram along the lines $\{x - t = X - T\}$ and $\{x + t = X + T\}$ emanating from this point (in more physical terms, this corresponds to two rays moving to the right and to the left at unit speed); these lines are called *characteristics*, and the method of solving (2.8), (2.9) by using the representation (2.10) is called the *method of characteristics* (see, e.g., the books by John [109] or Garabedian [78]).

2.3.3 Boundary Condition at the Moving Mirror

To obtain the boundary conditions at the stationary mirror, we note that the electric field, i.e., the temporal derivative of the vector potential, must vanish at this mirror, which yields the following "perfect reflection" boundary condition:

$$A_t(t,0) = 0 \ . \tag{2.12}$$

The boundary condition at the moving mirror can be easily obtained by performing a Lorenz transformation from the laboratory frame K to the inertial frame $\tilde{K}$ comoving with the moving mirror at some particular moment t. The temporal and spatial coordinates in K, t and x, are related to the ones in $\tilde{K}$, $\tilde{t}$ and $\tilde{x}$, by

$$
\begin{aligned}
t - t_0 &= \tilde{t}\cosh\zeta + \tilde{x}\sinh\zeta \\
x - a(t_0) &= \tilde{t}\sinh\zeta + \tilde{t}\cosh\zeta \ ,
\end{aligned}
\tag{2.13}
$$

where $\tanh\zeta = a'(t)$. In the comoving frame, the boundary condition is $\widetilde{A}_{\tilde{t}}(0,0) = 0$, which, together with (2.13), yields

$$\sqrt{1 - a'(t)^2}\, \widetilde{A}_{\tilde{t}}(0,0) = A_t(t,a(t)) + a'(t)\, A_x(t,a(t)) = 0 \ , \tag{2.14}$$

Note that (2.14) means that the derivative of A tangent to the spatial boundaries of the domain Σ vanishes.

Let us mention that the homogeneous Dirichlet boundary conditions, $A(t,0) = A(t,a(t)) = 0$, are a particular case of (2.12), (2.12). Thus, all

25

conclusions made by using (2.12), (2.12) will hold for the Dirichlet case. The homogeneous Neumann boundary conditions, $A_x(t,0) = A_x(t,a(t)) = 0$, however, yield a drastically different behavior – see Section 2.6.1.

2.3.4 Doppler Shift at Reflection

The method of characteristics developed in (2.10) and (2.11) for situations with no boundaries can be adapted to provide rather explicit solutions for systems in spatially bounded space-time domains satisfying (2.14) at the boundaries (see, e.g., the book by Weinberger [193, Chapter I]).

The prescription is the following. The solution of the boundary value problem (2.8), (2.9), (2.12), (2.14) in the domain Σ is a superposition of two functions that are constant on the straight pieces of the characteristics and change their sign at each reflection. To find $A(t,x)$, one has to consider the two characteristics, γ^- and γ^+, passing through (t,x), and propagate them backwards in time (according to the rule that, upon reaching a mirror, they change direction of propagation) until they reach the line $\{\text{time} = t_0\}$ at the points (t_0, x_0^-) and (t_0, x_0^+), resp. – see Figure 2.2. Then $A(t,x)$ is given by

$$A(t,x) = (-1)^{N_-} \Psi^-(x_0^-) + (-1)^{N_+} \Psi^+(x_0^+) , \qquad (2.15)$$

where $N_\mp$ are the number of reflections of $\gamma^\mp$ on the way back from (t,x) to $(t_0, x_0^\mp)$. In Section 2.3.5 we will give explicit formulae for $x_0^\mp$ and $A(t,x)$ in terms in circle maps.

Indeed, because the solution (2.15) is the sum of two functions constant

along the straight pieces of the characteristics, the wave equation is satisfied in the interior. Also, the initial conditions are easily verified because for $t - t_0$ small, x_0^- and x_0^+ are close to x [see (2.22)].

To check that this prescription also satisfies the boundary conditions, we need another argument. Consider the space-time diagram of the reflection of the field between two infinitesimally close characteristics reflected by the moving mirror at time θ, shown in Figure 2.3. The world line of the mirror is denoted by m, the angle δ between it and the time direction is connected with the mirror's velocity at reflection by $\tan \delta = a'(\theta)$. The Doppler factor at reflection, $D(\theta)$, is defined as the ratio of the spatial distances Δ and Δ' between the characteristics before and after reflection:

$$D(\theta) := \frac{\Delta}{\Delta'} = \tan\left(\frac{\pi}{4} - \delta\right) = \frac{1 - \tan \delta}{1 + \tan \delta} = \frac{1 - a'(\theta)}{1 + a'(\theta)} \ . \tag{2.16}$$

Thus, the absolute values of the temporal and spatial derivatives of the field increase by a factor of $D(\theta)$ after reflection. This implies that if in the space-time domain between the two characteristics, the values of the corresponding derivatives of the field before reflection are denoted by A_t and A_x, then after reflection they will become $-D(\theta)\mathsf{A}_t$ and $D(\theta)\mathsf{A}_x$, resp. Hence, in the space-time domain of the overlap the derivatives of the field will be

$$
\begin{aligned}
A_t(\theta, a(\theta)) &= \mathsf{A}_t - D(\theta)\mathsf{A}_t \\
A_x(\theta, a(\theta)) &= \mathsf{A}_x + D(\theta)\mathsf{A}_x \ .
\end{aligned}
\tag{2.17}
$$

Now, we will show that the modified method of characteristics is consistent with the boundary condition (2.14). We note that $\mathsf{A}_t = -\mathsf{A}_x$, which simply

27
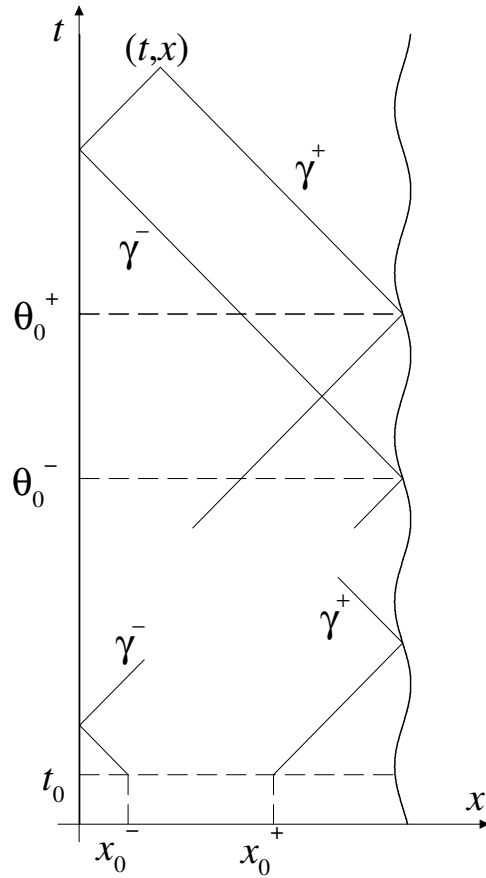
Figure 2.2: Finding $A(t, x)$ by the method of characteristics.

means that before reflection the rays are moving to the right at unit speed. If we multiply the second equation of (2.17) by

$$a'(\theta) = \frac{1 - D(\theta)}{1 + D(\theta)}$$

[which follows from (2.16)] and add it to the first, we obtain exactly the boundary condition (2.14).

The same prescription gives a solution of the Dirichlet problem $A(t, 0) =$
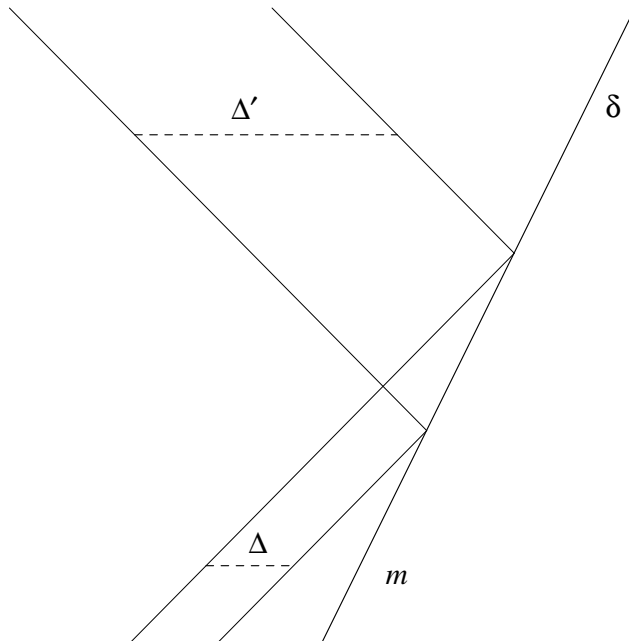
Figure 2.3: Reflection by the moving mirror.

$A(t, a(t)) = 0$. Similar methods can be developed for other boundary conditions. Unfortunately for the widely considered Neumann boundary conditions the representation by reflected characteristics is not straightforward when $a'(t) \neq 0$ – for details see Section 2.6.1 and our paper [190].

We note that the method of characteristics also yields information in the important case when the medium is inhomogeneous and perhaps time dependent. This is a physically natural problem since in many applications we have cavities filled with optically active media whose characteristics are changed by external perturbations. In this case, the method of characteristics does not yield an exact solution as above but rather, it is the main ingredient of an iterative procedure [78]. Physically, what happens is that in inhomoge-

neous media, the waves change shape while propagating in contrast with the propagation without change in shape in homogeneous media (2.10).

2.3.5   Using Circle Maps to Solve the Boundary Value Problem

We now reformulate the method of characteristics into a problem of circle maps.

We consider a particular characteristic and denote by $\{\tau_n\}$ the times at which it reaches the stationary mirror and $\{\theta_n\}$ the times at which it reaches the oscillating one; let $\ldots < \tau_n < \theta_n < \tau_{n+1} < \theta_{n+1} < \ldots$. Note that, with this notation,

$$\tau_n \;=\; \theta_n - a(\theta_n) = (\mathrm{Id} - a)(\theta_n)$$

$$(2.18)$$

$$\tau_{n+1} \;=\; \theta_n + a(\theta_n) = (\mathrm{Id} + a)(\theta_n) \;.$$

Therefore

$$\tau_{n+1} \;=\; (\mathrm{Id} + a) \circ (\mathrm{Id} - a)^{-1}(\tau_n) =: F(\tau_n)$$

$$(2.19)$$

$$\theta_{n+1} \;=\; (\mathrm{Id} - a)^{-1} \circ (\mathrm{Id} + a)(\theta_n) =: G(\theta_n) \;.$$

We refer to F and G as the time advance maps. They allow to compute the time of reflection on one side in terms of the time of the previous reflection on the same side. The conditions (2.5) on the range of a and a' guarantee that $(\mathrm{Id} - a)$ is invertible and that F and G are C^k (by the implicit function theorem).

30

When the function a is 1-periodic, F and G satisfy

$$F(t+1) = F(t) + 1 , \qquad G(t+1) = G(t) + 1 . \tag{2.20}$$

These relations mean that $F(t)$ and $G(t)$ depend only on the fractional part of t. In physical terms, we characterize a reflection of a ray by the *phase* of the oscillating mirror when the impact takes place, i.e., by the time of reflection modulo 1; if we know the phase at one reflection, we can compute the phase at the next impact. Mathematically, this means that F and G can be regarded as lifts of maps from $\mathbb{T} \equiv \mathbb{R}/\mathbb{Z}$ to $\mathbb{T}$ (see Section 2.4).

We want to argue that the study of the dynamics of the circle maps (2.19) leads to important conclusions for the physical problem, which we will take up after we collect some information about the mathematical theory of circle maps. In particular, many results in the mathematical literature are directly relevant for physical applications. This is natural because the long term behavior of the solution can be obtained by repeated application of the time advance maps [see (2.23)].

We call attention to the fact that

$$G = (\mathrm{Id} + a)^{-1} \circ F \circ (\mathrm{Id} + a) = (\mathrm{Id} - a)^{-1} \circ F \circ (\mathrm{Id} - a) , \tag{2.21}$$

so that

$$G^n = (\mathrm{Id} + a)^{-1} \circ F^n \circ (\mathrm{Id} + a) = (\mathrm{Id} - a)^{-1} \circ F^n \circ (\mathrm{Id} - a) .$$

In dynamical systems theory this is usually described as saying that the maps F and G are "conjugate" (see Section 2.4.4). In our situation, this comes from

the fact that F and G are physically equivalent descriptions of the relative phase of different successive reflections: F advances the τ variables while G advances the θ's, and the θ's are related to the τ's by (2.18).

Now, we use circle maps to derive an explicit formula for the solution of the boundary-value problem (2.8), (2.9), (2.12), (2.14) in the domain Σ. Let us trace back in time the characteristics γ^- and γ^+ coming "from the past" to the space-time point (t, x) – see Figure 2.2. Let $\theta_0^\pm := (\mathrm{Id} + a)^{-1}(t \pm x)$ be the last moments the characteristics $\gamma^\pm$ are reflected by the moving mirror, and let $\theta_{-k}^\pm := G^{-k}(\theta_0^\pm)$. After N_+, resp. N_-, reflections on the way backwards in time (out of which n_+, resp. n_-, are from the moving mirror), the characteristic γ^+, resp. γ^-, crosses the line $\{\mathrm{time} = t_0\}$. The spatial coordinate of the intersection of $\gamma^\pm$ and $\{\mathrm{time} = t_0\}$ can be easily seen to be

$$x_0^\pm = h(\theta_{-n_\pm}^\pm, t_0) := \left| (\mathrm{Id} - a)(\theta_{-n_\pm}^\pm) - t_0 \right| . \tag{2.22}$$

Thus, the formula for the vector potential is

$$\begin{aligned} A(t, x) &= (-1)^{N_-} \Psi^- \circ h\left(G^{-n_-} \circ (\mathrm{Id} + a)^{-1}(t - x), t_0 \right) \\ &\quad + (-1)^{N_+} \Psi^+ \circ h\left(G^{-n_+} \circ (\mathrm{Id} + a)^{-1}(t + x), t_0 \right) . \end{aligned} \tag{2.23}$$

If $\psi_1 \in C^2$, $\psi_2 \in C^1$, $a \in C^2$, then (2.22), (2.23) is a classical solution (i.e., the second partial derivatives exist in the classical sense) and it satisfies (2.8), (2.9), (2.12), (2.14).

Even if ψ_1, ψ_2 and a are less regular, (2.22), (2.23) can be shown to be a solution of (2.8) in the sense of distributions. Provided that ψ_1 and ψ_2

are continuous, (2.9) will be satisfied. Provided that $a \in C^1$, the argument presented above shows that (2.12), (2.14) are satisfied.

Remark 2.3.1. The argument we used to derive (2.11) also shows that, when $a \in C^1$, $\psi_1 \in C^1$, $\psi_2 \in C^0$ in (2.11), this is the only weak solution in the space of distributions. To that effect note that, in the coordinates $\xi = x + t$, $\eta = x - t$, equation (2.8) reads

$$\partial_\xi \partial_\eta A = 0. \tag{2.24}$$

The only distribution weak solutions of this equation are

$$A(\xi, \eta) = \Phi_1(\xi) + \Phi_2(\eta) \tag{2.25}$$

with Φ_1 and Φ_2 distributions.

The argument leading to (2.23) shows that the only distributions of the form (2.25) which satisfy the initial and the boundary conditions are precisely 2.23.

Of course, when $a \in C^2$, $\psi_1 \in C^2$, $\psi_2 \in C^1$, the solution is the only classical solution.

Even if the above argument is quite satisfactory in the case of constant coefficients, when the speed of light depends on the position or on the time, the uniqueness theory is more complicated since the equation does not reduce to the simple from (2.24) and one has to use energy methods etc. [193, Section II.7].

33

2.3.6   Energy of the Electromagnetic Field

The method of characteristics gives a very illuminating picture of the mechanism of the change of the field energy,

$$E(t) = \int_0^{a(t)} \mathfrak{T}^{00}(t, x) = \frac{1}{8\pi} \int_0^{a(t)} \left[A_t(t, x)^2 + A_x(t, x)^2 \right] \, dx \; , \qquad (2.26)$$

due to the distortion of the wave at reflection from the moving mirror. Indeed, consider the change of the energy of a very narrow wave packet at reflection from the moving mirror at time θ. Since at reflection the temporal and the spatial distances decrease by a factor of $D(\theta)$, $|A_t|$ and $|A_x|$ will increase by a factor of $D(\theta)$. Therefore, the integrand of the energy integral will increase $D(\theta)^2$ times, while the support of the integrand (i.e., the spatial width of the wave packet at time t) will shrink by a factor of $D(\theta)$. Hence, the energy of the wave packet after reflection will be $D(\theta)$ times greater than its energy before reflection.

In the general case, one can use (2.23) and obtain the energy of the system at time t. For the sake of simplicity, we will give the formula only under the assumption that at time t all the rays are going to the right, i.e., assuming that the vector potential is of the form $A(t, x) = (-1)^{N_-} \Psi^-(x_0^-)$. Let us introduce the "local Doppler factor"

$$D(t_0, x_0^-; t) := \left| \frac{\partial}{\partial t} h(\theta_{n_-}^-, t_0) \right| = \frac{1 - a'(\theta_{-n_-}^-)}{1 + a'(\theta_0^-)} \, (G^{-n_-})'(\theta_0^-) \; . \qquad (2.27)$$

It has the physical meaning of the ratio of the frequencies of the incident wave and the wave at time t [cf. (2.16)]. Note that $D(t_0, x_0^-; t)$ is equal to the

34

derivative of G^{-n_-} multiplied by a factor which is bounded and bounded away from 0 independently of n_- [due to the fact that $|a'(t)| < 1$]. From (2.23) and (2.22) we obtain that the square of $D(t_0, x_0^-; t)$ is the ratio of the energy density $\mathfrak{T}^{00}(t, x)$ and the initial energy density, $\mathfrak{T}^{00}(t_0, x_0^-)$:

$$\mathfrak{T}^{00}(t, x) = 2 \left|(\Psi^-)'(x_0^-)\right|^2 D(t_0, x_0^-; t)^2 = \mathfrak{T}^{00}(t_0, x_0^-) D(t_0, x_0^-; t)^2 .$$

On the other hand, $D(t_0, x_0^-; t)$ is connected with the Jacobian of the change of coordinates $x_0^- \mapsto x$ by

$$\left|\frac{\partial x}{\partial x_0^-}\right| = \left|\frac{\partial x_0^-}{\partial x}\right|^{-1} = D(t_0, x_0^-; t)^{-1} .$$

Hence, the energy of the system at time t is

$$E(t) = \int_0^{a(t)} \mathfrak{T}^{00}(t_0, x_0^-) D(t_0, x_0^-; t) \, dx_0^- . \tag{2.28}$$

Note that since the local Doppler factor squared is the ratio of the energy densities at two consecutive reflection points, then it satisfies the following multiplicative property. Let (t_1, x_1^-), (t_2, x_2^-), ..., (t_k, x_k^-) be space-time points on the characteristic connecting (t_0, x_0^-) and (t, x), such that at all of them the rays are going to the right, and let $t_0 < t_1 < \ldots < t_k < t$. Then

$$D(t_0, x_0^-; t) = D(t_0, x_0^-; t_1) D(t_1, x_1^-; t_2) \cdots D(t_{k-1}, x_{k-1}^-; t_k) D(t_k, x_k^-; t) .$$

As can be seen from (2.27), these multiplicative properties are closely related to the chain rule for diffeomorphisms,

$$(G^n)'(\theta) = G'(G^{n-1}(\theta)) G'(G^{n-2}(\theta)) \cdots G'(\theta) . \tag{2.29}$$

35

The mathematical theory of dynamical systems contains many results about derivatives of highly iterated maps as above (2.29). In Section 2.5.3 we will be able to translate some of them into asymptotic properties of the field energy.

A simple and intuitively clear formula for the rate of change of the field energy can be obtained by using (2.26), (2.8), (2.12), (2.14), and integrating by parts:

$$
\begin{aligned}
E'(t) &= -a'(t)\frac{1}{8\pi}\left[\frac{A_x(t,a(t)) + a'(t)\,A_t(t,a(t))}{\sqrt{1 - a'(t)^2}}\right]^2 \\
&= -a'(t)\frac{1}{8\pi}\widetilde{A}_{\tilde{x}}(0,0)^2 = -a'(t)\,\widetilde{\mathfrak{T}}^{11}(0,0) \\
&= -a'(t)\,\tilde{p}_{\mathrm{rad}}(\tilde{t} = 0) = -a'(t)\,p_{\mathrm{rad}}(t)\ ,
\end{aligned}
$$

where $\tilde{p}_{\mathrm{rad}}(\tilde{t} = 0) = \widetilde{\mathfrak{T}}^{11}(0,0)$ is the radiation pressure in $\tilde{K}$, and we have used the fact that the pressure is relativistic invariant (see the book by Pauli [159, Section 45]). This fact and (2.17) yield

$$
p_{\mathrm{rad}}(t) = 2\,\frac{1 - a'(t)}{1 + a'(t)}\frac{\mathsf{A}_x^2}{4\pi}\ .
$$

It is worth noting that the expression for the radiation pressure has been derived from the postulates of special relativity by Einstein in his famous first paper on the subject [67] (English translation: [136, pp. 35–65]). See also the book by Miller [143, Chapter 11] and Pauli [159, Section 32].

2.4   Maps of the Circle

In this section, we recall some facts from the theory of the dynamics of the orientation preserving homeomorphisms (OPHs) and diffeomorphisms (OPDs) of the circle $\mathbb{T}$, following the books by Katok and Hasselblatt [112, Chapter 11, 12], de Melo and van Strien [48], and Herman [94]. This is a very rich theory and we will only recall the facts that we will need in the physical application.

2.4.1   Circle Maps – Terminology and Notations

We identify $\mathbb{T}$ with the quotient $\mathbb{R}/\mathbb{Z}$ and use the universal covering projection

$$\pi : \mathbb{R} \to \mathbb{T} := \mathbb{R}/\mathbb{Z} : x \mapsto \pi(x) := x \,(\mathrm{mod}\,1) \ .$$

Another way of thinking about $\mathbb{T}$ is identifying it with the unit circle in $\mathbb{C}$ using the universal covering projection $x \mapsto e^{2\pi i x}$.

Let $f : \mathbb{T} \to \mathbb{T}$ be an OPH and $F : \mathbb{R} \to \mathbb{R}$ be its *lift* to $\mathbb{R}$, i.e., a map satisfying $f \circ \pi = \pi \circ F$. The fact that f is an OPH implies that $F(x+1) = F(x)+1$ for each $x \in \mathbb{R}$, which is equivalent to saying that $F - \mathrm{Id}$ is 1-periodic. The lift F of f is unique up to an additive integer constant. If a point $x \in \mathbb{T}$ is q-periodic, i.e., $f^q(x) = x$, then $F^q(x) = x + p$ for some $p \in \mathbb{N}$.

2.4.2   Rotation Number

A very important number to associate to a map of the circle is its rotation number, introduced by Poincaré. It is a measure of the average amount

of rotation of a point along an orbit.

Definition 2.4.1. Let $f : \mathbb{T} \to \mathbb{T}$ be an orientation preserving homeomorphism and $F : \mathbb{R} \to \mathbb{R}$ a lift of f. Define

$$\tau_0(F) := \lim_{n \to \infty} \frac{F^n(x) - x}{n} \ , \qquad \tau(f) := \tau_0(F) \, (\mathrm{mod} \, 1) \qquad (2.30)$$

and call $\tau(f)$ a *rotation number* of f.

It was proved by Poincaré that the limit in (2.30) exists and is independent of x. Hence, $\tau(f)$ is well defined.

The rotation number is a very important tool in classifying the possible types of behavior of the iterates of the OPHs of $\mathbb{T}$. The simplest example of an OPH of $\mathbb{T}$ is the *rotation* by α on $\mathbb{T} \equiv \mathbb{R}/\mathbb{Z}$, $r_\alpha : x \mapsto x + \alpha \, (\mathrm{mod} \, 1)$ (corresponding to a rotation by $2\pi\alpha$ radians on $\mathbb{T}$ thought of as the unit circle in $\mathbb{C}$). The map $R_\alpha : x \mapsto x + \alpha$ is a lift of r_α, and $\tau(r_\alpha) = \alpha \, (\mathrm{mod} \, 1)$. In the case of r_α there are two possibilities:

(a) If $\tau(r_\alpha) = p/q \in \mathbb{Q}$, then $R_{p/q}^q(x) = x + p$ for each $x \in \mathbb{R}$, so every point in $\mathbb{T}$ is q-periodic for $r_{p/q}$. If p and q are relatively prime, q is the minimal period.

(b) If $\tau(r_\alpha) \notin \mathbb{Q}$, then r_α has no periodic points; every point in $\mathbb{T}$ has a dense orbit. Thus, the α- and ω-limit sets of any point $x \in \mathbb{T}$ are the whole $\mathbb{T}$, which is usually described as saying that $\mathbb{T}$ is a *minimal set* for r_α. [Recall that $\alpha(x)$ is the set of the points at which the orbit of x

38

accumulates in the past, and $\omega(x)$ those points where it accumulates in the future.]

2.4.3 Types of Orbits of OPHs of the Circle

To classify the possible orbits of OPHs of the circle, we need the following definition (for the particular case $f : \mathbb{T} \to \mathbb{T}$).

Definition 2.4.2. (a) On orbit $\mathcal{O}$ of f is called *homoclinic* to an invariant set $T \in \mathbb{T} \setminus \mathcal{O}$ if $\alpha(x) = \omega(x) = T$ for any $x \in \mathcal{O}$.

(b) An orbit $\mathcal{O}$ of f is said to be *heteroclinic* to two disjoint invariant sets T_1 and T_2 if $\mathcal{O}$ is disjoint from each of them and $\alpha(x) = T_1$, $\omega(x) = T_2$ for any $x \in \mathcal{O}$.

With this definition, the possible types of orbits of circle OPHs were classified by Poincaré [162] as follows (for a modern pedagogical treatment see, e.g., [112, Section 11.2]):

(1) For $\tau(f) = p/q \in \mathbb{Q}$, all orbits of f are of the following types:

   (a) a periodic orbit with the same period as the rotation $r_{p/q}$ and ordered in the same way as an orbit of $r_{p/q}$;

   (b) an orbit homoclinic to the periodic orbit if there is only one periodic orbit;

   (c) an orbit heteroclinic to two different periodic orbits if there are two or more periodic orbits.

39

(2) When $\tau(f) \notin \mathbb{Q}$, the possible types of orbits are:

    (a) an orbit dense in $\mathbb{T}$ that is ordered in the same way as an orbit of $r_{\tau(f)}$ (as are the two following cases);

    (b) an orbit dense in a Cantor set;

    (c) an orbit homoclinic to a Cantor set.

We also note that in cases 2(b) and 2(c), the Cantor set that has a dense orbit is unique and can be obtained as the set of accumulation points of any orbit.

2.4.4   Conjugacies; Poincaré and Denjoy Theorems

Because of the simplicity of the rotations it is natural to ask whether a particular OPH of $\mathbb{T}$ is equivalent in some sense to a rotation. To state the results, we give a precise definition of "equivalence" and the important concept of topological transitivity.

Definition 2.4.3. Let $f : M \to M$ and $g : N \to N$ be C^m maps, $m \geq 0$.

    (a) The maps f and g are *topologically conjugate* if there exists a homeomorphism $h : M \to N$ such that $f = h^{-1} \circ g \circ h$.

    (b) The map g is a *topological factor* of f (or f is *semiconjugate* to g) if there exists a surjective continuous map $h : M \to N$ such that $h \circ f = g \circ h$; the map h is called a *semiconjugacy*.

(c) A map $f : M \rightarrow M$ is *topologically transitive* provided the orbit, $\{f^k(x)\}_{k \in \mathbb{Z}}$, of some point x is dense in M.

The meaning of the conjugacy is that g becomes f under a change of variables, so that from the point of coordinate independent physical quantities, f and g are equivalent. The meaning of the semiconjugacy is that, embedded in the dynamics of f, we can find the dynamics of g.

The following theorem of Poincaré [162] was the first theorem classifying circle maps.

Theorem 2.4.1 (Poincaré Classification Theorem). *Let $f : \mathbb{T} \rightarrow \mathbb{T}$ be an OPH with irrational rotation number. Then:*

(a) if f is topologically transitive, then f is topologically conjugate to the rotation $r_{\tau(f)}$;

(b) if f is not topologically transitive, then there exists a non-invertible continuous monotone map $h : \mathbb{T} \rightarrow \mathbb{T}$ such that $h \circ f = r_{\tau(f)} \circ h$; in other words, f is semiconjugate to the rotation $r_{\tau(f)}$.

If we restrict ourselves to considering not OPHs, but OPDs of the circle, we can say more about the conjugacy problem. An important result in this direction is the theorem of Denjoy [50].

Theorem 2.4.2 (Denjoy Theorem). *A C^1 OPD of S^1 with irrational rotation number and derivative of bounded variation is topologically transitive and*

41

hence (according to Poincaré theorem) topologically conjugate to a rotation. In particular, every C^2 OPD $f : \mathbb{T} \to \mathbb{T}$ is topologically conjugate to $r_{\tau(f)}$.

We note that this condition is sharp. For every $\varepsilon > 0$ there are $C^{2-\varepsilon}$ maps (see the definition later) with irrational rotation number, semiconjugate but not conjugate to a rotation (see [94, Section X.3.19]).

2.4.5 Smoothness of the Conjugacy

So far we have discussed only conditions for existence of a conjugacy h to a rotation, requiring h to be only a homeomorphism. Can anything more be said about the differentiability properties of h in the case of smooth or analytic maps of the circle? As we will see later, this is a physically important question since physical quantities such as energy density depend on the smoothness of the conjugacy. To answer this question precisely, we need two definitions.

Definition 2.4.4. A number ρ is called *Diophantine* of type (K, ν) (or simply of type ν) for $K > 0$ and $\nu \geq 1$, if

$$\left| \rho - \frac{p}{q} \right| > \frac{K}{|q|^{1+\nu}}$$

for all $\frac{p}{q} \in \mathbb{Q}$. The number ρ is called *Diophantine* if it is Diophantine for some $K > 0$ and $\nu \geq 1$. A number which is not Diophantine is called a *Liouville number*.

One can understand Diophantine numbers as "very irrational" numbers. If one wants to approximate them well by rational p/q, one needs to pay

by taking the denominator be large. It can be proved that for $K \to 0$, the set of all Diophantine numbers of type (K, ν) has Lebesgue measure as close to full as desired.

Definition 2.4.5. A function f is said to be $C^{m-\delta}$ where $m \geq 1$ is an integer and $\delta \in (0, 1)$, if it is C^{m-1} and its $(m-1)$st derivative is $(1-\delta)$-Hölder continuous, i.e.,

$$\left| D^{m-1} f(x) - D^{m-1} f(y) \right| < \text{const } |x - y|^{1-\delta} \ .$$

The first theorem answering the question about the smoothness of the conjugacy was the theorem of Arnol'd [3]. He proved that if the analytic map $f : \mathbb{T} \to \mathbb{T}$ is sufficiently close (in the sup-norm) to a rotation and $\tau(f)$ is Diophantine of type $\nu \geq 1$, then f is analytically conjugate to the rotation $r_{\tau(f)}$, i.e., there exists an analytic function $h : \mathbb{T} \to \mathbb{T}$ such that $h \circ f = r_{\tau(f)} \circ h$. The iterative technique applied by Arnol'd was fruitfully used later in the proof of the celebrated Kolmogorov-Arnold-Moser (KAM) theorem – see, e.g., Wayne [192]. The result of Arnol'd was extended to the case of finite differentiability by Moser [147]. In such a case, the Diophantine exponent ν has to be related to the number of derivatives one assumes for the map.

Arnol'd theorem is local, i.e., it is important that f is close to a rotation. Arnol'd conjectured that any analytic map with a rotation number in a set of full measure is analytically conjugate to a rotation. Herman [94] proved that there exists a set $\mathcal{A} \subset [0, 1]$ of full Lebesgue measure such that if $f \in$

C^k for $3 \leq k \leq \omega$ and $\tau(f) \in \mathcal{A}$, then the conjugacy is $C^{k-2-\varepsilon}$ for any $\varepsilon > 0$. After several improvements, notably Yoccoz [208], the best result on smooth conjugacy we know of, is the following version of Herman's theorem as extended by Katznelson and Ornstein [113].

Theorem 2.4.3 (Herman, Katznelson and Ornstein). *Assume that f is a C^k circle OPD whose rotation number is Diophantine of order ν, and $k > \nu + 1$. Then the homeomorphism h which conjugates f with the rotation $r_{\tau(f)}$ is of class $C^{k-\nu-\varepsilon}$ for any $\varepsilon > 0$.*

There are examples of $C^{2-\varepsilon}$ maps with a Diophantine rotation number arbitrarily close to a rotation and not conjugated by an absolutely continuous function to a rotation – see, e.g., Hawkins and Schmidt[92].

2.4.6 Devil's Staircase, Phase Locking, Arnol'd Tongues

Let $\{f_\alpha\}_{\alpha \in A}$ be a one-parameter family of circle OPHs such that $f_\alpha(x)$ is increasing in α for every x. Then the function $\alpha \mapsto \tau(f_\alpha)$ is non-decreasing. (Since the maps are only defined modulo an integer and so is the rotation number, what is meant precisely is that if one takes the numbers with their integer parts, they can be made increasing or non-decreasing; this is done in detail in [112, Section 11.1].)

For such a family the following fact holds: if $\tau(f_\alpha) \notin \mathbb{Q}$, then $\alpha \mapsto \tau(f_\alpha)$ is strictly increasing locally at α; on the other hand, if f_α has rational rotation number and the periodic point is attracting or repelling (i.e., there

is a neighborhood of the point that gets mapped into itself by forwards or backwards iteration), then $\alpha \mapsto \tau(f_\alpha)$ is locally constant at this particular value of α, i.e., for all α' sufficiently close to α, $\tau(f_{\alpha'}) = \tau(f_\alpha)$. The local constancy of the function $\alpha \mapsto \tau(f_\alpha)$ is known as *frequency (phase, mode) locking*. Note that, since the rotation number is continuous, when it indeed changes, it has to go through rational numbers. The described phenomenon suggests the following definition.

Definition 2.4.6. A monotone continuous function $\psi : [0,1] \to \mathbb{R}$ is called a *devil's staircase* if there exists a family $\{I_\xi\}_{\xi \in \Xi}$ of disjoint open subintervals of $[0,1]$ with dense union such that ψ takes constant values on these subintervals. (We call attention to the fact that the complement of the intervals in which the function is constant can be of positive measure.)

The devil's staircase is said to be *complete* if the union of all intervals I_ξ has a full Lebesgue measure.

A very common way of phase locking for differentiable mappings arises when the map we consider has a periodic point and that the derivative of the return map at the periodic point is not equal to 1. By the implicit function theorem, such a periodic orbit persists, and the existence of a periodic orbit implies that the rotation number is locally constant. At the end of the phase locking interval the map has derivative one and experiences a saddle-node (tangent) bifurcation.

We note that, unless certain combinations of derivatives vanish (see,

e.g., Ruelle [176]), the saddle-node bifurcation happens in a universal way. That is, there are analytic changes of variables sending one into another. This leads to quantitative predictions. For example, the Lyapunov exponents of a periodic orbit should behave as a square root of the distance of the parameter to the edge of the phase locking interval.

Of course, other things can happen in special cases: the fixed point may be attractive but only neutrally so, there may be an interval of fixed points, the family may be such that there are no frequency locking intervals (e.g., the rotation). Nevertheless, all these conditions are exceptional and can be excluded in concrete examples by explicit calculations. (For example, if the family of maps is analytic but not a root of the identity, it is impossible to have an interval of periodic points.)

In the example we will consider, we will not perform a complete proof that a devil's staircase occurs, but rather we will present numerical evidence. In particular, the square root behavior of the Lyapunov exponent with the distance to the edge of the phase locking interval seems to be verified.

Let us now consider two-parameter families of OPDs of the circle, $\{\phi_{\alpha,\beta}\}$, depending smoothly on α and β. Assume that when $\beta = 0$, the maps of the family are rotations by α, i.e., $\phi_{\alpha,0} = r_\alpha$. We will call β the *nonlinearity parameter*. Assume also that $\partial\phi_{\alpha,\beta}/\partial\alpha > 0$. An example of this type is the family studied by Arnol'd [3],

$$\eta_{\alpha,\beta} : \mathbb{T} \to \mathbb{T} : x \mapsto \eta_{\alpha,\beta}(x) := x + \alpha + \beta \sin 2\pi x \, (\mathrm{mod}\, 1) \,, \qquad (2.31)$$

where $\alpha \in [0, 1)$, $\beta \in (0, 1/2\pi)$.

The rotation number τ is a continuous map in the uniform topology, and $\phi_{\alpha,\beta}$ is a continuous function of α and β, so the function $(\alpha, \beta) \mapsto \tau(\phi_{\alpha,\beta}) =: \tau_\beta(\alpha)$ depends continuously on α and β. The map τ_β is non-decreasing; for $\beta > 0$, τ_β is locally constant at each α for which $\tau_\beta(\alpha)$ is rational and strictly increasing if $\tau_\beta(\alpha)$ is irrational. Thus, τ_β is a devil's staircase.

Since τ_β is strictly increasing for irrational values of $\tau_\beta(\alpha)$, the set $I_\nu := \{(\alpha, \beta) \mid \tau_\beta(\alpha) = \nu\}$ for an irrational $\nu \in [0, 1]$ is a graph of a continuous function. For a rational ν, I_ν has a non-empty interior and is bounded by two continuous curves. The wedges between these two curves are often referred to as *Arnol'd tongues*.

The fact that $\tau(\phi_{\alpha,0}) = \tau(r_\alpha) = \alpha$ implies that for $\beta = 0$, the set of α's for which there is frequency locking coincides with the rational numbers between 0 and 1, so its Lebesgue measure is zero. When $\beta > 0$, its Lebesgue measure is positive. The width of the Arnol'd tongues for small β for the Arnol'd map (2.31) is investigated, e.g., by Davie [43]. Much of this analysis carries out for more general functions such as the ones we encounter in the problem of the periodically pulsating resonator.

The total Lebesgue measure of the frequency locking intervals,

$$m(\{\tau_\beta^{-1}(\nu) \mid \nu \in \mathbb{Q} \cap [0, 1]\}) \,,$$

becomes equal to 1 when the family of circle maps consists of maps with a horizontal point (so that the map, even if having a continuous inverse, fails

to have a differentiable one) – see Jensen *et al* [105] and Lanford [120] for numerical results and Świątek [183] for analytical proof. With the Arnol'd map $\eta_{\alpha,\beta}$ this happens when $\beta = 1/2\pi$. In our case this happens when the mirror goes at one instant at the speed of light.

We note also that the numerical papers Shenker [179], Jensen *et al* [105], Lanford [120], Cvitanović *et al* [39] contain not only conjectures about the measure of the phase locking intervals but, perhaps more importantly, conjectures about scaling relations that hold "universally". In particular, the dimension of the set of parameters not covered by the phase locking intervals should be the same for all non-degenerate families. These universality conjectures are supported not only by numerical evidence but also by a renormalization group picture – see, e.g., Lanford [121, 123] and the references therein. These universality predictions have been verified in several physical contexts. Notably in turbulence by Glazier and Libchaber [80].

As we will see in Section 2.6.3, we do not expect that the families obtained in (2.19) for mirrors oscillating with different amplitudes belong to the same universality class as typical mappings, but they should have universality properties that are easy to figure out from those of the above references.

2.4.7 Ergodic Properties of Circle Maps

For the physical problem at hand it is also important to know how the iterates of the circle map $x \mapsto g(x) := G(x) \pmod 1$ are distributed. As we will see in lemma 2.5.3, if the iterates of g are well distributed (in an

48

appropriate sense), the energy of the field in the resonator does not build up. The distribution of an orbit is conveniently formalized by using the concept of invariant measures. We recall that a measure μ on X is *invariant* under the measurable map $f : X \to X$ if $\mu(f^{-1}(A)) = \mu(A)$ for each measurable set A.

Given a point $x \in \mathbb{T}$, the frequency of visit of the orbit of x to $I \subset \mathbb{T}$ can be defined by

$$\mu_x(I) := \lim_{n \to \infty} \frac{\#\{i \mid 0 \leq i \leq n \text{ and } f^i(x) \in I\}}{n} \ . \tag{2.32}$$

It is easy to check that if for every interval I, the limit (2.32) exists, it defines an invariant measure describing the frequency of visit of the orbit of x. Therefore, if there are orbits which have asymptotic frequencies of visit, we can find invariant measures.

A trivial example of the existence of such measures is when x is periodic. In such a case, the measure μ_x is a sum of Dirac delta functions concentrated on the periodic orbit. The measure of an interval is proportional to the number of points in the orbit it contains. We also note that it is easy to construct systems (see, e.g., Lanford [119]) for which the limits like the one in (2.32) do not exist except for measures concentrated on the fixed points, so that even the existence of such equidistributed orbits is not obvious.

There are also relations going in the opposite direction – if invariant measures exist, they imply the existence of well distributed orbits. We recall that the Krylov-Bogolyubov theorem [112, Thm. 4.1.1] asserts that any continuous map on a compact metrizable space has an invariant probability

measure. Moreover, the Birkhoff ergodic theorem [112, Thm. 4.1.2] implies that given any invariant measure μ, the set of points for which μ_x as in (2.32) does not exist has measure zero.

Certain measures have the property that $\mu_x = \mu$ for μ-almost all points. These measures are called *ergodic*. From the physical point of view, a measure is ergodic if all the points in the measure are distributed according to it. For maps of the circle, there are several criteria that allow to conclude that a map is ergodic.

For rotations of the circle with an irrational rotation number we recall the classical Kronecker-Weyl equidistribution theorem [112, Thm. 4.2.1] which shows that any irrational rotation is uniquely ergodic, i.e., has only one invariant measure – the Lebesgue measure m. (Such uniquely ergodic maps are ergodic because, by Birkhoff ergodic theorem, the limiting distribution has to exist almost everywhere, but, since there is only one invariant measure, all these invariant distributions have to agree with the original measure.) Thus, the iterates of any $x \in \mathbb{T}$ under an irrational rotation are uniformly distributed on the circle.

For general non-linear circle OPDs the situation may be quite different. As an example, consider Arnol'd map $\eta_{\alpha,\beta}$ (2.31). If it is conjugate to an irrational rotation by h, i.e., $\eta_{\alpha,\beta} = h^{-1} \circ r_{\tau(\eta_{\alpha,\beta})} \circ h$, then there is a unique invariant probability measure μ defined for each measurable set A by $\mu(A) := m(h(A))$. This implies that if I is an interval in $\mathbb{T}$, then the frequency with which a point x visits I is equal to $\mu(I)$.

50

On the other hand, if $\tau(\eta_{\alpha,\beta}) = p/q \in \mathbb{Q}$, then all orbits are periodic or asymptotic to periodic. Thus, the only possible invariant measure is concentrated at the periodic points and therefore singular, if the periodic points are isolated. Let us now assume that α is very close to $\tau_\beta^{-1}(p/q)$, but does not belong to it. Then $\eta_{\alpha,\beta}$ has no periodic orbits, but still there exists a point x which is "almost periodic", i.e., the orbits linger for an extremely long time near the points x, $\eta_{\alpha,\beta}(x)$, $\cdots$, $\eta_{\alpha,\beta}^{q-1}(x)$. So that, even if the invariant measure is absolutely continuous, one expects that it is nevertheless quite peaked around the periodic orbit – see Figure 2.6. The behavior of such maps is described quantitatively by the "intermittency theory" (Pomeau and Manneville [163]).

The continuity properties of the measures of the circle are not so easy to ascertain. Nevertheless, there are certain results that are easy to establish:

In the case that we have a rational rotation number and isolated periodic orbits, some of them attracting and some of them repelling, the only possible invariant measures are measures concentrated in the periodic orbits.

For the irrational rotation number case, the Kronecker-Weyl theorem implies that all the maps with an irrational rotation number – since they are semi-conjugate to a rotation by Poincaré theorem – are uniquely ergodic. In the situations where Herman's theorem applies, this measure will have a smooth density since it is the push-forward of Lebesgue measure by a smooth diffeomorphism.

We also recall that by Banach-Alaoglu theorem and the Riesz representation theorem, the set of Borel probability measures is compact when we give it the topology of $\mu_n \to \mu \iff \mu_n(A) \to \mu(A)$ for all Borel measurable sets A. (This convergence is called weak-* convergence by functional analysts and convergence in probability by probabilists.)

Lemma 2.4.4. *If λ is a parameter value for which f_λ admits only one invariant measure μ_λ, given μ_{λ_i} invariant measures for f_{λ_i}, with $\lambda_i \to \lambda$, then μ_i converges in the weak-* sense to μ_λ.*

Note that we are not assuming that f_{λ_i} are uniquely ergodic. In particular, the lemma says that in the set of uniquely ergodic maps, the map that a parameter associates the invariant measure is continuous if we give the measures the topology of weak-* convergence.

Proof. Let $\mu_{\lambda_{i_k}}$ be a convergent subsequence. The limit should be an invariant measure for f_λ. Hence, it should be μ_λ. It is an easy point set topology lemma that for functions taking values in a compact metrizable space, if all subsequences converge to the same point, then this point is a limit. The space of measures with weak-* topology is metrizable because by Riesz representation theorem is the dual of the space of continuous functions with sup-norm, which is metrizable. $\qquad\square$

We also point out that as a corollary of KAM theory (Arnol'd [3]) we can obtain that for non-degenerate families, if we consider the parameter

values for which the rotation number is Diophantine with uniform constants, the measures are differentiable jointly on x and in the parameter. (For the differentiability in the parameter, we need to use Whitney differentiability or, equivalently, declare that there is a family of densities differentiable both in x and in λ that agrees with the densities for these values of λ.)

On the other hand, we point out that there are situations where the invariant measure is not unique (e.g., a rational rotation or a map with more than one periodic orbit). In such cases, it is not difficult to approximate them by maps in such a way that the invariant measure is a discontinuous function of the parameter (in the weak-* topology). The discontinuity of the measures with respect to parameters, as we will see, has the physical interpretation that, by changing the oscillation parameters by arbitrarily small amounts, we can go from unbounded growth in the energy to the energy remaining bounded.

2.5   Applications of Circle Maps to the Resonator Problem

Now we return to the problem of a one-dimensional optical resonator with a periodically moving wall to discuss the physical implications of circle maps theory, and illustrate with numerical results in an example.

2.5.1   Circle Maps in the Resonator Problem

If we take $a(t)$ to depend on two parameters, α and β, as in (2.6), then, as we saw in Section 2.3.5, the time between the consecutive reflections at the

mirrors can be described in terms of the functions $F_{\alpha,\beta}$ and $G_{\alpha,\beta}$ defined by (2.19). These maps are lifts of circle maps that we will denote by $f_{\alpha,\beta}$ and $g_{\alpha,\beta}$. The restriction on the range of β in (2.6) implies that $f_{\alpha,\beta}$ and $g_{\alpha,\beta}$ are analytic circle OPDs. Therefore, we can apply the results about the types of orbits of OPHs of $\mathbb{T}$, Poincaré and Denjoy theorems, as well as the smooth conjugacy results and the facts about the distribution of orbits.

In an application where the motion of the mirror [i.e., $a(t)$] is given, one needs to compute $F_{\alpha,\beta}$ and $G_{\alpha,\beta}$ (2.19), which cannot be expressed explicitly from $a(t)$ but they require only to solve one variable implicit equation. In the numerical computations we used the subroutine ZEROIN (Forsythe *et al* [74]) to solve implicit equations. If $y = F_{\alpha,\beta}(t)$ and $z = G_{\alpha,\beta}(t)$, then for $a(t)$ given by (2.6), y and z are given implicitly by

$$-y + t + \alpha + 2\beta \sin[\pi(y+t)] = 0$$
$$-z + t + \alpha + \beta \left[\sin(2\pi t) + \sin(2\pi z)\right] = 0 \ .$$

Given t, we can find y, z applying ZEROIN.

2.5.2   Rotation Number, Phase Locking

In this section, our goal is to translate the mathematical statements from the theory of circle maps into physical predictions for the resonator problem.

The theory of circle maps guarantees that the measure of the frequency locking intervals for $g_{\alpha,\beta}$ is small when β is small and becomes 1 when $\beta =$

$1/2\pi$. The theory also guarantees for analytic maps that, unless a power of the map is the identity, the frequency locking intervals are non-trivial. For the example that we have at hand, it is very easy to verify that this does not happen and, therefore, we can predict that there will be frequency locking intervals and that as the amplitude of the oscillations of the moving mirror increases so that the maximum speed of the moving mirror reaches the speed of light, the devil's staircase becomes complete. Figure 2.4 shows a part of the
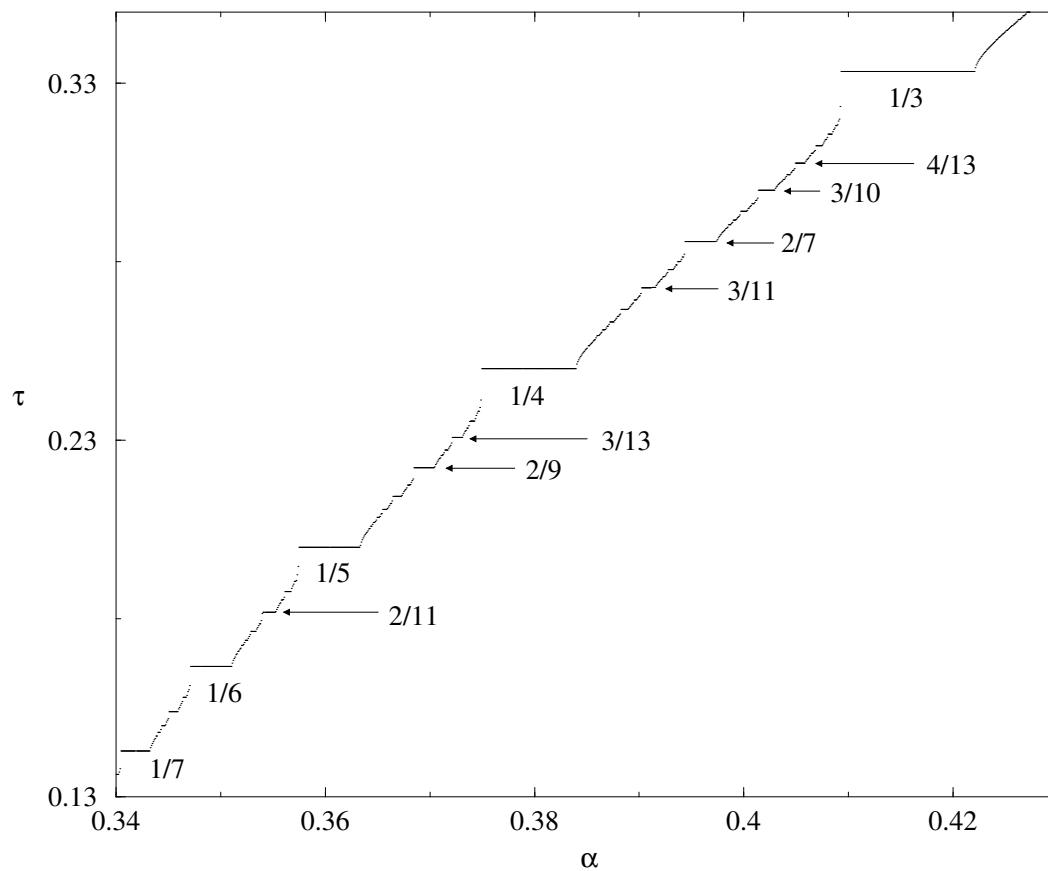
Figure 2.4: A part of the graph of $\tau(g_{\alpha,1/2\pi})$ vs. α.

complete devil's staircase – the situation which happens when the maps $g_{\alpha,\beta}$ and $f_{\alpha,\beta}$ lose their invertibility, i.e., for $\beta = 1/2\pi$.

We also recall that the theory of circle maps makes predictions about what happens for non-degenerate phase locking intervals. Namely, for parameters inside the phase locking interval the map has a periodic fixed point and the Lyapunov exponent is smaller than 0, while at the edges of the phase locking interval the map experiences a non-degenerate saddle-node bifurcation – provided that certain combinations of the derivatives do not vanish (Ruelle [176]).

We note that for parameters for which the map is in non-degenerate frequency locking, i.e., $\tau(g_{\alpha,\beta}) = p/q$ and the attractive periodic point of period q has a negative Lyapunov exponent, $\{G_{\alpha,\beta}^{nq}(x)\}_{n=0}^{\infty}$ will converge exponentially to the fixed point for all x in a certain interval, according to the results about the types of orbits of circle maps (Section 2.4.3). The whole circle can be divided into such intervals and a finite number of periodic points. Therefore, the graph of $G_{\alpha,\beta}^{nq}$, and hence of $g_{\alpha,\beta}^{nq}$, will look – up to errors exponentially small in n – like a piecewise-constant function with values (up to integers) in the fixed points of $g_{\alpha,\beta}^{q}$ – see Figure 2.5. The fact that certain functions tend to piecewise-constant functions for large values of the argument (which follows from what we found about $G_{\alpha,\beta}^{nq}$ for large n) was observed numerically for particular motions of the mirror in Law [128] and Cole and Schieve [28]. In physical terms, this means that the rays will be getting closer and closer together, so with the time the wave packets will become narrower and narrower
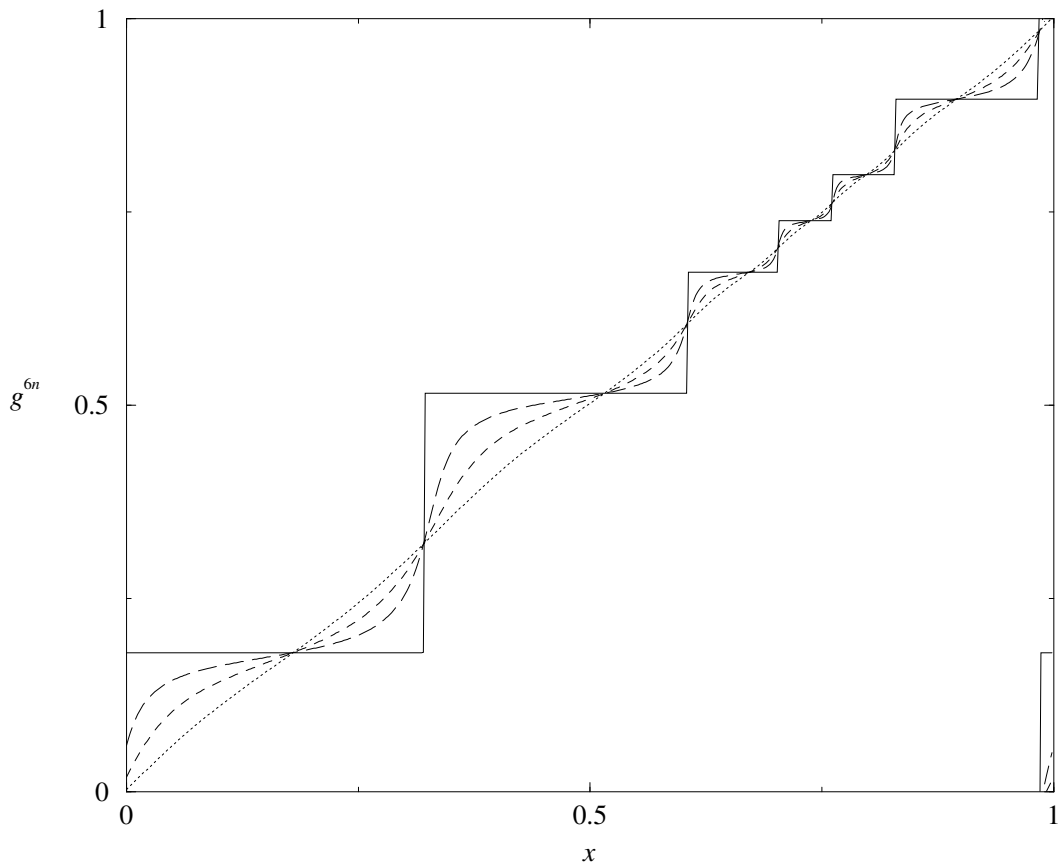
Figure 2.5: Development of the piecewise-constant structure of $g_{0.2545,\,0.1}^{6n}$ (the rotation number of $g_{0.2545,\,0.1}$ is $1/6$). Graphs of $g_{0.2545,\,0.1}^{6n}$ are plotted for $n = 1$ (dotted), $n = 5$ (dashed), $n = 10$ (long dashed), $n = 100$ (solid lines).

57

and more and more sharply peaked. The number of wave packets is equal to q. The number of reflections from the moving mirror per unit time will tend to the inverse of the rotation number. In the next section we discuss how this yields an increase of the field energy which happens exponentially fast on time.

The fact that for $\tau(g_{\alpha,\beta}) \in \mathbb{Q}$ the rays approach periodic orbits, is also interesting from a quantum mechanical point of view due to the relation between the periodic orbits in a classical system and the energy levels of the corresponding quantum system, given by the Gutzwiller's trace formula (see, e.g., the books by Gutzwiller [87] and Brack and Bhaduri [14, Chapter 5]).

We also note that we expect that slightly away from the edges of a phase locking interval, the invariant density will be sharply peaked around the points in which it was concentrated in the phase locking intervals. This is described by the "intermittency theory" (Pomeau and Manneville [163]).

To observe numerically in our example what happens when α enters or leaves a frequency locking interval, we set $N_\beta(\nu) := \{\alpha \in [0,1) \mid \tau(g_{\alpha,\beta}) = \nu\}$. Figure 2.6 represents the probability density of visit of the iterates, $d\mu/dm$.

The figure shows $d\mu/dm$ for α close to the left end of $N_{0.1}(1/6)$. When α approaches (from the left) the left end of $N_{0.1}(1/6)$, $d\mu/dm$ becomes sharply peaked at some points, and when α enters the frequency locking interval, the invariant measure becomes singular ($g_{\alpha,0.1}$ undergoes tangent bifurcation at $\alpha = 0.253977\ldots$). All seems to be consistent with the conjecture that all the frequency-locking intervals in the family (away of $\beta = 0$) are non-degenerate,
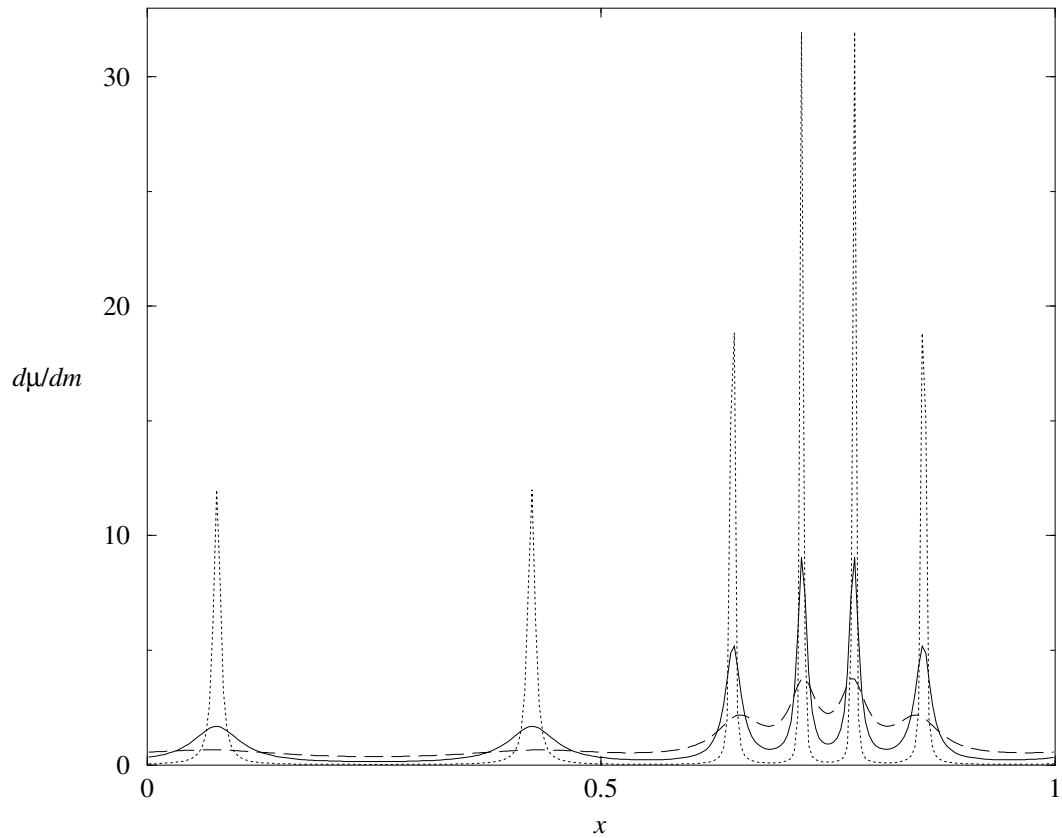
Figure 2.6: Density of the invariant measures for $\beta = 0.1$ and $\alpha = 0.253$ (dashed), $\alpha = 0.2539$ (solid), and $\alpha = 0.253975$ (dotted line).

i.e., that at the boundaries of the phase locking intervals the map satisfies the hypothesis of the saddle-node bifurcation theorem.

2.5.3   Doppler Shift

One of the most interesting parts of the applications of circle map theory is the ease with which we can describe the effect on the energy after repeated reflections.

59

Recall that in Section 2.3.6, we found the time dependence of the field energy under the assumption that at time t all rays are going to the right. This assumption is not very restrictive in the case of a rational rotation number since, as we found in Section 2.4.2, the field develops wave packets that become narrower with time, so (2.27) and (2.28) hold for the asymptotic behavior of the energy. Note that (2.27) expresses the Doppler shift factor in terms of the derivatives of the map G. This gives a very close relation between the dynamics and the behavior of the wave packets.

Proposition 2.5.1. *Let α and β be such that $\tau(g_{\alpha,\beta}) = p/q$, and that the map $G := G_{\alpha,\beta}$ has a stable periodic orbit $\Theta_q = \{\theta_1, \ldots, \theta_q\}$ such that $(G^q)'(\theta_1) < 1$. Assume that the initial electromagnetic field in the cavity is not zero at some space-time point for which the phase of the first reflection from the moving mirror is in the basin of attraction of Θ_q.*

Then the energy of the field in the resonator will be asymptotically increasing at an exponential rate:

$$E(t) \sim \exp\left\{\frac{\ln D(\Theta_q)}{p} t\right\} . \tag{2.33}$$

Remark 2.5.1. Dr. N. Gonzalez has kindly informed us that in his thesis [82] he has proved that if $(G^q)'(\theta_1) = 1$ (and some additional conditions are satisfied), the energy increases polynomially.

Proof. First, notice that the number of reflections from the moving mirror per unit time reaches a well defined limit (one and the same for all rays) –

the inverse of the rotation number. Secondly, as was discussed in Section 2.3, at reflection from the moving mirror at phase θ, a wave packet becomes narrower by a factor of $D(\theta)$ (2.16), which leads to a $D(\theta)$ times increase in its energy. Asymptotically, the phases at reflection will approach the stable periodic orbit $\Theta_q = \{\theta_1, \ldots, \theta_q\}$ of $g_{\alpha,\beta}$. The Doppler factors at reflection will tend correspondingly to $\{D(\theta_1), \ldots, D(\theta_q)\}$ (2.16). Hence, in time p each ray will undergo q reflections from the moving mirror, the total Doppler shift factor along the periodic orbit Θ_q being

$$D(\Theta_q) := \prod_{i=1}^{q} D(\theta_i) = \prod_{i=1}^{q} \frac{1 - a'(\theta_i)}{1 + a'(\theta_i)} \ .$$

On the other hand, the definition of the map G as the advance in the time between successive reflections from the moving mirror yields $\theta_i = G^{i-1}(\theta_1)$. The chain rule applied to the explicit expression (2.19) for G yields

$$(G^{q-1})'(\theta_1) = \prod_{j=1}^{q-1} G'(\theta_j) = \prod_{j=1}^{q-1} \frac{1 + a'(\theta_j)}{1 - a'(\theta_{j+1})} \ ,$$

which gives the following expression for $D(\Theta_q)$ [cf. (2.27)]:

$$D(\Theta_q) = \frac{1 - a'(\theta_1)}{1 + a'(\theta_q)} \left[(G^{q-1})'(\theta_1) \right]^{-1} = \frac{1 - a'(\theta_1)}{1 + a'(\theta_q)} (G^{1-q})'(\theta_q) \ . \qquad (2.34)$$

Hence, the energy density grows by a factor of $D(\Theta_q)^2$. Since after q reflections the wave packet is concentrated in a length $D(\Theta_q)$ times smaller, the total energy grows by a factor of $D(\Theta_q)$ in p units of time, which implies (2.33). $\qquad \square$
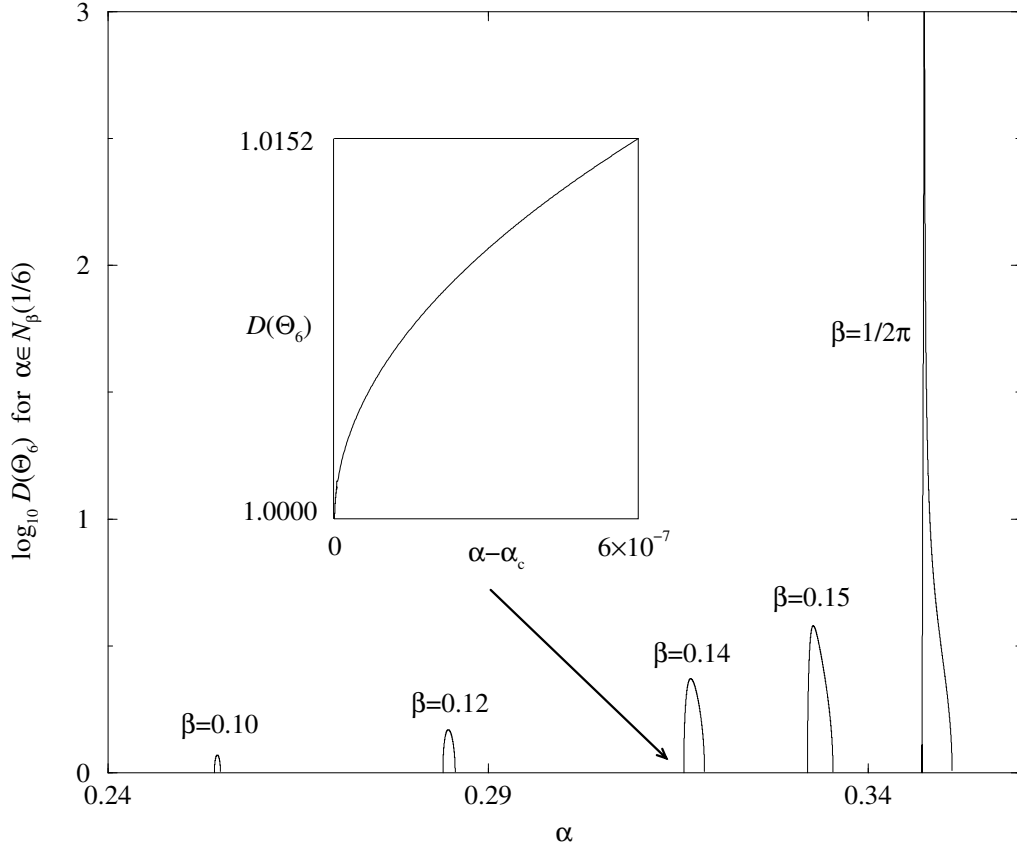
Figure 2.7: $\log_{10} D(\Theta_6)$ vs. $\alpha \in N_\beta(1/6)$ for different values of β.

The quantities $(G^n)'(\theta)$ that appear in (2.34) have been studied intensively in dynamical systems theory since they control the growth of infinitesimal perturbations of trajectories. Similarly, they are factors that multiply the invariant densities when they get transported, as we will see in (2.35).

We found numerically the total Doppler factors $D(\Theta_q)$ for some particular choices of the parameters. In Figure 2.7, $\log_{10} D(\Theta_6)$ is shown for different values of β and for $\alpha \in N_\beta(1/6)$. Obviously, the maximum value

of $D(\Theta_6)$ depends strongly on β, becoming infinite for $\beta = 1/2\pi$ and some $\alpha \in N_{1/2\pi}(1/6)$. For smaller values of β, the Doppler factor is much smaller. Moreover, the width of the frequency locking intervals for small β is small, so the probability of hitting a frequency locking interval with arbitrarily chosen α and β is small. [The likelihood of frequency locking for the Arnol'd map (2.31) is studied numerically by Lanford [120].]

In the case when Herman's theorem apply, the derivatives of G^n are bounded independently of n, which causes the energy of the system to be bounded for all times, which is proved in the following proposition.

Proposition 2.5.2. *If $G_{\alpha,\beta}$ is such that it satisfies the hypothesis of Herman's theorem, then the energy density remains bounded for all times.*

Proof. In such a case $G_{\alpha,\beta} = h^{-1} \circ R \circ h$ with h differentiable and R a rotation by $\tau(g_{\alpha,\beta})$. Therefore $G_{\alpha,\beta}^n = h^{-1} \circ R^n \circ h$ and

$$(G_{\alpha,\beta}^n)'(\theta) = (h^{-1})'(R^n \circ h(\theta)) \, (R^n)'(h(\theta)) \, h'(\theta) = (h^{-1})'(R^n \circ h(\theta)) \, h'(\theta)$$

because $(R^n)' = 1$. The two factors in the right-hand side of the above equation are bounded uniformly in θ and n. Thus, the "local Doppler factors" (2.27) will be bounded, which implies the boundedness of the energy (2.28). $\square$

There is an interesting connection between the invariant densities of the system and the growth of the electromagnetic energy density.

Recall that if a density μ is invariant, $\mu(G(\theta)) = \mu(\theta)/G'(\theta)$. Hence, if the density μ never vanishes, $G'(\theta) = \mu(\theta)/\mu(G(\theta))$ and, therefore, $(G^i)'(\theta) = \mu(\theta)/\mu(G^i(\theta))$. Let us assume that there is only one characteristic passing through the space-time point (t, x), and this characteristic is going to the right. Then, using the notations of Section 2.3.5, we can write the energy density at (t, x) as [cf. (2.27)]

$$\mathcal{T}^{00}(t, x) = \left[\frac{1 - a'(\theta_{-n_-}^-)}{1 + a'(\theta_0^-)} \frac{\mu(G^{n-}(\theta_{-n_-}^-))}{\mu(\theta_{-n_-}^-)} \right]^2 \mathcal{T}^{00}(t_0, x_0^-) . \qquad (2.35)$$

In the general case [with two characteristics through (x, t)], one can use (2.23) and (2.26) to prove the following result:

Lemma 2.5.3. *If a system has an invariant density μ which is bounded away from zero, then the electromagnetic energy density of C^1 initial A, A_t is smaller than $C\mu^2$ for all times.*

In the cases that Herman's theorem applies, there is an invariant density bounded away from zero (and also bounded). Hence, we conclude that there are values of the amplitude of mirror's oscillations for which the energy density of the field remains bounded. This set is typically a Cantor set interspersed with values for which the energy increases exponentially.

Some other results about the behavior of the energy with respect to time and parameters are obtained by Dittrich *et al* [53], and Gonzalez [82, 83].

The article by Gonzalez [83] contains an example with a periodically (piecewise linearly) moving boundary, in which the rotation number of the

circle map is rational, but the energy is bounded. In his example, however, the circle map is piecewise linear, so the qth iterate of its lift, F^q (where q is the denominator of its rotation number), is equal to the identity (up to an additive constant).

We call attention to the fact that Arnol'd [3] contains examples of analytic maps whose rotation numbers are very closely approximated by rationals and that are arbitrarily close to a rotation such that they preserve no invariant density and, therefore, are not smoothly conjugate to a rotation.

It is also known that for all rotation numbers one can construct $C^{2-\varepsilon}$ maps arbitrarily close to rotations with this rotation number and such that they do not preserve any invariant measures (Hawkins and Schmidt [92]).

Finally, let us remark that all conclusions about forming of wave packets remain valid for the case of homogeneous Dirichlet boundary conditions, $A(t, 0) = A(t, a(t)) = 0$, as explained in Section 2.3.3. For the case of Neumann boundary conditions, see Section 2.6.1.

2.6 Miscellaneous

2.6.1 On the Role of the Correct Boundary Conditions

Here we would like to give simple physical arguments showing that Neumann boundary conditions lead to very different predictions than the relativistic ones (2.12), (2.14). For more details see our article [190].

First note that the relativistic boundary conditions, (2.12), (2.14) are

equivalent to the Dirichlet ones,

$$A(t,0) = \text{const} , \quad A(t, a(t)) = \text{const} . \tag{2.36}$$

Therefore, the procedure for constructing the solution described in Section 2.3 can be successfully applied if instead of relativistic boundary conditions we had Dirichlet ones.

For Neumann boundary conditions, however, the situation is different (as we noticed in Section 2.3.4). To see why, let us consider the wave equation (2.8) with Neumann boundary conditions

$$A_x(t,0) = 0 , \quad A_x(t, a(t)) = 0 , \tag{2.37}$$

and initial conditions (2.9).

The most important observation is that by setting $u := A_x$, we transform the Neumann boundary value problem (2.8), (2.37), (2.9) into the Dirichlet boundary value problem

$$
\begin{aligned}
&u_{tt}(t,x) - u_{xx}(t,x) = 0 , &&(t,x) \in \Sigma , \\
&u(0,x) = \psi_1'(x) , \quad u_t(0,x) = \psi_2'(x) , &&x \in (0, a(0)) , \\
&u(t,0) = 0 , \quad u(t, a(t)) = 0 , &&t \geq 0 ,
\end{aligned}
\tag{2.38}
$$

which can be solved by applying our method from Section 2.3.

Recall that the reason for the energy growth in the case of relativistic or Dirichlet boundary conditions is the change of the distance between rays at reflection from the moving mirror, as shown in Figure 2.3. At the same time, the absolute value of the solution does not change at reflection. The effect of

66

this is increase of the first derivatives $D(\theta)$ times and decrease of the spatial distances $D(\theta)$ times, which results in increase of the energy (2.26) $D(\theta)$ times, where $D(\theta)$ is the Doppler factor at reflection at time θ (see Sections 2.3.4 and 2.3.6).

To simplify the exposition, let us consider only the case of motion of the boundary for which the system is in phase locking regime. Note that whether the system is phase locked does *not* depend on the boundary conditions, but only on the behavior of the characteristics (which in turn depends on the motion of the mirror). In this case the solution of the Dirichlet boundary value problem (2.38) will develop wave packets whose width will decrease exponentially in time. Note that for long enough times, when the wave packets are well separated, the solution $u(t, x)$ at each moment (except during the short periods of time when a wave packet undergoes a reflection) consists of *unidirectionally moving* wave packets. In general, the energy of the solution $A(t, x)$ of the Neumann boundary value problem (2.8), (2.37), (2.9) cannot be simply expressed in terms of the function u, but for unidirectionally moving wave packets it is approximately equal to

$$E(t) = \int_0^{a(t)} u(t, x)^2 \, dx \; . \tag{2.39}$$

To write (2.39), we neglected the overlap between different wave packets, and used the fact that for unidirectionally moving $A(t, x)$, the relations $A_t(t, x) = \pm A_x(t, x)$ hold (the sign depending on the direction of the motion). We see that in a phase locking regime the wave packets of the field u, whose energy

67

is given by (2.39), will become narrower at exponential rate, while the field u will only change sign at reflection, hence the integral of the square of u will *decrease* at exponential rate.

This simple physical argument shows that the behavior of the solutions of the relativistic (or Dirichlet) and the Neumann boundary value problems in a pulsating spatial domain behave very differently, the most dramatic difference being that in phase locking the energy of the former *increases* exponentially, while the energy of the latter *decreases* exponentially. The main reason for this is that the expression (2.39) for the energy of a solution of the Neumann boundary value problem is can be written in the form (2.39) which does not contain derivatives.

Similar phenomena have been previously noticed by Cooper and Koch [33], who observed that (in a slightly different context) the solutions may tend to zero in some Sobolev norms, but grow in others (see Section 2 and the end of Section 1 of their article), and by Dittrich *et al* [53]. The novelty of our approach is in giving an intuitively clear explanation of the phenomenon by linking it with the behavior of the characteristics of the wave equation.

2.6.2 The Inverse Problem: Determining the Mirror's Motion from the Circle Map

It is important to know whether the notion of a "typical" G is the same as the notion of a "typical" a or a "typical" F (in the mathematical literature people speak about "generic" maps, and in physical literature about

"universal" maps). We do not know the answer to this question, and here we will give some arguments showing that the answer is not obvious. We will not use "generic" or "universal". Rather we will make explicit the non-degeneracy assumptions so that they can be checked in the concrete examples. In Section 2.6.3 we will show that some universal properties for families of circle maps do not apply to G constructed according to (2.19) with $a(t) = \bar{a} + \varepsilon b(t)$.

While the function a can be expressed in terms of F as

$$
a = \frac{F - \mathrm{Id}}{2} \circ \left(\frac{F + \mathrm{Id}}{2} \right)^{-1} ,
$$

the relation between G and a is much harder to invert. We should have

$$
a(\theta) + a(G(\theta)) = \widetilde{G}(\theta) , \tag{2.40}
$$

where $\widetilde{G}(\theta) := G(\theta) - \theta$, so for any n,

$$
a(\theta) = \widetilde{G}(\theta) - \widetilde{G}(G(\theta)) + \cdots + (-1)^n \widetilde{G}(G^n(\theta)) + (-1)^{n+1} a(G^{n+1}(\theta)) .
$$

Hence, if $G^{2k}(\theta_0) = \theta_0 \,(\mathrm{mod}\,1)$, a necessary condition for the existence of a is that

$$
\sum_{i=0}^{2k-1} (-1)^i \widetilde{G}(G^i(\theta_0)) = 0 . \tag{2.41}
$$

An example of a G where the above condition is not satisfied can be readily constructed. We furthermore note that if a map fails to satisfy (2.41) and if $(G^{2k})'(\theta_0) \neq 1$, then all small C^1 perturbations will also fail to satisfy (2.41). Thus, there are C^1 neighborhoods of maps that cannot be realized as G for a moving mirror.

On the other hand, given very simple G's, it is easy to construct infinitely many a's that satisfy (2.40) and that therefore lead to the same G. For example, for $G(\theta) = \theta + \frac{1}{2}$, (2.40) amounts to $a(\theta + \frac{1}{2}) + a(\theta) = \frac{1}{2}$. If we prescribe a for θ in $[0, \frac{1}{2}]$, then this equation determines a on $[\frac{1}{2}, 1]$ (the only care needs to be exercised so that the two determinations of a match at $\theta = \frac{1}{2}$). A similar construction works when G permutes several intervals.

In the case when G is conjugate to an irrational rotation, $G = h^{-1} \circ R_\alpha \circ h$, then (2.40) is equivalent to

$$a \circ h^{-1} \circ R_\alpha + a \circ h^{-1} = h^{-1} \circ R_\alpha - h^{-1} \ .$$

Then $a \circ h^{-1}$ can be determined using Fourier analysis, setting $h^{-1}(\theta) = \theta + \sum_{k=-\infty}^{\infty} \widehat{\tau}_k e^{2\pi i k \theta}$, $a \circ h^{-1}(\theta) = \theta + \sum_{k=-\infty}^{\infty} \widehat{\psi}_k e^{2\pi i k \theta}$, which leads to

$$\left(e^{2\pi i k\alpha} + 1 \right) \widehat{\psi}_k = \left(e^{2\pi i k\alpha} - 1 \right) \widehat{\tau}_k \ . \tag{2.42}$$

If we assume that $|k\alpha - n - \frac{1}{2}| \geq \mathrm{const}\, |k|^{-\nu}$ for some $\nu \geq 1$ (a condition of this type is called a Diophantine condition – see definition 2.4.4), and that h^{-1} has r derivatives (which implies that its Fourier coefficients $\widehat{\tau}_k$ satisfy $|\widehat{\tau}^k| \leq \mathrm{const}\, |k|^{-r}$). Then if $r > \nu + 2$, then the coefficients $\widehat{\psi}_k$ define a smooth function (for more details see, e.g., Herman [94, Section XIII.4]). Of course, once we know $a \circ h^{-1}$, then, since h^{-1} depends only on G and is therefore determined, we can obtain a.

In summary, there are maps G that do not come from any a at all, come from infinitely many a's, or come from one and only one a. The maps F can always be obtained from one and only one a.

70

2.6.3 Behavior for Small Amplitude and Universality

We note that, even if all the motions of the mirror lead to a circle map as in (2.20), it does not seem clear to us that all the maps of the circle can appear as F, G for a certain a. This makes it impossible to conclude that the theory of generic circle maps applies directly to obtain conclusions for a generic motion of the mirror. Therefore, the very developed mathematical theory of generic or universal circle maps cannot be applied without caution to maps that appear as the result of generic or universal oscillations of the mirror. Of course, all the conclusions of the general theory that apply to all maps of the circle apply to our case. Those conclusions that require non-degeneracy assumptions will need that we verify the assumptions.

One aspect that we have found makes a big difference with the generic theory is the situation where the mirror oscillates with small amplitude, i.e., $a_\varepsilon(t) = \bar{a} + \varepsilon b(t)$ with b a periodic function of zero average and period 1, and $\varepsilon \ll 1$. The first parameter, $\bar{a}$, is the average length of the resonator, while $\varepsilon = 0$ is called the "nonlinearity parameter" for obvious reasons. If we denote by $F_{\bar{a},\varepsilon}$ and $G_{\bar{a},\varepsilon}$ the corresponding 2-parameter families of maps of the circle constructed according to (2.19), then we have, for three times differentiable families,

$$
\begin{aligned}
F_{\bar{a},\varepsilon}(t) &= t + 2\bar{a} + 2\varepsilon b(t + \bar{a}) + 2\varepsilon^2 b'(t + \bar{a})b(t + \bar{a}) + O(\varepsilon^3) \ , \\
G_{\bar{a},\varepsilon}(t) &= t + 2\bar{a} + \varepsilon[b(t) + b(t + 2\bar{a})] \\
&\quad + \varepsilon^2 b'(t + 2\bar{a})[b(t) + b(t + 2\bar{a})] + O(\varepsilon^3) \ .
\end{aligned}
\tag{2.43}
$$

71

Note that the term of order ε always has vanishing average. As we will immediately show, this property causes that some well known generic properties of families of circle mappings do not hold for families of maps constructed as in (2.19).

Indeed, if we consider the expressions for small amplitude developed in (2.43), we can write the maps as

$$H_\varepsilon(t) = t + 2\bar{a} + \varepsilon H_1(t) + \varepsilon^2 H_2(t) + O(\varepsilon^3) \ .$$

Since the conclusions of the theory of circle maps are independent of the coordinate system chosen, it is natural to try to choose a coordinate system where these expressions are as simple as possible. Hence, we choose $h_\varepsilon(t) := t + \varepsilon \eta(t)$, a perturbation of the identity, and consider $h_\varepsilon^{-1} \circ H_\varepsilon \circ h_\varepsilon$, which is just H_ε in another system of coordinates, related to the original one by h_ε. Then, up to terms of order ε^3, we have

$$\begin{aligned}
h_\varepsilon^{-1} \circ H_\varepsilon \circ h_\varepsilon(t) \ = \ \ & t + 2\bar{a} + \varepsilon \left[\eta(t) - \eta(t + 2\bar{a}) + H_1(t) \right] \\
& + \varepsilon^2 \{ \eta'(t + 2\bar{a}) \eta(t + 2\bar{a}) - \eta'(t + 2\bar{a}) \left[\eta(t) + H_1(t) \right] \\
& + H_1'(t) \eta(t) + H_2(t) \} \ .
\end{aligned}$$

We would like to choose η in such a way that the ε term is not present. Note that since $\int \eta(t + 2\bar{a}) \, dt = \int \eta(t) \, dt$, this is impossible unless $\int H_1(t) \, dt = 0$. When $\int H_1(t) \, dt = 0$, H_1 is smooth and $2\bar{a}$ is Diophantine, a well-known result (see, e.g., Herman [94, Section XIII.4]) shows that in such a case we can obtain one η satisfying

$$\eta(t) - \eta(t + 2\bar{a}) + H_1(t) = 0 \tag{2.44}$$

and $\overline{\eta} = 0$. [Such η is conventionally obtained by using Fourier coefficients. Note that in Fourier coefficients, (2.44) amounts to $\widehat{\eta}_k(e^{2\pi ik2\bar{a}} - 1) = \widehat{(H_1)}_k$. If H_1 is smooth, the Fourier coefficients decrease fast and if $2\bar{a}$ is Diophantine, then $(e^{2\pi ik2\bar{a}} - 1)^{-1}$ does not grow too fast. For more details we refer to the reference above.]

Since for the functions $F_{\bar{a},\varepsilon}$ and $G_{\bar{a},\varepsilon}$ the term of order ε has a zero average, we can transform these functions into lifts of rotations plus $O(\varepsilon^2)$. This implies, in particular, that their rotation number is $\tau(F_{\bar{a},\varepsilon}) = \tau(G_{\bar{a},\varepsilon}) = 2\bar{a} + O(\varepsilon^2)$. One could wonder if it would be possible to continue the process and eliminate also to order ε^2.

If we look at the ε^2 terms in (2.44), we see that $\overline{\eta'(t)\eta(t)} = 0$, and, when η is chosen as in (2.44),

$$\eta'(t + 2\bar{a})[\eta(t) + H_1(t)] = \eta'(t + 2\bar{a})\eta(t + 2\bar{a}) ,$$

which also has average zero. Therefore, a necessary condition for the ε^2 term in $h_\varepsilon^{-1} \circ H_\varepsilon \circ h_\varepsilon(t)$ to be zero is $\overline{H_1'(t)\eta(t)} + \overline{H_2(t)} = 0$.

For the $F_{\bar{a},\varepsilon}$ in (2.43) we see that F_2 has zero average. Nevertheless, the term $F_1'(t)\eta(t)$ does not in general have average zero as can be seen in examples. Hence, we see that the rotation number indeed changes by an order which is $O(\varepsilon^2)$ and not higher in general. This property is not generic for families of circle maps starting with a rotation $2\bar{a}$ and it puts them outside of the universality classes considered by Shenker [179], Lanford [121, 123], etc.,

since the correspondence between rotation numbers and parameters is not the same.

According to the geometric picture of renormalization developed by Lanford [121, 123], the space of circle maps is divided into slices of rational rotation numbers, which are – in appropriate sense – parallel. In that language – in which we think of families of circle maps as curves in the space of mappings – the families of advance maps $F_{\bar{a},\varepsilon}$ and $G_{\bar{a},\varepsilon}$ (for fixed $\bar{a}$) have second order tangency to the foliation of rational rotation numbers rather than being transversal. Hence, the scaling predicted by universality theory should be true for ε^2 in place of ε. We have not verified this prediction, but we expect to come back to it soon.

2.6.4 On the Formation of Wave Packets in the Quantum Treatment

In this section, we briefly show that the formation of wave packets in the quantum treatment of the problem can be easily explained within our formalism.

Recall (see Section 2.1.4) that a central object in the method suggested by Moore and studied extensively by other authors is the function $R(z)$ satisfying the property (2.1). Since the letter R has already been used in Section 2.4.2 to denote rotations, we introduce the function $S : \mathbb{R} \to \mathbb{R}$ by $S(z) := \frac{1}{2}R(z)$, which satisfies the property

$$S \circ F(\tau) = S(\tau) + 1 \,, \qquad \tau \in \mathbb{R} \tag{2.45}$$

74

(see the definition of the map F (2.19)).

We will show that in the case of phase locking, the function $S(t)$ develops a "staircase-like" structure, i.e., for large values of t its graph has almost horizontal pieces connected by almost vertical ones. This observation was made numerically by Cole and Schieve [28] and others, and interpreted as an indication that the field in the cavity develops wave packets. On the other hand, in the case when the associated with the mirror's motion circle map g is smoothly conjugate to a rotation, the first derivative of S stays bounded for all times, so staircase-like structure does not occur.

First we consider the case of phase locking with rotation number $\tau(g) = \tau(g) = \frac{p}{q}$. (Recall that the two phase advance maps f and g introduced in Section 2.3.5 are conjugate, so their rotation numbers are equal, hence f is phase-locked exactly when f is phase-locked.) In this case, the map f has an attractive periodic orbit of period q. Let $\bar{t}$ belong to this q-periodic orbit. Then it is a fixed point for the iterated map f^q, and satisfies

$$F^q(\bar{t}) = \bar{t} + p , \qquad (2.46)$$

where F is a lift of f. To be closer to the physical interpretation, let F stands for the "physical" time advance map, i.e., the only lift satisfying $F(0) = f(0)$.

Set

$$\bar{t}_1 := \bar{t} , \qquad \bar{t}_j := F(\bar{t}_{j-1}) , \quad j = 2, \ldots, q .$$

The function F^q maps the interval $[\bar{t}_1, \bar{t}_1 + q)$ onto $[\bar{t}_1 + q, \bar{t}_1 + 2q)$, the interval $[\bar{t}_1 + q, \bar{t}_1 + 2q)$ onto $[\bar{t}_1 + 2q, \bar{t}_1 + 3q)$, etc. Moreover, it acts on each of these

75

intervals "in the same way", or, more precisely, shifting the argument of the function F^q by nq (n is an arbitrary integer) shifts the value by np:

$$F^q(\bar{t}_1 + nq + t) = F^q(\bar{t}_1 + t) + np , \qquad t \in [0, nq) .$$

Assume that we know the values of the function S on the interval $[t, F(t))$ where $t \in \mathbb{R}$ is arbitrary. Then by using the property (2.45), we can construct S on the whole real line. Note that (2.46) and (2.45) imply

$$S(\bar{t}_k + np) = S \circ F^{nq}(\bar{t}_k) = S(\bar{t}_k) + nq .$$

This means, in particular, that S maps the interval $[\bar{t}_1, \bar{t}_1 + p)$ onto $[\bar{t}_1 + p, \bar{t}_1 + 2p)$, the interval $[\bar{t}_1 + p, \bar{t}_1 + 2p)$ onto $[\bar{t}_1 + 2p, \bar{t}_1 + 3p)$, etc. Let us define the series of functions

$$S_n : [\bar{t}_1, \bar{t}_1 + p) \to [\bar{t}_1, \bar{t}_1 + p) , \qquad n \in \mathbb{Z} ,$$

by

$$S_n(t) := S(t + np) - nq .$$

The functional series $\{S_n\}_{n \in \mathbb{Z}}$ contains the whole information about the function S, and we can study the asymptotic behavior of S by studying the limit $\lim_{n \to \infty} S_n$.

First note that, by (2.46) and (2.45), the values of S_n at the points $\bar{t}_k$ are the same for all n:

$$S_n(\bar{t}_k) = S(\bar{t}_k) \qquad k = 1, 2, \ldots, q . \tag{2.47}$$

Next, let us study the first derivative of S. Here it is convenient to use the notations from the beginning of Section 2.3.5, so let us recall them briefly. The symbols τ_n and θ_n stand for the times of reflection of one particular ray from the stationary and the moving mirror, respectively, and they are ordered as follows: $\ldots < \tau_n < \theta_n < \tau_{n+1} < \theta_{n+1} < \ldots$. Recall also the relations

$$\tau_n = (\mathrm{Id} - a)(\theta_n) \, , \qquad \tau_{n+1} = (\mathrm{Id} + a)(\theta_n) \, .$$

With these notations, the expression for the derivative of F at τ_n can be written as

$$F'(\tau_n) = \frac{1 + a'(\theta_n)}{1 - a'(\theta_n)} = \frac{1}{D(\theta_n)} \, ,$$

where $D(\theta_n)$ is the Doppler factor for reflection at time θ_n. This formula yields

$$(F^{mq})'(\tau_n) = \prod_{j=1}^{mq} F'\left(F^{j-1}(\tau_{n+j-1})\right) = \left[\prod_{j=1}^{mq} D(\theta_{n+j-1})\right]^{-1} . \qquad (2.48)$$

Differentiating the relation $S \circ F^{mq}(\tau) = S(\tau) + mq$ (which is simply (2.45) iterated $mq - 1$ times), and using (2.48), we obtain

$$S'(F^{mq}(\tau_n)) = \left[\prod_{j=1}^{mq} D(\theta_{n+j-1})\right]^{-1} S'(\tau_n) \, . \qquad (2.49)$$

Since we are in the phase locking case, the times of reflection of any ray except the ones that correspond to the unstable q-periodic orbit of f will converge exponentially fast to the rays corresponding to the stable q-periodic orbit of f. This means that for large m's, the product

$$\lim_{m\to\infty} \prod_{j=mq+1}^{(m+1)q} D(\theta_{n+j-1}) = \prod_{j=1}^{q} D(\bar{\theta}_j) \, , \qquad (2.50)$$

77

where $\{\bar{\theta}_1, \bar{\theta}_2, \ldots, \bar{\theta}_q\}$ is the attractive q-periodic orbit of the map g. The stability of this periodic orbit corresponds to the fact that the product in the right-hand side of (2.50) is greater than 1. The implication of this fact on the values of the derivative of S (2.49) unless t is such that $t \bmod 1$ belongs to the unstable q-periodic orbit of f, the derivative of S at t is very close to 0.

If, instead of talking about large values of the argument, we talk about large indices of the functional sequence $\{S_n\}$, we can say that for large m the relation

$$S_m(t) = S(t + mp) - mq \approx S \circ F^{mq}(t) - mq$$

implies

$$S'_n(t) \approx \left[\prod_{j=1}^{q} D(\bar{\theta}_j) \right]^{-1} S'_{n-1}(t) ,$$

so the derivatives at a fixed value of the argument decrease exponentially when the index of the function increases.

Let us recapitulate our findings about the behavior of the function S, or, equivalently, about the functional sequence $\{S_n\}$. For any $S_0 := S|_{[\bar{t}_1, \bar{t}_1+p)}$, the functions S_n for large n are going to be staircase-like, with almost horizontal pieces and almost vertical pieces between them; the values of S_n at the horizontal pieces will tend to the values $S(\bar{t}_k)$ as $n \to \infty$ (cf. (2.47)).

2.6.5 Two Moving Mirrors

As mentioned in Section 2.1.6, our approach allows us to give a very clear treatment of the problem in the case when both mirrors are moving.

Let T_1 and T_2, respectively, be the periods of the motion of two mirrors. If the frequencies, T_1^{-1} and T_2^{-1}, of the two mirrors are rationally related, i.e., if there exist integers, m_1 and m_2 (both different from 0), such that

$$m_1 T_1^{-1} + m_2 T_2^{-1} = 0 \ , \tag{2.51}$$

then set T equal to the least common multiple of T_1 and T_2, and rescale the units to make T equal to 1, after which our analysis carries over with obvious modifications – e.g., if the positions of the left and the right mirrors are given by $x = a_1(t)$ and $x = a_2(t)$, respectively, then the the phase advance map G will be

$$G = (\mathrm{Id} - a_2)^{-1} \circ (\mathrm{Id} - a_1) \circ (\mathrm{Id} + a_1)^{-1} \circ (\mathrm{Id} + a_2)$$

(compare with (2.19)). It is again a circle map, and the whole analysis of the problem is practically the same as in the case of one periodically moving mirror.

It would be interesting to apply our method to the case $a_2 = a_1 + \mathrm{const}$, i.e., when the cavity is moving as a whole, its length being constant.

If the periods T_1 and T_2 do not satisfy (2.51), then the mathematical description of the problem cannot be reduced to study of a circle map. However, it can be described in terms of maps of the 2-torus $\mathbb{T}^2$. We study this case (and its far generalizations) in Chapter 3.

2.6.6   Schwarzian Derivative in the Problem of Moving Mirrors

Fulling and Davies [76] calculated the energy-momentum tensor in the two-dimensional quantum field theory of a massless scalar field influenced by the motion of a perfectly reflecting mirror (see also Mostepanenko and Trunov [151, Section 2.7]). They obtained that the "renormalized" vacuum expectation value of the energy density radiated by a moving mirror into initially empty space is

$$\mathcal{T}^{00}(u) = -\frac{1}{24\pi} \left[\frac{F'''(u)}{F'(u)} - \frac{3}{2} \left(\frac{F''(u)}{F'(u)} \right)^2 \right] ,$$

where $u = t - x$, and F is related to the law of the motion of the mirror, $x = a(t)$, by (2.19). The right-hand side of this equation is nothing but (up to a constant factor) the Schwarzian derivative of F – a differential operator which naturally appears in complex analysis, e.g., it is invariant under a fractional linear transformation; vanishing Schwarzian derivative of a function is the necessary and sufficient condition that the function is fractional linear transformation, etc. More interestingly, the Schwarzian derivative has been used as an important tool in the proof of several important theorems in the theory of circle maps – see, e.g., Yoccoz [208], Herman [95], of Graczyk and Świątek [84]. In the light of the connection between the solutions of the wave equation in a periodically pulsating domain and the theory of circle maps it is not impossible that this is not just a coincidence.

Chapter 3

Torus Maps and a Quasiperiodically Pulsating Cavity

In this chapter we study the problem of the asymptotic behavior of the electromagnetic field in an optical resonator one of whose walls is at rest and the other one is moving quasiperiodically (with $d \geq 2$ incommensurate frequencies).

We show that this problem can be reduced to a problem about the behavior of the iterates of a map of the d-dimensional torus that preserves a foliation by irrational straight lines. In particular, the Jacobian of this map has $(d-1)$ eigenvalues equal to 1.

We study several dynamical features of such maps and translate them into into properties for the field in the cavity. Among them, we show that when the torus map satisfies a KAM theorem – it happens for a Cantor set of positive measure of parameters – the energy of the electromagnetic field remains bounded. When the torus map is in a resonant region – it happens in open sets of parameters inside the gaps of the previous Cantor set – the energy grows exponentially.

3.1 Introduction

In the present chapter, we study a generalization of the problem of the behavior of the electromagnetic field in a cavity with one stationary and one moving perfectly reflecting boundaries to the case of a quasiperiodic motion of the mirror. We are interested in the asymptotic behavior of the electromagnetic field in the resonator. We use an approach similar to the one used in Chapter 2, and reformulate the problem in terms of certain maps of the torus. This allows us to draw conclusions about the asymptotic behavior of the field in the resonator in terms of the dynamical properties of these torus maps.

In particular, we obtain that if we consider typical families of motions described by several parameters (e.g., the Fourier coefficients of the motion of the boundary), then there exists an open and nonempty set of parameters for which the electromagnetic field has exponentially growing energy (this situation is called "resonance"), and another set of parameters for which the energy remains bounded. In the case that the energy is unbounded, the electromagnetic field concentrates in pulses of exponentially decreasing width which move quasiperiodically. In the case that the energy does not grow, the derivatives of the field remain uniformly bounded for all times. Both sets of parameters interpenetrate each other. The set with bounded energy is a Cantor set and the unbounded growth lies in the gaps of this Cantor set.

The torus maps that appear in our treatment of pulsating cavities have several special properties, the most striking one being that they preserve an irrational foliation (see Sections 3.2.2 and 3.3.4). This leads to several dy-

namical consequences, notably that there is only one Lyapunov exponent that may be nonzero. The set of parameters for which this exponent is negative are the phase locked regions. We will give a description of these regions and will show that, when the dynamical system is in the phase locked region, the field in the cavity has an exponentially growing energy. Moreover, we will derive a relationship between the rate of increase of the energy (the "Doppler factor") and the nonzero Lyapunov exponent.

Another region where the dynamics can be understood is a region where KAM (Kolmogorov-Arnol'd-Moser) techniques apply. In such a case, the derivatives of the electromagnetic field remain bounded and, as a consequence, the energy of the electromagnetic field remains bounded.

There may be regions in parameter space that are not covered by the above descriptions. At the moment, we do not know what behavior to expect there.

We present a numerical study of the phase locked regions, which, besides giving a description of the boundaries of the regions of unbounded energy, suggests several questions of a more dynamical nature.

A physical problem similar to the one studied in this article has been studied in [204], from a very different point of view.

The chapter is organized as follows. In Section 3.2 we describe the physical model, and derive the associated torus map (omitting many details that are the same as in Chapter 2). In Section 3.3 we define the basic concepts used

in the classification of torus maps, paying special attention to the particular type of torus maps occurring in the analysis of the resonator problem, discuss the KAM theory for these maps, and derive an expression for the Lyapunov exponent of such maps. In Section 3.4 we explore the torus maps numerically. In Section 3.5 we apply the conclusions drawn from the mathematical theory and the numerical study to the problem of the electromagnetic field in the resonator, and, in particular, derive a simple relationship between the Lyapunov exponent of the torus map and the Doppler factor at reflection from the moving mirror. Finally, we give simple reasoning about the asymptotic behavior of the energy for the boundary conditions for the optical resonator.

3.2 Derivation of the Mathematical Model

In this section we describe the physical model of the electromagnetic field in the resonator (Section 3.2.1), and derive the torus map describing the evolution of the electromagnetic field (Section 3.2.2).

3.2.1 Physical Setup

Consider the classical (i.e., not quantized) electromagnetic field between two flat infinite perfectly reflecting mirrors, both of them perpendicular to the x-axis (see Figure 2.1). Let one of them be at rest at $x = 0$, and the other one be moving quasiperiodically, its position being given by

$$x = a(t) = \Phi(\boldsymbol{\omega}t) \ , \tag{3.1}$$

where the function $\Phi : \mathbb{R}^d \to \mathbb{R}$ is periodic of period 1 in each argument:

$$\Phi(\Xi_1, \ldots, \Xi_{j-1}, \Xi_j + 1, \Xi_{j+1}, \ldots, \Xi_d)$$
$$= \Phi(\Xi_1, \ldots, \Xi_{j-1}, \Xi_j, \Xi_{j+1}, \ldots, \Xi_d) . \tag{3.2}$$

For the moment, and in a good part of this chapter, we will not need to make any assumptions on $\boldsymbol{\omega} \in \mathbb{R}^d$. In some parts, we will assume that $\boldsymbol{\omega}$ is incommensurate (see Definition 3.3.2) or, sometimes, that it is Diophantine (Definition 3.3.3).

The vector $\boldsymbol{\omega}$ is called the *frequency vector* (note that this convention differs from the one usually used in physics by a factor of 2π).

Since only the fractional parts of Ξ_j matter (due to (3.2)), we call the fractional parts of the Ξ_j's *phases* of the motion of the mirror.

We also impose the physically natural conditions

$$a(t) = \Phi(\boldsymbol{\omega}t) \geq \Phi_{\min} > 0 \quad \forall t \in \mathbb{R} \tag{3.3}$$

(positive length of the resonator), and

$$|a'(t)| = |\boldsymbol{\omega} \cdot \nabla\Phi(\boldsymbol{\omega}t)| \leq a'_{\max} < 1 \quad \forall t \in \mathbb{R} \tag{3.4}$$

(the speed of the mirror does not exceed the speed of light).

In our numerical simulations we study the case of two frequencies ($d = 2$) and the map

$$\Phi(\Xi_1, \Xi_2) \;=\; \frac{\alpha}{2} + \beta \left[\sin\left(2\pi\Xi_1\right) + \gamma \sin\left(2\pi\Xi_2\right)\right] , \tag{3.5}$$
$$\boldsymbol{\omega} \;=\; (1, \sigma_{\mathrm{G}}) , \quad \sigma_{\mathrm{G}} := \tfrac{\sqrt{5}-1}{2} , \tag{3.6}$$

85

with the constants α, β and γ chosen in such a way that (3.5) satisfies (3.3) and (3.4). Note that for $\gamma = 0$, the map Φ stops depending on Ξ_2, and becomes a periodic function of Ξ_1, i.e., in this case we are back to the case of a periodically moving boundary considered in Chapter 2.

Since our considerations in Sections 2.3.2, 2.3.3, and 2.3.4 did not depend on the nature of the function $a(t)$ giving the motion of the boundary, everything in these sections works without any modification for the case of a quasiperiodic motion of the mirror. Namely, after imposing Coulomb gauge condition, we arrive at the boundary-value problem (2.8), (2.9), (2.12), (2.14) for the function $A(t, x)$ defining the vector potential, $\mathbf{A}(t, x) = A(t, x) \, \mathbf{e}_y$. The method of characteristics again can be used to solve the boundary value problem, and, in particular, the mechanism of the change of the energy of the electromagnetic field again is through Doppler effect at reflection from the moving mirror. The considerations about the asymptotic behavior of the energy of the electromagnetic field from Section 2.3.6 can be easily adapted to the case of a quasiperiodic $a(t)$.

3.2.2 Derivation of the Torus Map

The asymptotic behavior of the characteristics – and hence the electromagnetic field – can be studied quite effectively by the following device.

We denote by $\boldsymbol{\pi} : \mathbb{R}^d \to \mathbb{T}^d := \mathbb{R}^d / \mathbb{Z}^d$ the projection

$$\Xi \mapsto \boldsymbol{\xi} := \boldsymbol{\pi}(\Xi) = (\Xi_1 \bmod 1, \, \ldots, \, \Xi_d \bmod 1) . \tag{3.7}$$

This projection appears naturally in the study of quasiperiodic motions since, due to (3.2), the state of the moving mirror is completely characterized by the phase $\boldsymbol{\xi} := \boldsymbol{\pi}(\boldsymbol{\omega} t)$ which determines not only the position $a(t) = \Phi(\boldsymbol{\omega} t)$, but also the derivatives $a'(t)$ and all future and past phases at reflection.

We adopt the convention of referring to the objects in $\mathbb{T}^d$ as the *phases* and denote them by lower case boldface letters, while the objects in $\mathbb{R}^d$ will be denoted by uppercase boldface letters.

Let θ_n be the time of the nth reflection of a particular characteristic ("ray") from the moving mirror (we use the notations of Section 2.3.5). We will see that there is a very explicit expression that gives θ_{n+1} in terms of θ_n. It is clear that

$$\theta_{n+1} - a(\theta_{n+1}) = \theta_n + a(\theta_n) \tag{3.8}$$

(cf. (2.18)).

Let $\mathbf{G}$ be the map that gives $\boldsymbol{\omega}\theta_{n+1}$ in terms of $\boldsymbol{\omega}\theta_n$:

$$\mathbf{G} : \mathbb{R}^d \to \mathbb{R}^d : \boldsymbol{\omega}\theta_n \mapsto \boldsymbol{\omega}\theta_{n+1} \ .$$

Multiplying (3.8) by $\boldsymbol{\omega}$ and taking into account (3.1), we obtain the following expression for $\mathbf{G}$ (cf. (2.19)):

$$\mathbf{G} = (\mathrm{Id} - \boldsymbol{\omega}\Phi)^{-1} \circ (\mathrm{Id} + \boldsymbol{\omega}\Phi) \ . \tag{3.9}$$

Remark 3.2.1. Due to the condition (3.4), $\mathrm{Id} - \boldsymbol{\omega}\Phi$ is always invertible, so $\mathbf{G}$ (and the map $\mathbf{g}$ defined below) are well-defined.

87

Now let us note that due to (3.2), we do not need to know the Ξ_j's, but only their fractional parts – the phases $\xi_j = \Xi_j \bmod 1 \in \mathbb{T}^1$. Because of this, we define the map $\mathbf{g} : \mathbb{T}^d \to \mathbb{T}^d$ as follows. Let $\boldsymbol{\xi} \in \mathbb{T}^d$ and $\boldsymbol{\Xi} \in \mathbb{R}^d$ be a *lift* of $\boldsymbol{\xi}$, i.e., $\xi_j = \Xi_j \bmod 1$ for each $j = 1, \ldots, d$. Then we define the map

$$\mathbf{g} := (g_1,\, g_2,\, \ldots,\, g_d) : \mathbb{T}^d \to \mathbb{T}^d$$

by

$$g_j(\boldsymbol{\xi}) := G_j(\boldsymbol{\Xi}) \bmod 1 \ . \tag{3.10}$$

In mathematical language, $\mathbf{g}$ can be defined as the only map satisfying

$$\mathbf{g} \circ \boldsymbol{\pi} = \boldsymbol{\pi} \circ \mathbf{G} \ , \tag{3.11}$$

where $\boldsymbol{\pi}$ is given by (3.7). We will call $\mathbf{g}$ the *phase advance map*.

Remark 3.2.2. Note that $\mathbf{G}$ has the form

$$\mathbf{G}(\boldsymbol{\Xi}) = \boldsymbol{\Xi} + \Gamma(\boldsymbol{\Xi})\boldsymbol{\omega} \ , \tag{3.12}$$

where Γ is a strictly positive real-valued function (since the length of the cavity is bounded from below by $\Phi_{\min} > 0$ (3.3)). The physical interpretation of $\Gamma(\boldsymbol{\Xi}) = \Gamma(\boldsymbol{\omega}\theta)$ is the time spent between the reflection from the moving mirror at moment θ when the phase of the mirror's motion is $\boldsymbol{\xi} = \boldsymbol{\pi}(\boldsymbol{\omega}\theta)$, and the next reflection from the moving mirror. Torus maps satisfying (3.12) are a very particular class of torus maps, as explained in Section 3.3.4.

Maps of the type (3.12) have appeared in the mathematical literature as reparametrizations of irrational flows on the torus (Fayad [70]). We

note, however, that there are many maps of the form (3.12) which are not reparametrizations of irrational flows. Fayad [70] constructed reparametrizations of irrational flows on the torus (hence maps of the form (3.12)) with very complicated ergodic properties which we will not discuss further here.

A particular case of the above construction is when $a(t) := \bar{a} = \text{const}$, i.e., when the right mirror is at rest at a constant distance $\bar{a} = \text{const}$ from the left one. In this case, (3.9) reduces to

$$\mathbf{G}(\mathbf{\Xi}) = \mathbf{\Xi} + 2\bar{a}\boldsymbol{\omega} \ .$$

3.3 Analysis of the Torus Map

In this section we give a short exposition of the facts from the theory of torus maps necessary for the analysis of the torus map $\mathbf{g}$ (3.10), and explain some rigorous results for torus maps. In Section 3.4 we will present numerical results and in Section 3.5 we will discuss the interpretations for the cavity problem of the rigorous and numerical results of Sections 3.3 and 3.4, respectively.

This section is organized as follows. First in Sections 3.3.1, 3.3.2, and 3.3.3, we briefly introduce some concepts from the theory of torus homeomorphisms (continuous torus maps whose inverse is also continuous) which we shall call torus maps for brevity (for more details see, e.g., Baesens *et al* [7]). Then, in Sections 3.3.4 we discuss in more detail the case of the torus maps occurring in the physical problem at hand.

The main tools of the analysis are the KAM theory developed in Section 3.3.5, and the theory of Lyapunov exponents in Section 3.3.6. Since the general theory of KAM and Lyapunov exponents is much more subtle than for the case that we have in mind, we will just study what we need.

We point out that the literature on the dynamical properties of torus maps is quite extensive both in the mathematical and the physical literature. Torus maps appear in ergodic theory (see, e.g., Arnol'd and Avez [5]), in the description of systems of coupled oscillators (Baesens *et al* [7]), play a central role in the Ruelle-Takens-Newhouse scenario for transition to turbulence (Newhouse *et al* [153]; see also Eckmann [64] and Grebogi *et al* [85]), Schrödinger's equation with a quasiperiodic potential (Dinaburg and Sinai [52], Chulaevsky and Sinai [25], Dinaburg [51]), Hill's equation with a quasiperiodic forcing (Broer and Simo [18]); bifurcations of quasiperiodic tori have been studied in detail in Broer *et al* [19].

3.3.1 Rotation Set

A basic concept in the theory of torus maps is the concept of the rotation set of the orbits of a map.

Let $\mathbf{g}$ be a torus map, and $\mathbf{G}$ be a *lift* of $\mathbf{g}$, i.e., a map of $\mathbb{R}^d$ to itself that is related to $\mathbf{g}$ by (3.11) (any torus map has infinitely many lifts, differing by an integer vector $\mathbf{p} \in \mathbb{Z}^d$).

Definition 3.3.1. Let $\mathbf{G}$ be a lift of the torus map $\mathbf{g}$ and let $\boldsymbol{\xi} \in \mathbb{T}^d$, and $\boldsymbol{\Xi} \in \mathbb{R}^d$ be any lift of $\boldsymbol{\xi}$, (i.e., $\boldsymbol{\pi}(\boldsymbol{\Xi}) = \boldsymbol{\xi}$). The *rotation set* $\boldsymbol{\tau}(\boldsymbol{\xi}, \mathbf{g})$ of the point

90

$\boldsymbol{\xi}$ under the map $\mathbf{g}$ is the set of the limit points of

$$\boldsymbol{\pi}\left(\frac{\mathbf{G}^n(\boldsymbol{\Xi}) - \boldsymbol{\Xi}}{n}\right) , \quad n \in \mathbb{N} . \tag{3.13}$$

If the limit

$$\boldsymbol{\tau}(\boldsymbol{\xi}, \mathbf{g}) := \boldsymbol{\pi}\left(\lim_{n\to\infty} \frac{\mathbf{G}^n(\boldsymbol{\Xi}) - \boldsymbol{\Xi}}{n}\right) , \tag{3.14}$$

exists (i.e., if $\boldsymbol{\tau}(\boldsymbol{\xi}, \mathbf{g})$ consists of one point), then it is called the *rotation vector* of $\boldsymbol{\xi}$ under $\mathbf{g}$.

Remark 3.3.1. The rotation set is always nonempty, compact and connected (Llibre and MacKay [135]), and it does not depend on the choice of a lift of $\mathbf{g}$.

Remark 3.3.2. For circle maps $(d = 1)$, the limit in the right-hand side of (3.14) always exists and does not depend on $\xi \in \mathbb{T}$ (see Section 2.4.2). In other words, the rotation set of the map consists of only one number called the *rotation number* of the map.

Remark 3.3.3. When $d > 1$, the structure of the rotation set could be very complicated for a generic map of the torus (see, e.g., Kwapisz [118] and references therein).

One could hope that for maps of the form (3.12), it would be possible to develop a more systematic theory. Using KAM theory, it is possible to show that for families of maps close to rotations and satisfying suitable non-degeneracy assumptions there are large measure sets parameters for which the rotation set consists only of one point – see de la Llave and Vano [134] and Yamaguchi [204] (a summary of the main results of [134] are given in

91

Section 3.3.5). See also Cortez [36] for a proof of existence of a rotation vector for maps of the form (3.12) under the hypothesis of area preservation.

3.3.2 Arithmetic Properties of Vectors

Below, we summarize some number-theoretic properties of vectors that are important for our exposition.

Definition 3.3.2. A vector $\boldsymbol{\rho} \in \mathbb{T}^d$ is called:

(A) *incommensurate* if for any $\mathbf{m} \in \mathbb{Z}^d$ and $k \in \mathbb{Z}$ the equality

$$\mathbf{m} \cdot \boldsymbol{\rho} = k \tag{3.15}$$

implies that $\mathbf{m} = \mathbf{0}$, $k = 0$;

(B) *commensurate* if (3.15) holds for some $\mathbf{m} \in \mathbb{Z}^d \setminus \{\mathbf{0}\}$ and $k \in \mathbb{Z}$;

(B)$_1$ *rational* if $\boldsymbol{\rho} = \mathbf{p}/q$ for some $\mathbf{p} \in \mathbb{Z}^d$, $q \in \mathbb{N}$.

Remark 3.3.4. In the above definition, by $\mathbf{p}/q$ we always mean the *primitive* fraction, i.e., the one for which there is no common factor for p_1, …, p_d, q.

Remark 3.3.5. Obviously, all rational vectors are commensurate.

Important concepts needed for the KAM-type theorems for torus maps are given in the following definition.

Definition 3.3.3. A vector $\boldsymbol{\rho} \in \mathbb{R}^d$ is *Diophantine* if there exist constants $C > 0$, $\nu \geq d$ such that

$$|\mathbf{m} \cdot \boldsymbol{\rho} - k| \geq \frac{C}{|\mathbf{m}|^\nu} \tag{3.16}$$

for each $\mathbf{m} \in \mathbb{Z}^d \setminus \{\mathbf{0}\}$, $k \in \mathbb{Z}$ (here $|\mathbf{m}| := \sum_{j=1}^d |m_j|$); we will denote this by $\boldsymbol{\rho} \in D_{C,\nu}$.

The vector $\boldsymbol{\omega} \in \mathbb{R}^d$ is called *Diophantine affine* if it satisfies

$$|\mathbf{m} \cdot \boldsymbol{\rho}| \geq \frac{C}{|\mathbf{m}|^\nu} \ , \tag{3.17}$$

for each $\mathbf{m} \in \mathbb{Z}^d \setminus \{\mathbf{0}\}$.

Remark 3.3.6. Note that all Diophantine vectors are incommensurate. Also, all Diophantine vectors are Diophantine affine.

Remark 3.3.7. If $\boldsymbol{\rho} \in \mathbb{R}^d$ is Diophantine affine, so is $t\boldsymbol{\rho}$ for any $t \in \mathbb{R} \setminus \{0\}$. On the other hand, the set of Diophantine vectors is totally disconnected.

Remark 3.3.8. For $\boldsymbol{\omega} \in \mathbb{R}^d$ which satisfies (3.17), the set

$$\mathcal{A} := \{t \in \mathbb{R} \,|\, t\boldsymbol{\omega} \text{ is Diophantine}\}$$

is of full measure in the real line (see de la Llave and Vano [134] for the argument).

3.3.3 Translations on the Torus

The simplest example of a torus map is the translation $\mathbf{t}_{\boldsymbol{\eta}}$ ($\boldsymbol{\eta} \in \mathbb{T}^d$), whose lift, $\mathbf{T}_{\boldsymbol{\eta}}$, is given by

$$\mathbf{T}_{\boldsymbol{\eta}}(\boldsymbol{\Xi}) = \boldsymbol{\Xi} + \boldsymbol{\eta} \ .$$

Each orbit of $\mathbf{t}_{\boldsymbol{\eta}}$ has rotation vector equal to $\boldsymbol{\eta}$.

Depending on the properties of the rotation vector $\boldsymbol{\rho} \in \mathbb{R}^d$, one can talk about the following cases.

- If $\boldsymbol{\rho}$ is incommensurate, then the orbit of each $\boldsymbol{\xi} \in \mathbb{T}^d$ is dense in $\mathbb{T}^d$.

- If $\boldsymbol{\rho}$ is rational, say $\boldsymbol{\rho} = \mathbf{p}/q \in \mathbb{Q}$, then for the lift $\boldsymbol{\Xi}$ of any $\boldsymbol{\xi} \in \mathbb{T}^d$, we have $\mathbf{G}^q(\boldsymbol{\Xi}) = \boldsymbol{\Xi} + \mathbf{p}$, therefore, each $\boldsymbol{\xi} \in \mathbb{T}^d$ is *periodic* of period q: $\mathbf{g}^q(\boldsymbol{\xi}) = \boldsymbol{\xi}$.

- If $\boldsymbol{\rho}$ is commensurate but not rational, the orbit of each $\boldsymbol{\xi}$ under $\mathbf{g}$ is dense in some d'-dimensional torus $(0 < d' < d)$, where $d - d'$ is the number of independent relations $\mathbf{m} \cdot \boldsymbol{\rho} = k$ satisfied by $\boldsymbol{\rho}$.

  For example, if $\boldsymbol{\rho} = (\frac{1}{3}, \frac{2}{3}, \sqrt{2})$, then (3.15) is satisfied by the 2-parameter family $\mathbf{m} = (3a, 3b, 0)$, $k = a + 2b$, $(a, b) \in \mathbb{Z}^2 \setminus \{(0,0)\}$, hence $\mathbb{T}^3$ in this case is foliated by the orbits each of which is dense in a torus of dimension $d' = 1$; if $\mathbb{T}^3$ is visualized as the unit cube (with the corresponding sides identified), then the invariant one-dimensional tori are parallel to the ξ_3-axis.

3.3.4   Torus Maps Preserving a Foliation

Because of (3.12), the maps of the torus we have derived in Section 3.2.2 are of a very special nature. The main feature is that a straight line with direction $\boldsymbol{\omega}$ is transformed by $\mathbf{G}$ into itself. In mathematical terms this is described by saying that the maps are *foliation-preserving* – they preserve the leaves of $\mathcal{F}_{\boldsymbol{\omega}}$, the one dimensional foliation with direction $\boldsymbol{\omega}$. Indeed, if $\boldsymbol{\Xi} = \widetilde{\boldsymbol{\Xi}} + s\boldsymbol{\omega}$, then

$$\mathbf{G}(\boldsymbol{\Xi}) = \mathbf{G}(\widetilde{\boldsymbol{\Xi}}) + [\Gamma(\boldsymbol{\Xi}) - \Gamma(\widetilde{\boldsymbol{\Xi}}) + s]\,\boldsymbol{\omega} \; . \tag{3.18}$$

94

The existence of a preserved foliation is a severe restriction on the maps **g** of interest for us. Hence, phenomena typical in the class of all torus maps, may not be present in our case. Similarly, phenomena that are persistent in our family may not be persistent in the case of general torus maps.

The existence of a preserved foliation implies, in particular, that the rotation set is a rotation interval parallel to $\boldsymbol{\omega}$.

In the physical problem at hand, we will study only the case of an incommensurate $\boldsymbol{\omega}$, because in the case of a commensurate (but not rational) $\boldsymbol{\omega}$ one can study only the d'-dimensional invariant tori.

If $\boldsymbol{\omega}$ is incommensurate – which in the case $d = 2$ simply means that ω_1 and ω_2 are rationally independent, – each line of the foliation $\mathcal{F}_{\boldsymbol{\omega}}$ is dense when projected ("folded back") to the torus $\mathbb{T}^d$.

We also note that since $\boldsymbol{\omega}$ is incommensurate and $\Gamma(\boldsymbol{\Xi})$ (defined in (3.12)) is bounded away from 0, the torus map **g** cannot have any periodic points. (Indeed, observe that the line $\boldsymbol{\xi} + \boldsymbol{\omega}t$ is mapped to itself. Since Γ is positive, the motion on this line is monotone. Because $\boldsymbol{\omega}$ is incommensurate, two different points on the line correspond to two different points on the torus.)

3.3.5   KAM Theory

Due to the simplicity of the translations on the torus, it is important to know whether a general torus map is "equivalent" to a translation (up to a change of variables).

As we will see in Lemma 3.5.3, the fact that the torus maps appearing in the cavity problem are smoothly equivalent to a rotation has important consequences for the behavior in time of the the electromagnetic field, in particular for the growth of the energy.

The formal definition of equivalence is the following.

Definition 3.3.4. The torus maps $\mathbf{g} : \mathbb{T}^d \to \mathbb{T}^d$ and $\mathbf{g}' : \mathbb{T}^d \to \mathbb{T}^d$ are *(topologically, C^r, analytically) conjugate* if there exists a (continuous, C^r, analytic) map $\mathbf{h} : \mathbb{T}^d \to \mathbb{T}^d$ such that

$$\mathbf{g} = \mathbf{h}^{-1} \circ \mathbf{g}' \circ \mathbf{h} . \tag{3.19}$$

We note that if two maps are topologically conjugate, then the rotation sets (Definition 3.3.1) of the two maps are the same.

Simplifying somewhat, the main result of standard KAM theory is as follows:

Given any Diophantine vector $\boldsymbol{\omega}_0$ and a family of maps $\mathbf{f}^{\boldsymbol{\lambda}}$ that depends on the d-dimensional parameter $\boldsymbol{\lambda}$, satisfies some non-degeneracy conditions (see below), and is close to the translation $\mathbf{t}_{\boldsymbol{\omega}_0}$, we can find a Cantor set $\mathcal{C} \subset \mathbb{R}^d$ of (Diophantine) frequencies such that for each $\boldsymbol{\omega} \in \mathcal{C}$ we can find a parameter value $\boldsymbol{\lambda}(\boldsymbol{\omega})$ (which depends on $\boldsymbol{\omega}$) such that the map $\mathbf{t}^{\boldsymbol{\lambda}(\boldsymbol{\omega})}$ is smoothly conjugate to the translation by the vector $\boldsymbol{\omega}$. The degree of smoothness of the conjugacy depends on the degree of smoothness of the maps and the Diophantine exponent of $\boldsymbol{\omega}_0$.

Theorems on stability of translations under these hypotheses can be found in Moser [147, 148], Herman [94], Arnol'd [4]. A pedagogical exposition of these and other KAM theorems can be found in de la Llave [130].

Remark 3.3.9. The reason why we need a d-dimensional parameter $\boldsymbol{\lambda}$ is to be able to adjust the frequency change due to the perturbation. For example, the translation $\mathbf{t}_{\boldsymbol{\omega}_0 + \boldsymbol{\Delta}}$ cannot be conjugated to $\mathbf{t}_{\boldsymbol{\omega}_0}$ no matter how small $\boldsymbol{\Delta}$ is. The problem of lack of parameters is discussed in the book of Moser [149, Section V.4]; for recent developments see Sevryuk [178] and de la Llave [130].

A precise definition of the non-degeneracy assumption in the standard KAM theory is that the function

$$\boldsymbol{\varphi}(\boldsymbol{\lambda}) := \int_{\mathbb{T}^d} \left[\mathbf{f}^{\boldsymbol{\lambda}}(\boldsymbol{\xi}) - \boldsymbol{\xi} \right] \, d\boldsymbol{\xi} \tag{3.20}$$

satisfies

$$\det D\boldsymbol{\varphi}(\mathbf{0}) \neq 0 \, . \tag{3.21}$$

More geometrically, we require that $D\boldsymbol{\varphi}(\mathbf{0})$ has full range.

When the nondegeneracy assumption (3.21) is satisfied, by adjusting the parameters one can make sure that the rotation vector is kept at the value we want.

Another problem considered in KAM theory is estimating the measure of the set of parameters for which there exists a conjugacy between $\mathbf{f}^{\boldsymbol{\lambda}}$ and a rotation. This is particularly relevant for our applications since the measure of the set of parameters relates to the observability of the phenomena. A positive

(or large) measure of parameters will indicate that, picking parameter values at random, there is a (good) chance of observing the phenomena.

Unfortunately, the standard results of KAM theory do not apply for the maps of the form (3.12) appearing in the quasiperiodic cavity problem.

There are three reasons for this: one is that KAM theory does not apply straightforwardly to maps of the form (3.12) since the function $\boldsymbol{\varphi}$ defined in (3.20) has one dimensional range (in the direction of $\boldsymbol{\omega}$). Hence, $D\boldsymbol{\varphi}(\boldsymbol{\lambda})$ has range contained in a one dimensional vector space.

As a second difficulty in our situation, we note that the parameters that appear in the problem (3.5), (3.6) are 1-dimensional rather than d-dimensional as required by standard KAM theory. Hence, we are considering one-parameter families of maps of the form (3.12).

Finally, we note that the families of maps that appear in the resonant cavity problem are also rather specialized in the class of maps of the form (3.12). As we see below, families of maps of the form (3.9), which appear naturally in the study of the cavity are more degenerate than the general maps of the form (3.12).

More explicitly, if we consider a system with the motion of the wall being a small perturbation of a constant, i.e., $\Phi(\boldsymbol{\Xi}) = \frac{\alpha}{2} + \lambda b(\boldsymbol{\Xi})$ (cf. (3.5), (3.6)), then we have for small λ

$$\mathbf{G}^{\lambda}(\boldsymbol{\Xi}) = \boldsymbol{\Xi} + \alpha\boldsymbol{\omega} + \lambda\left[-b(\boldsymbol{\xi} + \tfrac{\alpha}{2}\boldsymbol{\omega}) + b(\boldsymbol{\xi})\right] + O(\lambda^2) . \qquad (3.22)$$

Since $\int_{\mathbb{T}^d}[-b(\boldsymbol{\xi} + \frac{\alpha}{2}\boldsymbol{\omega}) + b(\boldsymbol{\xi})]\,d\boldsymbol{\xi} = \mathbf{0}$, we obtain that for the families (3.9) we have that $D\boldsymbol{\varphi}(\mathbf{0}) = \mathbf{0}$, which is a more severe degeneracy than even that of a typical foliation-preserving map (3.12).

The application of KAM theory to one dimensional parameter foliation preserving families of maps, which may be degenerate as above (but which satisfy other weaker non-degeneracy conditions), is developed by de la Llave and Vano [134]. This reference also contains estimates on the measure of the parameters for which KAM theorem applies. In what follows, we will summarize the results of this paper.

We recall that a family $\mathbf{f}^\lambda$ of mappings is said to be a C^r family when $\mathbf{f}^\lambda(\boldsymbol{\xi})$ is a C^r function of both $\boldsymbol{\xi}$ and λ. (i.e., that it has continuous mixed derivatives of order up to r with respect to either $\boldsymbol{\xi}$ or λ).

Theorem 3.3.1. *Let $\boldsymbol{\omega}_0 \in \mathbb{R}^d$ be an affine Diophantine vector of exponent ν. Let $\mathbf{f}^\lambda$ be a one-parameter C^r family of foliation-preserving mappings as in (3.12) such that $\mathbf{f}^0 = \mathbf{t}_{\boldsymbol{\omega}_0}$.*

Assume that the function $\tilde{\varphi}$ defined by $\tilde{\varphi}(\lambda)\boldsymbol{\omega}_0 = \int_{\mathbb{T}^d}[\mathbf{f}^\lambda(\boldsymbol{\xi}) - \boldsymbol{\xi}]\,d\boldsymbol{\xi}$ satisfies

$$\frac{d^N}{d\lambda^N}\tilde{\varphi}(\lambda)|_{\lambda=0} \neq 0$$

for some positive $N < r$. Assume also that the regularity r is large enough depending on the Diophantine exponent of $\boldsymbol{\omega}_0$.

Then, there is a set $\mathcal{B} \subset [-1, 1]$ such that:

99

a) *For $\lambda \in \mathcal{B}$, $\mathbf{f}^\lambda$ is conjugate to the translation $\mathbf{t}_{u(\lambda)\boldsymbol{\omega}_0}$, i.e., there exists a diffeomorphism $\mathbf{h}^\lambda$ of the torus such that*

$$\mathbf{f}^\lambda = (\mathbf{h}^\lambda)^{-1} \circ \mathbf{t}_{u(\lambda)\boldsymbol{\omega}_0} \circ \mathbf{h}^\lambda \ . \tag{3.23}$$

b) *For some $C > 0$, and for all sufficiently small $\delta > 0$*

$$|[-\delta, \delta] \cap \mathcal{B}^c| \leq C\delta^{1/N} \ ,$$

where $|\ |$ denotes the Lebesgue measure, and $\mathcal{B}^c$ is the complement of $\mathcal{B}$.

In typical situations, the set $\mathcal{B}$ is a Cantor set (i.e., it is a totally disconnected closed set).

Remark 3.3.10. Note that a corresponding result for higher-dimensional parameters can be obtained from the one-dimensional case by decomposing the several-parameter family into several one-parameter families and repeatedly applying the one dimensional result.

Remark 3.3.11. The results of de la Llave and Vano [134] also include that the maps $\lambda \mapsto \mathbf{h}^\lambda$ and $\lambda \mapsto u(\lambda)$ can be extended to C^s functions on $[-1, 1]$ where s is a number that depends on r and the Diophantine exponent ν. (Of course, the extended family will only satisfy (3.23) when $\lambda \in \mathcal{B}$.) This is sometimes referred to as saying that the function $\mathbf{h}^\lambda$ is *differentiable in the sense of Whitney* since Whitney [194] gave an intrinsic characterization of functions defined in closed sets that can be extended to smooth functions.

Numerical explorations in Section 3.4 indicate that in the intervals of the complement of $\mathcal{B}$ (i.e., in the gaps of $\mathcal{B}$) one often has dynamics with negative Lyapunov exponent. Of course, this observation could be false for situations not covered by our numerical experiments, in particular for very Liouville rotation vectors (see Fayad [70]).

3.3.6 Structure of $D\mathbf{g}$, Lyapunov Exponents, and Hyperbolicity

An important measure of instability of a map $\mathbf{f} : \mathbb{T}^d \to \mathbb{T}^d$ is its *Lyapunov exponent* defined by

$$\mu(\boldsymbol{\xi}, \mathbf{v}) := \lim_{n \to \infty} \frac{1}{n} \log \| D\mathbf{f}^n(\boldsymbol{\xi}) \, \mathbf{v} \| \, . \tag{3.24}$$

We recall that, by Oseledets theorem [157] (see also Ruelle [175] and Barreira and Pesin [9]), the limits in (3.24) exist for all $\mathbf{v}$ and m-almost all $\boldsymbol{\xi}$ for any $\mathbf{f}$-invariant Borel measure m. It is clear that for every $\boldsymbol{\xi}$, there are at most d possible values of the limit in (3.24).

Lyapunov exponents are a rather weak notion of exponential growth of perturbations (or decay if they are negative). In particular, they ignore polynomial growth, and can be reached non-uniformly, i.e., at different rate for different points $\boldsymbol{\xi}$.

A notion which in principle is stronger than the existence of a positive Lyapunov exponent is that of uniform hyperbolicity. In our case, since we only have one direction with non-trivial expansion, this notion reduces to the following:

Definition 3.3.5. We say that a set $\mathcal{L} \subset \mathbb{T}^d$ invariant by $\mathbf{f}$ as in (3.9) is *uniformly attracting* (respectively *uniformly expanding*) when there exist constants $C > 0$, $\alpha > 0$, such that we can find a splitting $T_{\boldsymbol{\xi}}\mathbb{T}^d = (\mathrm{span}\,\boldsymbol{\omega}) \oplus E_{\boldsymbol{\xi}}^s$ (respectively $T_{\boldsymbol{\xi}}\mathbb{T}^d = (\mathrm{span}\,\boldsymbol{\omega}) \oplus E_{\boldsymbol{\xi}}^u$) such that

$$\|D\mathbf{f}^n(\boldsymbol{\xi})\,\mathbf{v}\| \leq Ce^{-\alpha n}\|\mathbf{v}\|\,, \quad \forall\, n \in \mathbb{N}\,, \quad \boldsymbol{\xi} \in \mathcal{L}\,, \quad \mathbf{v} \in E_{\boldsymbol{\xi}}^s$$

$$(\text{ resp. } \|D\mathbf{f}^n(\boldsymbol{\xi})\,\mathbf{v}\| \geq Ce^{\alpha n}\|\mathbf{v}\|\,, \quad \forall\, n \in \mathbb{N}\,, \quad \boldsymbol{\xi} \in \mathcal{L}\,, \quad \mathbf{v} \in E_{\boldsymbol{\xi}}^s\,)\,.$$

These general notions can be made more precise for foliation-preserving maps. Notably, all but one of their Lyapunov exponents are zero.

Proposition 3.3.2. *Let* $\mathbf{g}$ *be a* $C^1 : \mathbb{T}^d \to \mathbb{T}^d$ *map foliation-preserving map of the form* (3.12)*. Then for every point* $\boldsymbol{\xi} \in \mathbb{T}^d$, $d-1$ *of the Lyapunov exponents of* $\mathbf{g}$ *are 0. Beside these* $d-1$ *trivial exponents, for* m-*almost every* $\boldsymbol{\xi}$, *there is one Lyapunov exponent corresponding to the direction of* $\boldsymbol{\omega}$.

Proof. For foliation preserving maps $\mathbf{g}$,

$$D\mathbf{g}(\boldsymbol{\xi})\,\boldsymbol{\omega} = [1 + \boldsymbol{\omega} \cdot \nabla\Gamma(\boldsymbol{\xi})]\,\boldsymbol{\omega} := \lambda(\boldsymbol{\xi})\,\boldsymbol{\omega}\,. \tag{3.25}$$

Let us choose a system of (affine) coordinate patches of $\mathbb{T}^d$ in the following way: Choose an orthonormal frame $\mathbf{v}_1, \ldots, \mathbf{v}_d$ in $\mathbb{R}^d$ in such a way that $\mathbf{v}_1 = \boldsymbol{\omega}$. Let U be the orthogonal matrix that transforms the standard basis of $\mathbb{R}^d$ into $\mathbf{v}_1, \ldots, \mathbf{v}_d$. Define the charts $\boldsymbol{\psi}_i : B_{1/10} \to \mathbb{T}^d$ (where $B_{1/10}$ is the ball of radius $\frac{1}{10}$ around the origin in $\mathbb{R}^d$) by

$$\boldsymbol{\psi}_i(\mathbf{x}) = \boldsymbol{\pi}(U\mathbf{x} + \mathbf{t}_i)\,, \tag{3.26}$$

102

where $\boldsymbol{\pi}$ is given by (3.7), and $\{\mathbf{t}_i\}$ is a finite set of translations in a grid of size, say, $\frac{1}{100}$, to ensure that the union $\cup_i \psi_i(B_{1/10})$ cover the whole $\mathbb{T}^d$. Then in all coordinate patches, the differential $D\mathbf{g}(\boldsymbol{\xi})$ has the form

$$
D\mathbf{g}(\boldsymbol{\xi}) = U^{-1}
\begin{pmatrix}
\lambda(\boldsymbol{\xi}) & * & * & \cdots & * \\
0 & 1 & 0 & \cdots & 0 \\
0 & 0 & 1 & \cdots & 0 \\
\vdots & \vdots & \vdots & \ddots & \vdots \\
0 & 0 & 0 & \cdots & 1
\end{pmatrix}
U \ ,
\tag{3.27}
$$

where the stars represent numbers that are nonzero in general. Hence, the differential of the iterated map, $D\mathbf{g}^n(\boldsymbol{\xi})$, after conjugating with U, is also upper triangular with the first element in the diagonal equal to $\lambda(\mathbf{g}^{n-1}(\boldsymbol{\xi})) \cdots \lambda(\boldsymbol{\xi})$, and all other diagonal terms equal to 1. This makes it clear that $d-1$ Lyapunov numbers are equal to 0.

According to Birkhoff ergodic theorem,

$$
\frac{1}{n} \log \left[\lambda(\mathbf{g}^{n-1}(\boldsymbol{\xi})) \cdots \lambda(\boldsymbol{\xi}) \right] = \frac{1}{n} \left[\log \lambda(\mathbf{g}^{n-1}(\boldsymbol{\xi})) + \cdots + \log \lambda(\boldsymbol{\xi}) \right]
$$

has a limit as $n \to \infty$ for m-almost every $\boldsymbol{\xi}$, for any $\mathbf{g}$-invariant probability measure m. This limit is, of course, another Lyapunov exponent besides the previously found $d-1$ equaling zero. $\qquad\square$

In particular, the differential $D\mathbf{g}$ of the torus map $\mathbf{g}$ (3.9) is

$$
D\mathbf{g}(\boldsymbol{\xi}) = \left[\mathrm{Id} - \boldsymbol{\omega} \otimes \nabla\Phi(\mathbf{g}(\boldsymbol{\xi})) \right]^{-1} \left[\mathrm{Id} + \boldsymbol{\omega} \otimes \nabla\Phi(\boldsymbol{\xi}) \right] \ .
\tag{3.28}
$$

Therefore,

$$
D\mathbf{g}(\boldsymbol{\xi})\,\boldsymbol{\omega} = \lambda(\boldsymbol{\xi})\boldsymbol{\omega} \ ,
$$

103

where

$$\lambda(\boldsymbol{\xi}) := \frac{1 + \boldsymbol{\omega} \cdot \nabla\Phi(\boldsymbol{\xi})}{1 - \boldsymbol{\omega} \cdot \nabla\Phi(\mathbf{g}(\boldsymbol{\xi}))} \ . \tag{3.29}$$

Hence,

$$D\mathbf{g}^n(\boldsymbol{\xi})\,\boldsymbol{\omega} = \lambda(\mathbf{g}^{n-1}(\boldsymbol{\xi})) \cdots \lambda(\boldsymbol{\xi})\,\boldsymbol{\omega} \ ,$$

so the Lyapunov exponent in the direction of $\boldsymbol{\omega}$ is equal to the average of the logarithm of λ along the orbit of $\boldsymbol{\xi}$, and the other $d-1$ Lyapunov exponents are equal to 0.

Uniformly attracting or uniformly repelling sets have some remarkable properties. For example, the general theory of persistence of normally hyperbolic sets (Hirsch and Pugh [97], Fenichel [72]) implies, for our case, the following theorem.

Theorem 3.3.3. *Let* $\mathbf{g}$ *be a map of the form* (3.12).

Assume that there exists a compact set $\mathcal{L} \subset \mathbb{T}^d$ *invariant under* $\mathbf{g}$ *such that*

   (i) $\mathcal{L}$ *is a* C^1 *manifold without boundary;*

   (ii) $\mathcal{L}$ *is transversal to* $\operatorname{span}\boldsymbol{\omega}$ *at each point:* $T_{\boldsymbol{\xi}}\mathcal{L} \oplus \operatorname{span}\boldsymbol{\omega} = \mathbb{R}^d$;

   (iii) $\mathbf{g}|_{\mathcal{L}}$ *is uniformly attracting (respectively repelling).*

Then, for any torus map $\mathbf{g}'$ *sufficiently* C^1-*close to* $\mathbf{g}$, *we can find a set* $\mathcal{L}'$, *invariant under* $\mathbf{g}'$ *and satisfying (i), (ii) and (iii).*

The existence of these invariant manifolds for maps of the form (3.12) is an analogue of the phase locking which happens frequently in torus maps.

Theorem 3.3.3 is interesting from our point of view because its hypotheses are verified on open sets of parameters (we will argue that these sets are non-empty and will discuss their abundance in numerical exploration) and, at the same time, they have important consequences for the behavior of the electromagnetic field in the cavity.

3.3.7   Resonances

Resonances are a generalization of the phase locking encountered in circle maps with rational rotation numbers, when the circle map has an attracting or repelling periodic point. Recall that the origin of the phase locking is that, by the implicit function theorem, these periodic points persist, hence the rotation number remains constant for small enough perturbations of the map. For higher dimensional tori, there are analogous phenomena, but the geometry is significantly more complicated.

Definition 3.3.6. We say that a rotation vector $\boldsymbol{\omega}$ is $(\mathbf{k}, n)$-*resonant* (for $\mathbf{k} \in \mathbb{Z}^d \setminus \{\mathbf{0}\}$, $n \in \mathbb{Z}$) if

$$\mathbf{k} \cdot \boldsymbol{\omega} = n \ .$$

The set of $(\mathbf{k}, n)$-resonant vectors is a hyperplane of codimension one in the space of frequencies. Hence, given a vector $\boldsymbol{\omega}_0$ that is incommensurate (and, therefore, not perpendicular to any $\mathbf{k} \in \mathbb{Z}^d \setminus \{\mathbf{0}\}$), we can find $t \in \mathbb{R}$ such that $t\boldsymbol{\omega}_0$ is $(\mathbf{k}, n)$-resonant.

The intuition is that rotations by resonant vectors are unstable under perturbations since KAM theorem does not apply to them. Note that, when one tries to eliminate the perturbations from a rotation one is lead to denominators of the form $e^{2\pi i \mathbf{k} \cdot \boldsymbol{\omega}} - 1$. Hence, if ω is $(\mathbf{k}, n)$-resonant, we are lead to terms that cannot be eliminated from the perturbation.

Galkin [77] have studied the width of the resonant regions for a particular type of torus maps.

We plan to study rigorously the resonances for torus maps occurring in the cavity problem in near future.

3.4 Numerical Study of the Resonance Regions

In this section we show the results of our numerical investigation of the map $\mathbf{g} : \mathbb{T}^2 \to \mathbb{T}^2$ corresponding to the motion of the boundary given by (3.1), (3.5), (3.6). Unless otherwise specified, in the whole section $\mathbf{g}$ will stand for this particular map.

3.4.1 General Remarks

As we noted in Section 3.3.4, the rotation set of $\mathbf{g}$ must be an interval proportional to the frequency vector $\boldsymbol{\omega}$, which for motion of the mirror given by (3.5), (3.6) is $\boldsymbol{\omega} = (1, \sigma_{\mathrm{G}})$. Based on our numerical investigations, we adopt the working hypothesis that the rotation set for the torus maps in our problem consists only of one element which we call a rotation vector.

For the map (3.5), (3.6), the rotation vector $\boldsymbol{\tau}(\mathbf{g})$ has only one independent component, because it has to be a multiple of $\boldsymbol{\omega}$:

$$\boldsymbol{\tau}(\mathbf{g}) = \rho\boldsymbol{\omega} = \rho\left(1, \sigma_{\mathrm{G}}\right) . \tag{3.30}$$

For reasons that will become clear in Section 3.4.2, we will call the first component, $\tau_1(\mathbf{g}) = \rho\omega_1 = \rho$, of $\boldsymbol{\tau}(\mathbf{g})$ a *rotation number* of the map $\mathbf{g}$. Note that because of the incommensurability of $\boldsymbol{\omega}$ and the condition (3.3), the map $\mathbf{g}$ has no periodic points.

Due to the existence of an invariant foliation $\mathcal{F}_{\boldsymbol{\omega}}$, the problem we have to solve numerically is essentially one-dimensional for any dimension d of the torus. Indeed, let θ_n be the moment of the nth reflection of a particular ray from the moving mirror, and $\boldsymbol{\xi}_n = \boldsymbol{\omega}\theta_n$ be the vector of the phases of the mirror's motion at that moment. To find $\boldsymbol{\xi}_{n+1} = \mathbf{g}(\boldsymbol{\xi}_n)$, we first find the time θ_{n+1} of the $(n+1)$st reflection of this ray from the moving mirror by solving numerically the equation (3.8). To compute θ_{n+1}, we used the zero finding routine ZBRENT from Press *et al* [165] (using long double precision). Having found θ_{n+1}, we compute $\boldsymbol{\xi}_{n+1} = \mathbf{g}(\boldsymbol{\xi}_n)$ from

$$\boldsymbol{\xi}_{n+1} = \boldsymbol{\pi}\left(\boldsymbol{\xi}_n + (\theta_{n+1} - \theta_n)\boldsymbol{\omega}\right) .$$

3.4.2 Distribution of the Iterates on $\mathbb{T}^2$

To hone up our intuition and to make a connection with the case $d = 1$, let us start with the case of the map (3.5) with $\gamma = 0$, in which the phase ξ_2 has no effect on the motion of the mirror, so the dynamics of the map $\mathbf{g}$ can

107

be derived completely from the dynamics of the projection of $\mathbf{g}$ on the ξ_1 axis. If $\pi_1 : \mathbb{T}^2 \to \mathbb{T}^1 : (\xi_1, \xi_2) \mapsto \xi_1$ is the projection onto the ξ_1 axis, then the map $\tilde{g}$ defined by

$$\pi_1 \circ \mathbf{g} = \tilde{g} \circ \pi_1$$

is a circle map.

If $\tilde{g}$ is conjugate to a rotation, then there are two cases:

- If the vector

$$\boldsymbol{\tau}(\mathbf{g}) = (\tau(\tilde{g}),\, \tau(\tilde{g})\sigma_G)$$

  is incommensurate, then the iterates of $\mathbf{g}$ fill $\mathbb{T}^2$ densely.

- If $\boldsymbol{\tau}(\mathbf{g})$ is commensurate of type (m_1, m_2, k) (with $m_2 \neq 0$, because otherwise $\tau(\tilde{g})$ would be rational), then the iterates of any point of $\mathbb{T}^2$ lie on a one-dimensional manifold, which is topologically a circle "wrapped around" $\mathbb{T}^2$ – more precisely, making m_2 turns in ξ_1 direction and $-m_1$ turns in ξ_2 direction.

The other extreme case of a map $\mathbf{g}$ with $\gamma = 0$ is the case when the circle map $\tilde{g}$ is phase locked, $\tau(\tilde{g}) = \frac{p}{q}$ – in this case $\mathbf{g}$ is in $(q, 0, p)$ resonance. As an example, let us consider the map $\tilde{g}$ for $\beta = 0.1$, $\gamma = 0$, in which case the phase locking interval of values of α for which $\tilde{g}$ is phase locked with rotation number $\frac{1}{5}$ is

$$[0.273630763679 \,, 0.275033857936] \, .$$

108

In Figure 3.1 we show 10000 iterates of **g** for $\alpha = 0.273631$, $\beta = 0.1$, $\gamma = 0$; the initial point is circled. Since for these values of the parameters the map **g** is $(5, 0, 1)$-resonant, the iterates accumulate on an attractor consisting of five "vertical" lines.

The case in which the map $\tilde{g}$ is phase locked is of particular interest for us, because the case of a small "incommensurate perturbation" (which for our particular phase advance map **g** corresponds to small values of γ in (3.5)) can be considered as a small perturbation to the "unperturbed" map **g** (by "unperturbed" we mean the map with $\gamma = 0$). The theory of normally hyperbolic systems guarantees that if γ is small enough, the map **g** will remain $(q, 0, p)$-resonant. Examples of this phenomenon will be shown in Section 3.4.3.

3.4.3 Bifurcation Diagrams

To give a rough idea what the resonant zones in the (α, γ) parameter plane look like for fixed $\beta = 0.13$, we show in Figure 3.2 the areas with Lyapunov exponents smaller than -0.03 (the Lyapunov exponents have been calculated for a discrete set of α's and γ's, and if the Lyapunov exponent for given values of α and γ is smaller than the threshold -0.03, the corresponding point is shown as a dot in the picture). The types of some resonances are given in the figure. The resonances of type $(3, 0, 2)$ and $(4, 0, 3)$ come from the $\frac{2}{3}$ and $\frac{3}{4}$ phase lockings of the map **g** with $\beta = 0.13$ and $\gamma = 0$, while the other resonances shown in the figure appear because of the incommensurate forcing.

In Figure 3.3, we show 10000 iterates of the map **g** for parameter values
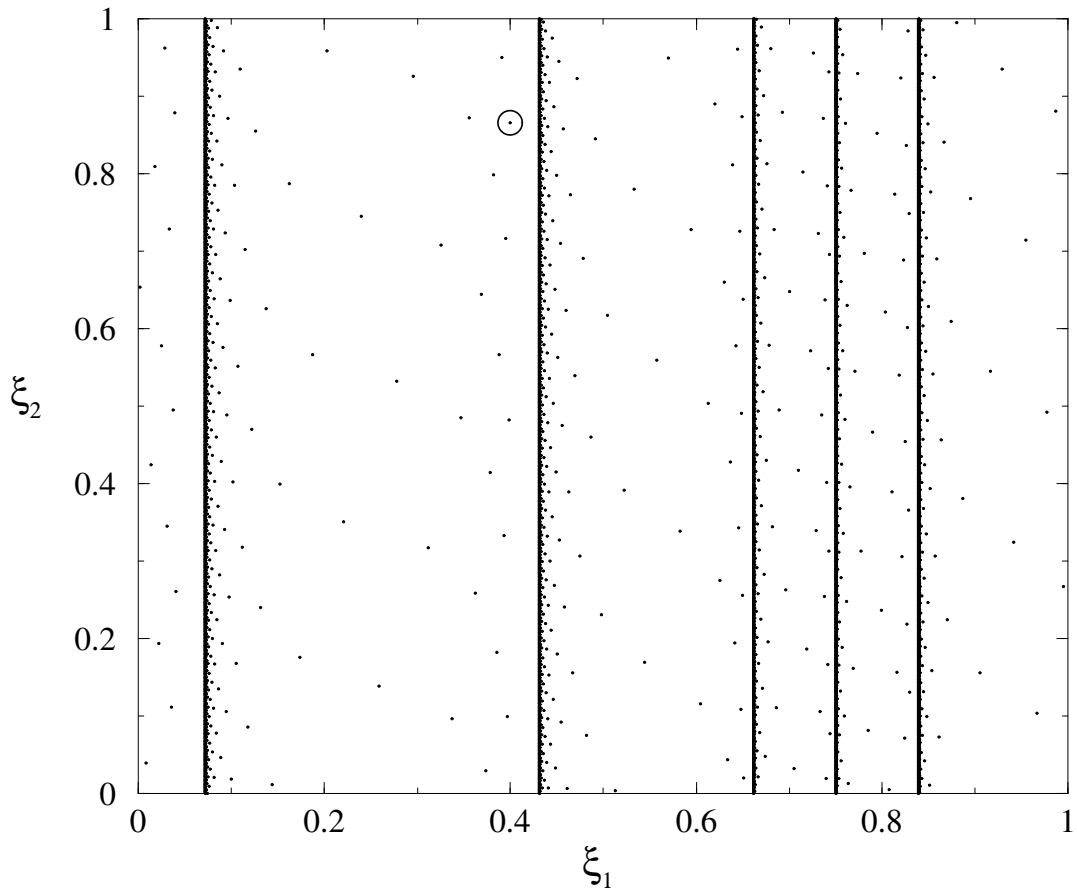
Figure 3.1: Iterates of **g** (with $\gamma = 0$) in the case of $\tau = 1/5$ phase locking with $\gamma = 0$ i.e., $(5, 0, 1)$-resonance.
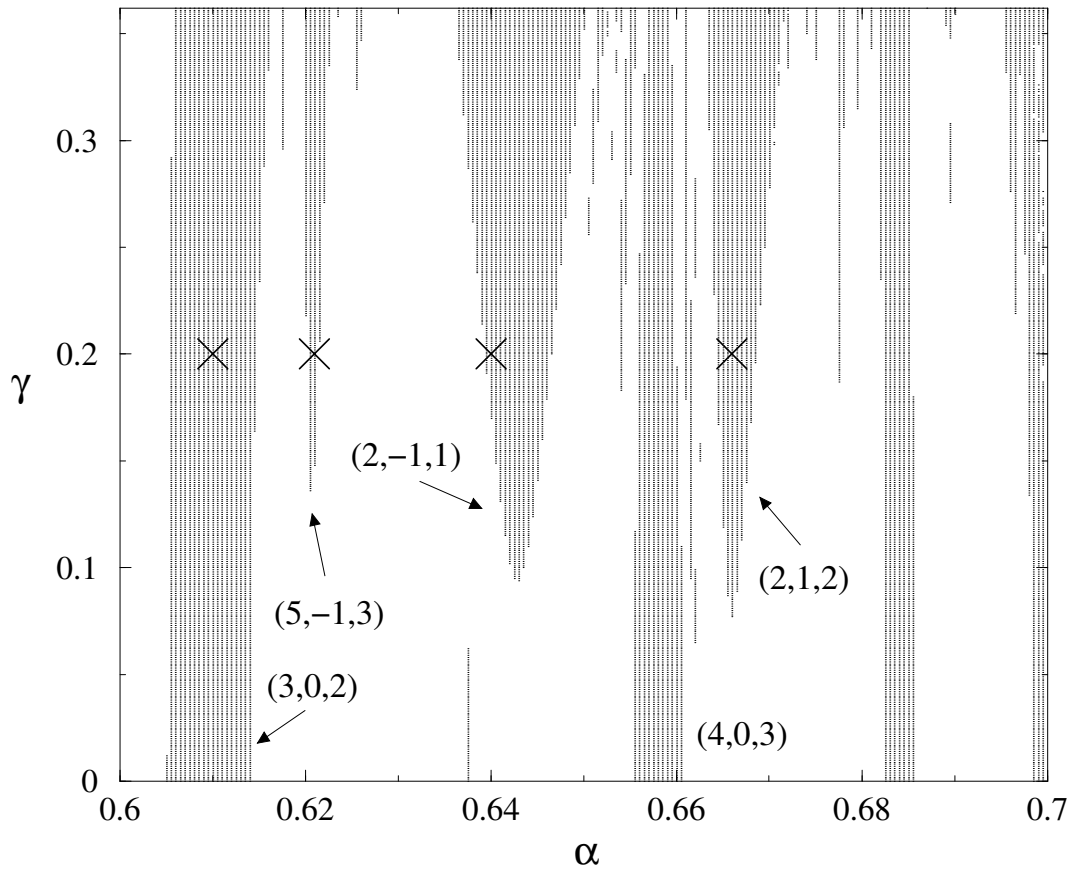
Figure 3.2: Rough sketch of the most intensive phase resonant regions in the (α, γ) plane for $\beta = 0.13$.
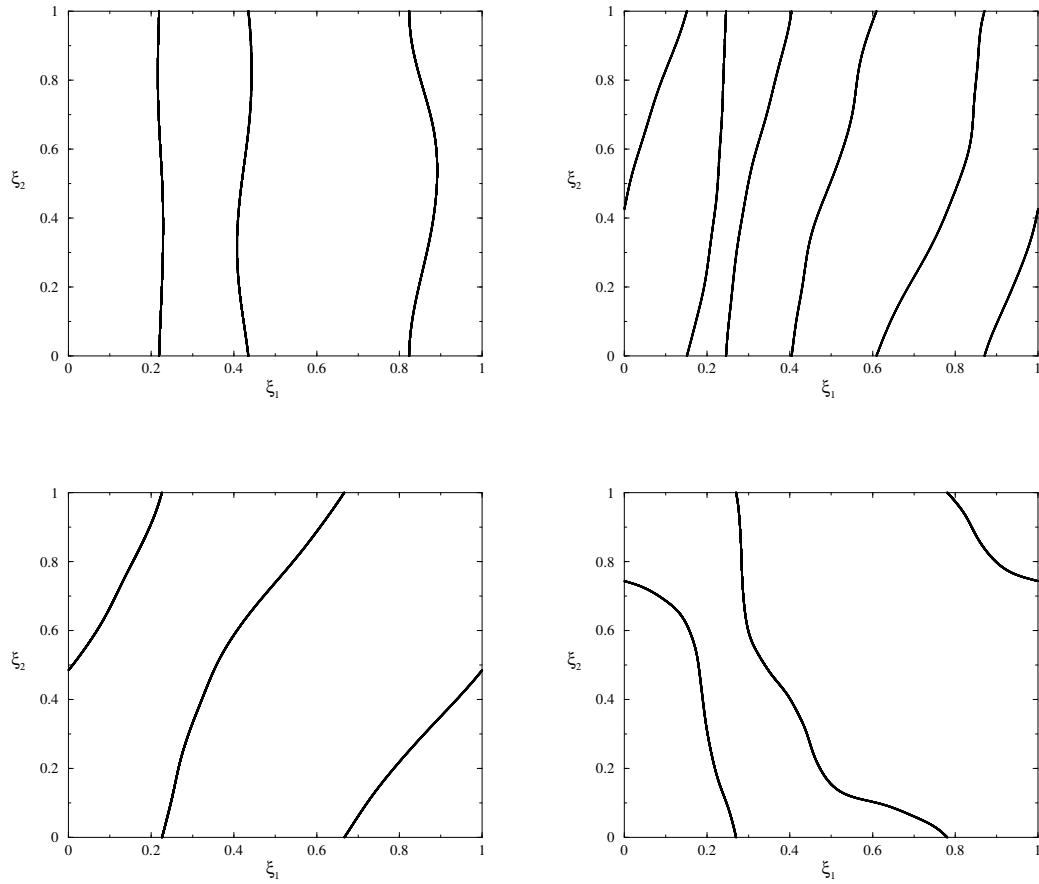
Figure 3.3: Iterates of $(3, 0, 2)$-, $(5, -1, 3)$-, $(2, -1, 1)$-, and $(2, 1, 2)$-resonant maps.

for which the map is $(3, 0, 2)$-, $(5, -1, 3)$-, $(2, -1, 1)$-, and $(2, 1, 2)$-resonant, respectively; the parameters α and γ for these points correspond to the points shown with x's in the figure (the initial point has been first iterated 10^6 times). The values of α are 0.610, 0.621, 0.640, and 0.666, respectively.

In Figure 3.4, we give more detailed information about the Lyapunov exponents of the map $\mathbf{g}$ for $\beta = 0.13$ for the same range of α and γ as in Fig-

ure 3.2. The blue color corresponds to Lyapunov exponents with the smallest absolute value, the green one to the intermediate values, and the red one to the largest values.

To give a better idea about how rich the structure of the (α, γ) plane is, we show in Figure 3.5 iterates of the map **g** for the same values of β and γ ($\beta = 0.13$, $\gamma = 0.2$) and different values of α. The values of α are very close to the value of α for the $(2, -1, 1)$-resonant map from Figure 3.3. The values of α and the type of resonance are shown in the table; for $\alpha = 0.6389$, the map is $(2, -1, 1)$-resonant as in the lower left corner of Figure 3.3.

Figure	α	ρ	Resonance type
3.5 (upper left)	0.6387	$0.72192451\dots$	$(53, -23, 28)$
3.5 (upper right)	0.6386	$0.72125379\dots$	$(37, -15, 20)$
3.5 (lower left)	0.6385	$0.72074231\dots$	Non-resonant
3.5 (lower right)	0.6384	$0.72025004\dots$	$(25, -9, 14)$

Even resonances with small m_1, m_2, and k, can occur for very close values of the parameters – e.g., the $(4, 3, 4)$ and $(5, -1, 3)$ resonances for the map **g** occur for

$$\rho = \frac{4}{4 + 3\sigma_G} = 0.683281572999747\dots$$

$$\rho = \frac{3}{5 - \sigma_G} = 0.684624205732747\dots ,$$

respectively (where the meaning of ρ is the same as in (3.30)).

3.4.4 "Pinching" of the Resonant Regions

In Figure 3.6 we show the domain of the values of the parameters α and γ for which the map **g** is $(5, 0, 1)$-resonant with $\beta = 0.1$. As we see
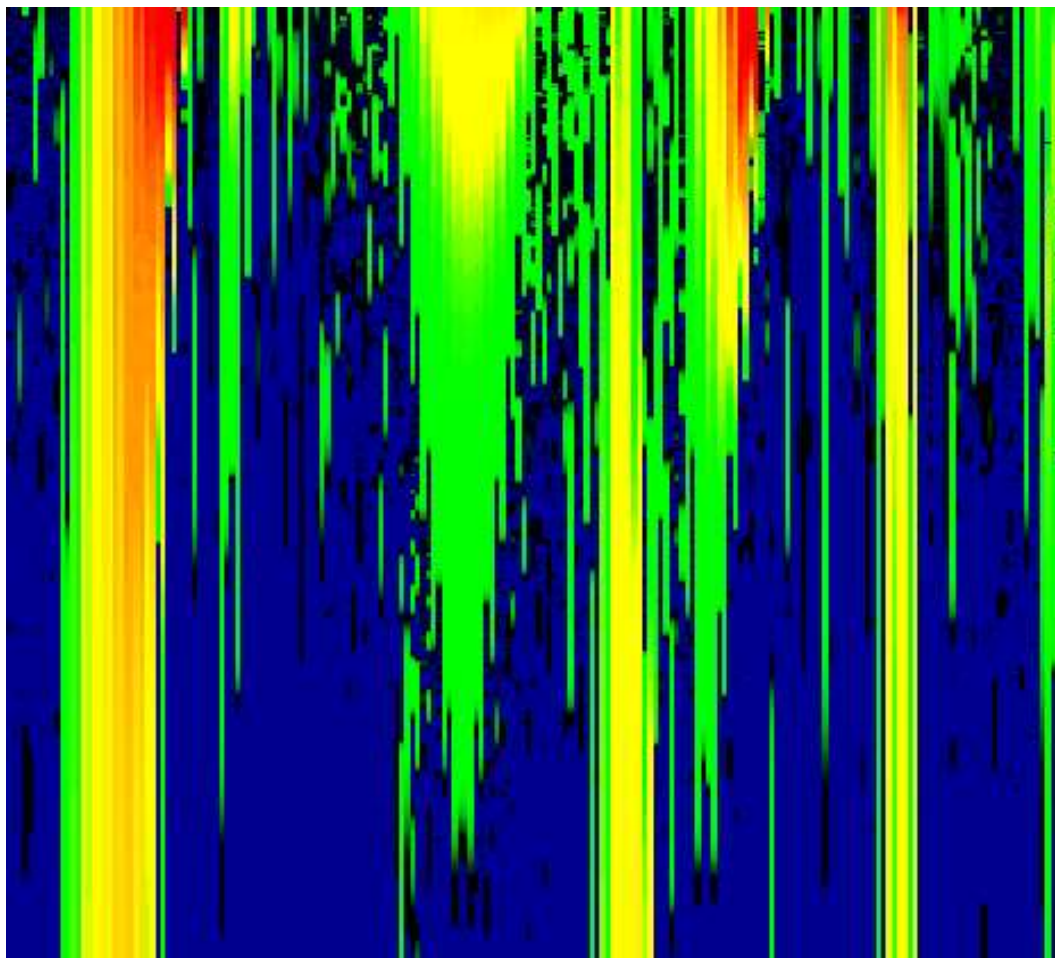
Figure 3.4: Lyapunov exponents of the map **g** for $\beta = 0.13$ in the (α, γ)-plane for $\alpha \in [0.6, 0.7]$ (on the horizontal axis), and $\gamma \in [0, 0.362]$ (on the vertical axis).
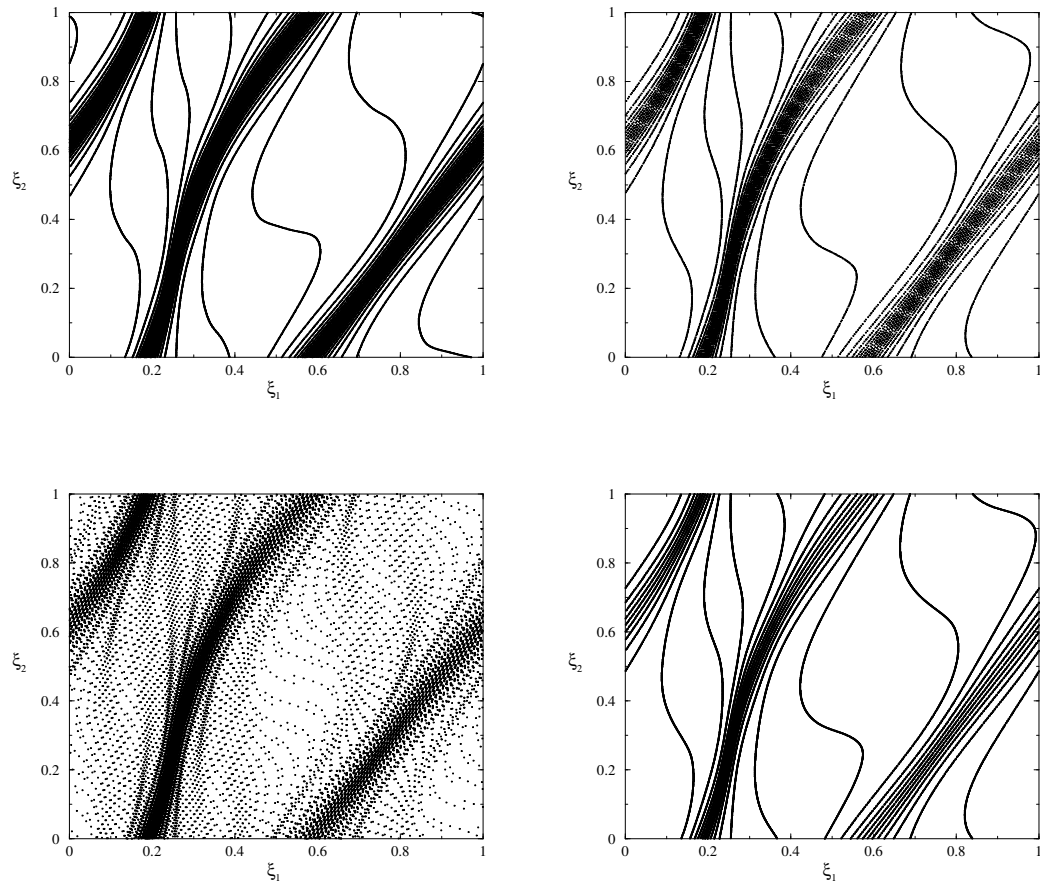
Figure 3.5: Iterates of **g** for close values of the parameter α (all for $\beta = 0.13$, $\gamma = 0.2$). Clockwise, from top left: $\alpha = 0.6387$ – $(53, -23, 28)$-resonance, $\alpha = 0.6386$ – $(37, -15, 20)$-resonance, $\alpha = 0.6385$ – nonresonant, $\alpha = 0.6384$ – $(25, -9, 14)$-resonance.
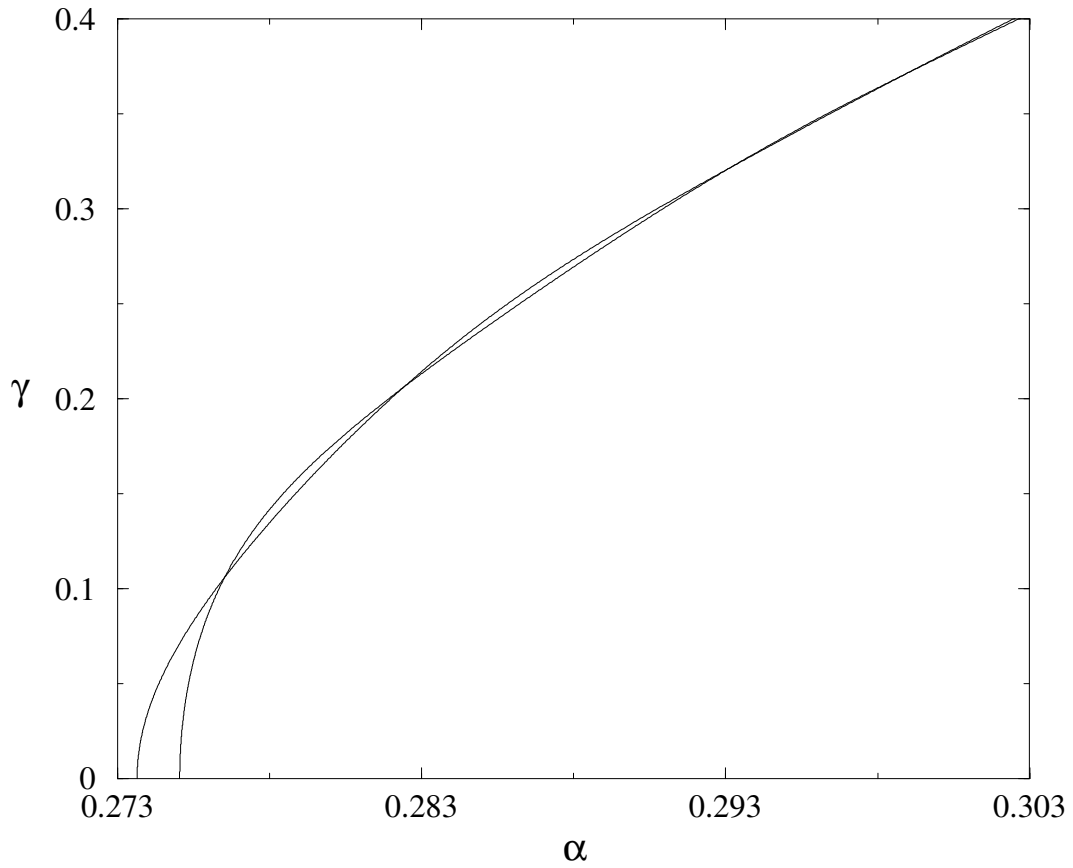
Figure 3.6: Boundaries of the $\beta = 0.1$, $(5, 0, 1)$-resonant region in the (α, γ) plane.

116
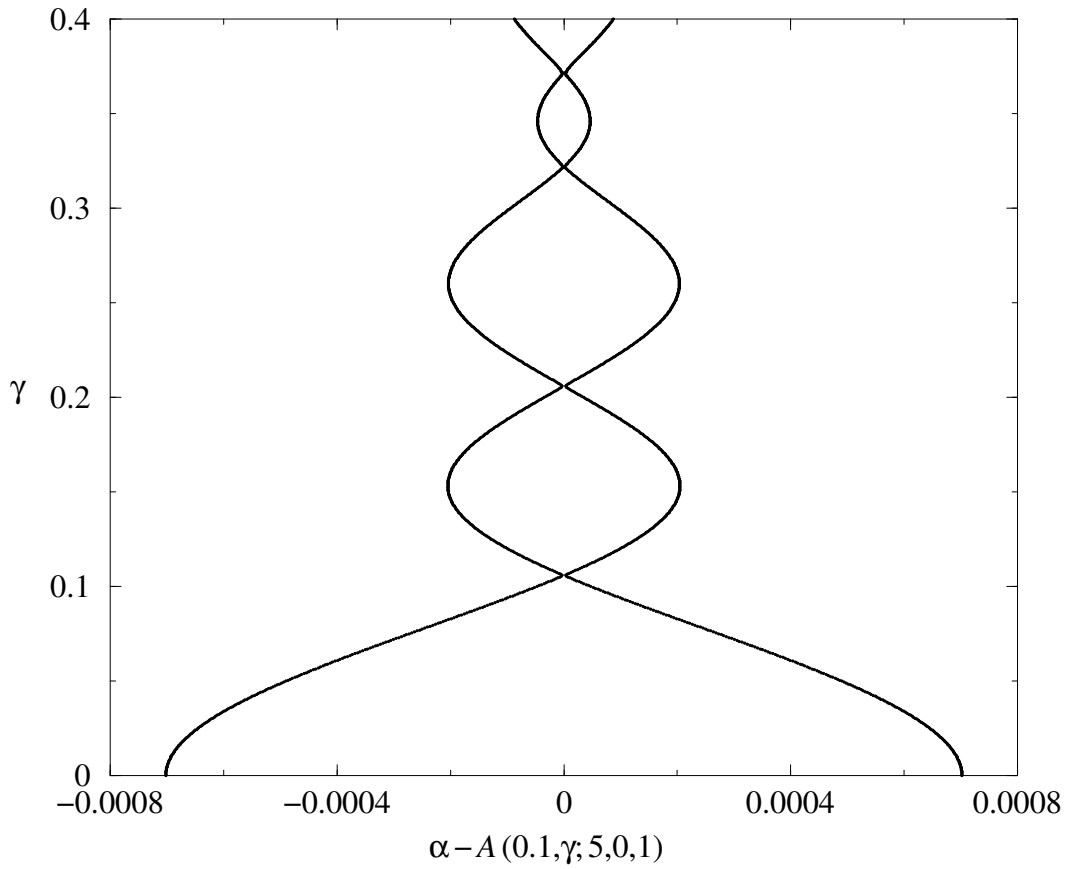
Figure 3.7: "Magnified" plot of the resonant domain shown in Figure 3.6 – the domain is "straightened out" and expanded around its center line.

in the figure, the width of the interval of values of α for which the $(5, 0, 1)$-resonance occurs depends on the amplitude of the incommensurate forcing of the mirror (which for the map $\mathbf{g}$ is $\beta\gamma$). For certain values of γ, the width of this phase locking domain becomes very small. To illustrate this phenomenon better, in Figure 3.7 we show the same phase locked region as in Figure 3.6, but "magnified", i.e., expanded proportionally around the "center line"; here

117

$A(\beta, \gamma; m_1, m_2, k)$ is the average of the two extreme values of α for which the map **g** is (m_1, m_2, k)-resonant for the particular values of β and γ. Our numerical study shows that the width of the phase locked domain when "pinching" occurs is smaller than 10^{-9}, but we cannot say whether the "pinching" there is complete, i.e., whether the width of the phase-locked domain in the (α, γ) plane becomes zero. The article of Glendinning *et al* [81] contains a study of the structure of the phase locked regions of another quasiperiodically forced circle map.

"Pinching" does not occur for some resonances, for example for the $(3, 0, 2)$-resonance domain shown in Figure 3.2 – the $(3, 0, 2)$-resonance domain even becomes wider for larger values of γ. We do not know the reason for the different behavior of the resonant domains.

3.4.5 Occurrence of Resonances Absent for Periodic Motion of the Mirror

In Section 2.6.3, we emphasized that the family of circle maps occurring in the case of periodically pulsating cavity is non-generic. One of the manifestations of this nongenericity is the absence of phase locking with rotation number $\frac{1}{2}$. To illustrate this phenomenon, we show in Figure 3.8 the $(2, 0, 1)$-resonant domain (in the (α, γ)-plane) for $\beta = 0.1$. Note that in the unperturbed case $(\gamma = 0)$, there is no phase locking with rotation number $\frac{1}{2}$, so the appearance of the $(2, 0, 1)$ resonance for $\gamma > 0$ is due to the incommensurate forcing.
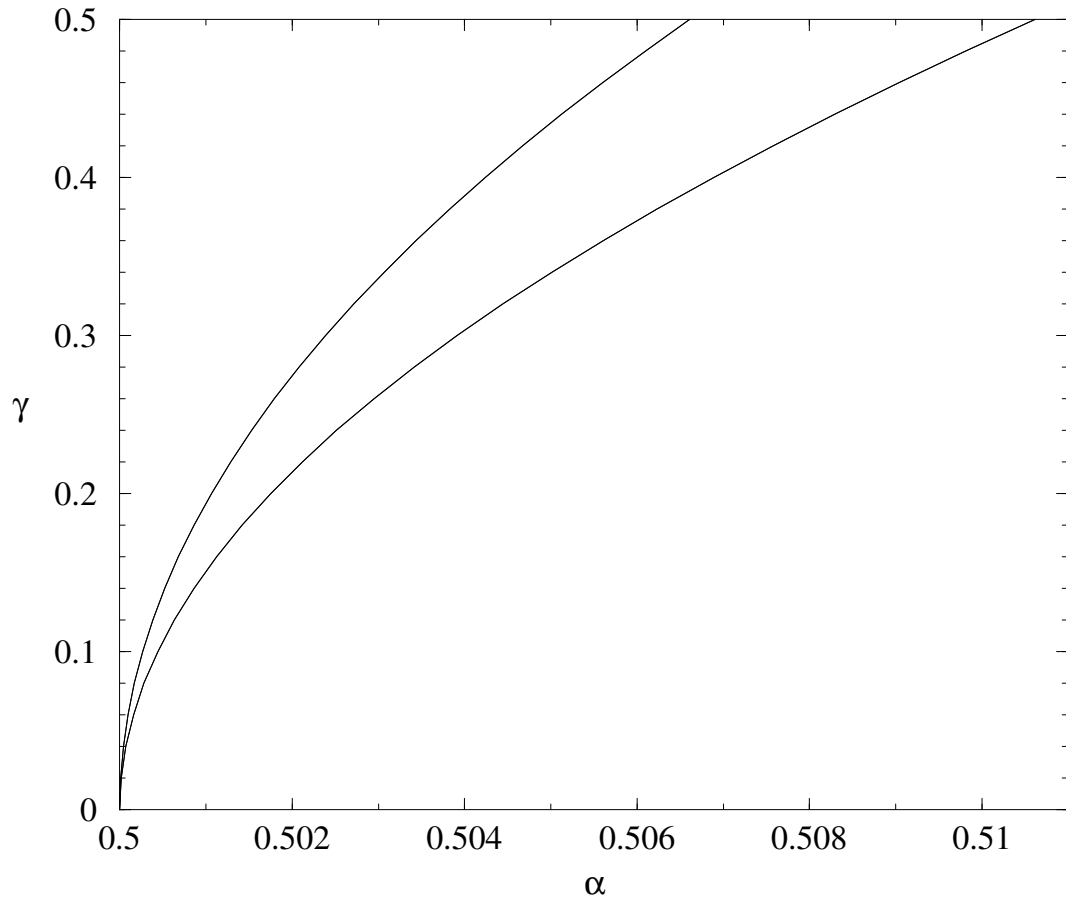
Figure 3.8: An example of a resonance missing in the "unperturbed" case.
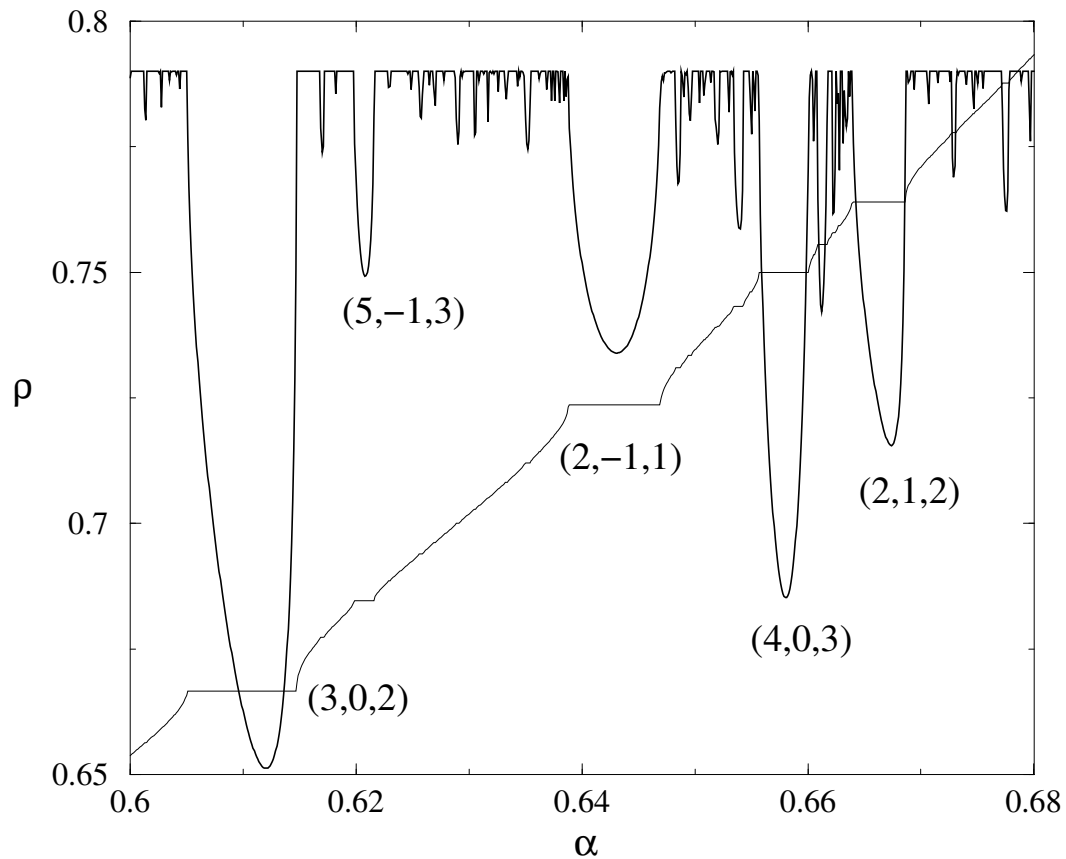
Figure 3.9: Plot of the first component, ρ, of the rotation vector $\boldsymbol{\tau}(\mathbf{g})$, and the Lyapunov exponent of the map $\mathbf{g}$ as functions of α for $\beta = 0.13$, $\gamma = 0.2$.

3.4.6 "Rotation Number" and Lyapunov Exponent

In Figure 3.9, the thin line is the first component, ρ, of the rotation vector $\boldsymbol{\tau}(\mathbf{g})$ (see (3.30)), and the Lyapunov exponent of $\mathbf{g}$ as a function of α for $\beta = 0.13$, $\gamma = 0.2$. The scale on the vertical axis gives the values of ρ. The thick line is the Lyapunov exponent of $\mathbf{g}$ in arbitrary units, and shifted up by 0.79. The types of some resonances are shown. We see that the resonant domains

occur for parameter values for which the Lyapunov exponent is negative. The values of β and γ used to make Figure 3.9 correspond to a horizontal line through the x's in Figure 3.2, and the "strong" resonances visible there can be seen clearly identified in Figures 3.2 and 3.4. Moreover, the resonances of type $(q, 0, p)$ exist in the "unperturbed" $(\gamma = 0)$ case, and in Figure 3.9 we see that they occur at rational values of ρ, namely, for $\rho = \frac{p}{q}$. On the other hand, the resonances that are due to the incommensurate forcing (i.e., of type (m_1, m_2, k) with $m_2 \neq 0$) occur at irrational values of ρ:

$$\rho = \frac{k}{m_1 + m_2 \sigma_G} \notin \mathbb{Q} \ .$$

3.5 Consequences of the Dynamical Systems Phenomena for the Field in the Resonator

In this section we discuss how the dynamical results for torus maps (which were obtained rigorously or found numerically in the previous sections) imply results for the cavity problem.

In Section 3.5.1 we recall briefly the results of Chapter 2 for a periodic motion of the mirror and explain their relation with the case of quasiperiodic motion.

In Section 3.5.2 we derive a simple relationship between the asymptotic behavior of the Doppler factor for the physical system and the Lyapunov exponent of the torus map.

In Section 3.5.3, we explain our method for numerical computation of

the energy density.

In Section 3.5.4 and 3.5.5, we discuss the resonant and the KAM cases, respectively.

In Section 3.5.6, we give a simple physical argument showing that the energy of the electromagnetic field in the cavity cannot decrease asymptotically.

3.5.1 Comparison with the Case of a Periodically Moving Mirror

Let us start by recalling some of the results of Chapter 2 obtained for the case of a periodic motion of the mirror. In the case of phase locking, i.e., if the circle map has an attracting periodic orbit of period q, the characteristics starting in a set of positive measure are attracted to this periodic orbit, so the electromagnetic field concentrates in q (or fewer) pulses of exponentially decreasing width and, hence, exponentially growing energy. Each of these narrow wave packets bounces back and forth between the two mirrors. The motion of the wave packets is asymptotically periodic – if the rotation number of the circle map is $\frac{p}{q}$, then the period of the motion of the wave packets is p.

In contrast, if KAM theory applies and reduces the circle map to a rotation, then the characteristics are well distributed and the electromagnetic field remains uniformly smooth and, hence, the electromagnetic energy remains uniformly bounded in time.

These two results have generalizations for maps of higher dimensional tori and imply results for the cavity pulsating quasiperiodically.

The analogue of the phase locking in the quasiperiodic case is the existence of a commensurate rotation vector with a uniformly attracting invariant torus of positive codimension. If such a lower-dimensional invariant torus exists, the iterates of the torus map quickly concentrate on this torus, and asymptotically the dynamics happens in it (this is illustrated for $d = 2$ in Figure 3.1). The nontrivial eigenvalue of $D\mathbf{g}$, λ (3.29), is negative, and the energy of the system increases exponentially see Section 3.5.2). The only essential difference with the case of a periodically moving mirror is that the motion of the wave packets is quasiperiodic (for more details in this case see Section 3.5.4).

When the KAM theorem applies, the energy of the system stays uniformly bounded in time similarly to the case of a circle map (see Section 3.5.5).

3.5.2 Lyapunov Exponent and Doppler Factor

In Section 2.3.4, we derived the expression (2.16) for the Doppler factor, $\mathcal{D}(\theta)$, at reflection from the moving mirror at time θ. Here we derive an expression of the asymptotic behavior of the rate of change of the energy of the electromagnetic field, which generalizes our treatment in Section 2.5.3.

Let one particular characteristic "ray" be reflected from the moving mirror at times θ_0, θ_1, θ_2, ..., and let $\boldsymbol{\xi}_n := \boldsymbol{\pi}(\boldsymbol{\omega}\theta_n)$ be the vectors of the phases of the mirror's motion at the moments of reflection. By the definition of the corresponding torus map $\mathbf{g}$ (3.10), $\boldsymbol{\xi}_n$ are iterates of $\mathbf{g}$:

$$\boldsymbol{\xi}_n = \mathbf{g}(\boldsymbol{\xi}_{n-1}) = \cdots = \mathbf{g}^n(\boldsymbol{\xi}_0) \ .$$

Using the expression for the nontrivial eigenvalue of $D\mathbf{g}$, λ (3.29) (Section 3.3.6), we obtain for the only nontrivial Lyapunov exponent of $\mathbf{g}$

$$
\begin{aligned}
\Lambda &:= \lim_{N\to\infty} \frac{1}{N} \log \prod_{n=1}^{N} \lambda(\boldsymbol{\xi}_n) \\
&= \lim_{N\to\infty} \frac{1}{N} \log \prod_{n=1}^{N} \frac{1 + \boldsymbol{\omega}\cdot\nabla\Phi(\boldsymbol{\xi}_n)}{1 - \boldsymbol{\omega}\cdot\nabla\Phi(\boldsymbol{\xi}_{n+1})} \\
&= \lim_{N\to\infty} \frac{1}{N} \log \prod_{n=1}^{N} \frac{1 + \boldsymbol{\omega}\cdot\nabla\Phi(\boldsymbol{\xi}_n)}{1 - \boldsymbol{\omega}\cdot\nabla\Phi(\boldsymbol{\xi}_n)} \\
&= -\lim_{N\to\infty} \frac{1}{N} \log \prod_{n=1}^{N} \mathcal{D}(\theta_n) \\
&= -\lim_{N\to\infty} \frac{1}{N} \sum_{n=1}^{N} \log \mathcal{D}(\theta_n) \ .
\end{aligned}
\tag{3.31}
$$

Let the average time interval between two consecutive reflections from the moving mirror be $\langle\Delta\theta\rangle$. This means that asymptotically, in a time interval of length $N\langle\Delta\theta\rangle$, the energy E changes by a factor of $\prod_{n=1}^{N}\mathcal{D}(\theta_n)$. Therefore, in unit time interval, $\log E$ increases on average by

$$
\frac{1}{\langle\Delta\theta\rangle}\frac{1}{N}\log\prod_{n=1}^{N}\mathcal{D}(\theta_n) \approx -\frac{\Lambda}{\langle\Delta\theta\rangle} \ .
$$

Taking all this into account, we obtain

Proposition 3.5.1. *The only nontrivial Lyapunov exponent Λ of the torus map $\mathbf{g}$ is equal to the negative of the averaged over a trajectory logarithm of the Doppler factor at reflection from the moving mirror:*

$$
\begin{aligned}
\Lambda &= -\langle\log\mathcal{D}(\theta_n)\rangle_{\text{averaged over } n} \\
&:= -\lim_{N\to\infty} \frac{1}{N} \sum_{n=1}^{N} \log \mathcal{D}(\theta_n) \ .
\end{aligned}
$$

124

If the initial conditions of the boundary value problem for the vector potential A are continuous, then the asymptotic behavior of the energy of the electromagnetic field is given by

$$E(t) \sim E(0) \exp \left(-\frac{\Lambda}{\langle \Delta \theta \rangle} t \right) \ .$$

3.5.3   Method for Computing the Energy Density

Before we discuss the resonant and the KAM cases in Sections 3.5.4 and 3.5.5, let us explain how we made the pictures of the evolution of a wave packet given in these sections.

The main idea is to employ the methods of geometric optics in order to avoid solving partial differential equations. We used the fact that the energy density of the electromagnetic field is proportional (up to an overall factor) to the spatial density of the characteristics. We took into account that at each reflection the electromagnetic field changes sign, so to find the density of the energy of the field in a small spatial interval $[x_1, x_2]$ at a particular moment t, we subtracted the number of characteristics going through the line connecting the points (t, x_1) and (t, x_2) on the space-time diagram and going to the left from the ones passing through this line and going to the right, and took the absolute value of the difference. We note that this algorithm is very similar to ray tracing in computer graphics and is quite parallelizable.

3.5.4 The Resonant Case

In the case when there exists a uniformly attracting invariant torus, one can make somewhat more precise predictions for the behavior of the electromagnetic field.

Lemma 3.5.2. *Let* **g** *be a map of the form* (3.10) *describing a cavity with quasiperiodically moving boundary as in Section 3.2.2. Assume that* **g** *has an invariant torus* $\mathcal{L}$ *which is uniformly attracting (Definition 3.3.5) with exponent* λ. *Let the initial condition be supported on the basin of attraction of* $\mathcal{L}$.

Then $A(t, x)$ *consists of a pulse of width decreasing exponentially with exponent* λ. *The energy of the pulse is increasing exponentially with the same exponent* λ. *The support of the pulse contains a point which is moving quasiperiodically along the torus* $\mathbb{T}^d$.

Proof. Recall that the map **g** describes the characteristics at the time of collision with the moving boundary. The assumption implies that the characteristics emanating at the support are getting exponentially contracted under the map **g**.

As a consequence, the times of collision with the moving mirror of each of the characteristics are getting also exponentially close from which it follows that the time of collision with the characteristics is concentrated in an interval of exponentially decreasing width.

The argument for the growth of the energy is given in Section 3.5.2. $\square$
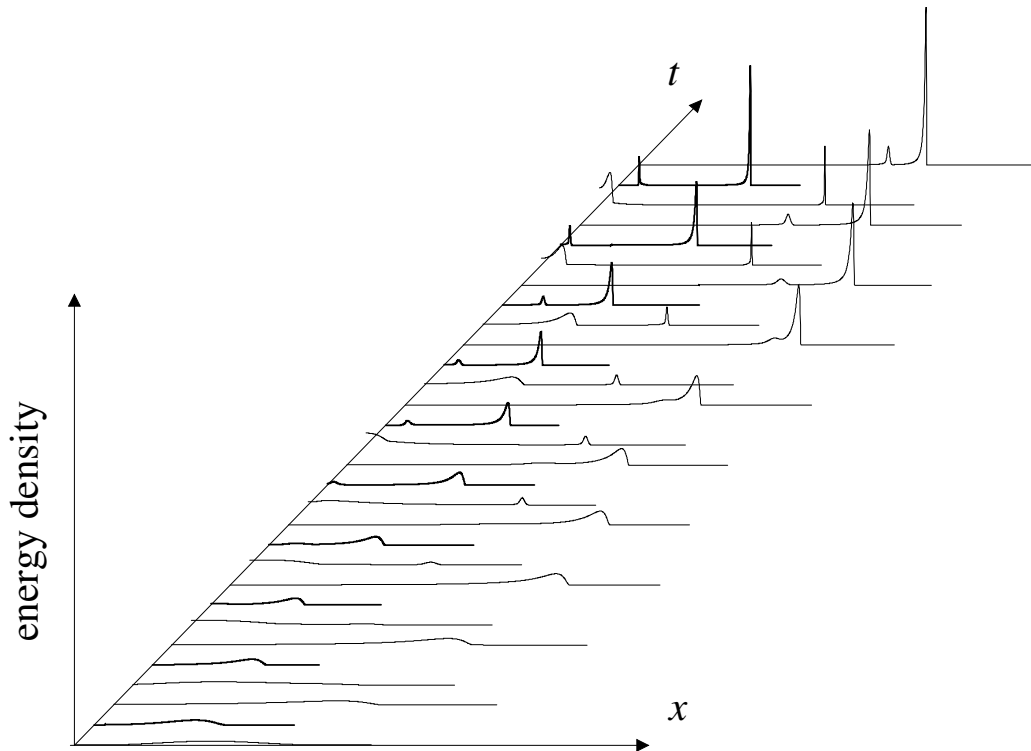
Figure 3.10: Evolution of a wave packet in a $(3, 0, 2)$-resonant case.

From the point of view of direct observations, the above Lemma means that if the hypotheses are met, we will see that the electromagnetic field concentrates in lumps and that the center of the lumps moves quasiperiodically along the cavity (up to an exponentially decreasing error).

In Figure 3.10, we show the evolution of a wave packet in the resonant case. The parameters of the mirror's motion are $\alpha = 0.61$, $\beta = 0.13$, $\gamma = 0.2$ (this point is shown in Figure 3.2), and for these parameter values the torus map $\mathbf{g}$ is $(3, 0, 2)$-resonant. At the initial moment $(t = 0)$, the wave packet was supported on the interval $x \in [0.03, 0.24]$, and was moving to the right.

The figure shows the energy density of the electromagnetic field (in arbitrary units) at times $t = 0$, $\frac{2}{3}$, $\frac{4}{3}$, $\frac{6}{3}$, ..., $\frac{58}{3}$; each third snapshot starting from $t = \frac{2}{3}$ is shown with a thick line. The wave packet splits in two wave packets, and these two wave packets become narrower and higher with time at a rate that is asymptotically exponential. This is especially clear if one looks at the density at the moments shown with thick line. The fact that the associated torus map $\mathbf{g}$ is $(3, 0, 2)$-resonant means that, asymptotically, the motion of the wave packets is such that at some particular moment t the positions of the wave packets is close to their positions at time $t - 2$ (in terms of the torus map, this means that a point from some attractive invariant circle, iterated 3 times, comes to the same invariant circle – see more details below). This is the reason for drawing every third snapshot with a thick line – the elapsed time between two adjacent such snapshots is 2 seconds.

To make Figure 3.10, we used $2^{21} \approx 2 \times 10^6$ rays with initial density corresponding to the initial energy density of the wave packet, and studied their distribution in 2048 bins.

To understand better why the wave packet splits into two wave packets, we show in Figure 3.11 the evolution of the wave packet, depicted as the motion of the iterates of the associated torus map $\mathbf{g}$ in $\mathbb{T}^2$. To produce this figure, we took 22 points,

$$x^{(1)} = 0.03 \; , \quad x^{(2)} = 0.04 \; , \quad x^{(3)} = 0.05 \; , \quad \dots \; , \quad x^{(22)} = 0.24 \; ,$$

equidistributed on the support of the wave packet from Figure 3.10 at the

128
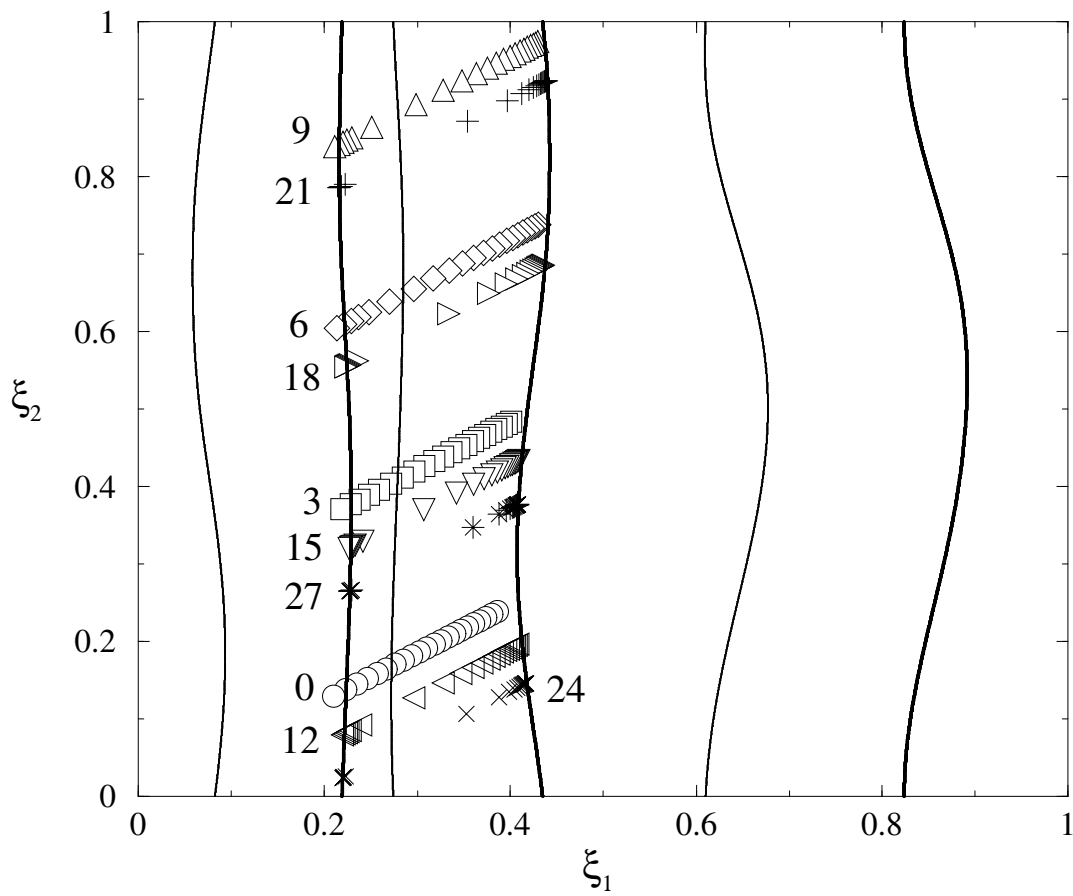
Figure 3.11: Evolution of the wave packet of Figure 3.10, depicted as iterates under $\mathbf{g}^{3n}$ of points from the support of the wave packet at $t = 0$.

initial moment $t = 0$. First we found the times $\theta_0^{(k)}$ ($k = 1$, 2, ..., 22) of the first reflection from the moving mirror of the right-moving characteristic emanating from each point $x^{(k)}$ at $t = 0$, i.e., from the point $(0, x^{(k)})$ in the space-time diagram. These times are represented in the figure by the points $\boldsymbol{\xi}^{(k)} := \boldsymbol{\pi}(\boldsymbol{\omega}\theta_0^{(k)}) \in \mathbb{T}^2$, are depicted as 22 circles with a number 0 to the left of them. Then we illustrated the evolution of these points by showing their 3rd iterates $\mathbf{g}^3(\boldsymbol{\xi}^{(k)})$ (the squares with a number 3 next to them), 6th iterates $\mathbf{g}^6(\boldsymbol{\xi}^{(k)})$ (the diamonds with a 6), 9th iterates $\mathbf{g}^9(\boldsymbol{\xi}^{(k)})$ (the triangles with a 9), ..., 27th iterates $\mathbf{g}^{27}(\boldsymbol{\xi}^{(k)})$ (the stars with a 27).

The map $\mathbf{g}$ for these values of the parameters of the mirror's motion is $(3, 0, 2)$-resonant, and its attracting invariant circles are shown with thick lines in the figure, while the repelling ones are represented with thin lines. The points $\boldsymbol{\xi}^{(k)}$ (the circles) belong to the basins of attraction of the first and the second from the left invariant circles in the figure, six points being in the basin of attraction of the leftmost one. These six points are being attracted to the leftmost invariant circle, and the others are being attracted to the other invariant circle. From the figure, it is very clear how the points are being pushed away from the repelling invariant circle and accumulate on the attractive ones, which means that the electromagnetic field forms two packets with exponentially growing energy. For these parameter values the electromagnetic field can form up to three wave packets – the actual number of the wave packets depends on the support of the electromagnetic field at $t = 0$.

130

3.5.5 The KAM Case

In contrast with Section 3.5.4, we have

Lemma 3.5.3. *Assume that the map* $\mathbf{g}$ *is* C^r *conjugate to a translation (e.g., when the KAM theorem applies).*

Then, given any C^r *initial data, the* C^r *norm of the electromagnetic field remains uniformly bounded for all time.*

In particular, when $r \geq 1$, *the energy of the electromagnetic field remains bounded for all time.*

Remark 3.5.1. We note that, according to Theorem 3.3.1, given a family of motions, the behavior described in Lemma 3.5.3 will happen in Cantor sets of parameters of positive measure. Typically, in the gaps of these Cantor sets there are intervals for which Theorem 3.3.3 applies. Hence, we have that for the physical problem, situations with unbounded energy and with bounded energy are intimately mixed in the space of parameters.

Proof. We note that $\mathbf{g} = \mathbf{h}^{-1} \circ \mathbf{t}_{\boldsymbol{\tau}(\mathbf{g})} \circ \mathbf{h}$ yields $\mathbf{g}^n = \mathbf{h}^{-1} \circ \mathbf{t}_{\boldsymbol{\tau}(\mathbf{g})}^n \circ \mathbf{h}$, therefore (taking into account that $D\mathbf{t}_{\boldsymbol{\tau}(\mathbf{g})} = \mathrm{Id}$)

$$D\mathbf{g}^n = (D\mathbf{h}^{-1} \circ \mathbf{t}_{\boldsymbol{\tau}(\mathbf{g})}^n \circ \mathbf{h}) \cdot (D\mathbf{h}) \ .$$

Hence

$$\|D\mathbf{g}^n\|_{C^0} \leq \|D\mathbf{h}^{-1}\|_{C^0} \|D\mathbf{h}\|_{C^0} \leq \|\mathbf{h}^{-1}\|_{C^1} \|\mathbf{h}\|_{C^1} \ .$$

More generally, we obtain

$$\|D^r\mathbf{g}^n\|_{C^0} \leq K \|\mathbf{h}^{-1}\|_{C^r} \|\mathbf{h}\|_{C^r} \ ,$$

131

where K is a constant depending on r.

Once we have that $\mathbf{g}^n$ is uniformly C^r, we observe that the map that gives the position of the characteristic at time θ is obtained by composing $\mathbf{g}^n$ with a map which gives the solution from the time of the last reflection to θ. (These arguments are very similar to the ones in Sections 2.3.5 and 2.5.3; see especially equation (2.23)). From here the result follows easily. □

In Figure 3.12, we show the evolution of a wave packet for motion of the mirror that corresponds to the KAM case (parameter values: $\alpha = 0.2745$, $\beta = 0.09$, $\gamma = 0.05$), for $t = 0$, 500, 1000, 1500, 2000, 2500, 3000, and 3500. At $t = 0$, the wave packet is moving to the right. On the vertical axis we give the energy density in arbitrary units. We see that, although the shape of the wave packet changes, its energy stays bounded. The shape of the packets for different t is different, although this cannot be clearly seen in the picture.

3.5.6 The Energy Cannot Decrease Asymptotically

Here we make an important observation about the Doppler factor and, hence, about the nontrivial Lyapunov exponent Λ of $\mathbf{g}$. Recall that the energy of a narrow wave packet decreases at the moment θ of reflection of the wave packet from the moving mirror (i.e., $\mathcal{D}(\theta) < 1$) only if the width of the wave packet increases, which in turn happens exactly when the mirror is moving outwards , i.e., $a'(\theta) > 0$. Now notice that if the wave packet is spreading over a long time interval, it will stop existing, i.e., the situation when the
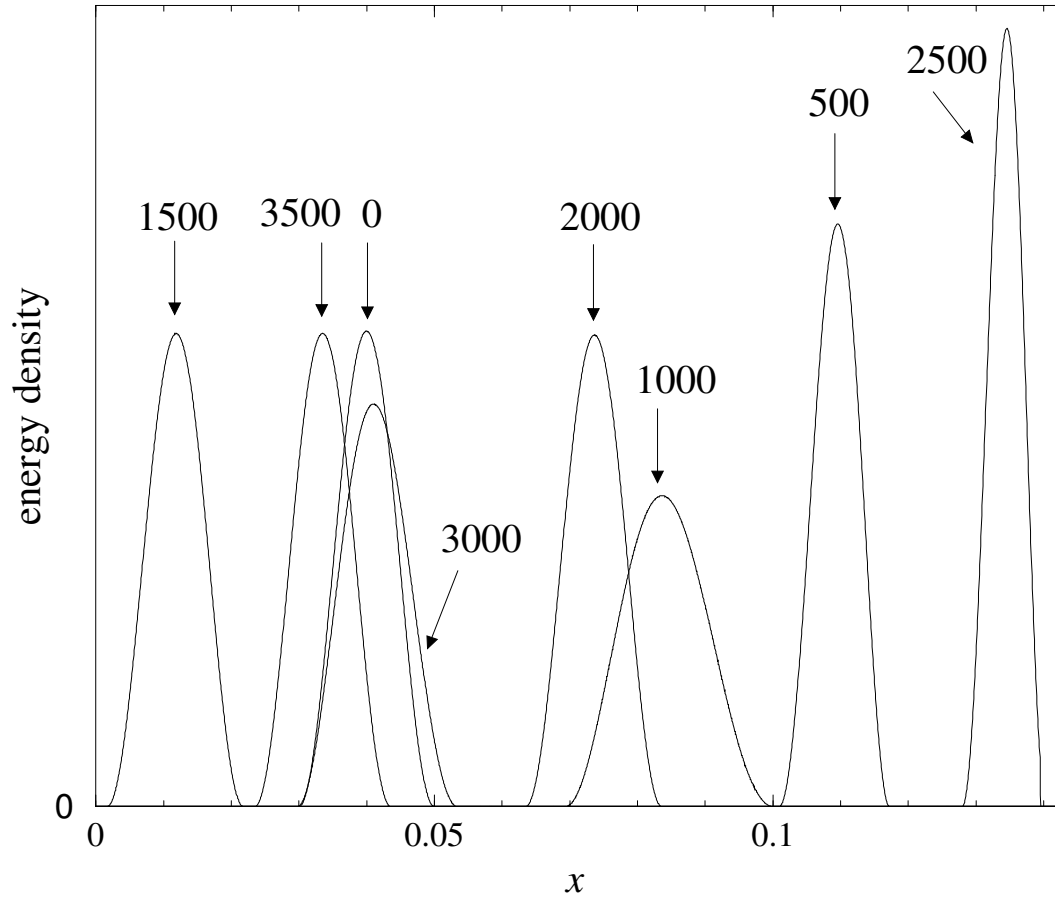
Figure 3.12: Evolution of a wave packet in the KAM case.

133

Doppler factor is less than 1, or, equivalently, when the Lyapunov exponent is strictly negative, is asymptotically unstable. Hence, the energy cannot decrease asymptotically – it either increases or stays bounded.

Chapter 4

Global Hölder Regularity of Conjugacies Between (Critical) Circle Maps

4.1 Introduction and Literature Review

Classification of circle homeomorphisms under changes of variables is an old and famous problem in mathematics. It was initiated by Poincaré in [162] motivated by studies in differential equations more than a century ago, and has been actively studied ever since.

Circle maps are important also because of their applications to natural sciences. They appear in the Pomeau-Manneville scenario for transition to turbulence through intermittency [163], second order ODEs with periodic potentials (see, e.g., Moser and Pöschel [150]), cardiac arrhythmias (Glass [79]), oscillations in plasma (Ignatov [100]), electronic devices (see, e.g., Bohr *et al* [11]), optical resonators with a periodically moving wall (see our article [131]), to name just a few. We would like to draw the reader's attention to the collections of reprints edited by Cvitanović [38] and Bai Lin Hao [89] which contain many articles devoted to circle maps and their applications.

The main dynamical invariant of homeomorphisms of the circle is the rotation number (see Section 2.4.2). It was quickly realized that it is an

135

invariant under topological equivalence (Poincaré [162]) and that for C^2 maps it is a complete invariant for topological conjugacy (Denjoy [50]). The theory of smooth equivalence of smooth diffeomorphisms is by now very well understood (see, e.g., the articles by Herman [94] and Katznelson and Ornstein [113]).

Nevertheless, the theory of smooth equivalence of "critical circle maps", i.e., smooth circle maps that are homeomorphisms but not diffeomorphisms (the simplest one – and the only one that we will consider in this paper – being a smooth map with a critical point), is much less developed. This will be the main subject of our empirical studies.

In the articles of Shenker [179], Feigenbaum *et al* [71], Ostlund *et al* [158], Rand *et al* [168], it was found numerically that cubic critical circle maps exhibit interesting "universal" properties – for large classes of circle maps there exist numbers and functions that are the same for all functions in the class – similar to the Feigenbaum-Coullet-Tresser universality of unimodal maps of the interval. (Lately similar studies were carried out for maps with critical points of higher degrees by Dixon *et al* [55] and Briggs *et al* [17]). Shortly after the initial numerical studies, a renormalization theory that explains these properties was developed and some parts of the theory were put of a firm mathematical basis in the papers of Feigenbaum *et al* [71], Rand *et al* [168], Shraiman [180], Epstein [68], Eckmann and Epstein [65, 66], Lanford [121–123], Rand [169, 170], Kim and Ostlund [114], Epstein [69], Rand [167], Veerman and Tangerman [191], Tangerman and Veerman [186], Pinto and Rand [161], Rand [171]. Recently there has been a significant progress in the renormalization

theory of critical circle maps – see Świątek [185], de Melo [47], Yampolsky [207], de Faria [44], de Faria and de Melo [45, 46].

Shenker In [179] studied numerically a one parameter family of smooth circle maps, $\{f_K\}$, all of rotation number equal to the golden mean, $\sigma_G = \frac{\sqrt{5}-1}{2}$. He found that if f_K is a diffeomorphism, the conjugacy between f_K and the rotation by σ_G is a smooth function (as predicted by the general theory [94]). However, if f_K has a cubic critical point, the conjugacy between f_K and the rotation becomes very rough. Moreover, it was noticed that the conjugacy has a self-similar structure (which he found by studying the first 400 Fourier coefficients of the conjugacy).

In the present paper, we study numerically the smoothness of the conjugacies between non-critical, cubic critical, and quintic critical circle maps. To estimate the smoothness of the conjugacies, we use finite difference method and tools from harmonic analysis (Littlewood-Paley theory and wavelet theory). In some cases, we are able to calculate reliably millions of Fourier coefficients, so we hope that our numerical estimates are quite convincing.

We expect that the numerical methodology developed here will be used to study several other problems in the theory of critical phenomena in dynamical systems in which the regularity of functions and their self-similar properties play a role. Since the theory of circle maps has a well developed mathematical literature, it seemed a good starting point to asses the validity of the methods.

We also find evidence that the conjugating functions are asymptoti-

cally self-similar confirming by very different methods the results obtained previously for cubic critical maps. (See the numerical studies by Arneodo and Holschneider [2].)

The fact that we have precise numbers for the regularity of the conjugacies predicted in the theorems allows us to observe that in some cases some simple upper bounds for the regularity of the conjugacies appear to be sharp, whereas in other cases they seem to be very far from optimal. This indicates that possibly there are conceptually different phenomena at play. (See Section 4.7.)

This chapter is organized as follows. In Section 4.2.2, we review some definitions and rigorous results about circle maps and conjugacies between them (the results for the noncritical maps were discussed in Section 2.4 In Section 4.3 we discuss how the conjugacies are calculated and explore them visually. In Section 4.4 we collect some results from harmonic analysis and in Section 4.5 we discuss them from point of view of numerically implementations. In Section 4.6 we show the results from our analysis. It Section 4.7, we develop some mathematically rigorous arguments that show that if certain scaling relations are present, the regularity of the conjugacies are bounded from above. The scaling relations can be verified numerically. We compare these upper bounds with the regularities calculated directly. In the Conclusion, we briefly recapitulate our findings.

4.2 Critical Circle Maps

4.2.1 Consequences of the Nondifferentiability of the Inverse Map in Denjoy's Theorem

Recall that Denjoy theorem (Theorem 2.4.2) says that a circle diffeomorphism F with irrational rotation number and derivative of bounded variation (in particular, every C^2 circle map) is topologically conjugate to a rotation. In this theorem, it is important that f^{-1} is differentiable. If f^{-1} is not differentiable, one cannot guarantee the existence of a conjugacy to a rotation even by assuming that f is C^∞. The article of Hall [88] contains an example of a C^∞ circle map with rotation number ρ (for any irrational $\rho \in [0, 1)$) which has no dense orbit and therefore cannot be conjugate to r_ρ. This map is onto, has no periodic orbits and has no more than two points where the derivative of the map vanishes (in fact, one can construct such a map with one critical point only).

In striking contrast with the C^∞ Denjoy counterexamples of [88], it was shown by Yoccoz [209] that the maps exhibiting the behavior of those in [88] cannot be real analytic. More precisely,

Theorem 4.2.1 (Yoccoz). *Any real analytic circle map with no periodic orbits is topologically conjugate to a rotation.*

This theorem guarantees that any two real analytic circle maps with irrational rotation number are topologically conjugate (we will use this fact in Section 4.3.3).

The above result was extended by Świątek [184, 185].

4.2.2 Results for Critical Circle Maps

We recall that a *critical* circle map is a circle homeomorphism such that the derivative is positive except for one point where it is zero of with finite order. The order of the zero is called the *type* of the critical map.

The following result was proved recently (de Faria and de Melo [45, 46], see also de Melo [47], de Faria [44], Yampolsky [207]):

Theorem 4.2.2. *Let f and g be real analytic critical circle maps with the same rotation number ρ of bounded type. Then f and g are $C^{1+\alpha}$ conjugate for some $\alpha \in (0,1)$ depending only on the combinatorial type, $N := \sup_n \rho_n$, of ρ.*

It was conjectured in [47] that the Hölder exponent of the conjugacy between two critical circle maps whose critical points are if the same order and which have the same rotation number of bounded type does not depend on N (although in the proof of Theorem 4.2.2 α does depend on N).

For the regularity of the conjugacies between critical maps and rotations, which exist because of Theorem 4.2.1, the sharpest result we are aware of is from Świątek [185], whose Theorem 1.1 (the theorem and a previous proof are credited to an unpublished manuscript of M. Herman) implies:

Theorem 4.2.3. *Let f be an analytic critical circle map with an irrational rotation number. The conjugacy between the map and a rotation is quasi-symmetric if and only if the rotation number is of constant type.*

We note that it is a well-known fact in the theory of quasi-conformal maps that the quasi-symmetric maps are Hölder (Väisälä [189, Section 18]). Hence, we can conclude that the conjugacy between a critical map and a rotation is Hölder. Therefore, the conjugacies between critical circle maps of the same rotation number have to be Hölder with exponent 1.

It is not difficult to show that, when the critical maps have different order, the conjugacy between them cannot have Hölder exponent 1.

Putting together Theorem 4.2.3, the Hölder regularity of quasi-symmetric maps and Theorem 4.2.2, we obtain:

Corollary 4.2.4. *The conjugacy between critical circle maps with golden mean rotation number is Hölder. The Hölder exponent depends only on the order of the critical points of the two functions.*

The above results seem to give very little information about what the actual values of these regularities are. In this paper, we will develop methods that allow us to compute these numbers as well as to explore numerically some geometric properties of the conjugacies.

4.2.3 Some General Heuristic Remarks on Renormalization and Conjugacies

A unifying point of view in the study of long term dynamics – especially in one-dimensional systems – has been provided by the scaling and renormalization group ideas.

Formulated somewhat loosely, the unifying idea of renormalization group can be formulated as saying that "highly iterated maps, when observed in small scales, have forms that are largely independent of the map" (the universal properties can be different in sets of maps of positive codimension).

In this section, we want to present a heuristic point of view on the relations of the renormalization and smoothness of conjugacy which seems to be applicable to a wide variety of models.

The main connection of the study of regularity properties of conjugacies and renormalization group arises from the fact that the regularity of the conjugacies is a very good test of universality properties.

Note that regularity depends on very fine scales. Moreover, formula (4.8) that we will establish later, makes it clear that the conjugacies in increasingly small scales are determined by the increasingly long recurrence times.

The fact that some conjugacies examined in very small scales are self-similar leads, at least in an informal way, to several consequences of universality for the conjugacies that we will later explore empirically.

(A1) The regularity of the conjugacies between maps of the same universality class is a "universal number".

Note that for the case of golden mean circle maps this is a consequence of Corollary 4.2.4.

(A2) These universal regularities between maps in the same class are higher than those between maps of different classes.

Note that for circle maps, this follows from the observation that critical circle maps can be only Hölder of exponent less than one conjugate to maps with critical points of different order and that by Theorem 4.2.2, the conjugacies between maps of the same order is $C^{1+\alpha}$.

(A3) The functions giving the conjugacies are asymptotically self-similar.

If h_1 and h_2 are conjugacies of maps f_1, f_2 to the golden mean rotation, (i.e., $f_1 \circ h_1 = h_1 \circ r_{\sigma_G}$, $f_2 \circ h_2 = h_2 \circ r_{\sigma_G}$), then $f_1 \circ h_1 \circ h_2^{-1} = h_1 \circ h_2^{-1} \circ f_2$. The fact that we observe that $h_1 \circ h_2^{-1} = k$, $h_1^{-1} \circ h_2 = \ell$ are very smooth means that $h_1 = k \circ h_2$, $h_1 = h_2 \circ \ell^{-1}$, in other words, we can obtain h_1 from h_2 by composing with a very smooth map. This makes precise the notion that h_1 and h_2 are very similar. Even if each of them is rather rough, the roughness of one is very precisely comparable to that of the other.

We hope that the present work could serve as a stimulus for further mathematical investigations. Our numerics are precise enough that we can even study the corrections to (A3). We formulate them as

(A4) The convergence to self-similarity is exponentially fast.

Somewhat more precisely (but still very far from a mathematically rigorous statement), we can write conjugacies in the form

$$h(x) = \sum_n \lambda_1^n H_1(\alpha^n x) + \sum_n \lambda_2^n H_2(\alpha^n x) + \cdots \tag{4.1}$$

for some $|\alpha| > 1$, $1 > \lambda_1 > \lambda_2 > \cdots$, where μ, λ_1, λ_2, ... are universal numbers.

Of course, scalings such as those in (4.1) do not, strictly speaking, make sense in the case that the variables are in the circle. Nevertheless, since (4.1) is supposed to hold in the asymptotic sense of the very small scales, we can identify the whole circle with the real line.

We also note the following conjecture that seems to be reasonable for many areas in which renormalization applies. For the case of period doubling it is studied extensively by de la Llave and Schafer [133].

Conjecture 4.2.1. Consider the set $\mathcal{M}_\nu$ (for odd integer $\nu \geq 1$) of analytic maps of the circle such that:

(a) The maps are homeomorphisms.

(b) They are of the form $f(x) = Ax^\nu + O(x^{\nu+1})$ with A a nonzero constant (hence f is a homeomorphism but not a diffeomorphism).

(c) Their rotation number is the golden mean σ_G.

Note that the sets $\mathcal{M}_\nu$ are manifolds.

Then in an open set $\mathcal{B}_\nu \in \mathcal{M}_\nu$ we can find foliations $\mathcal{F}^i$, integers d_i, and numbers λ_i ($d_i > d_{i+1}$, $\lambda_i < \lambda_{i+1}$, $\lambda_i \to \infty$) such that, if $\mathcal{W}^i_f$ is the leaf of $\mathcal{F}^i$ passing through the map f, then:

(1) $\mathcal{W}^i_f \subset \mathcal{W}^{i+1}_f$.

(2) $\mathcal{W}^i_f$ is a smooth submanifold of $\mathcal{M}_\nu$ of codimension d_i.

(3) The foliations $\mathcal{F}^i$ are Hölder (i.e., the ∞-jets of the leaves $\mathcal{W}^i_f$ are Hölder with respect to f).

(4) If $f \in \mathcal{W}^i_g$, then f is $C^{\lambda_i - \varepsilon}$ conjugate to g for each $\varepsilon > 0$.

(5) if $f \notin \mathcal{W}^i_g$, then f is not $C^{\lambda_i + \varepsilon}$ conjugate to g for each $\varepsilon > 0$.

The most important consequence of this conjecture is that the conjugacies between maps in the classes $\mathcal{M}_\nu$ can only have regularities which belong to a discrete set $\{\lambda_i\}$ (ignoring the ε's which are as small as desired). In particular, if we know that a conjugacy is $C^{\lambda_i + \varepsilon}$, we can conclude that it is $C^{\lambda_{i+1} - \varepsilon}$.

In the rest of the paper, we will present methods that allow us to carry high precision calculation of golden mean circle maps as well as an array of methods that asses the regularity of their conjugacies. By comparing the results of these different methods among themselves and with the results of the mathematical literature, we can asses their validity and hope to apply them to other contexts.

In the process of doing that, we also obtain some information about the relation between the regularity and renormalization. In particular, in Section 4.7, we obtain indications that the regularities may be limited by other mechanisms that just simple scaling phenomena.

4.3 Computing the Conjugacies

4.3.1 Examples Studied

Let f and g be analytic circle maps whose derivatives possibly vanish at one point; without loss of generality we can take this point to be $x = 0$. We studied numerically the following families of analytic circle maps (for values of K for which the maps are invertible):

(i) the noncritical (N) family $(0 \leq K < 1)$

$$f_{K,\omega}^{\mathrm{N}}(x) = \left(x + \omega - \tfrac{K}{2\pi}\sin 2\pi x\right) \quad \bmod 1 ; \tag{4.2}$$

(ii) the cubic critical (C) family $(0 \leq K < \tfrac{4}{3})$

$$f_{K,\omega}^{\mathrm{C}}(x) = \left[x + \omega - \tfrac{1}{2\pi}(K\sin 2\pi x + \tfrac{1-K}{2}\sin 4\pi x)\right] \quad \bmod 1 , \tag{4.3}$$

where the coefficients are chosen in such a way that for every K,

$$f_{K,\omega}^{\mathrm{C}}(x) = \omega + \tfrac{2\pi^2(4-3K)}{3}x^3 + \mathcal{O}(x^5) ;$$

(iii) the quintic critical (Q) family $(\tfrac{1}{2} \leq K < \tfrac{3}{2})$

$$f_{K,\omega}^{\mathrm{Q}}(x) = \left[x + \omega - \tfrac{1}{2\pi}(K\sin 2\pi x + \tfrac{9-8K}{10}\sin 4\pi x + \tfrac{3K-4}{15}\sin 6\pi x)\right] \quad \bmod 1 ,$$

where the coefficients are chosen in such a way that for every K,

$$f_{K,\omega}^{\mathrm{Q}}(x) = \omega + \tfrac{8\pi^4(3-2K)}{5}x^5 + \mathcal{O}(x^7) .$$

146

Of course, there are similar formulae for higher order critical points, but the numerics cannot be carried out easily.

We studied the case of rotation number equal to the golden mean σ_G:

$$\tau(f_{K,\omega}^\bullet)\big|_{\omega=\Omega^\bullet(K)} = \sigma_G \ , \tag{4.4}$$

where $\bullet$ stands for N, C, or Q. The golden mean is chosen because its continued fraction expansion is periodic (and simple). Hence, renormalization arguments can be expressed in terms of operators and, since all partial quotients of σ_G are 1, renormalization operators are as simple as possible.

Since we have to iterate $f_{K,\omega}^\bullet$, we need to know the value of $\Omega^\bullet(K)$ with a very high precision. To achieve this, we used the C++ software package `doubledouble` developed by Briggs [16]. This package allowed us to use about 30 decimal places floating point precision arithmetic and to find 24–25 digits of the parameter $\Omega^\bullet(K)$ in the case of N circle maps and about 16 digits of $\Omega^\bullet(K)$ in the C and Q cases.

To double-check the results, we also used the GNU MP library [187] – a public domain library for arbitrary precision arithmetic. We wrote subroutines for high precision trigonometric functions, which we did by using local Taylor series expansion, and tested them by using the following elegant and numerically stable method.

For x, y positive, define $x_1 := x$, $y_1 := y$, and

$$x_{n+1} := \frac{x_n + y_n}{2} \ , \quad y_{n+1} := \sqrt{x_n y_n}$$

for $n \in \mathbb{N}$. The sequences $\{x_n\}$ and $\{y_n\}$ converge quadratically to a common limit called the arithmetic-geometric mean (AGM) of x and y, $\mathsf{M}(x, y)$ (see, e.g., Borwein and Borwein [13]). The AGM has many remarkable properties, e.g.,

$$\frac{2}{\pi} \int_0^{\pi/2} \frac{d\zeta}{\sqrt{x^2 \cos^2 \zeta + y^2 \sin^2 \zeta}} = \frac{1}{\mathsf{M}(x, y)}$$

(in particular, elliptic integrals can be calculated through the AGM). To calculate precisely trigonometric functions, e.g., sin, one can use the fact that

$$\arcsin x = \frac{x}{\mathsf{M}(\sqrt{1 - x^2}, 1)} \ ,$$

and calculate sin as the inverse function by using, for instance, the program ZEROIN (which is quadratically convergent, so each iteration doubles the number of correct digits).

The AGM has been used for precise computations, e.g., in Brent [15]; see also the discussion in Borwein and Borwein [12] (both papers reprinted in Berggren *et al* [10]).

4.3.2 Calculating the Parameters for Rotation Number the Golden Mean

Having chosen some K (for which $f_{K,\omega}^{\bullet}$ is a homeomorphism), we first have to determine the value $\Omega^{\bullet}(K)$ such that (4.4) is satisfied. To achieve this, we use the following method (Greene [86], Shenker [179]). First we determine the phase-locking intervals

$$I_{K,n}^{\bullet} := \left\{ \omega \in [0, 1] \ \middle| \ \tau(f_{K,\omega}^{\bullet}) = \tfrac{Q_n}{Q_{n+1}} \right\}$$

148

$(n \in \mathbb{N})$. It is guaranteed that the value $\Omega^\bullet(K)$ we are looking for is between $I^\bullet_{K,n}$ and $I^\bullet_{K,n+1}$. If $\Omega^\bullet_n(K)$ is the end of $I^\bullet_{K,n}$ that is closer to $I^\bullet_{K,n+1}$, then we assume that

$$\Omega^\bullet_n(K) = \Omega^\bullet(K) + C\beta^n_\bullet \ , \tag{4.5}$$

for some constants $-1 < \beta_\bullet < 0$ and C ($\beta_\bullet$ is a universal number that depends only on the degree of the critical point, while C is different for different maps), and find $\Omega^\bullet(K)$ by Aitken extrapolation (see Press *et al* [165]). This assumption does not affect the validity of our results, but it speeds up our searches since the rotation numbers of fewer maps are computed. We note that the renormalization group picture also predicts (4.5). Moreover, this assumption is in an excellent agreement with our numerics:

(a) in the N case, we find

$$\beta_{\mathrm{N}} = -0.381966011250 \pm 10^{-12} = -\sigma_G{}^{\kappa_{\mathrm{N}}}$$

for $|\kappa_{\mathrm{N}} - 2| < 6 \times 10^{-12}$ (according to Theorem 2.4.3, $\kappa_{\mathrm{N}} = 2$);

(b) in the C case, we find

$$\beta_{\mathrm{C}} = -0.3529067 \pm 10^{-7} = -\sigma_G{}^{\kappa_{\mathrm{C}}}$$

for $\kappa_{\mathrm{C}} = 2.1644347 \pm 0.0000006$;

(c) in the Q case, we find

$$\beta_{\mathrm{Q}} = -0.32858 \pm 10^{-5} = -\sigma_G{}^{\kappa_{\mathrm{Q}}}$$

for $\kappa_{\mathrm{Q}} = 2.31286 \pm 0.00006$.

149

The values we found are in perfect agreement with those found by Shenker [179] (for the C case), and, for different families of circle maps, by Hu *et al* [99], Delbourgo and Kenny [49]. Note that what we call β is called in these papers δ^{-1}).

To find the phase-locking interval $I_{K,n}^\bullet$, we used that when ω enters this interval, the map

$$x \mapsto (F_{K,\omega}^\bullet)^{Q_{n+1}}(x) - Q_n$$

(where $F_{K,\omega}^\bullet$ is the lift of $f_{K,\omega}^\bullet$, i.e., it is given by the same formula as $f_{K,\omega}^\bullet$, but without the mod 1) undergoes a tangent bifurcation. To determine the values at which bifurcations occur, we used the subroutines FMIN and ZEROIN from Forsythe *et al* [74] (translated into C and slightly modified).

We will denote by $f_K^\bullet$ the map $f_{K,\Omega^\bullet(K)}^\bullet$ for $\Omega^\bullet(K)$ such that $\tau(f_K^\bullet) = \sigma_G$. In the table below we give the values of $\Omega^\bullet(K)$ for the values of K we studied numerically.

Map	$\Omega^\bullet(K)$
$f_{0.2}^{\mathrm{N}}$	0.617425455584922780978570
$f_{0.3}^{\mathrm{N}}$	0.616692360605785021928
$f_{0.5}^{\mathrm{N}}$	0.614526387677448776559862
$f_{0.8}^{\mathrm{N}}$	0.610074405308465212053842071
$f_{0.3}^{\mathrm{C}}$	0.626871059546737818
$f_{0.6}^{\mathrm{C}}$	0.617607758640542315
$f_{0.7}^{\mathrm{C}}$	0.6148131852529150525
$f_{1.0}^{\mathrm{C}}$	0.606661063470112017
$f_{0.6}^{\mathrm{Q}}$	0.633133040895040332
$f_{0.9}^{\mathrm{Q}}$	0.616330501795706578
$f_{1.2}^{\mathrm{Q}}$	0.60250115301615805
$f_{4/3}^{\mathrm{Q}}$	0.59694625982733198

150

4.3.3 Calculating the Conjugacies on an Equidistant Grid

Having found appropriate values of the parameters of the maps f and g such that $\tau(f) = \tau(g) = \sigma_G$, we construct numerically the conjugacy h between them. Instead of h, it is more convenient to study

$$\theta := h - \mathrm{Id} \ . \tag{4.6}$$

because θ is a periodic function, hence it is better suited for harmonic analysis. For brevity, we will denote the map θ defined by (4.6) for h being a conjugacy between, say, an N map f and a C map g by θ^{NC}, and will call θ a "conjugacy".

From (2.4.3) we obtain

$$h \circ f^n = g^n \circ h \ . \tag{4.7}$$

Theorem 4.2.1 guaranteeing the existence of the conjugacies between f (resp. g) and the rotation r_{σ_G} allows us to impose the condition $h(0) = 0$ or, equivalently, $\theta(0) = 0$. This implies that $\theta(f^n(0)) = g^n(0) - f^n(0)$, so the points

$$(f^n(0),\, g^n(0) - f^n(0)) \tag{4.8}$$

belong to the graph of θ and fill it densely. It is apparent that one can compute the points in (4.8) by iterating f and g on 0.

One problem with the calculation above is that the points in (4.8) do not have first coordinates that are distributed on a equidistant grid, and to apply fast Fourier of wavelet transforms, we need to know the values of θ on an equidistant grid. We used the grid

$$x_\ell := 2^{-L}\ell \ , \quad \ell = 0,\, 1,\, \ldots,\, 2^L - 1 \tag{4.9}$$

for some $L \in \mathbb{N}$ (typically about 20). Since the iterates $\{f^n(0)\}$ are not equidistantly distributed, we used interpolation and calculated the values of the interpolating function at the points $\{x_\ell\}_{\ell=0}^{2^L-1}$. To this end, we used the cubic interpolation subroutines SPLINE and SEVAL from Forsythe *et al* [74] (the periodicity of θ was taken into account).

An important source of difficulty for the numerical computation is the fact that the iterates of a C or a Q map are very nonuniformly distributed. To give an idea about the seriousness of the problem, we have shown in Figure 4.1 the distribution of four million iterates of $f_{0.6}^Q$ and, for comparison, of $f_{0.3}^N$, in 256 bins, each of size $\frac{1}{256}$, between 0 and 1. The number of iterates of $f_{0.6}^Q$ in a bin varies from 15 to 118304; for $f_{0.5}^N$ it varies from 13076 to 18739. The largest gap between the iterates of $f_{0.6}^Q$ is 0.001308.

If the gaps are very large, it is complicated and unstable to compute the values of the interpolating function at the gaps. The way we found to deal with this problem is to use a large number of iterates which, however, is very memory consuming and leads to accumulation of numerical error. This problem becomes more severe when the order of the critical point is higher. This is the main reason why our investigation did not cover critical maps of degree higher than 5.

4.3.4 Conjugacies – Visual Explorations

Theorem 2.4.3 guarantees that each θ^{NN} (recall that this means a conjugacy between two N circle maps) is analytic, but does not say anything
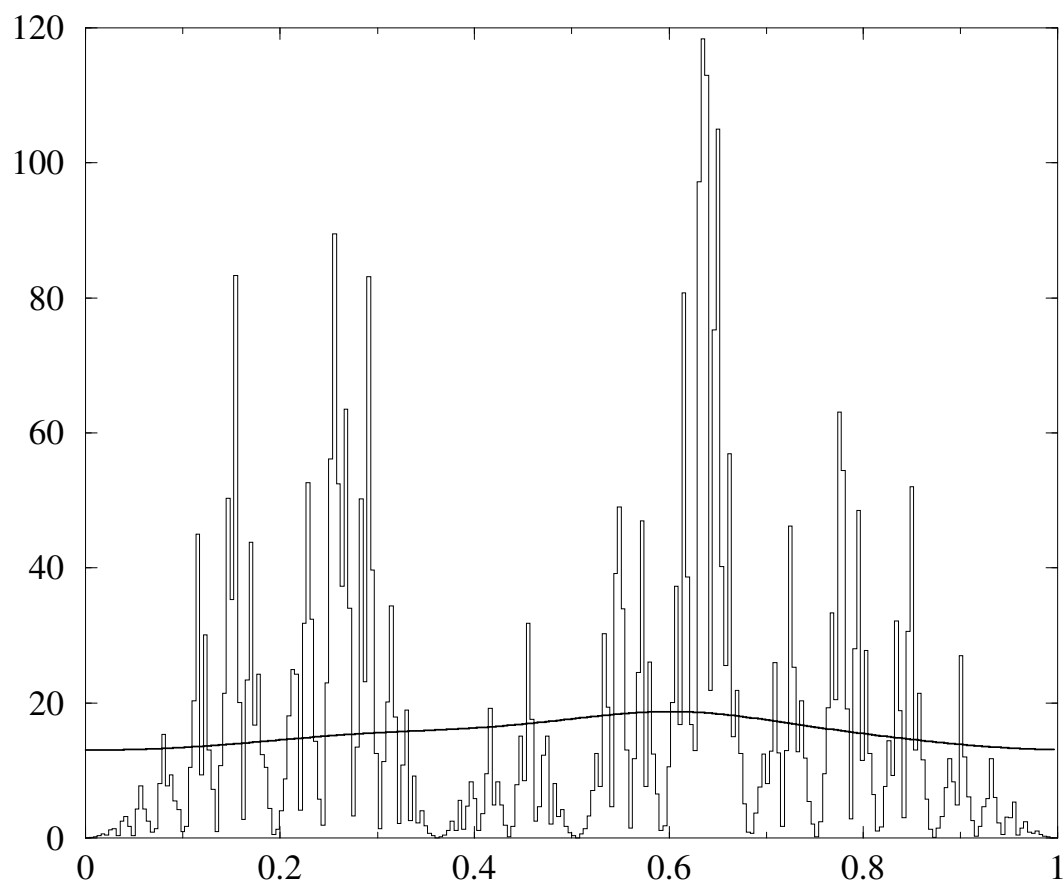
Figure 4.1: Density of the iterates of a Q map. The number of iterates in a bin (in thousands) vs. the position of the bin, for four million iterates of $f_{0.6}^{Q}$ (thin line) and of $f_{0.5}^{N}$ (thick line), in 256 bins.

about critical circle maps. The goal of this paper is to study the conjugacies of critical circle maps to a golden mean rotation and assess their regularity and asymptotic scaling properties.

To motivate our subsequent analysis, we start with some preliminary visual explorations.

In Figure 4.2 we show two θ^{NC} and one θ^{CC}. Obviously the θ^{NC}'s are less differentiable then the θ^{CC}; visually, θ^{CC} is smoother than C^1.

In Figure 4.3 we show the conjugacies between a map of type N (resp. C, Q) and a Q map. Again, the conjugacy between two maps of the same type is evidently more differentiable than the ones between maps of different types.

Another observation is the self-similar structure of the conjugacy between an N map and a critical (C or Q) map. To illustrate this, in Figure 4.4 we show magnified regions of the conjugacy between $f_{0.8}^{\mathrm{N}}$ and $f_{0.9}^{\mathrm{Q}}$. The self-similarity of the conjugacies between an N and a C map is one of the predictions of the theory of renormalization for C maps; we observed a self-similar structure in the case of the conjugacy between an N map and a Q map as well.

The self-similarity of the conjugacies of type θ^{NC} and θ^{NQ} can be seen distinctly from their Fourier spectra displayed in log-log form (Figures 4.5 and 4.6). The self-similarity manifests itself in the "periodicity" of the Fourier spectrum for large $|k|$'s.

This effect becomes even more prominent in the plot of $\log_{10}(|k|^{\lambda}|\hat{\theta}_k|)$

154
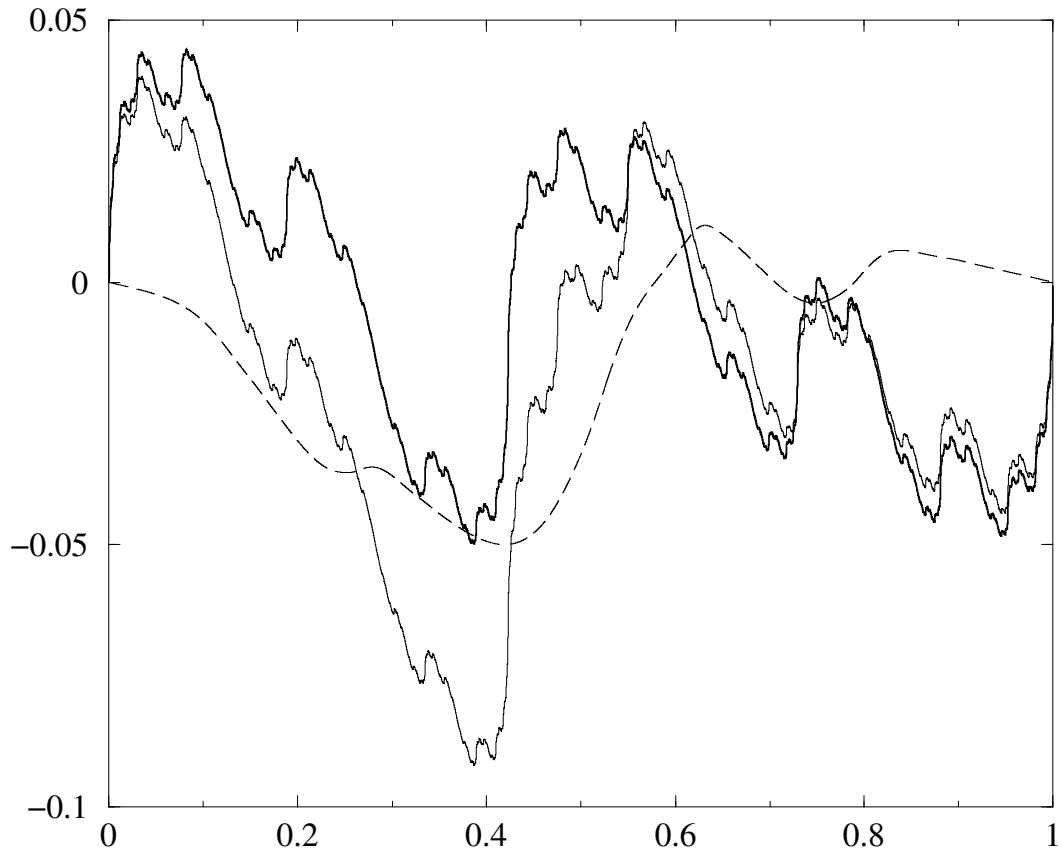
Figure 4.2: Conjugacies θ between: $f_{0.2}^{\mathrm{N}}$ and $f_{0.3}^{\mathrm{C}}$ (thin solid line), $f_{0.2}^{\mathrm{N}}$ and $f_{0.6}^{\mathrm{C}}$ (thick solid line), and $f_{0.6}^{\mathrm{C}}$ and $f_{0.3}^{\mathrm{C}}$ (dashed line).
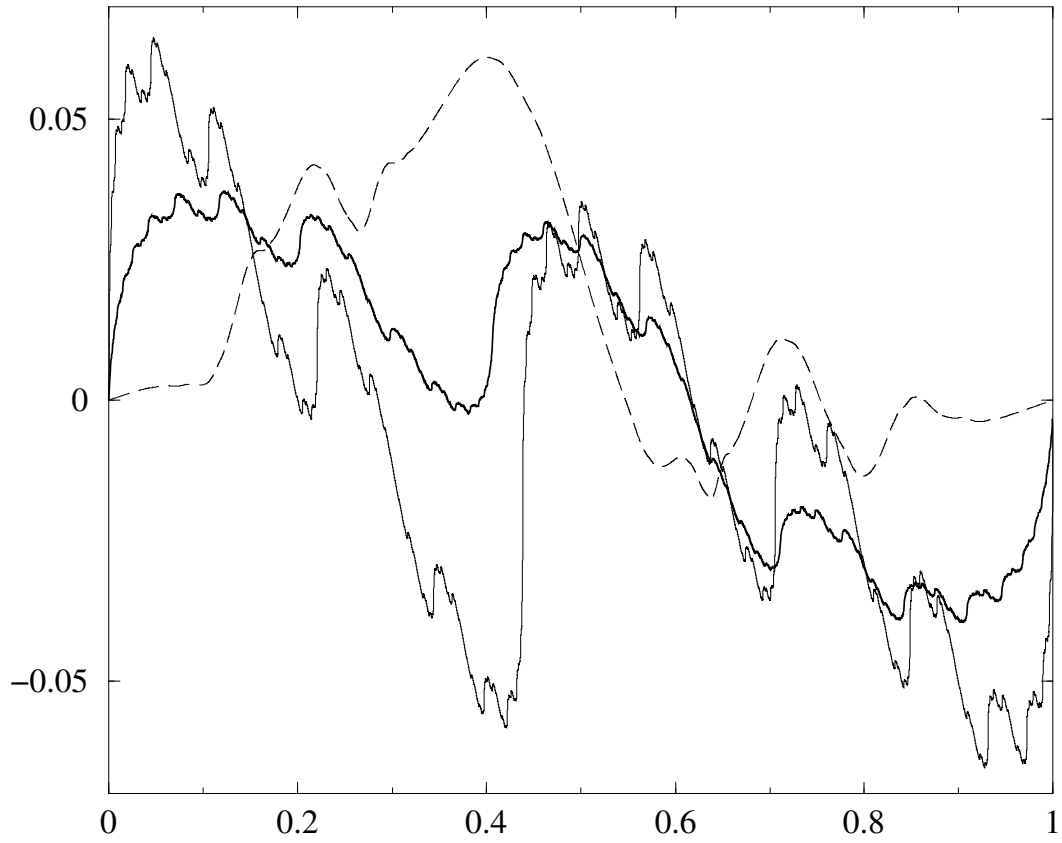
Figure 4.3: Conjugacies θ between: $f^{\mathrm{N}}_{0.3}$ and $f^{\mathrm{Q}}_{0.9}$ (thin solid line), $f^{\mathrm{C}}_{0.6}$ and $f^{\mathrm{Q}}_{0.9}$ (thick solid line), and $f^{\mathrm{Q}}_{0.6}$ and $f^{\mathrm{Q}}_{0.9}$ (dashed line).
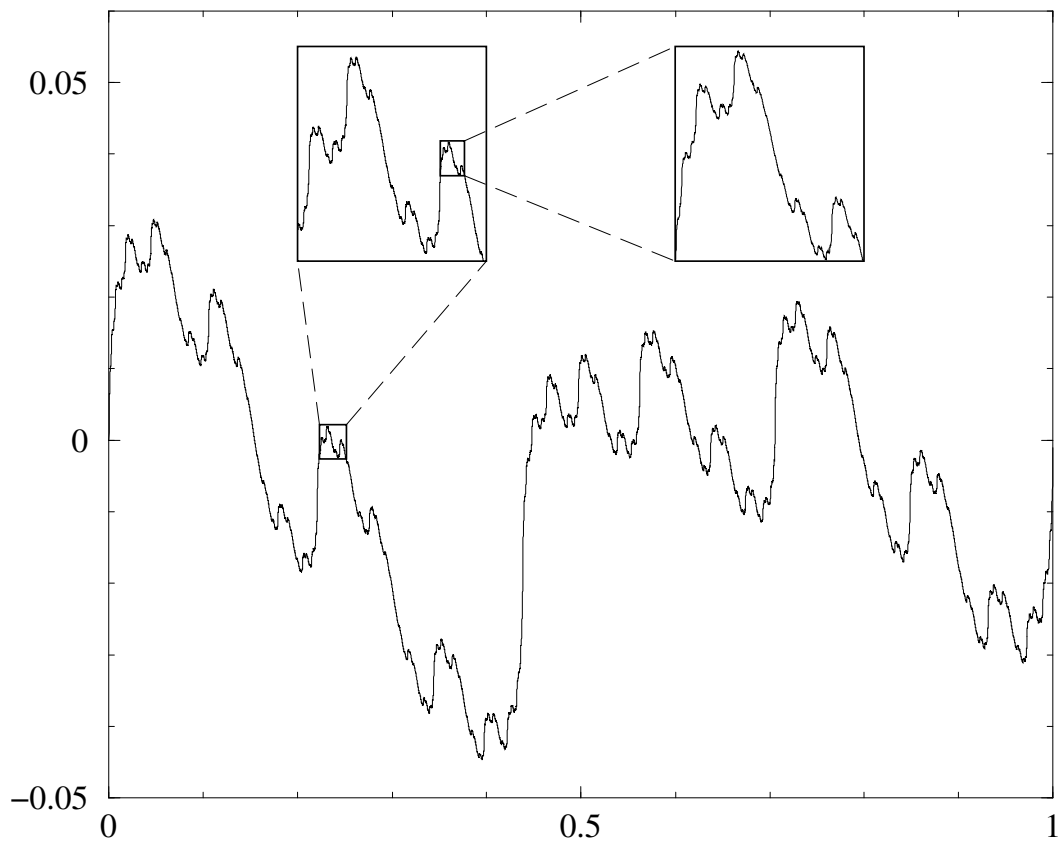
Figure 4.4: Zooming in the graph of the conjugacy between $f_{0.8}^{\mathrm{N}}$ and $f_{0.9}^{\mathrm{Q}}$.

vs. $\log_{10} |k|$, as shown in Figures 4.7 (for θ^{NC}, $\lambda = 1.29$) and 4.8 (for θ^{NQ}, $\lambda = 1.19$). In both cases, the width of the "periodic windows" is approximately equal to $\log_{10} \sigma_G$, as predicted by renormalization theory.
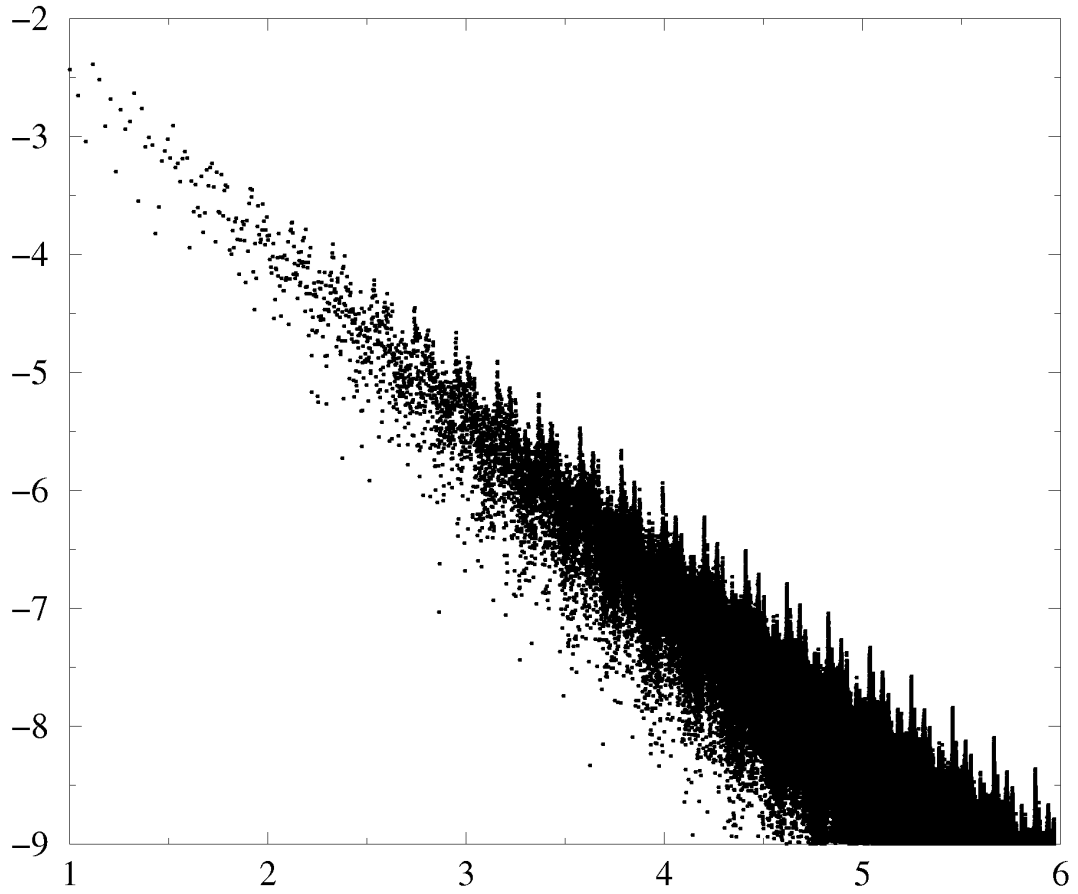
Figure 4.5: Plot of $\log_{10} |\hat{\theta}_k|$ vs. $\log_{10} k$ where θ is the conjugacy between $f_{0.2}^{\mathrm{N}}$ and $f_{0.6}^{\mathrm{C}}$.
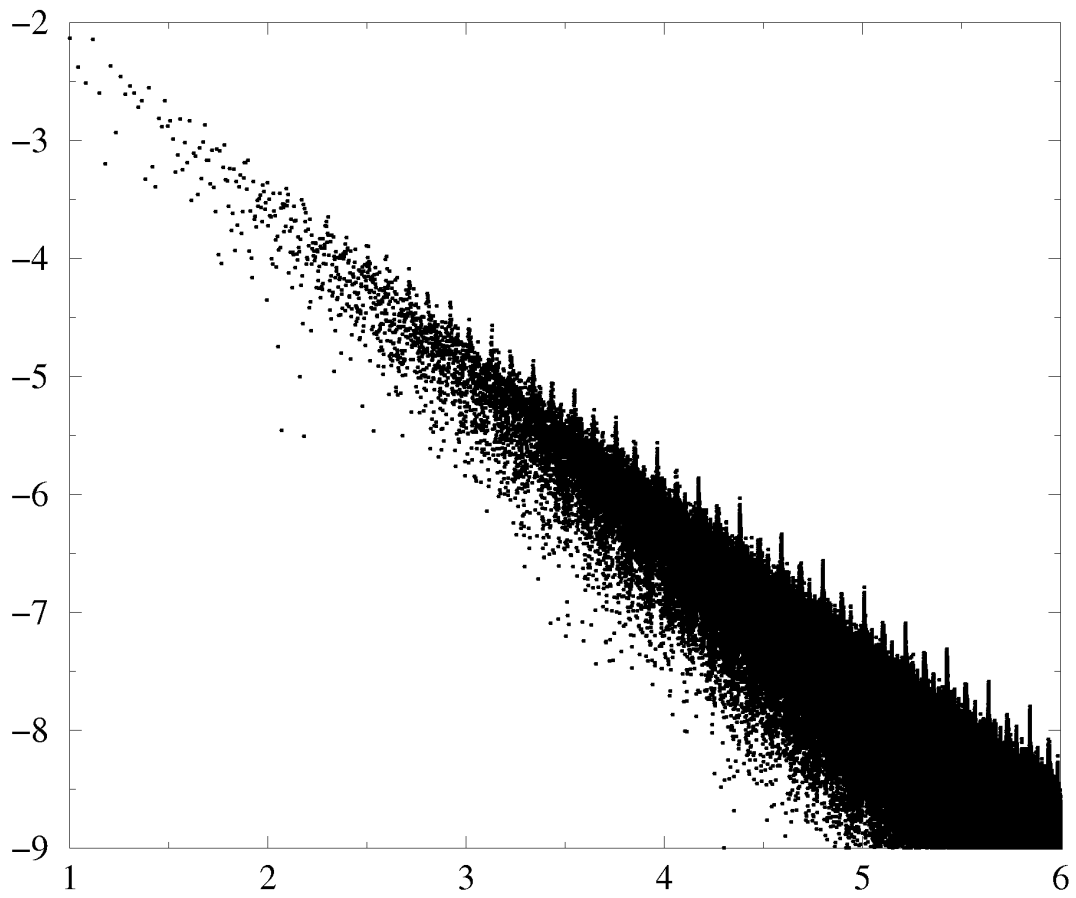
Figure 4.6: Plot of $\log_{10} |\hat{\theta}_k|$ vs. $\log_{10} k$ where θ is the conjugacy between $f_{0.3}^{\mathrm{N}}$ and $f_{0.9}^{\mathrm{Q}}$.
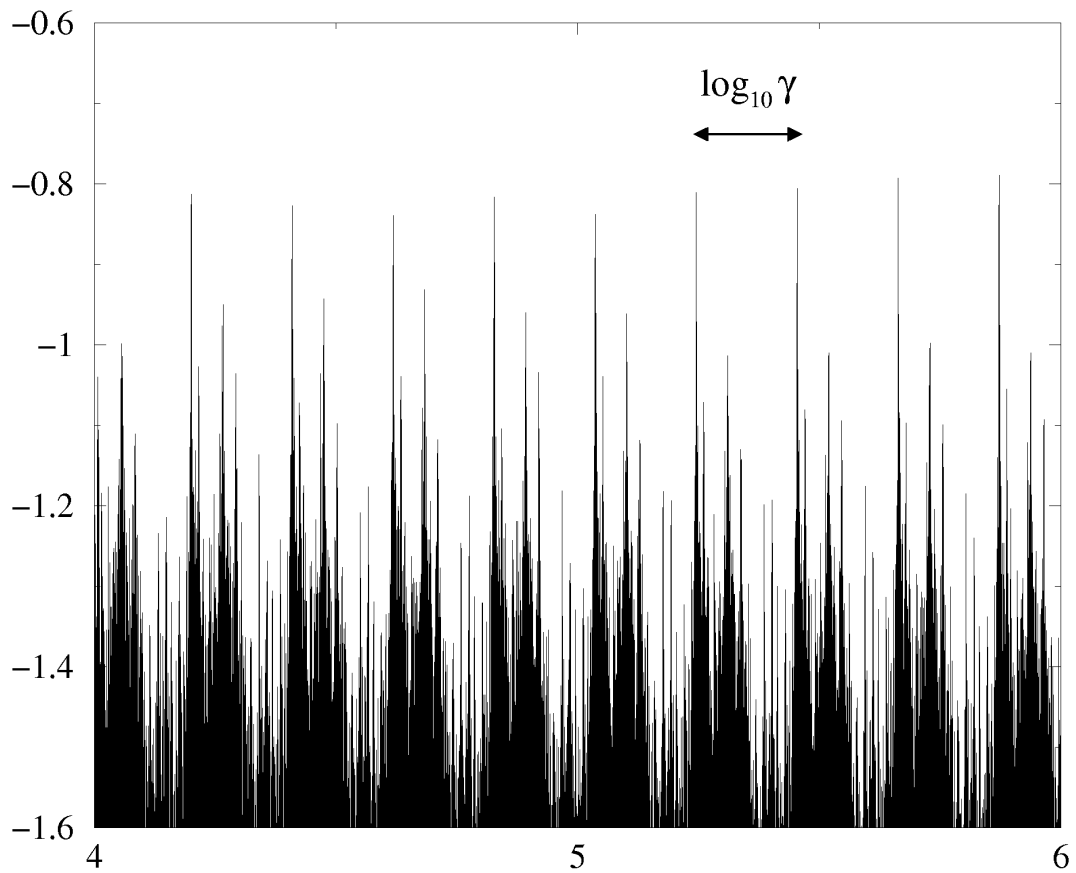
Figure 4.7: Plot of $\log_{10}(|k|^{1.29}|\hat{\theta}_k|)$ vs. $\log_{10}|k|$ where θ is the conjugacy be-tweeh $f_{0.2}^{\mathrm{N}}$ and $f_{1.0}^{\mathrm{C}}$.
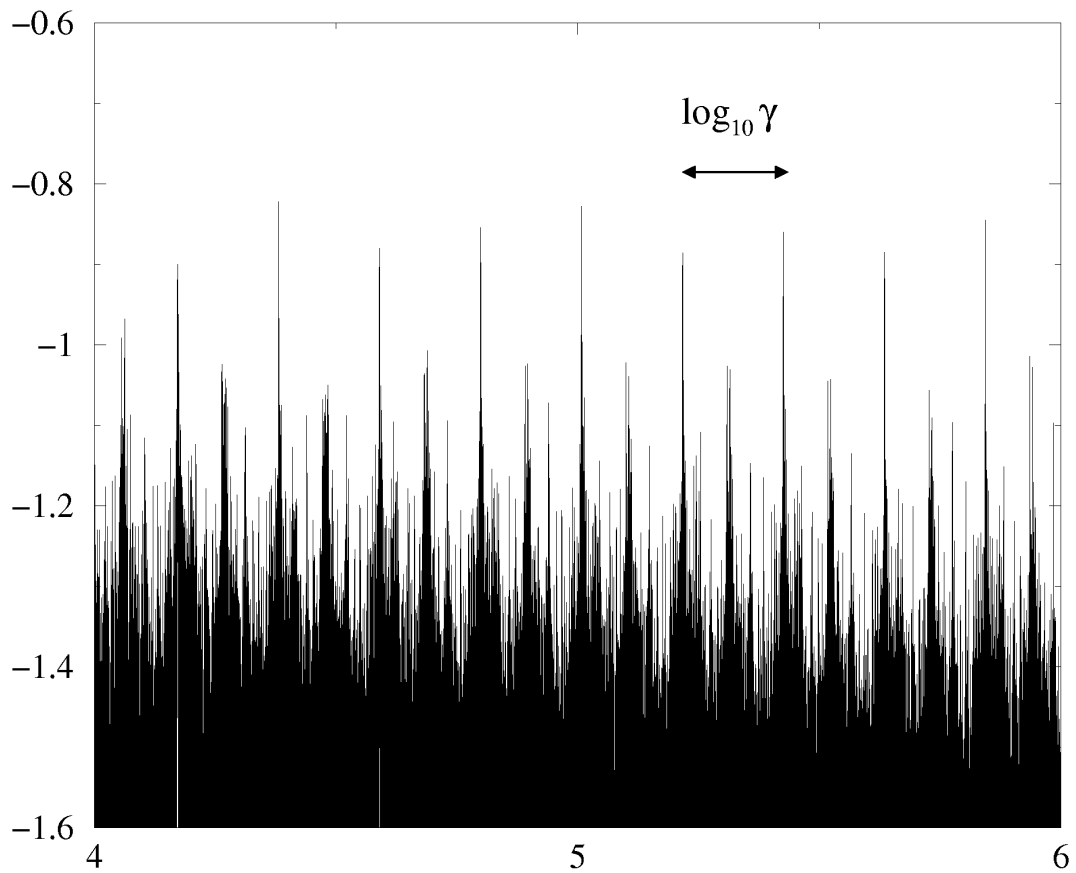
Figure 4.8: Plot of $\log_{10}(|k|^{1.19}|\hat{\theta}_k|)$ vs. $\log_{10}|k|$ where θ is the conjugacy between $f_{0.2}^{\mathrm{N}}$ and $f_{0.6}^{\mathrm{Q}}$.

4.4 Methods for Studying the Regularity

In this section we describe the function spaces studied and collect the theorems from harmonic analysis we used to compute the regularity of conjugacies.

4.4.1 Hölder Spaces

Let $C^n(\mathbb{T})$ ($n \in \mathbb{N}$) stand for the space of n times continuously differentiable functions on $\mathbb{T}$.

Definition 4.4.1. The *Hölder spaces* $\Lambda_\alpha(\mathbb{T})$ are defined as follows.

- For $\alpha \in (0, 1)$:

$$\|\theta\|_{\Lambda_\alpha(\mathbb{T})} := \sup_{|y|>0} \frac{|\theta(x+y) - \theta(x)|}{|y|^\alpha} \,,$$

$$\Lambda_\alpha(\mathbb{T}) := \left\{ \theta \in L^\infty(\mathbb{T}) \ : \ \|\theta\|_{\Lambda_\alpha(\mathbb{T})} < \infty \right\} \,,$$

- For $\alpha = n + \alpha'$ ($n \in \mathbb{N}$, $\alpha' \in (0, 1)$):

$$\Lambda_\alpha(\mathbb{T}) := \left\{ \theta \in C^n(\mathbb{T}) \ : \ \theta^{(n)} \in \Lambda_{\alpha'}(\mathbb{T}) \right\} \,.$$

- For $\alpha = 1$:

$$\|\theta\|_{\Lambda_1(\mathbb{T})} := \|\theta\|_{L^\infty(\mathbb{T})} + \sup_{|y|>0} \frac{|\theta(x+y) + \theta(x-y) - 2\theta(x)|}{|y|} \,,$$

$$\Lambda_1(\mathbb{T}) := \left\{ \theta \in L^\infty(\mathbb{T}) \cap C^0(\mathbb{T}) \ : \ \|\theta\|_{\Lambda_1(\mathbb{T})} < \infty \right\} \,.$$

- For $\alpha = n \in \{2, 3, 4, \ldots\}$:

$$\Lambda_n(\mathbb{T}) := \left\{ \theta \in L^\infty(\mathbb{T}) \cap C^{n-1}(\mathbb{T}) \ : \ \theta^{(n-1)} \in \Lambda_1(\mathbb{T}) \right\} \ .$$

Remark 4.4.1.   1. $C^1(\mathbb{T}) \subset \mathrm{Lip}\,(\mathbb{T}) \subset \Lambda_1(\mathbb{T})$ and $C^n(\mathbb{T}) \subset \Lambda_n(\mathbb{T})$ $(n \geq 2)$; all these inclusions are strict.

2. Every $\theta \in \Lambda_\alpha(\mathbb{T})$ $(0 < \alpha)$ may be modified on a set of measure zero so that it becomes continuous (Stein [182, Section V.4.1]).

The spaces in these scales have several characterizations some of which lead to algorithms that can be used to assess the regularity of functions. Some of these characterizations will de discussed in Sections 4.4.2, 4.4.3, 4.4.4. The numerical implementation of these methods will be discussed in Section 4.5.

4.4.2   Finite Differences Method

In this subsection we discuss the characterization of Hölder spaces by means of finite differences (FD) (Krantz [116]).

Let $\mathcal{D}_y^n$ be the finite difference operator,

$$\left(\mathcal{D}_y^n \theta\right)(x) := \sum_{j=0}^n (-1)^j \binom{n}{j} \theta(x + (n - 2j)y) \ .$$

Theorem 4.4.1 (FD). *Let* $\theta \in L^\infty(\mathbb{T}) \cap C^0(\mathbb{T})$ *and* $0 < \alpha < n \in \mathbb{Z}$. *Then* $\theta \in \Lambda_\alpha(\mathbb{T})$ *if and only if* $\exists\, C > 0$ *such that* $\forall\, y \in \mathbb{T}$

$$\|\mathcal{D}_y^n \theta\|_{L^\infty(\mathbb{T})} \leq C|y|^\alpha \tag{4.10}$$

for all $y \in \mathbb{T}$.

164

The FD method is simple and convenient to use if one can compute the values of the function in points that are arbitrarily close and equally spaced. As mentioned before, this requires to use intepolation between the iterates $f^n(0)$.

4.4.3 Fourier Methods – Littlewood-Paley Theorem

The trigonometric system $\{e^{2\pi i k x}\}_{k \in \mathbb{Z}}$ is an orthonormal basis of $L^2(\mathbb{T}, dx)$, hence, according to the Plancherel's theorem, a function

$$\theta(x) = \sum_{k \in \mathbb{Z}} \hat{\theta}_k\, e^{2\pi i k x} \tag{4.11}$$

belongs to $L^2(\mathbb{T})$ if and only if

$$\sum_{k \in \mathbb{Z}} |\hat{\theta}_k|^2 < \infty\ .$$

The main result of Littlewood-Paley theory is that similar characterization of $L^p(\mathbb{T})$ $(1 < p < \infty)$ can be obtained by grouping the terms of the Fourier series in dyadic blocks. Define the decomposition

$$\theta = \sum_{M=1}^{\infty} \mathcal{L}_M \theta$$

of $\theta \in L^1(\mathbb{T})$ in *dyadic partial sums*

$$(\mathcal{L}_M \theta)(x) := \sum_{A^{M-1} \le |k| < A^M} \hat{\theta}_k\, e^{2\pi i k x}\ ,$$

$(M \in \mathbb{N})$, $\mathcal{L}_0 \theta := \hat{\theta}_0$, and $A > 1$.

Remark 4.4.2. Usually A is taken to be 2, since the precise value does not make any difference for the mathematical treatment.

In the numerical applications, we will find it convenient to use some A's different from 2. Nevertheless, we have not introduced A in the notation, since it will be clear from the context, and we follow the standard practice of calling the decomposition "dyadic".

The dyadic blocks can be written as

$$\mathcal{L}_M \theta = (\phi_{A^M} - \phi_{A^{M-1}}) * \theta \ , \tag{4.12}$$

where the function

$$\phi_N(x) := \sum_{|k| < N} e^{2\pi i k x} \tag{4.13}$$

plays a role of a "low-pass filter", or, in the terminology of physicists, introduces an "ultraviolet" cutoff.

To formulate the celebrated Littlewood-Paley (LP) theorem, let us introduce the Littlewood-Paley d-function,

$$d(\theta)(x) := \left(\sum_{M=0}^{\infty} |\mathcal{L}_M \theta(x)|^2 \right)^{1/2} \ ,$$

and its "continuous" analog, the G-function,

$$G(\theta)(x) := \left(\int_0^1 (1-s) \left| \left(\frac{dP_s}{ds} * \theta \right)(x) \right|^2 ds \right)^{1/2} \ ,$$

where

$$\begin{aligned} P_s(x) \ &= \ \sum_{k \in \mathbb{Z}} s^{|k|} e^{2\pi i k x} \\ &= \ \frac{1 - s^2}{1 - 2s \cos 2\pi x + s^2} \ , \quad s \in [0, 1) \end{aligned} \tag{4.14}$$

166

is the periodic Poisson kernel. Note that if Δ is the Laplacian, then

$$
\begin{aligned}
P_{\exp(-2\pi t)} * \theta(x) &= e^{-t\sqrt{-\Delta}}\,\theta(x) \\
&= \sum_{k \in \mathbb{Z}} \hat{\theta}_k\, e^{-2\pi t|k|}\, e^{2\pi i k x} \ .
\end{aligned}
$$

Heuristically, it seems clear that the partial sums, $\phi_n * \theta$, behave like the Abel means, $P_{1-\frac{1}{n}} * \theta$. In fact, one can prove that the $L^p(\mathbb{T})$ norms of $d(\theta)$ and $G(\theta)$ are equivalent for $1 < p < \infty$ if $\hat{\theta}_0 = 0$.

Remark 4.4.3. The Poisson kernel can also be considered as defined on the real line. In that case, it can be given by the formula $P_t = e^{-t\sqrt{-\Delta}}$ or as the convolution with the kernel $P_t(x) = \pi^{-1/2}\, t/(x^2 + t^2)$.

Note that we can consider a periodic function of period 1 on the real line as a function on the circle. When we apply the real Poisson kernel to a periodic function of period 1, it also produces a periodic function of period 1.

It is well known and not difficult to check (Poisson summation formula) that it is the same to apply the real Poisson kernel to a periodic function of period one defined on $\mathbb{R}$ or to consider the function as defined on the circle and to apply the periodic Poisson kernel (4.14).

Remark 4.4.4. On the real line it makes sense to define scaling transformations and to investigate how the Poisson kernel behaves under scalings. It is very easy to check that, for every $\lambda > 0$, the Poisson kernel on $\mathbb{R}$ satisfies

$$
P_{\lambda t}(\lambda x) = \lambda^{-1} P_t(x) \ . \tag{4.15}
$$

On the circle, we cannot speak about scaling, therefore the relation (4.15) does not, strictly speaking, make sense for the Poisson kernel on the circle when λ is not an integer. Nevertheless, for small scales, the circle can be identified with the real line, so that the scalings of the periodic Poisson kernel can be used when examining asymptotic features in small scales.

Theorem 4.4.2 (Littlewood-Paley). *If $\theta \in L^p(\mathbb{T})$, $1 < p < \infty$, then there exist positive constants A_p and B_p such that*

$$A_p \, \|\theta\|_{L^p(\mathbb{T})} \leq \|d(\theta)\|_{L^p(\mathbb{T})} \leq B_p \, \|\theta\|_{L^p(\mathbb{T})} \ .$$

Analogous inequalities hold for $G(\theta)$ in place of $d(\theta)$.

Theorem 4.4.2 has many important implications. In particular, it gives useful characterizations of Sobolev, Hölder, Hardy, Besov spaces – see, e.g., Stein [182, Chapter 5], Hernández and Weiss [96, Chapter 6], Meyer [141, Chapter 6], Frazier *et al* [75].

In our numerical explorations, we used methods based on the following two corollaries of Theorem 4.4.2, which we will call "discrete" (DLP) and "continuous" (CLP) versions of the Littlewood-Paley theorem.

Theorem 4.4.3 (DLP). **[116, Theorem 5.9]** *The function θ (4.11) is of class $\Lambda_\alpha(\mathbb{T})$ ($\alpha \in \mathbb{R}_+$) if and only if there exists a $C > 0$ such that for any $M \in \mathbb{N}$*

$$\|\mathcal{L}_M \theta\|_{L^\infty(\mathbb{T})} \leq C \, A^{-\alpha M} \ . \tag{4.16}$$

Theorem 4.4.4 (CLP). [182, Chapter 5, Lemma 5] *The function θ (4.11) is of class $\Lambda_\alpha(\mathbb{T})$ ($\alpha \in \mathbb{R}_+$) if and only if for each $\eta \geq 0$ there exists a $C > 0$ such that for any $t > 0$*

$$\left\| \left(\frac{\partial}{\partial t} \right)^\eta e^{-t\sqrt{-\Delta}} \theta \right\|_{L^\infty(\mathbb{T})} \leq C \, t^{\alpha-\eta} . \tag{4.17}$$

4.4.4 Wavelet Methods

In this section we discuss the application of wavelet theory.

The guiding idea of wavelet theory is to decompose functions systematically into functions that have definite scales decreasing geometrically. This is, of course, related to the decompositions used in Littlewood-Paley (cf. (4.12)). Since the formalism is quite systematic, it is well suited for numerical implementations.

Expansions in wavelet bases are very well suited to studying the local properties of functions because of their localization in space. Wavelet methods are especially appropriate for analyzing self-similar functions like some of the conjugacies between circle maps studied in this paper. Below we introduce the notations and collect the basic theoretical results about regularity of functions expanded in wavelet bases. For more details we refer the reader to Meyer [141], Daubechies [42], Mallat [138], Hernández and Weiss [96], Härdle *et al* [90], Louis *et al* [137].

Let $L^2(\mathbb{T})_{2^L}$ be the "discrete" version of the space of square integrable circle maps, i.e., the 2^L-dimensional space of the circle maps defined on the

grid $x_\ell = 2^{-L}\ell$, $\ell = 0, 1, \ldots, 2^L - 1$. We use the following multiresolution analysis of $L^2(\mathbb{T})_{2^L}$:

$$V_0 \subset V_1 \subset \cdots \subset V_{L-1} \subset V_L = L^2(\mathbb{T})_{2^L} .$$

Let W_j be the orthogonal complement of V_j in V_{j+1}, so that

$$L^2(\mathbb{T})_{2^L} = V_0 \oplus \left(\bigoplus_{j=0}^{L-1} W_j \right) ;$$

$$\dim V_j = \dim W_j = 2^j .$$

The space W_j is spanned by $\{\psi_{jk}\}_{k=0}^{2^j-1}$, where

$$\psi_{jk}(x) = 2^{j/2}\psi(2^j x - k)$$

and ψ is the "mother wavelet". Let $\theta_{2^L} := \{\theta(x_\ell)\}_{\ell=0}^{2^L-1} \in L^2(\mathbb{T})_{2^L}$ be the discrete representation of the function θ, and

$$\Pi_J : L^2(\mathbb{T})_{2^L} \to V_J : \theta_{2^L} \mapsto \sum_{j=0}^{J} \sum_{k=0}^{2^j-1} \langle \theta, \psi_{jk} \rangle \, \psi_{jk}$$

be the projections onto V_J, $J = 0, 1, \ldots, L$.

Littlewood-Paley theorem can be generalized to bases other than the trigonometric one by observing that the proofs do not use the explicit form of ϕ_N (4.13) and P_s (4.14), but only some of their properties, so that the results are valid for larger function classes. In particular, the following theorem holds:

Theorem 4.4.5. [96, Th. 7.16] *If $\psi \in \Lambda_\alpha(\mathbb{T})$, then the function θ is of class $\Lambda_\alpha(\mathbb{T})$ if and only if there exists a $C > 0$ such that for any $j \in \mathbb{N}$*

$$\sup_{0 \le k \le 2^j - 1} |\langle \theta, \psi_{jk} \rangle| \le C \, 2^{-j(\alpha+\frac{1}{2})} . \tag{4.18}$$

Another formulation which is useful for numerical computations is

Theorem 4.4.6. *If* $\psi \in \Lambda_\alpha(\mathbb{T})$*, then the function* θ *is of class* $\Lambda_\alpha(\mathbb{T})$ *if and only if there exists a* $C > 0$ *such that for any* $j \in \mathbb{N}$

$$\|\theta - \Pi_j\theta\|_{L^\infty(\mathbb{T})} \leq C\, 2^{-j\alpha} \ . \tag{4.19}$$

For more subtle results on applications of wavelets to studies of local regularity of functions, see Jaffard and Meyer [103], Holschneider and Tchamitchian [98], Jaffard [102], Meyer [142].

In this paper we will not explore local regularity, even if our numerical methods are related to the results in Jaffard [102].

4.5 Numerical Implementation

In this subsection we discuss the numerical implementation of the theorems from Section 4.4.

4.5.1 General Remarks

The numerical implementation brings us a wealth of issues which we will try to discuss.

One issue is that the characterizations mentioned above involve inequalities that have to be satisfied for an infinite number of integers. Obviously, the numerical calculation can only compute the Fourier and wavelet transform up to a finite order. It is conceivable that the behavior of the functions is different for high Fourier modes than for the values that can be explored.

In spite of the above solipsistic argument, there are good reasons (a renormalization group description) that strongly suggest that the functions we are studying are asymptotically self-similar, so that the the study of a finite number of scales predicts accurately the behavior at all scales. Indeed, we find empirically that the upper bounds giving the regularity become approximately identities. We see that, after a very short transient, the upper bounds become identities up to a small periodic error whose interpretation we discuss in Section 4.5.5.

Because of this empirical observation and the renormalization group description, we believe that it is reasonable to extrapolate from the observed values and conclude that the upper bounds giving regularity are saturated to all scales.

Another issue that one has to discuss in numerical implementations is the effect of the round off and discretization error. This analysis is very similar to the standard considerations of numerical analysis.

Finding numerically the regularity of functions that are very smooth is difficult because their Fourier/wavelet coefficients decrease faster. That is why we were not able to asses the precise values of the smoothness of the conjugacies of type θ^{CC} and θ^{QQ}, whose smoothness is more than one.

In these two cases, as well as for all conjugacies between f and g for f being critical (C or Q), an important issue is the presence of big gaps between the iterates $f^n(0)$ (see Section 4.3.3). This is due to the fact that we perform

Fast Fourier Transform (FFT) or Discrete Wavelet Transform (DWT) not on the exact values of θ at the points x_ℓ (4.9), but on the values of the interpolating cubic polynomials at these points, which significantly deteriorates the precision of the spectra.

For the FFT, we used the routines FOUR1 and REALFT from Press et al [165] (for long double precision).

For the DWT, we used the freely available C routines documented in detail in the book by Wickerhauser [195].

For the graphing and some of the data analysis, we used the plotting tool `ACE/gr`.

Numerically, the most important restriction on the number of Fourier or wavelet coefficients computed was not the speed, but the memory usage (in some of the cases about 200 Mb).

4.5.2   Calibration of the Methods

To asses the validity of the numerical methods that have been employed, we have taken an empirical approach, testing them on functions whose regularity is known.

One particularly good class of functions for calibration are the Weierstrass functions

$$w_{a,b}(x) = \sum_{k=1}^{\infty} a^k \sin(2\pi b^k x) \ , \tag{4.20}$$

where $a < 1$, $b \in \mathbb{N}$. As it is well known, $w_{a,b} \in \Lambda_{-\log_b a}$ and for any $\delta > 0$,

173

$w_{a,b} \notin \Lambda_{-\log_b a + \delta}$.

To calibrate our numerical methods, we have generated the $w_{a,b}$ functions at points obtained by iterating the diffeomorphisms we are studying. Then, we obtained the regularity applying the methods outlined above.

This procedure gave us an idea of the severity of the problem of the lack of equidistribution of the iterates.

We think that the use of Weierstrass function to calibrate the methods is appropriate because the working hypothesis (A3) asserts that the functions we are studying are very similar to the functions (4.20). Hence, one can hope that the problems of interpolation and lack of distribution can be assessed by testing the methods on (4.20).

4.5.3 Finite Differences Method

We applied Theorem 4.4.1 for $y = 2^{-j}$, in which case (4.10) yields

$$\log_2 \|\mathcal{D}_{2^{-j}}^n \theta\|_{L^\infty(\mathbb{T})} \leq \text{const} - \alpha j$$

(naturally, one can consider the case of arbitrary y's). As examples of the results obtained by applying this method, we show in Figure 4.9 the plot of $\log_2 \|\mathcal{D}_{2^{-j}}^1 \theta\|_{L^\infty(\mathbb{T})}$ as a function of j for four conjugacies of type NC (x's) and four ones of type CQ (circles); to calculate θ^{NC}, we used 10^7 iterates and 2^{22} interpolated values, while for θ^{CQ} these numbers were 2×10^6 and 2^{22}, respectively.

In the favorable case (NC), we see that the numerical results correspond

174
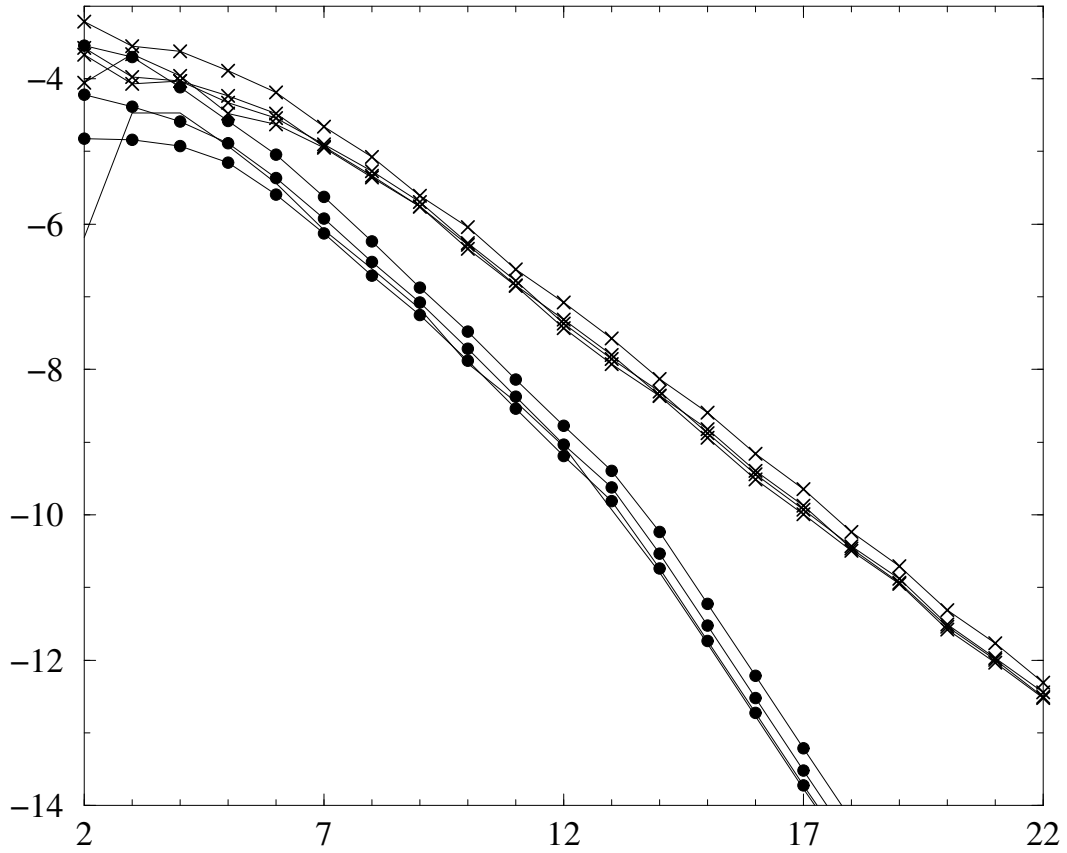
Figure 4.9: Plot of $\log_2 \|\mathcal{D}_{2^{-j}}^1 \theta\|_{L^\infty(\mathbb{T})}$ vs. j for four θ^{NC}'s (x's) and four θ^{CQ}'s (circles).

to parallel straight lines that cover the whole range plotted. On the other hand, in the unfavorable case (CQ), the numerical results present two straight lines joined by a break.

This can be clearly explained because the graph presented for the NC case includes computations of in which many of the points in the finite difference operator are included in the gaps. Hence, the finite difference operator is observing the regularity of the interpolating spline.

In the NC case the gaps between the iterates did not exceed 1.5×10^{-7}. At the same time, in the CQ case the maximum gap was about $2 \times 10^{-4} \approx 2^{-12}$, which corresponds quite exactly to the position of the break in the graph.

When we restrict the differences to regions which are larger than the gaps, the method produces results consistent with the other methods.

4.5.4   DLP Method

Theorem 4.4.3 implies that

$$\log_A \|\mathcal{L}_M \theta\|_{L^\infty(\mathbb{T})} \leq \text{const} - \alpha M \ ,$$

i.e., the Hölder exponent of θ is the negative of the slope of the graph of $\log_A \|\mathcal{L}_M \theta\|_{L^\infty(\mathbb{T})}$ vs. M.

Graphs of this type for some classes of conjugacies are shown in Figure 4.10. Each case is represented by two conjugacies, the first one depicted by a big empty shape, and the second one – by a small full shape: $(f_{0.3}^N, f_{0.6}^C)$ and $(f_{0.3}^N, f_{0.7}^C)$ – circles, $(f_{0.5}^N, f_{0.6}^Q)$ and $(f_{0.5}^N, f_{0.9}^Q)$ – squares, $(f_{0.6}^C, f_{0.6}^Q)$ and $(f_{0.3}^C,$

$f_{0.9}^{\mathrm{Q}}$) – diamonds, ($f_{0.6}^{\mathrm{C}}$, $f_{0.3}^{\mathrm{C}}$) and ($f_{0.7}^{\mathrm{C}}$, $f_{0.6}^{\mathrm{C}}$) – triangles down, ($f_{0.6}^{\mathrm{Q}}$, $f_{0.9}^{\mathrm{Q}}$) and ($f_{0.9}^{\mathrm{Q}}$, $f_{1.2}^{\mathrm{Q}}$) – triangles up. Clearly, the smoothness of the conjugacies of different classes is different, but this graph does not allow us to find the smoothness of the conjugacies precisely (and for θ^{CC} and θ^{QQ} the results are very poor). The reasons for this are the following.

Firstly, each point on this graph is computed by using not all Fourier coefficients of θ, but only a dyadic block of them, so for small M the points on the graph are based on a small number of Fourier coefficients. For large M the points are based on larger number of Fourier coefficients, but these coefficients are affected by the numerical noise. Also, the number of points in the figure is of order $\log_A$ of the number of Fourier coefficients found, i.e., it is significantly smaller than the number of coefficients. In our explorations we used values of A around 1.5.
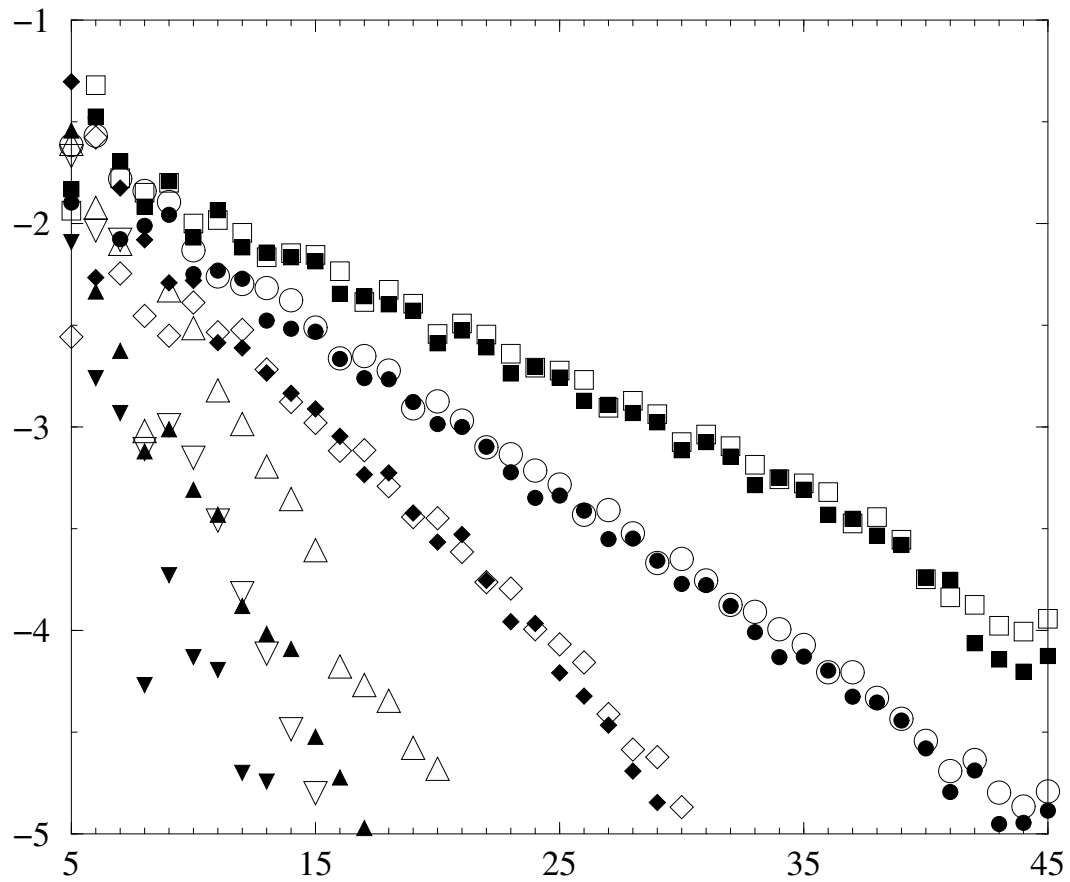
Figure 4.10: Plot of $\log_{10} \|\mathcal{L}_M \theta\|_{L^\infty(\mathbb{T})}$ vs. M (for $A = 1.4$) for pairs of conjugacies of five different types.

4.5.5 CLP Method

From numerical point of view, CLP method (based on Theorem 4.4.4) is much better than DLP.

First of all, we can calculate $\|\frac{\partial^\eta}{\partial t^\eta} e^{-t\sqrt{-\Delta}} f\|_{L^\infty(\mathbb{T})}$ for as many values of t as we wish. Furthermore, for each value of t, the value of this norm is based on the values of *all* known Fourier coefficients of f. Finally, one can perform calculations for different values of η and check whether they yield the same value of α – this is a very good test of the reliability of the numerical results.

To illustrate how well this method works, we show in Figure 4.11 plots of $\log_{10} \|\frac{\partial^2}{\partial t^2} e^{-t\sqrt{-\Delta}} w_{0.57,3}\|_{L^\infty(\mathbb{T})}$ vs. $\log_{10} t$ for 2^{22} (circles), 2^{13} (x's), and 2^{10} (pluses) Fourier components based on the values of $w_{0.57,3}$ at the points $(f_{0.5}^N)^n(0)$ for $n = 0, \ldots, 2^{21} - 1$. Evidently, the position of the plateau for small t's depends on the number of Fourier coefficients used in the computation. Theoretically, the regularity of $w_{0.57,3}$ is $-\log_3 0.57 = 0.5117\ldots$. The slope of the straight line that fits best the full circles in the figure is -1.4908, so the numerically found regularity according to (4.17) is $2 - 1.4908 = 0.5092$ – a value that differs from the exact one by only 0.002.

Figure 4.12 shows graphs of $\log_{10} \|\frac{\partial^\eta}{\partial t^\eta} e^{-t\sqrt{-\Delta}} \theta\|_{L^\infty(\mathbb{T})}$ vs. $\log_{10} t$ for $\eta = 1, 2, 3$; θ is the conjugacy between $f_{0.2}^N$ and $f_{0.6}^C$. The results of the linear regression of these data are the presented in the table. The uncertainties are just the the standard errors of the regression.

179
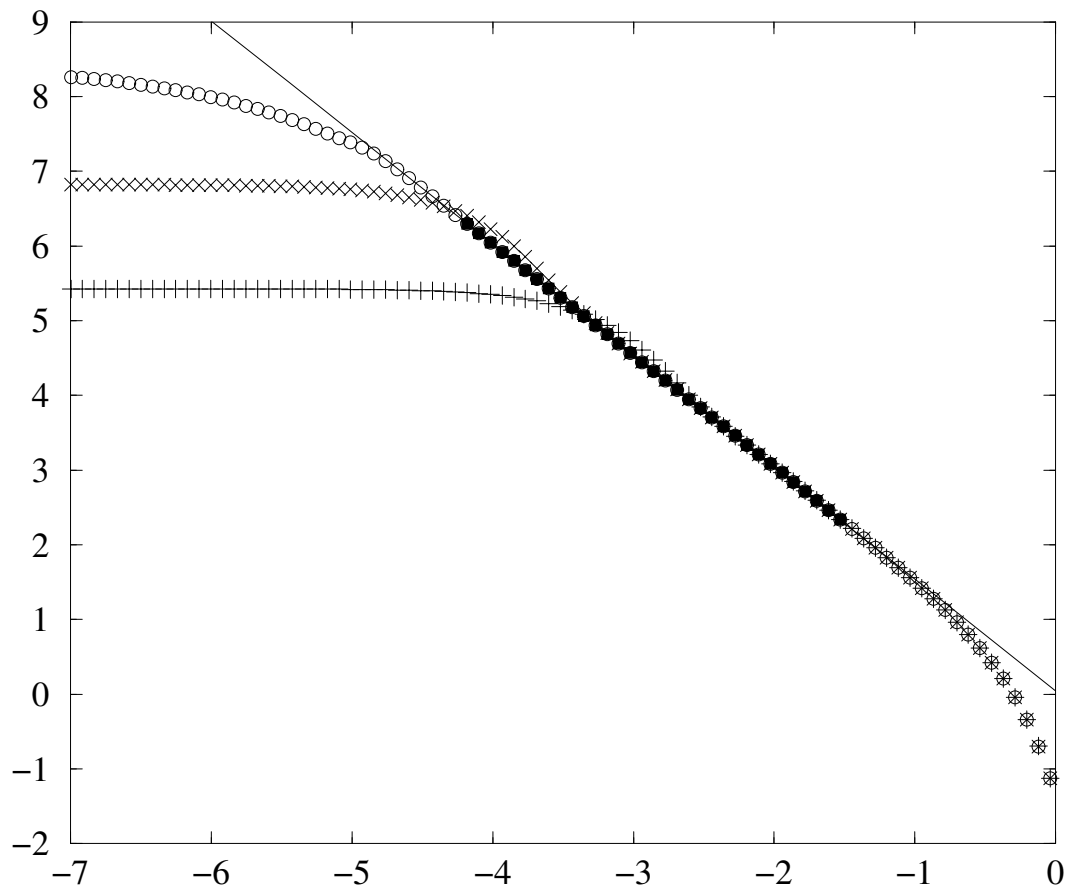
Figure 4.11: Plot of $\log_{10} \left\| \frac{\partial^2}{\partial t^2} e^{-t\sqrt{-\Delta}} w_{0.57, 3} \right\|_{L^\infty(\mathbb{T})}$ vs. $\log_{10} t$.

180
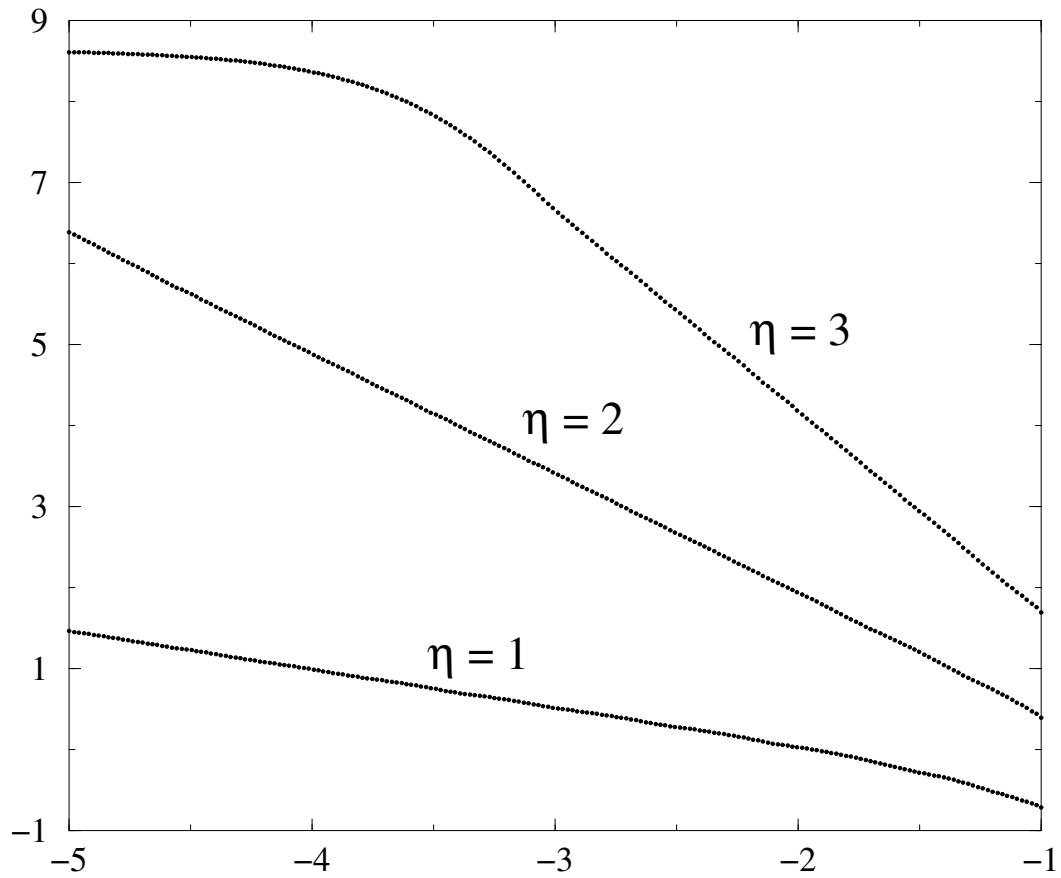
Figure 4.12: Plot of $\log_{10} \|\frac{\partial^\eta}{\partial t^\eta} e^{-t\sqrt{-\Delta}}\theta\|_{L^\infty(\mathbb{T})}$ vs. $\log_{10} t$ for $\eta = 2$ and $\eta = 3$ of all 12 conjugacies between an N and a C map for four N and three C maps with different parameter values. Each line connects 146 points; to obtain each point, we have used 10^6 iterates and $2^{21} \approx 10^6$ spline points.

181

η	Range of $\log_{10} t$	Regularity
1	$[-5.0, -4.0]$	0.5247 ± 0.0009
2	$[-3.5, -2.5]$	0.5253 ± 0.0012
3	$[-3.0, -1.5]$	0.5244 ± 0.0008

In Figure 4.13, we show $\log_{10} \|\frac{\partial^\eta}{\partial t^\eta} e^{-t\sqrt{-\Delta}}\theta\|_{L^\infty(\mathbb{T})}$ vs. $\log_{10} t$ for $\eta = 1$, 2 for all the 16 conjugacies between the four N and four C maps we considered. We call attention to the fact that not only the lines are parallel, but they are also very close.

The CLP method can be used also to test some features of the expansion (4.1). Since (4.1) is supposed to hold only in the asymptotic limit of very small scales, we can use Remark 4.4.4 and the scalings (4.15). Note that, taking the convolution of (4.1) with the Poisson kernel and using (4.15), we obtain:

$$
\begin{aligned}
P_t \ * \ & \left[\sum_n \lambda_1^n (H_1 \circ \alpha^n)(x) + \lambda_2^n (H_2 \circ \alpha^n)(x) + \cdots \right] \\
= \ & \sum_n \left[\lambda_1^n \left[P_{\alpha^n t} * H_1 \right] (\alpha^n x) + \lambda_2^n \left[P_{\alpha^n t} * H_2 \right] (\alpha^n x) + \cdots \right] .
\end{aligned}
$$

If we take suprema in x and then logarithms, we obtain that the structure of the main term for the resulting function considered as a function of $\log t$ is a sum of a linear function and a function that is periodic. The slope of the linear function is, of course, according to Theorem 4.4.4, the degree of differentiability, but if we subtract off the linear part, we should see the periodicity.

This exploration of the first differences is undertaken in Figure 4.14, where we plot the first differences of the graph of $\log_{10} \|\frac{\partial^\eta}{\partial t^\eta} e^{-t\sqrt{-\Delta}}\theta\|_{L^\infty(\mathbb{T})}$ as a function of $\log_{10} t$ (for $\eta = 2$, 3) at equally spaced points.

Figure 4.13: Plot of $\log_{10} \|\frac{\partial^\eta}{\partial t^\eta} e^{-t\sqrt{-\Delta}}\theta\|_{L^\infty(\mathbb{T})}$ vs. $\log_{10} t$ for $\eta = 1, 2$ for 16 conjugacies of type NC.

183
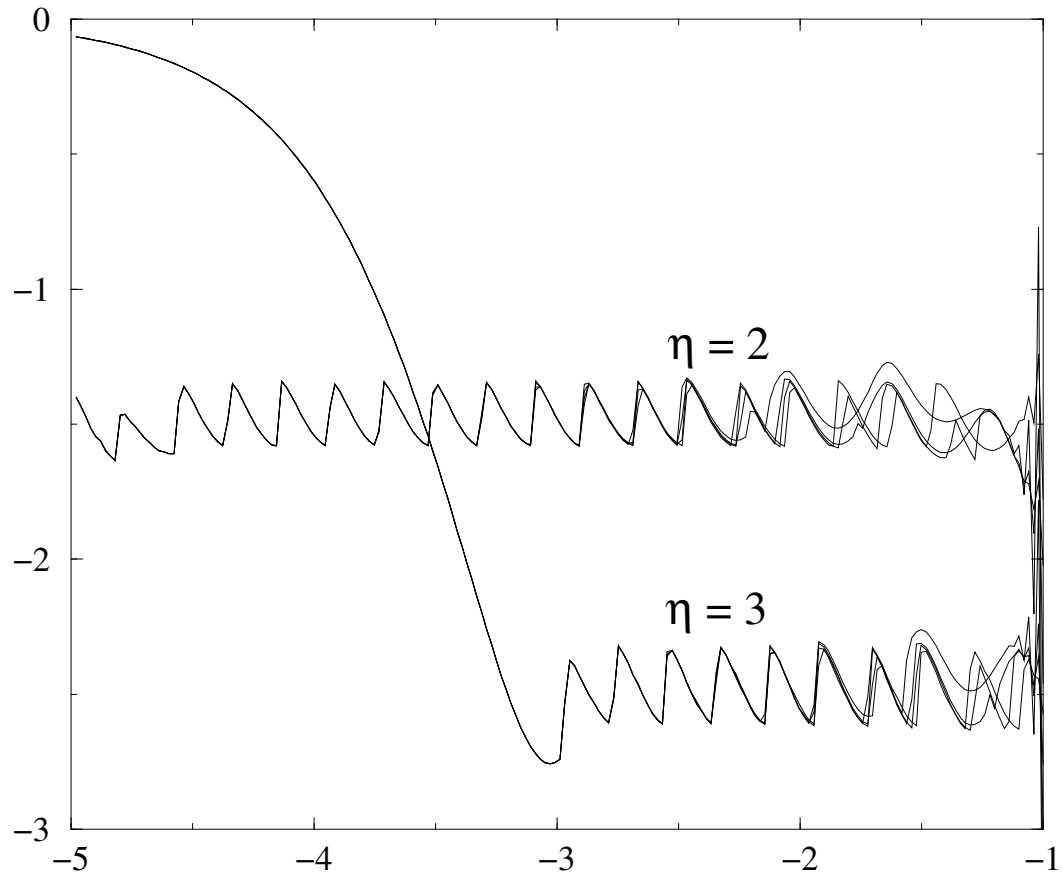
Figure 4.14: Plot of the first differences of the graph of $\log_{10} \|\frac{\partial^\eta}{\partial t^\eta} e^{-t\sqrt{-\Delta}}\theta\|_{L^\infty(\mathbb{T})}$ (in arbitrary units) vs. $\log_{10} t$ for $\eta = 2$ and $\eta = 3$ for four θ of type NC.

Note that taking first differences turns a linear function into a constant and a periodic function into a periodic function. Higher order differences eliminate the linear function and receive contributions of the periodic part.

In Figure 4.15, we show the same plot as above for four conjugacies of type NQ and the first and second differences of the plot.

We call attention to the fact that the periodic corrections we plot quickly become independent of the functions we start with which corresponds to the fact that the function H_1 is universal. This is particularly remarkable for the case of second differences since they are very susceptible to numerical errors. Hence, this gives us confidence on the reliability of the methods we have used.

We note that the computation of first differences is one of the data analysis features included in `ACE/gr`, so that it is quite feasible to carry out these explorations in an interactive way for a variety of functions.
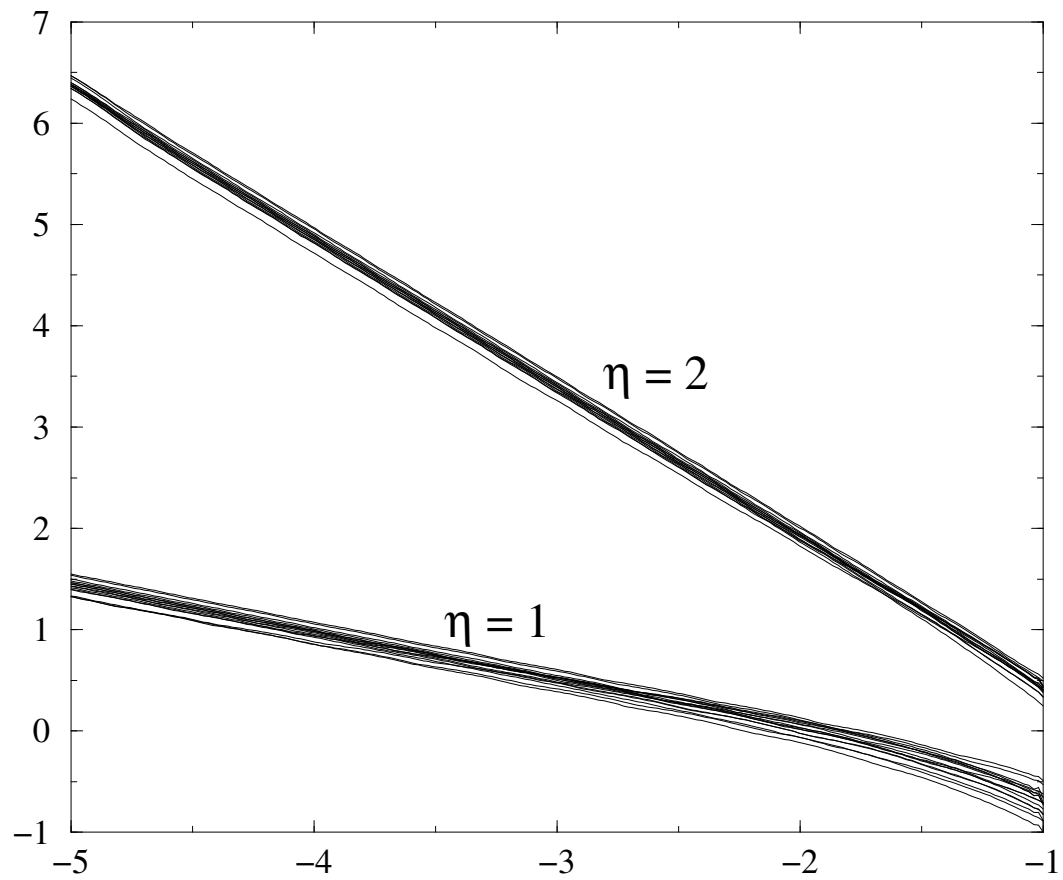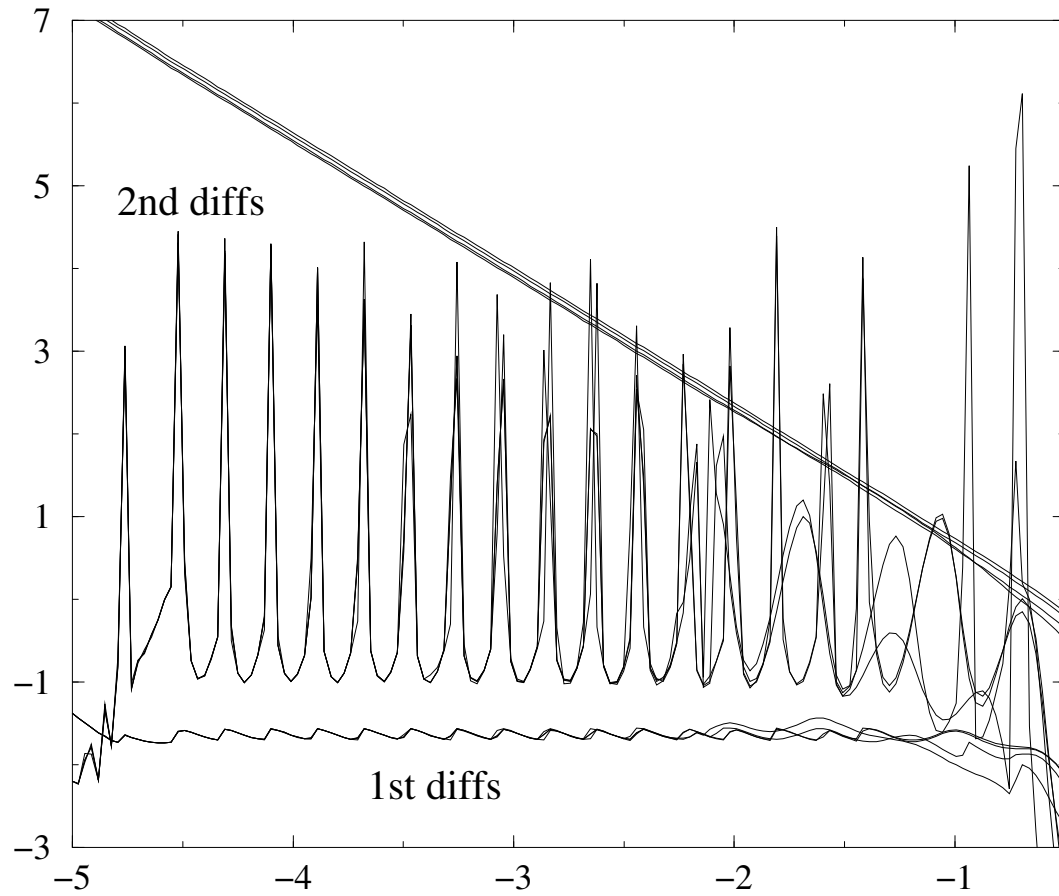
Figure 4.15: Plot of $\log_{10} \|\frac{\partial^2}{\partial t^2} e^{-t\sqrt{-\Delta}}\theta\|_{L^\infty(\mathbb{T})}$ vs. $\log_{10} t$ for four θ of type NC and the first and second differences.

186

4.5.6   Decay of Wavelet Coefficients

Theorem 4.4.5 can be used to asses the regularity of the functions we study by examining the decay of the coefficients of wavelet transform.

Nevertheless, we do not think that for our functions it is necessary to appeal to Theorem 4.4.5.

Note that the working hypothesis (A4) gives a representation of the function.

It is not difficult to show that, for functions of the form (4.1) in the working hypothesis (A4), the degree of regularity is a simple ratio between the logarithms of λ and the scaling factor α defined in (4.1).

For functions of this form, the logarithm of the size of the projections on a space V_j should decay linearly with j irrespective of what is the wavelet used. In particular, one does not need to use wavelets which are smoother than the regularity observed to obtain the scaling exponents, which also give the regularity.

In our numerical studies we have used Daubechies wavelets of order 4, 10, 20, which we will denote as D4, D10, D20 respectively. It is known that D4$\in \Lambda_{0.55...}$ and not in any more regular space. For large N, D2$N \in \Lambda_{l_N}$ where $l_N \approx 0.20775\, N$ (see, e.g., Härdle *et al* [90, Section 7.1]).

We note that even if Theorem 4.4.5 does not apply to the measurements of regularity with D4 in some of the cases we consider, nevertheless, we obtain decays which are extremely similar to those obtained using D10 or D20, for

which Theorem 4.4.5 does apply and also extremely similar to the regularities obtained by other methods.

Moreover, we also note that the upper bounds given by Theorem 4.4.5 are identities.

We interpret the coincidence of the rates of decays obtained by any wavelets and the saturation of the bounds as (at least circumstantial) evidence that the the asymptotic scalings in (4.1) indeed hold. As we will discuss later, similar coincidences are observed for other methods.

In Figure 4.16 we show $\log_2 \sup_k |\langle \theta, \psi_{jk} \rangle|$ vs. j for several θ^{QN} and θ^{NQ} maps. The slope of the straight lines on this graph is $-(\alpha + \frac{1}{2})$.

There is one reason why this method works much better with wavelet instead of Fourier coefficients (cf. Figure 4.10): The cubic interpolation in the large gaps distorts all Fourier coefficients. At the same time, in the case of wavelets it only affects the ones whose support intersects the gap; moreover, the "artificial local smoothing" due to the interpolation decreases the wavelets supported at the gap, which does not change $\sup_k |\langle \theta, \psi_{jk} \rangle|$ for fixed j.
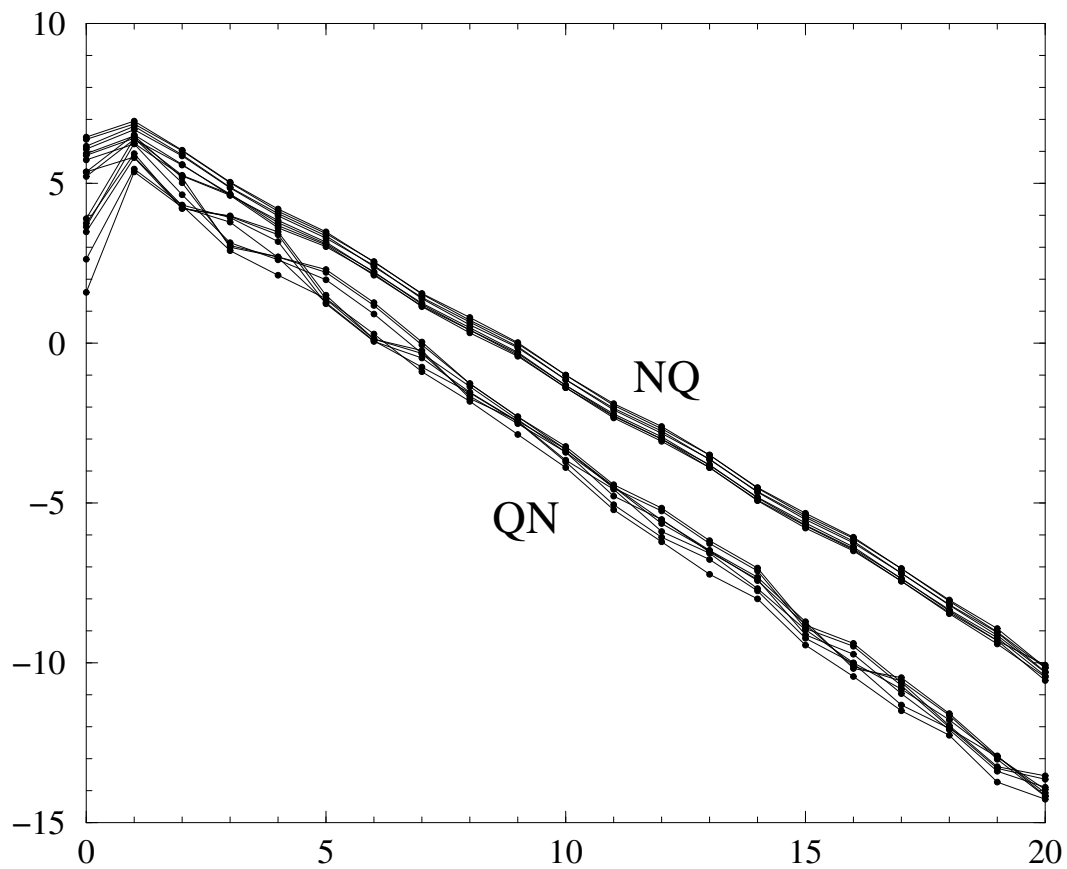
Figure 4.16: Plot of $\log_2 \sup_k |\langle \theta, \psi_{jk} \rangle|$ vs. j for 12 conjugacies of type NQ (for 2^{22} interpolated values based on 10^7 iterates) and 12 of type QN (for 2^{21} interpolated values based on 10^6 iterates).

4.5.7 Approximation with Wavelets

The method based on Theorem 4.4.6 yields very good results. In Figure 4.17 we show plots of $\log_2 \|\theta - \Pi_j \theta\|_{L^\infty(\mathbb{T})}$ vs. j for several θ^{NC} and θ^{CN}. The slope of the straight lines in this graph is $-\alpha$.

As in the previous case, we note that we have used D4, D10 and D20. Theorem 4.4.6 does not apply to D4 in some cases. We, nevertheless, find the same linear decay as with the other methods and we interpret it as a confirmation of the asymptotic scaling of the function.
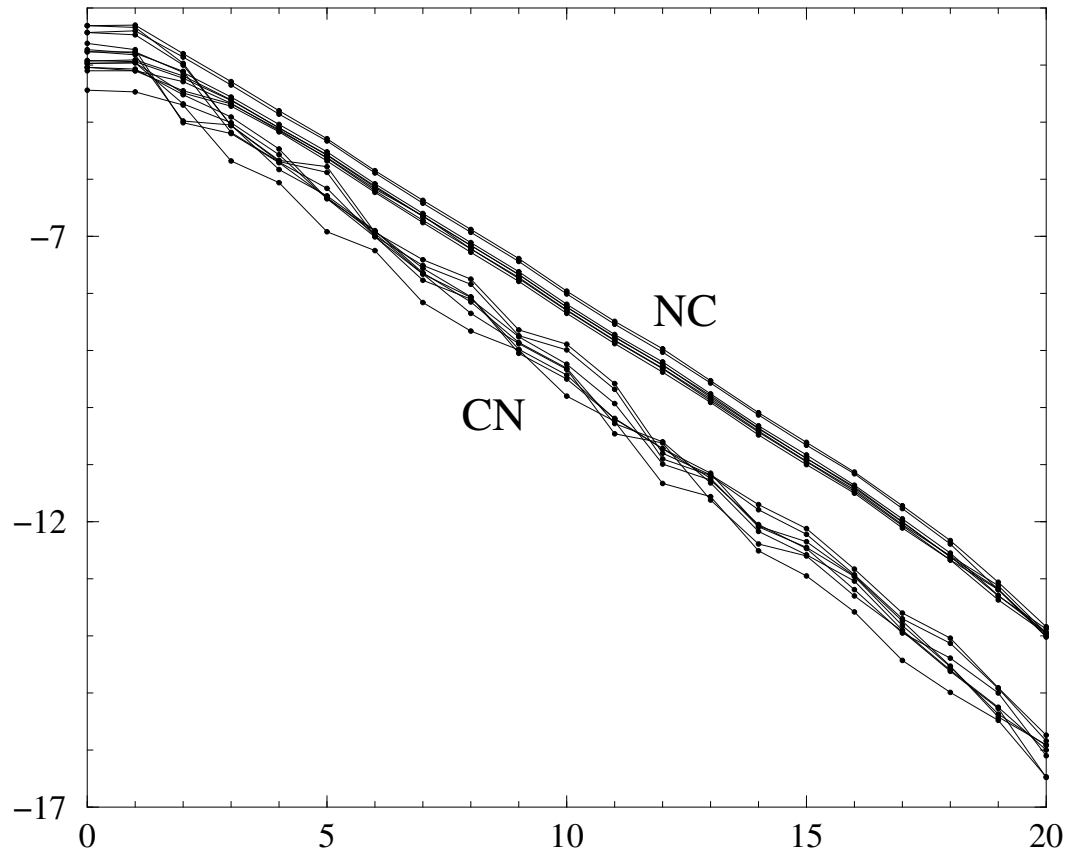
Figure 4.17: Plot of $\log_2 \|\theta - \Pi_j \theta\|_{L^\infty(\mathbb{T})}$ vs. j for 12 conjugacies of type NC (for 2^{22} interpolated values based on 10^7 iterates) and 12 of type CN (for 2^{21} interpolated values based on 2×10^6 iterates).

4.6   Results

In this section we give the numerical values of the Hölder exponents of the conjugacies.

To determine these values, we used the methods based on Theorems 4.4.1, 4.4.3, 4.4.4, 4.4.5, 4.4.6.

To find the smoothness of a particular type of conjugacy, we applied all these methods to study numerically the smoothness of the conjugacies between all possible combinations of circle maps studied (four N, four C,and four Q maps).

As an example, we show in the tables below the results of our analysis of the regularity of the conjugacies between N and Q maps as well as the results of the same methods applied to the test functions $w_{0.66745,3}$, whose Hölder exponent, 0.36800..., is close to the one of the conjugacies of type θ^{NQ}.

The column "Function" indicates the function analyzed: "w on $f_{0.2}^{\mathrm{N}}$" means the regularity of the function $w_{0.66745,3}$ calculated at the points $(f_{0.2}^{\mathrm{N}})^n(0)$, and θ $(f_{0.2}^{\mathrm{N}}/f_{4/3}^{\mathrm{Q}})$ means the conjugacy between $f_{0.2}^{\mathrm{N}}$ and $f_{4/3}^{\mathrm{Q}}$.

The column "Finite diffs" shows the results of the smoothness found by using the finite difference method.

The columns "CLP, $\eta = 1, 2, 3$" display the results of the CLP analysis for different numbers of derivatives.

"Decay D4, D10, D20" contain the results of analysis of the decay rate of the coefficients of Daubechies 4 (resp. 10, 20) wavelets, while "Approx D4,

D10, D20" shows the results of the study of the speed of the approximation using these wavelets.

The meaning of the notations below is the following: $0.3661(13)$ means 0.3661 ± 0.0013. The error is the standard error of the linear regression.

Function	Finite diffs	CLP, $\eta = 1$	CLP, $\eta = 2$	CLP, $\eta = 3$
w on $f_{0.2}^{\mathrm{N}}$	0.3508(162)	0.3556(4)	0.3661(13)	0.3683(94)
w on $f_{0.3}^{\mathrm{N}}$	0.3511(156)	0.3625(2)	0.3659(13)	0.3680(93)
w on $f_{0.5}^{\mathrm{N}}$	0.3483(155)	0.3632(2)	0.3661(13)	0.3681(94)
w on $f_{0.8}^{\mathrm{N}}$	0.3486(155)	0.3634(4)	0.3660(13)	0.3682(94)
$\theta\ (f_{0.2}^{\mathrm{N}}/f_{4/3}^{\mathrm{Q}})$	0.3652(33)	0.3611(10)	0.3682(8)	0.3676(2)
$\theta\ (f_{0.2}^{\mathrm{N}}/f_{0.6}^{\mathrm{Q}})$	0.3642(34)	0.3622(12)	0.3675(9)	0.3710(6)
$\theta\ (f_{0.2}^{\mathrm{N}}/f_{1.2}^{\mathrm{Q}})$	0.3649(33)	0.3613(10)	0.3681(8)	0.3670(3)
$\theta\ (f_{0.2}^{\mathrm{N}}/f_{0.9}^{\mathrm{Q}})$	0.3684(29)	0.3623(11)	0.3680(8)	0.3667(3)
$\theta\ (f_{0.3}^{\mathrm{N}}/f_{4/3}^{\mathrm{Q}})$	0.3635(27)	0.3616(10)	0.3685(8)	0.3677(3)
$\theta\ (f_{0.3}^{\mathrm{N}}/f_{0.6}^{\mathrm{Q}})$	0.3626(28)	0.3625(12)	0.3679(10)	0.3703(5)
$\theta\ (f_{0.3}^{\mathrm{N}}/f_{1.2}^{\mathrm{Q}})$	0.3633(28)	0.3618(10)	0.3684(8)	0.3671(3)
$\theta\ (f_{0.3}^{\mathrm{N}}/f_{0.9}^{\mathrm{Q}})$	0.3615(29)	0.3628(11)	0.3685(8)	0.3668(3)
$\theta\ (f_{0.5}^{\mathrm{N}}/f_{4/3}^{\mathrm{Q}})$	0.3646(25)	0.3610(10)	0.3677(9)	0.3671(2)
$\theta\ (f_{0.5}^{\mathrm{N}}/f_{0.6}^{\mathrm{Q}})$	0.3641(27)	0.3616(11)	0.3672(9)	0.3684(3)
$\theta\ (f_{0.5}^{\mathrm{N}}/f_{1.2}^{\mathrm{Q}})$	0.3647(27)	0.3612(10)	0.3676(9)	0.3666(3)
$\theta\ (f_{0.5}^{\mathrm{N}}/f_{0.9}^{\mathrm{Q}})$	0.3757(36)	0.3620(10)	0.3681(9)	0.3664(3)
$\theta\ (f_{0.8}^{\mathrm{N}}/f_{4/3}^{\mathrm{Q}})$	0.3674(28)	0.3607(10)	0.3680(9)	0.3654(4)
$\theta\ (f_{0.8}^{\mathrm{N}}/f_{0.6}^{\mathrm{Q}})$	0.3640(26)	0.3615(10)	0.3681(9)	0.3645(3)
$\theta\ (f_{0.8}^{\mathrm{N}}/f_{1.2}^{\mathrm{Q}})$	0.3666(28)	0.3612(10)	0.3679(9)	0.3649(5)
$\theta\ (f_{0.8}^{\mathrm{N}}/f_{0.9}^{\mathrm{Q}})$	0.3592(37)	0.3624(10)	0.3683(7)	0.3649(5)

Function	Decay D4	Decay D10	Decay D20	Approx D4	Approx D10	Approx D20
w on $f_{0.2}^{N}$	0.3548(126)	0.3455(340)	0.3558(461)	0.3672(36)	0.3658(102)	0.3636(136)
w on $f_{0.3}^{N}$	0.3563(126)	0.3460(350)	0.3554(469)	0.3685(38)	0.3657(101)	0.3650(141)
w on $f_{0.5}^{N}$	0.3569(123)	0.3478(344)	0.3550(461)	0.3659(32)	0.3642(100)	0.3645(140)
w on $f_{0.8}^{N}$	0.3559(126)	0.3482(345)	0.3514(455)	0.3678(33)	0.3641(101)	0.3620(138)
$\theta\ (f_{0.2}^{N}/f_{4/3}^{Q})$	0.3686(104)	0.3667(247)	0.3643(161)	0.3713(12)	0.3706(75)	0.3664(69)
$\theta\ (f_{0.2}^{N}/f_{0.6}^{Q})$	0.3674(106)	0.3556(160)	0.3670(161)	0.3717(11)	0.3710(76)	0.3660(72)
$\theta\ (f_{0.2}^{N}/f_{1.2}^{Q})$	0.3684(105)	0.3670(249)	0.3647(162)	0.3711(12)	0.3702(75)	0.3661(70)
$\theta\ (f_{0.2}^{N}/f_{0.9}^{Q})$	0.3677(105)	0.3744(217)	0.3629(155)	0.3710(13)	0.3672(49)	0.3658(70)
$\theta\ (f_{0.3}^{N}/f_{4/3}^{Q})$	0.3692(108)	0.3658(246)	0.3638(155)	0.3701(8)	0.3691(71)	0.3669(67)
$\theta\ (f_{0.3}^{N}/f_{0.6}^{Q})$	0.3686(109)	0.3632(270)	0.3661(155)	0.3703(7)	0.3698(73)	0.3665(68)
$\theta\ (f_{0.3}^{N}/f_{1.2}^{Q})$	0.3691(108)	0.3695(234)	0.3644(155)	0.3698(8)	0.3688(72)	0.3666(67)
$\theta\ (f_{0.3}^{N}/f_{0.9}^{Q})$	0.3684(108)	0.3546(345)	0.3630(169)	0.3700(8)	0.3725(61)	0.3665(67)
$\theta\ (f_{0.5}^{N}/f_{4/3}^{Q})$	0.3694(106)	0.3631(249)	0.3735(164)	0.3712(9)	0.3772(77)	0.3728(70)
$\theta\ (f_{0.5}^{N}/f_{0.6}^{Q})$	0.3696(107)	0.3641(195)	0.3812(140)	0.3712(9)	0.3780(79)	0.3724(72)
$\theta\ (f_{0.5}^{N}/f_{1.2}^{Q})$	0.3694(106)	0.3663(216)	0.3742(165)	0.3710(9)	0.3766(77)	0.3725(70)
$\theta\ (f_{0.5}^{N}/f_{0.9}^{Q})$	0.3689(106)	0.3642(308)	0.3847(166)	0.3709(10)	0.3594(58)	0.3723(70)
$\theta\ (f_{0.8}^{N}/f_{4/3}^{Q})$	0.3676(105)	0.3682(249)	0.3629(181)	0.3684(7)	0.3687(73)	0.3692(66)
$\theta\ (f_{0.8}^{N}/f_{0.6}^{Q})$	0.3673(107)	0.3701(239)	0.3560(186)	0.3685(7)	0.3699(66)	0.3695(68)
$\theta\ (f_{0.8}^{N}/f_{1.2}^{Q})$	0.3675(105)	0.3681(250)	0.3634(182)	0.3683(7)	0.3686(73)	0.3691(66)
$\theta\ (f_{0.8}^{N}/f_{0.9}^{Q})$	0.3619(101)	0.3355(325)	0.3440(218)	0.3687(7)	0.3550(86)	0.3694(66)

As seen from the tables above, the results obtained by using different methods are consistent, the most precise being the ones based on using CLP. In the table below, we give the Hölder exponent of the conjugacy between the maps f and g. The margins of error are determined empirically, and only in very few cases outliers are ignored.

In the case of conjugacies of types CC and QQ for reasons explained in the text, we were not able to determine the smoothness of the conjugacies, but only to give a rough estimates.

$\downarrow f \quad g \ \rightarrow$	N	C	Q
N	Analytic	0.527 ± 0.003	0.368 ± 0.003
C	0.63 ± 0.02	$1.4_{-0.2}^{+0.4}$	0.71 ± 0.03
Q	0.54 ± 0.05	0.86 ± 0.02	1.7 ± 0.5

4.7 Some Bounds on the Regularity of Conjugacies

In this section, we derive some bounds for the regularities of the congugacies.

4.7.1 Some Simple Bounds

It follows directly from the definition of Λ_α, $0 < \alpha < 1$, that if $h_1 \in \Lambda_{\alpha_1}$, $h_2 \in \Lambda_{\alpha_2}$, then $h_1 \circ h_2 \in \Lambda_{\alpha_1 \alpha_2}$. It is not difficult to produce functions that saturate the above bounds (just take $h_i(x) = |x|^{\alpha_i}$) as well as functions for this bound is not optimal (take $h_1(x) = |x|^{\alpha_1}$, $h_2 = |x - 0.1|^{\alpha_2}$).

We also note that if $h^{1,2} \circ f_1 = f_2 \circ h^{1,2}$, $h^{2,3} \circ f_2 = f_3 \circ h^{2,3}$, and we define $h^{1,3}$ by $h^{1,3} = h^{1,2} \circ h^{2,3}$, we have $h^{1,3} \circ f_1 = f_3 \circ h^{1,3}$.

Let $\rho^{a,b}$ (where a, b are among N, C, Q) be the regularities of the conjugacy between golden mean circle maps of class a to circle maps of class b, i.e., the entries in the table above.

It follows from the regularity of the composition that when a, b, c are such that $a \neq b$, $b \neq c$, we should have

$$\rho^{a,c} \geq \rho^{a,b} \rho^{b,c} \tag{4.21}$$

The inequality (4.21) can be verified in two cases in the table that we have. Namely, we can take $a = $ N, $b = $ C, $c = $ Q, or $a = $ Q, $b = $ C, $c = $ N. When we carry out this verification, we find out that, up to the error of the calculation, we obtain that (4.21) becomes an identity.

195

This is presumably not a coincidence. We believe that it is again a manifestation of the self-similarity of the function at small scales. If we compose two functions that in each small scale have oscillations comparable to those allowed by the Hölder exponent, the resulting function will also have oscillations that are comparable to the product of the Hölder exponents. Note however that this argument does not suggest that there is a simple relation between the regularity of a function and its inverse.

We note that the equation (4.21) can be described as saying that the regularities of the conjugacies as indexed by the classes form a multiplicative supercocycle. We find empirically it is a cocycle.

In the following section, we will derive upper bounds for the regularity that are cocycles.

4.7.2 Scalings of the Recurrence and Upper Bounds on Hölder Exponents of Conjugacies

In this section, we discuss the relation between the scaling properties and smoothness of the conjugacy.

Scalings have been studied numerically from the beginning of renormalization theory. Some of them have been probed to hold.

In this section, we will report some rigorous results that show that if certain scalings hold, then there are bounds for the regularity of the conjugacy.

Since these scaling relations – hypothesis to our lemma – are numerically accessible, we can use the rigorous results to obtain numerical upper

bounds.

One of the first numerical observations that were made in the study of the golden mean rotation number critical circle maps was that

$$(f^\bullet)^{Q_n}(0) \approx \iota_\bullet^{-n} , \tag{4.22}$$

where $\bullet$ stands for N, C, Q, and $\iota_\bullet$ are universal constants. The numbers $\iota_\bullet$ play a fundamental role in the fixed point equations.

For non-critical maps, because of Theorem 2.4.3, ι_N is the same as for rotations by golden mean, and, by using the well-known relation

$$\frac{Q_n}{Q_{n+1}} = \sigma_G + C(-\sigma_G{}^2)^n + o(\sigma_G{}^{2n}) ,$$

we obtain $\iota_N = \sigma_G{}^{-1}$.

We note that for the cubic critical case, there are unpublished computer assisted proofs (Mestel [140], Lanford and de la Llave [124]) that establish the existence of the ι_C, upper and lower bounds for it, and the fact that (4.22) holds for maps in open sets.

Some relation between the scaling properties of the returns and the regularity of the conjugacy is given by

Lemma 4.7.1. *Let*

$$f_1^{Q_n}(0) = C_1 \iota_1^{-n} + o(\iota_1^{-n}) \tag{4.23}$$

$$f_2^{Q_n}(0) = C_2 \iota_2^{-n} + o(\iota_2^{-n}) \tag{4.24}$$

and

$$\alpha := \log|\iota_2|/\log|\iota_1| \notin \mathbb{N}. \tag{4.25}$$

Then, if h satisfies $h \circ f_1 = f_2 \circ h$, $h(0) = 0$, then, for every $\delta > 0$,
$h \notin \Lambda_{\alpha+\delta}$.

Proof. For any $\chi > 0$ we have

$$\frac{h \circ f_1^{Q^n}(0) - h(0)}{\left[f_1^{Q^n}(0) - 0\right]^\chi} = \frac{f_2^{Q^n}(0)}{\left[f_1^{Q^n}(0)\right]^\chi} = \frac{C_2\iota_2^{-n} + o(\iota_2^{-n})}{C_1^\chi \iota_1^{-\chi n} + o(\iota_1^{-\chi n})} . \tag{4.26}$$

We argue by contradiction: if $h \in \Lambda_\chi$ for some $\chi > \alpha$, we use (4.26) to prove by induction that $h^{(n)}(0) = 0$ for all $n \leq \alpha$, $n \in \mathbb{N}$. Then we note that $h \in \Lambda_{\alpha+\delta}$ (for any $\delta > 0$) would imply that if we substitute $\chi = \alpha + \delta$ in (4.26), the left-hand side is bounded uniformly in n. At the same time, the right-hand side of (4.26) is unbounded in n. $\qquad\square$

We emphasize that Lemma 4.7.1 does not conclude anything when $\beta \in \mathbb{N}$; in particular, it does not conclude anything in the cases when f_1 and f_2 have the same scaling factor ι, which happens when f_1 and f_2 are in the same universality class.

We have verified the relations (4.22) for the maps we considered and obtained values of ι as follows:

$$\iota_C = -1.2886 , \qquad \iota_Q = -1.194 , \tag{4.27}$$

198

which agree with the values reported in Shenker [179] (for the C case), and those in the papers Hu *et al* [99], Delbourgo and Kenny [49], even though they consider functions that are periodized versions of polynomials which are not C^1.

Taking the values in (4.27) and the exact value for ι_N, we obtain the following upper bounds for the regularity of the conjugacies between the maps f and g.

$\downarrow f \quad g \rightarrow$	N	C	Q
N	?	0.5269	0.368
C	1.898	?	0.70
Q	2.72	1.43	?

We note that the in the cases NC, NQ, CQ, the upper bounds obtained applying Lemma 4.7.1 agree within the margin of error with the values of the regularity reported. In the other cases, the results are absurd.

We conjecture that indeed the upper bounds produced by applying Lemma 4.7.1 are sharp for those cases.

Note that the fact that the upper bounds that work in one case are far off in another seem to imply that there are different mechanisms limiting the regularity. In the cases CN, QN, QC, these mechanisms cannot be just a simple scaling argument.

We note that since the α defined in (4.25) is the ratio of a quantity depending on the domain and a quantity depending on the range, the upper bounds that we have derived form a multiplicative cocycle.

199

For the sake of completeness, we also point out that there is a very similar argument that gives upper bounds for the regularity of the conjugacy for the maps in the same class. The following set of ideas was found useful in de la Llave and Schafer [133]. There it is shown that this argument produced upper bounds that were sharp in the case of conjugacies of limiting sets of unimodal maps.

Lemma 4.7.2. *Assume that*

$$
\begin{aligned}
f_1^{Q_n}(0) &= C_1 \iota^{-n} + D_1 \tilde{\iota}^{-n} + o(\tilde{\iota}^{-n}) \\
f_2^{Q_n}(0) &= C_2 \iota^{-n} + D_2 \tilde{\iota}^{-n} + o(\tilde{\iota}^{-n})
\end{aligned}
$$

with $|\iota| < |\tilde{\iota}|$, $C_1 C_2 \neq 0$,

$$
D_2 \neq (C_2/C_1)D_1 \tag{4.28}
$$

and $\alpha := \log |\tilde{\iota}| / \log |\iota| \notin \mathbb{N}$. Then, if h satisfies $h \circ f_1 = f_2 \circ h$, $h(0) = 0$, then $h \notin \Lambda_{\alpha+\delta}$ for any $\delta > 0$.

Proof. The argument is very similar to the argument that proved Lemma 4.7.1.

Note that the assumptions imply that $\alpha > 1$. Hence we are only excluding regularities higher than C^1.

We argue by contradiction, assuming that $h \in \Lambda_{\alpha+\delta}$. We note that

$$
h \circ f_1^{Q_n}(0) - h(0) = f_2^{Q_n}(0) . \tag{4.29}
$$

Since $h \in \Lambda_{\alpha+\delta}$, and $\alpha > 1$, we conclude that $h'(0) = C_2/C_1 \neq 0$. Hence h is invertible in a neighborhood of zero and $h^{-1} \in \Lambda_{\alpha+\delta}$.

We note that $h(t) = P(t) + R(t)$ where $P(t)$ is a polynomial of degree $[\alpha]$ and $|R(t)| \leq |t|^{\alpha+\delta}$.

Given the assumptions on the degrees we have made, we have

$$P(C_1 \iota^{-n} + D_1 \tilde{\iota}^{-n} + o(\tilde{\iota}^{-n})) = h'(0)\tilde{\iota}^{-n} + \sum_j C_j(\iota^j)^{-n} + o(\iota^{-n([\beta]+1)})$$

We also note that $R(C_1 \iota^{-n} + D_1 \tilde{\iota}^{-n} + o(\tilde{\iota}^{-n})) = o(\tilde{\iota}^{-n})$.

Equating the coefficients of the $\tilde{\iota}^{-n}$ in (4.29), we obtain $D_2 = (C_2/C_1)D_1$, which contradicts our assumption (4.28). This is the desired contradiction with the assumption that h admitted a Taylor expansions near 0 with Hölder bounds. $\qquad\square$

Note that in contrast with Lemma 4.7.1, Lemma 4.7.2 contains a hypothesis (4.28) which could fail for a finite codimension set of maps. This is to be expected since the other hypothesis allows to take $f_1 = f_2$, $h = $ Id. In this situation, the conjugacy h is very regular. The elementary theory of renormalization tells us that (4.28) indeed occurs in a set which is of positive codimension.

The conjecture 4.2.1 amounts to the fact that the upper bounds produced by applying Lemma 4.7.2 are sharp.

At the moment, unfortunately, we do not have accurate enough values for the $\tilde{\iota}$ for cubic critical or quintic critical maps and, hence, cannot give concrete values for the upper bounds of the regularity in the CC or QQ cases. It is interesting to remark that in the NN case, these bounds are far from optimal.

4.8   Conclusion

We have studied the problem of the smoothness of maps of the circle with critical points and golden mean rotation number.

The first step was to obtain an extremely precise calculation of the parameters of the function that put us in the correct universality class.

The most important step is to develop a numerical toolkit based on a wide array of methods from harmonic analysis (Littlewood-Paley, wavelets) to study the regularity and the fine scale structure of these functions.

We have used the combination of the methods applied to critical circle maps to asses their range of validity.

We have found indication that the regularity of critical circle maps is limited by considerations other than just scaling of recurrences.

Appendices

Appendix A

Fermi Acceleration

In this Appendix we give more details on the derivation of the map related to the Fermi acceleration, mentioned in Section 2.1.10. The derivation is very similar to the derivation of the circle maps in Section 2.3.5, and we are going to use very similar notations.

Let the ball be moving along the x axis between two (infinitely heavy) walls perpendicular to the x axis and having x coordinates 0 and $a(t)$, respectively. Assume that the collisions of the ball with the walls are elastic.

Let $\{\tau_n\}$ be the times at which the ball bounces back from the stationary wall, $\{\theta_n\}$ the times at which it reaches the oscillating wall (these notations are the same as the one in Figure 2.2, but now the piecewise linear lines correspond to the "world lines" of the ball). Let v_n be the magnitude of the velocity of the ball just before it hits the moving wall for nth time, i.e.,

$$v_n = \lim_{t \to \theta_n - 0} v(t) \ .$$

Since the collision is elastic,

$$v_{n+1} = |v_n - 2a'(\theta_n)| \ .$$

The ball is moving at a speed $v_n + 1$ in the time interval (θ_n, θ_{n+1}), during which it travels from the moving to the stationary wall and back to the stationary one, so the total traveled distance is $a(\theta_n) + a(\theta_{n+1})$. Thus,

$$\theta_{n+1} = \theta_n + \frac{a(\theta_n) + a(\theta_{n+1})}{v_{n+1}} \ .$$

Now recall that the function a is periodic of period 1, so we do not need to know θ, but only $\theta \,(\mathrm{mod}\,1)$. The speed v can take any nonnegative values, so we obtain the map

$$\mathbf{W} : \mathbb{T} \times \mathbb{R}_+ \to \mathbb{T} \times \mathbb{R}_+ : (\theta_n, \, v_n) \mapsto (\theta_{n+1}, \, v_{n+1}) \ ,$$

defined implicitly by

$$
\begin{aligned}
\theta_{n+1} &= \left[\theta_n + \frac{a(\theta_n) + a(\theta_{n+1})}{v_{n+1}} \right] \mathrm{mod}\,1 \\
v_{n+1} &= |v_n - 2a'(\theta_n)| \ .
\end{aligned}
$$

The map $\mathbf{W}$ is two-dimensional, so its dynamics is much more complicated than the dynamics of the circle maps occurring in our treatment of the problem of pulsating optical resonator.

Note that since the map $\mathbf{W}$ is implicitly defined, a simplified (explicit) version of it, which is similar to the standard (Chirikov-Taylor) map, was often studied in the literature instead of $\mathbf{W}$.

Bibliography

[1] M. A. Andreata and V. V. Dodonov. Energy density and packet formation in a vibrating cavity. *J. Phys. A*, 33(16):3209–3223, 2000.

[2] A. Arneodo and M. Holschneider. Fractal dimensions and homeomorphic conjugacies. *J. Statist. Phys.*, 50(5-6):995–1020, 1988.

[3] V. I. Arnol'd. Small denominators. I. Mapping the circle onto itself. *Izv. Akad. Nauk SSSR Ser. Mat.*, 25:21–86, 1961. Correction: 28:479–480, 1964; English translation: *Amer. Math. Soc. Transl. (2)*, 46:213–284, 1965.

[4] V. I. Arnol'd. *Geometrical Methods in the Theory of Ordinary Differential Equations*. Springer-Verlag, New York, second edition, 1988.

[5] V. I. Arnol'd and A. Avez. *Ergodic Problems of Classical Mechanics*. W. A. Benjamin, New York-Amsterdam, 1968.

[6] Thomas Kwok-keung Au and X.-S. Lin. Off-center reflections: caustics and chaos. *Experiment. Math.*, 10(2):287–301, 2001.

[7] C. Baesens, J. Guckenheimer, S. Kim, and R. S. MacKay. Three coupled oscillators: mode-locking, global bifurcations and toroidal chaos. *Phys. D*, 49(3):387–475, 1991.

[8] N. Balazs. On the solution of the wave equation with moving boundaries. *J. Math. Anal. Appl.*, 3(3):472–484, 1961.

[9] L. Barreira and Ya. B. Pesin. *Lyapunov Exponents and Smooth Ergodic Theory.* American Mathematical Society, Providence, RI, 2002.

[10] L. Berggren, J. Borwein, and P. Borwein. *Pi: A Source Book.* Springer-Verlag, New York, second edition, 2000.

[11] T. Bohr, P. Bak, and M. H. Jensen. Transition to chaos by interaction of resonances in dissipative systems. II. Josephson junctions, charge-density waves, and standard maps. *Phys. Rev. A (3)*, 30(4):1970–1981, 1984.

[12] J. M. Borwein and P. B. Borwein. The arithmetic-geometric mean and fast computation of elementary functions. *SIAM Rev.*, 26(3):351–366, 1984.

[13] J. M. Borwein and P. B. Borwein. *Pi and the AGM: A Study in Analytic Number Theory and Computational Complexity.* John Wiley & Sons, New York, 1987.

[14] M. Brack and R. K. Bhaduri. *Semiclassical Physics.* Addison-Wesley, Reading, Mass., 1997.

[15] R. P. Brent. Fast multiple-precision evaluation of elementary functions. *J. Assoc. Comput. Mach.*, 23(2):242–251, 1976.

[16] K. M. Briggs. The doubledouble homepage.
http://www.labs.bt.com/people/briggsk2/doubledouble.html.

[17] K. M. Briggs, T. W. Dixon, and G. Szekeres. Analytic solutions of the Cvitanović-Feigenbaum and Feigenbaum-Kadanoff-Shenker equations. *Internat. J. Bifur. Chaos Appl. Sci. Engrg.*, 8(2):347–357, 1998.

[18] H. Broer and C. Simó. Hill's equation with quasi-periodic forcing: resonance tongues, instability pockets and global phenomena. *Bol. Soc. Brasil. Mat. (N.S.)*, 29(2):253–293, 1998.

[19] H. W. Broer, G. B. Huitema, F. Takens, and B. L. J. Braaksma. Unfoldings and bifurcations of quasi-periodic tori. *Mem. Amer. Math. Soc.*, 83(421):viii+175, 1990.

[20] G. Calucci. Casimir effect for moving bodies. *J. Phys. A*, 25(13):3873–3882, 1992.

[21] H. B. G. Casimir. On the attraction between two perfectly conducting plates. *Proc. Konink. Nederl. Akad. Wetensch.*, 51(7):793–795, 1948.

[22] M. Castagnino and R. Ferraro. The radiation from moving mirrors: the creation and absorption of particles. *Ann. Physics*, 154(1):1–23, 1984.

[23] L. Chen, N. Goldenfeld, and Y. Oono. Renormalization group and singular perturbations: Multiple scales, boundary layers, and reductive perturbation theory. *Phys. Rev. E*, 54(1):376–394, 1996.

[24] L. Y. Chen, N. Goldenfeld, and Y. Oono. Renormalization group theory for global asymptotic analysis. *Phys. Rev. Lett.*, 73(10):1311–1315, 1994.

[25] V. A. Chulaevsky and Ya. G. Sinaǐ. Anderson localization for the 1-D discrete Schrödinger operator with two-frequency potential. *Comm. Math. Phys.*, 125(1):91–112, 1989.

[26] K. Colanero and M.-C. Chu. Resonances of the system of a particle in an oscillating spherical cavity. *Phys. Rev. A*, 60(3):1845–1849, 1999.

[27] C. K. Cole. The quantum vacuum in a cavity with moving boundaries. *Ph.D. Thesis, University of Texas*, 1996.

[28] C. K. Cole and W. C. Schieve. Radiation modes of a cavity with a moving boundary. *Phys. Rev. A*, 52(6):4405–4415, 1995.

[29] C. K. Cole and W. C. Schieve. Resonant energy exchange between a moving boundary and radiation modes of a cavity. *Phys. Rev. A*, 64(2):023813, 9, 2001.

[30] J. Cooper. Scattering of electromagnetic fields by a moving boundary: the one-dimensional case. *IEEE Trans. Antennas and Propagation*, 28(6):791–795, 1980.

[31] J. Cooper. Asymptotic behavior for the vibrating string with a moving boundary. *J. Math. Anal. Appl.*, 174(1):67–87, 1993.

[32] J. Cooper. Long-time behavior and energy growth for electromagnetic waves reflected by a moving boundary. *IEEE Trans. Antennas and Propagation*, 41(10):1365–1370, 1993.

[33] J. Cooper and H. Koch. The spectrum of a hyperbolic evolution operator. *J. Funct. Anal.*, 133(2):301–328, 1995.

[34] J. Cooper and W. Strauss. Scattering of waves by periodically moving bodies. *J. Funct. Anal.*, 47(2):180–229, 1982.

[35] J. Cooper and W. A. Strauss. Energy boundedness and decay of waves reflecting off a moving obstacle. *Indiana Univ. Math. J.*, 25(7):671–690, 1976.

[36] A. J. Cortez. Dynamics of diffeomorphisms of the torus. *Ph.D. Thesis, University of California*, 2002.

[37] M. Crocce, D. A. R. Dalvit, and Mazzitelli F. D. Resonant photon creation in a three-dimensional oscillating cavity. *Phys. Rev. A*, 64(1):013808, 10, 2001.

[38] P. Cvitanović, editor. *Universality in Chaos*. Adam Hilger, Bristol, second edition, 1989.

[39] P. Cvitanović, B. Shraiman, and B. Söderberg. Scaling laws for mode lockings in circle maps. *Phys. Scripta*, 32(4):263–270, 1985.

[40] D. A. R. Dalvit and F. D. Mazzitelli. Renormalization-group approach to the dynamical Casimir effect. *Phys. Rev. A*, 57(3):2113–2119, 1998.

[41] D. A. R. Dalvit and F. D. Mazzitelli. Creation of photons in an oscillating cavity with two moving mirrors. *Phys. Rev. A*, 59(4):3049–3059, 1999.

[42] I. Daubechies. *Ten Lectures on Wavelets*. SIAM, Philadelphia, PA, 1992.

[43] A. M. Davie. The width of Arnold tongues for the sine circle map. *Nonlinearity*, 9(2):421–432, 1996.

[44] E. de Faria. Asymptotic rigidity of scaling ratios for critical circle mappings. *Ergodic Theory Dynam. Systems*, 19(4):995–1035, 1999.

[45] E. de Faria and W. de Melo. Rigidity of critical circle mappings. I. *J. Eur. Math. Soc. (JEMS)*, 1(4):339–392, 1999.

[46] E. de Faria and W. de Melo. Rigidity of critical circle mappings. II. *J. Amer. Math. Soc.*, 13(2):343–370, 2000.

[47] W. de Melo. Rigidity and renormalization in one-dimensional dynamical systems. In *Proceedings of the International Congress of Mathematicians, Vol. II (Berlin, 1998)*, number Extra Vol. II, pages 765–778 (electronic), 1998.

[48] W. de Melo and S. van Strien. *One-Dimensional Dynamics.* Springer-Verlag, Berlin, 1993.

[49] R. Delbourgo and B. G. Kenny. Relations between universal scaling constants for the circle map near the golden mean. *J. Math. Phys.*, 32(4):1045–1051, 1991.

[50] A. Denjoy. Sur les courbes définies par les équations différentielles à la surface du tore. *J. Math. Pures et Appl. (9. série)*, 11:333–375, 1932.

[51] E. I. Dinaburg. Some problems in the spectral theory of discrete operators with quasiperiodic coefficients. *Uspekhi Mat. Nauk*, 52(3(315)):3–52, 1997. English translation: *Russian Math. Surveys*, 52(3):451–499, 1997.

[52] E. I. Dinaburg and Ja. G. Sinaĭ. The one-dimensional Schrödinger equation with quasiperiodic potential. *Funkcional. Anal. i Priložen.*, 9(4):8–21, 1975. English translation: *Functional Anal. Appl.*, 9(4):279–289, 1975.

[53] J. Dittrich, P. Duclos, and N. Gonzalez. Stability and instability of the wave equation solutions in a pulsating domain. *Rev. Math. Phys.*, 10(7):925–962, 1998.

[54] J. Dittrich, P. Duclos, and P. Šeba. Instability in a classical periodically driven string. *Phys. Rev. E*, 49(4):3535–3538, 1994.

[55] T. W. Dixon, B. G. Kenny, and K. M. Briggs. On the universality of singular circle maps. *Phys. Lett. A*, 231(5-6):359–366, 1997.

[56] V. V. Dodonov. Resonance photon generation in a vibrating cavity. *J. Phys. A*, 31(49):9835–9854, 1998.

[57] V. V. Dodonov and M. A. Andreata. Squeezing and photon distribution in a vibrating cavity. *J. Phys. A*, 32(39):6711–6726, 1999.

[58] V. V. Dodonov and A. B. Klimov. Generation and detection of photons in a cavity with a resonantly oscillating boundary. *Phys. Rev. A*, 53(4):2664–2682, 1996.

[59] V. V. Dodonov, A. B. Klimov, and V. I. Man'ko. Generation of squeesed states in a resonator with a moving wall. *Phys. Lett. A*, 149(4):225–228, 1990.

[60] V. V. Dodonov, A. B. Klimov, and D. E. Nikonov. Quantum phenomena in nonstationary media. *Phys. Rev. A*, 47(5):4422–4429, 1993.

[61] V. V. Dodonov, A. B. Klimov, and D. E. Nikonov. Quantum phenomena in resonators with moving walls. *J. Math. Phys.*, 34(7):2742–2756, 1993.

[62] R. Douady. Systèmes dynamiques non autonomes: démonstration d'un théorème de Pustyl'nikov. *J. Math. Pures Appl. (9)*, 68(3):297–317, 1989.

[63] S. A. Dovbysh. Kolmogorov stability, the impossibility of Fermi acceleration, and the existence of periodic solutions in some systems of Hamiltonian type. *Prikl. Mat. Mekh.*, 56(2):218–229, 1992. English translation: *J. Appl. Math. Mech.*, 56(2):188–197, 1992.

[64] J.-P. Eckmann. Roads to turbulence in dissipative dynamical systems. *Rev. Mod. Phys.*, 53:643–654, 1981.

[65] J.-P. Eckmann and H. Epstein. On the existence of fixed points of the composition operator for circle maps. *Comm. Math. Phys.*, 107(2):213–231, 1986.

[66] J.-P. Eckmann and H. Epstein. Fixed points of composition operators. In *VIIIth International Congress on Mathematical Physics (Marseille, 1986)*, pages 517–530. World Sci. Publishing, Singapore, 1987.

[67] A. Einstein. Zur Electrodynamik bewegter Körper. *Ann. Phys. (Leipzig)*, 17:891–921, 1905.

[68] H. Epstein. New proofs of the existence of the Feigenbaum functions. *Comm. Math. Phys.*, 106(3):395–426, 1986.

[69] H. Epstein. Fixed points of composition operators. II. *Nonlinearity*, 2(2):305–310, 1989.

[70] B. R. Fayad. Weak mixing for reparametrized linear flows on the torus. *Ergodic Theory Dynam. Systems*, to appear.

[71] M. J. Feigenbaum, L. P. Kadanoff, and S. J. Shenker. Quasiperiodicity in dissipative systems: a renormalization group analysis. *Phys. D*, 5(2-3):370–386, 1982.

[72] N. Fenichel. Asymptotic stability with rate conditions for dynamical systems. *Bull. Amer. Math. Soc.*, 80:346–349, 1974.

[73] E. Fermi. On the origin of the cosmic radiation. *Phys. Rev. (2)*, 75(8):1169–1174, 1949.

[74] G. E. Forsythe, M. A. Malcolm, and C. B. Moler. *Computer Methods for Mathematical Computations*. Prentice-Hall, Englewood Cliffs, N.J., 1977.

[75] M. Frazier, B. Jawerth, and G. Weiss. *Littlewood-Paley Theory and the Study of Function Spaces*. Published for the Conference Board of the Mathematical Sciences, Washington, DC, 1991.

[76] S. A. Fulling and P. C. W. Davies. Radiation from a moving mirror in two dimensional space-time: conformal anomaly. *Proc. Roy. Soc. London Ser. A*, 348(1654):393–414, 1976.

[77] O. G. Galkin. Phase-locking for dynamical systems on the torus and perturbation theory for Mathieu-type problems. *J. Nonlinear Sci.*, 4(2):127–156, 1994.

[78] P. R. Garabedian. *Partial Differential Equations*. John Wiley & Sons, New York, 1964.

[79] L. Glass. Cardiac arrhythmias and circle maps – a classical problem. *Internat. J. Bifur. Chaos Appl. Sci. Engrg.*, 5(2):359–371, 1995.

[80] J. A. Glazier and A. Libchaber. Quasi-periodicity and dynamical systems: an experimentalist's view. *IEEE Trans. Circuits and Systems*, 35(7):790–809, 1988.

[81] P. Glendinning, U. Feudel, A. S. Pikovsky, and J. Stark. The structure of mode-locked regions in quasi-periodically forced circle maps. *Phys. D*, 140(3–4):227–243, 2000.

[82] N. Gonzalez. *Ph.D. Thesis, University of Toulon and Czech Technical University*, 1997.

[83] N. Gonzalez. An example of pure stability for the wave equation with moving boundary. *J. Math. Anal. Appl.*, 228(1):51–59, 1998.

[84] J. Graczyk and G. Świątek. Critical circle maps near bifurcation. *Comm. Math. Phys.*, 176(2):227–260, 1996.

[85] C. Grebogi, E. Ott, and J. A. Yorke. Attractors on an N-torus: quasiperiodicity versus chaos. *Phys. D*, 15(3):354–373, 1985.

[86] J. M. Greene. A method for determining a stochastic transition. *J. Math. Phys.*, 20(6):1183–1201, 1979.

[87] M. C. Gutzwiller. *Chaos in Classical and Quantum Mechanics*. Springer-Verlag, New York, 1990.

[88] G. R. Hall. A C^∞ Denjoy counterexample. *Ergodic Theory Dynamical Systems*, 1(3):261–272 (1982), 1981.

[89] Bai Lin Hao, editor. *Chaos.* World Sci. Publishing, Singapore, 1984.

[90] W. Härdle, G. Kerkyacharian, D. Picard, and A. Tsybakov. *Wavelets, Approximation, and Statistical Applications.* Springer-Verlag, New York, 1998.

[91] T. H. Havelock. Some dynamical illustrations of the pressure of radiation and of the adiabatic invariance. *Phil. Mag.*, 47(280):754–771, 1924.

[92] J. Hawkins and K. Schmidt. On C^2-diffeomorphisms of the circle which are of type III$_1$. *Invent. Math.*, 66(3):511–518, 1982.

[93] W. C. Henneberger and H. J. Schulte. Optical pulses produced by laser length variation. *J. Appl. Phys.*, 37(5):2189, 1965.

[94] M.-R. Herman. Sur la conjugaison différentiable des difféomorphismes du cercle à des rotations. *Inst. Hautes Études Sci. Publ. Math.*, (49):5–233, 1979.

[95] M.-R. Herman. Simple proofs of local conjugacy theorems for diffeomorphisms of the circle with almost every rotation number. *Bol. Soc. Brasil. Mat.*, 16(1):45–83, 1985.

[96] E. Hernández and G. Weiss. *A First Course on Wavelets*. CRC Press, Boca Raton, FL, 1996.

[97] M. W. Hirsch and C. C. Pugh. Stable manifolds and hyperbolic sets. In *Global Analysis (Proc. Sympos. Pure Math., Vol. XIV, Berkeley, Calif., 1968)*, pages 133–163. Amer. Math. Soc., Providence, R.I., 1970.

[98] M. Holschneider and Ph. Tchamitchian. Pointwise analysis of Riemann's "nondifferentiable" function. *Invent. Math.*, 105(1):157–175, 1991.

[99] B. Hu, A. Valinia, and O. Piro. Universality and asymptotic limits of the scaling exponents in circle maps. *Phys. Lett. A*, 144(1):7–10, 1990.

[100] A. M. Ignatov. Trivelpiece-Gould modes in a corrugated plasma slab. *Phys. Rev. E (3)*, 51(2):1391–1399, 1995.

[101] J. D. Jackson. *Classical Electrodynamics*. John Wiley & Sons, New York, second edition, 1975.

[102] S. Jaffard. Multifractal formalism for functions. I. Results valid for all functions. II. Self-similar functions. *SIAM J. Math. Anal.*, 28(4):944–970, 971–998, 1997.

[103] S. Jaffard and Y. Meyer. Wavelet methods for pointwise regularity and local oscillations of functions. *Mem. Amer. Math. Soc.*, 123(587):x+110, 1996.

[104] M. Janowicz. Evolution of wave fields and atom-field interactions in a cavity with one oscillating mirror. *Phys. Rev. A*, 57(6):4784–4790, 1998.

[105] M. H. Jensen, P. Bak, and T. Bohr. Transition to chaos by interaction of resonances in dissipative systems. I. Circle maps. *Phys. Rev. A (3)*, 30(4):1960–1969, 1984.

[106] J.-Y. Ji, H.-H. Jung, J.-W. Park, and K.-S. Soh. Production of photons by the parametric resonance in the dynamical Casimir effect. *Phys. Rev. A*, 57(6):4440–4444, 1997.

[107] J.-Y. Ji, H.-H. Jung, and K.-S. Soh. Interference phenomena in the photon production between two moving mirrors. *Phys. Rev. A*, 57(6):4952–4955, 1998.

[108] J.-Y. Ji, K.-S. Soh, R.-G. Cai, and S. P. Kim. Electromagnetic fields in a three-dimensional cavity and in a waveguide with oscillating walls. *J. Phys. A*, 31(24):L457–L462, 1998.

[109] F. John. *Partial Differential Equations.* Springer-Verlag, New York, fourth edition, 1982.

[110] H. Johnston and S. Sarkar. Moving mirrors and time-dependent dielectrics. *Phys. Rev. A*, 51(5):4109–4115, 1995.

[111] H. Johnston and S. Sarkar. A re-examination of the quantum theory of optical cavities with moving mirrors. *J. Phys. A*, 29(8):1741–1746, 1996.

[112] A. Katok and B. Hasselblatt. *Introduction to the Modern Theory of Dynamical Systems*. Cambridge University Press, Cambridge, 1995.

[113] Y. Katznelson and D. Ornstein. The differentiability of the conjugation of certain diffeomorphisms of the circle. *Ergodic Theory Dynam. Systems*, 9(4):643–680, 1989.

[114] S. Kim and S. Östlund. Universal scaling in circle maps. *Phys. D*, 39(2-3):365–392, 1989.

[115] J. Koiller, R. Markarian, S. Oliffson Kamphorst, and S. Pinto de Carvalho. Time-dependent billiards. *Nonlinearity*, 8(6):983–1003, 1995.

[116] S. G. Krantz. Lipschitz spaces, smoothness of functions, and approximation theory. *Exposition. Math.*, 1(3):193–260, 1983.

[117] T. Krüger, L. D. Pustyl'nikov, and S. E. Troubetzkoy. Acceleration of bouncing balls in external fields. *Nonlinearity*, 8(3):397–410, 1995.

[118] J. Kwapisz. Every convex polygon with rational vertices is a rotation set. *Ergodic Theory Dynam. Systems*, 12(2):333–339, 1992.

[119] O. E. Lanford, III. Introduction to the mathematical theory of dynamical systems. In *Chaotic Behavior of Deterministic Systems (Les Houches, 1981)*, pages 3–51. North-Holland, Amsterdam, 1983.

[120] O. E. Lanford, III. A numerical study of the likelihood of phase locking. *Phys. D*, 14(3):403–408, 1985.

[121] O. E. Lanford, III. Renormalization group methods for circle mappings. In *Statistical Mechanics and Field Theory : Mathematical Aspects (Groningen, 1985)*, pages 176–189. Springer-Verlag, Berlin, 1986.

[122] O. E. Lanford, III. Renormalization group methods for critical circle mappings with general rotation number. In *VIIIth international Congress on Mathematical Physics (Marseille, 1986)*, pages 532–536. World Sci. Publishing, Singapore, 1987.

[123] O. E. Lanford, III. Renormalization group methods for circle mappings. In *Nonlinear Evolution and Chaotic Phenomena (Noto, 1987)*, pages 25–36. Plenum, New York, 1988.

[124] O. E. Lanford, III and R. de la Llave. Solution of the functional equation for critical circle mappings with golden rotation number. *Manuscript*, 1984.

[125] Sir J. Larmor. On the dynamics of radiation. In *Proceedings of the Fifth International Congress of Mathematicians, Cambridge, 1912*, volume 1, pages 197–216. Cambridge University Press, Cambridge, 1913. With and Appendix by T. Levi-Civita, pages 217–220.

[126] C. K. Law. Interaction between a moving mirror and radiation pressure: A Hamiltonian formulation. *Phys. Rev. A*, 51(3):2537–2541, 1955.

221

[127] C. K. Law. Effective Hamiltonian for the radiation in a cavity with a moving mirror and a time-varying dielectric medium. *Phys. Rev. A*, 49(1):433–437, 1994.

[128] C. K. Law. Resonance responce of the quantum vacuum to an oscillating boundary. *Phys. Rev. Lett.*, 73(4):1931–1934, 1994.

[129] A. J. Lichtenberg and M. A. Lieberman. *Regular and Chaotic Dynamics*. Springer-Verlag, New York, second edition, 1992.

[130] R. de la Llave. A tutorial on KAM theory. In *Smooth Ergodic Theory and Its Applications (Seattle, WA, 1999)*, pages 175–292. Amer. Math. Soc., Providence, RI, 2001.

[131] R. de la Llave and N. P. Petrov. Theory of circle maps and the problem of one-dimensional optical resonator with a periodically moving wall. *Phys. Rev. E (3)*, 59(6):6637–6651, 1999.

[132] R. de la Llave and N. P. Petrov. Regularity of conjugacies between critical circle maps: an experimental study. *Experiment. Math.*, to appear, 2001.

[133] R. de la Llave and R. P. Schafer. Rigidity properties of one dimensional expanding maps and applications to renormalization. *Manuscript*, 1996.

[134] R. de la Llave and J. Vano. A Nash-Moser implicit function theorem with Whitney regularity. *Manuscript*, 2001.

[135] J. Llibre and R. S. MacKay. Rotation vectors and entropy for homeomorphisms of the torus isotopic to the identity. *Ergodic Theory Dynam. Systems*, 11(1):115–128, 1991.

[136] H. A. Lorentz, A. Einstein, H. Minkowski, and H. Weyl. *The Principle of Relativity*. Dover, New York, 1923.

[137] A. K. Louis, P. Maaß, and A. Rieder. *Wavelets: Theory and Applications*. John Wiley & Sons, Chichester, 1997.

[138] S. Mallat. *A Wavelet Tour of Signal Processing*. Academic Press, San Diego, CA, 1998.

[139] O. Méplan and C. Gignoux. Exponential growth of a wave in a 1D vibrating cavity: Application to the quantum vacuum. *Phys. Rev. Lett.*, 76(3):408–410, 1996.

[140] B. Mestel. Computer assisted proof of universality of cubic critial maps of the circle with golden mean rotation number. *Ph.D. Thesis, University of Warwick*, 1984.

[141] Y. Meyer. *Ondelettes et opérateurs. I.* Hermann, Paris, 1990.

[142] Y. Meyer. *Wavelets, Vibrations and Scalings*. Amer. Math. Soc., Providence, RI, 1998.

[143] A. I. Miller. *Albert Einstein's Special Theory of Relativity*. Addison-Wesley, Reading, Mass., 1981.

[144] H. Minkowski. Raum und Zeit. *Phys. Z.*, 10(3):104–111, 1909.

[145] V. E. Mkrtchian and R. v. Baltz. Dynamical electromagnetic modes for an expanding sphere. *J. Math. Phys.*, 41(4):1956–1960, 2000.

[146] G. T. Moore. Quantum theory of the electromagnetic field in a variable-length one-dimensional cavity. *J. Math. Phys.*, 11(9):2679–2691, 1970.

[147] J. Moser. A rapidly convergent iteration method and non-linear differential equations. II. *Ann. Scuola Norm. Sup. Pisa (3)*, 20:499–535, 1966.

[148] J. Moser. A rapidly convergent iteration method and non-linear partial differential equations. I. *Ann. Scuola Norm. Sup. Pisa (3)*, 20:265–315, 1966.

[149] J. Moser. *Stable and Random Motions in Dynamical Systems.* Princeton University Press, Princeton, N. J., 1973.

[150] J. Moser and J. Pöschel. An extension of a result by Dinaburg and Sinaǐ on quasiperiodic potentials. *Comment. Math. Helv.*, 59(1):39–85, 1984.

[151] V. M. Mostepanenko and N. N. Trunov. *The Casimir Effect and Its Applications.* Clarendon Press, Oxford, 1997.

[152] D. F. Mundarain and P. A. Maia Neto. Quantum radiation in a cavity with moving mirrors. *Phys. Rev. A*, 57(2):1379–1390, 1998.

[153] S. Newhouse, D. Ruelle, and F. Takens. Occurrence of strange Axiom A attractors near quasiperiodic flows on $T^m, m \geq 3$. *Comm. Math. Phys.*, 64(1):35–40, 1978/79.

[154] E. L. Nicolai. On a dynamical illustration of the pressure of radiation. *Phil. Mag.*, 49(289):171–177, 1925.

[155] J. U. Nöckel and R. R. Chang. 2d microcavities: theory and experiment. In R. D. van Zee and J. P. Looney, editors, *Cavity-Enhanced Spectroscopies*, Experimental Methods in the Physical Sciences. Academic Press, San Diego, 2002.

[156] S. Oliffson Kamphorst and S. Pinto de Carvalho. Bounded gain of energy on the breathing circle billiard. *Nonlinearity*, 12(5):1363–1371, 1999.

[157] V. I. Oseledec. A multiplicative ergodic theorem. Characteristic Ljapunov, exponents of dynamical systems. *Trudy Moskov. Mat. Obšč.*, 19:179–210, 1968. English translation: *Trans. Moscow Math. Soc.* 19:197–231, 1968.

[158] S. Ostlund, D. Rand, J. Sethna, and E. D. Siggia. Universal properties of the transition from quasiperiodicity to chaos in dissipative systems. *Phys. D*, 8(3):303–342, 1983.

[159] W. Pauli. *Theory of Relativity*. Pergamon Press, New York, 1958.

[160] N. P. Petrov, R. de la Llave, and J. A. Vano. Torus maps and the problem of a one-dimensional optical resonator with a quasiperiodically moving wall. *Preprint*, 2002.

[161] A. A. Pinto and D. A. Rand. Global phase space universality, smooth conjugacies and renormalization. II. The $C^{k+\alpha}$ case using rapid convergence of Markov families. *Nonlinearity*, 5(1):49–79, 1992.

[162] H. Poincaré. Sur le courbes définies par les équations différentielles. *J. Math. Pures et Appl. (4. série)*, 1:167–244, 1885.

[163] Y. Pomeau and P. Manneville. Intermittent transition to turbulence in dissipative dynamical systems. *Comm. Math. Phys.*, 74(2):189–197, 1980.

[164] G. Popov and Ts. V. Rangelov. Exponential growth of the local energy for moving obstacles. *Osaka J. Math.*, 26(4):881–895, 1989.

[165] W. H. Press, S. A. Teukolsky, W. T. Vetterling, and B. P. Flannery. *Numerical Recipes in C: The Art of Scientific Computing*. Cambridge University Press, Cambridge, second edition, 1992.

[166] L. D. Pustyl'nikov. Stable and oscillating motions in nonautonomous dynamical systems. II. *Trudy Moskov. Mat. Obšč.*, 34:3–103, 1977. English translation: *Trans. Moscow Math. Soc.*, 1978, *Issue 2*, American Mathematical Society, Providence, R.I., 1978, pages 1–101.

[167] D. Rand. Universality and renormalisation in dynamical systems. In *New Directions in Dynamical Systems*, pages 1–56. Cambridge Univ. Press, Cambridge, 1988.

[168] D. Rand, S. Ostlund, J. Sethna, and E. D. Siggia. Universal transition from quasiperiodicity to chaos in dissipative systems. *Phys. Rev. Lett.*, 49(2):132–135, 1982.

[169] D. A. Rand. Fractal bifurcation sets, renormalization strange sets and their universal invariants. *Proc. Roy. Soc. London Ser. A*, 413(1844):45–61, 1987.

[170] D. A. Rand. Global phase space universality, smooth conjugacies and renormalisation. I. The $C^{1+\alpha}$ case. *Nonlinearity*, 1(1):181–202, 1988.

[171] D. A. Rand. Existence, nonexistence and universal breakdown of dissipative golden invariant tori. I. Golden critical circle maps. *Nonlinearity*, 5(3):639–662, 1992.

[172] Lord Rayleigh (J. W. Strutt). On the pressure of vibrations. *Phil. Mag.*, 3:338–346, 1902.

[173] Lord Rayleigh (J. W. Strutt). *Scientific Papers*. Dover, New York, 1964.

[174] M. Razavy and J. Terning. Quantum ratiation in a one-dimensional cavity with moving boundaries. *Phys. Rev. D*, 31(2):307–313, 1985.

[175] D. Ruelle. Ergodic theory of differentiable dynamical systems. *Inst. Hautes Études Sci. Publ. Math.*, (50):27–58, 1979.

[176] D. Ruelle. *Elements of Differentiable Dynamics and Bifurcation Theory.* Academic Press, Boston, MA, 1989.

[177] E. Sassaroli, Y. N. Srivastava, and A. Widom. Photon production by dynamical Casimir effect. *Phys. Rev. A*, 50(2):1027–1034, 1994.

[178] M. B. Sevryuk. The lack-of-parameters problem in the KAM theory revisited. In *Hamiltonian Systems with Three or More Degrees of Freedom (S'Agaró, 1995)*, pages 568–572. Kluwer Acad. Publ., Dordrecht, 1999.

[179] S. J. Shenker. Scaling behavior in a map of a circle onto itself: empirical results. *Phys. D*, 5(2–3):405–411, 1982.

[180] B. I. Shraiman. Transition from quasiperiodicity to chaos: a perturbative renormalization-group approach. *Phys. Rev. A (3)*, 29(6):3464–3466, 1984.

[181] P. W. Smith. Phase locking of laser modes by continuous cavity length variation. *Appl. Phys. Lett.*, 10(2):51–53, 1967.

[182] E. M. Stein. *Singular Integrals and Differentiability Properties of Functions.* Princeton University Press, Princeton, N.J., 1970.

[183] G. Świątek. Rational rotation numbers for maps of the circle. *Comm. Math. Phys.*, 119(1):109–128, 1988.

[184] G. Świątek. Circle homeomorphisms with flat critical points. *Fund. Math.*, 138(3):205–217, 1991.

[185] G. Świątek. On critical circle homeomorphisms. *Bol. Soc. Brasil. Mat. (N.S.)*, 29(2):329–351, 1998.

[186] F. M. Tangerman and J. J. P. Veerman. Scalings in circle maps. II. *Comm. Math. Phys.*, 141(2):279–291, 1991.

[187] GMP Team. The gmp home page. `http://www.swox.com/gmp/`.

[188] S. M. Ulam. On some statistical properties of dynamical systems. In *Proc. 4th Berkeley Sympos. Math. Statist. and Prob., Vol. III*, pages 315–320. Univ. California Press, Berkeley, Calif., 1961.

[189] J. Väisälä. *Lectures on n-Dimensional Quasiconformal Mappings*. Springer-Verlag, Berlin, 1971. Lecture Notes in Mathematics, Vol. 229.

[190] J. A. Vano, R. de la Llave, and N. P. Petrov. On the role of the boundary conditions in resonant cavities with moving walls. *Preprint*, 2002.

[191] J. J. P. Veerman and F. M. Tangerman. Scalings in circle maps. I. *Comm. Math. Phys.*, 134(1):89–107, 1990.

[192] C. E. Wayne. An introduction to KAM theory. In *Dynamical Systems and Probabilistic Methods in Partial Differential Equations (Berkeley, CA, 1994)*, pages 3–29. Amer. Math. Soc., Providence, RI, 1996.

[193] H. F. Weinberger. *A First Course in Partial Differential Equations with Complex Variables and Transform Methods*. Blaisdell, New York, 1965.

[194] H. Whitney. Differentiable functions defined in arbitrary subsets of Euclidean space. *Trans. Amer. Math. Soc.*, 40(2):309–317, 1936.

[195] M. V. Wickerhauser. *Adapted Wavelet Analysis from Theory to Software*. A K Peters, Wellesley, MA, 1994. Software available at
`http://www.math.wustl.edu/~victor/`

[196] Ying Wu, K. W. Chan, M.-C. Chu, and P. T. Leung. Radiation modes of a cavity with a resonantly oscillating boundary. *Phys. Rev. A*, 59(2):1662–1666, 1999.

[197] Ying Wu, M.-C. Chu, and P. T. Leung. Dynamics of the quantized radiation field in a cavity vibrating at the fundamental frequency. *Phys. Rev. A*, 59(4):3032–3037, 1999.

[198] M. Yamaguchi. Note on quasiperiodic solutions of undamped linear wave equations. *Proc. Fac. Sci. Tokai Univ.*, 12:3–10, 1977.

[199] M. Yamaguchi. Almost periodic solutions of one-dimensional wave equations with periodic coefficients. *J. Math. Kyoto Univ.*, 29(3):463–487, 1989.

[200] M. Yamaguchi. Nonexistence of bounded solutions of one-dimensional wave equations with quasiperiodic forcing terms. *J. Differential Equations*, 127(2):484–497, 1996.

[201] M. Yamaguchi. Quasiperiodic motions of vibrating string with periodically moving boundaries. *J. Differential Equations*, 135(1):1–15, 1997.

[202] M. Yamaguchi. Periodic motions of vibrating string with a periodically moving boundary. *Discrete Contin. Dynam. Systems*, (Added Volume II):303–314, 1998. Dynamical Systems and Differential Equations, Vol. II (Springfield, MO, 1996).

[203] M. Yamaguchi. 3D wave equations in sphere-symmetric domain with periodically oscillating boundaries. *Discrete Contin. Dynam. Systems*, 7(2):385–396, 2001.

[204] M. Yamaguchi. Vibrating string problem with quasiperiodically moving boundaries, 2001.

[205] M. Yamaguchi and I. Imai. Nonexistence of bounded solutions of some linear evolution equation with periodic forcing term. *Proc. Fac. Sci. Tokai Univ.*, 27:17–26, 1992.

[206] M. Yamaguchi and H. Yoshida. Nonhomogeneous string problem with periodically moving boundaries. In *Operator Theory and Its Applications (Winnipeg, MB, 1998)*, pages 565–574. Amer. Math. Soc., Providence, RI, 2000.

231

[207] M. Yampolsky. Complex bounds for renormalization of critical circle maps. *Ergodic Theory Dynam. Systems*, 19(1):227–257, 1999.

[208] J.-C. Yoccoz. Conjugaison différentiable des difféomorphismes du cercle dont le nombre de rotation vérifie une condition diophantienne. *Ann. Sci. École Norm. Sup. (4)*, 17(3):333–359, 1984.

[209] J.-C. Yoccoz. Il n'y a pas de contre-exemple de Denjoy analytique. *C. R. Acad. Sci. Paris Sér. I Math.*, 298(7):141–144, 1984.

[210] V. Zharnitsky. Instability in Fermi-Ulam "ping-pong" problem. *Nonlinearity*, 11(6):1481–1487, 1998.

[211] V. Zharnitsky. Invariant curve theorem for quasiperiodic twist mappings and stability of motion in the Fermi-Ulam problem. *Nonlinearity*, 13(4):1123–1136, 2000.

[212] V. Zharnitsky. Invariant tori in Hamiltonian systems with impacts. *Comm. Math. Phys.*, 211(2):289–302, 2000.

Vita

Nikola Petrov Petrov was born in Plovdiv, Bulgaria on 6 July 1965, the son of Petar Nikolov Petrov and Maria Georgieva Petrova. He received the Bachelor of Science degree in Physics (specialization Nuclear and Elementary Particle Physics) from the University of Sofia, Bulgaria, in 1990. From 1991 to 1993 he was a graduate student in Theoretical and Mathematical Physics at the Theoretical Physics Division of the University of Sofia. From 1993 to 1995 he worked as a full-time Lecturer in Physics at the Experimental Technological School of Electronic Systems of the Technical University, Sofia, Bulgaria. In 1995 he was accepted in the Graduate Program in Physics of the University of Texas at Austin. He is also working towards a Master of Arts degree in Mathematics from the University of Texas at Austin. Starting in the Fall of 2002, he will be working for three years as an Assistant Professor at the Department of Mathematics of the University of Michigan at Ann Arbor.

Permanent address: 13 Iztochen Blvd., Apt. 15
4000 Plovdiv, BULGARIA

This dissertation was typeset with LaTeX[†] by the author.

[†]LaTeX is a document preparation system developed by Leslie Lamport as a special version of Donald Knuth's TeX Program.